THE UNIVERSITY OF EDINBURGH

EDINBURGH
UNIVERSITY
LIBRARY

Shelf Mark CHEMISTRY LIBRARY

ROBERTS, PhD 2007

30150 023357293

THE CHARACTERISATION OF MAMMALIAN PHOSPHO1: *AN ENZYME INVOLVED IN BONE MINERALISATION?*

Scott John Roberts

A thesis submitted for the degree of Doctor of Philosophy at the University of Edinburgh

2007

**Department of Gene Function and Development,
Roslin Institute, Edinburgh**

I would like to thank both my supervisors Colin Farquharson and Peter Sadler for their help and guidance throughout this project. I would also like to thank my funding bodies, the BBSRC and Immunodiagnostic Systems Ltd. for their financial support, without which this project would never have occurred.

A kind thank you should also be paid to Claudia Blindauer and Rald Schmid for their work on the PHOSPHO1 and PHOSPHO2 modelling which ultimately provided figures and results which complemented experimental data that I accrued. I would also like to thank Jose Luis Millan for allowing me to travel to California to conduct chemical library screening and Steve Vasile for his assistance while there. In addition all of the people within the Roslin Institute who have aided me in this project deserve appreciation.

A special thank you also has to be paid to my partner, family and friends for their support and encouragement over the last three years.

"In light of knowledge attained, the happy achievement seems almost a matter of course, and any intelligent student can grasp it without too much trouble. But the years of anxious searching in the dark, with their intense longing, their alterations of confidence and exhaustion, and the final emergence into the light - only those who have experienced it can understand it."

Einstein, Albert (1879-1955)

Abstract

Skeletal mineralisation is dependent on the generation of inorganic phosphate (Pi), which has traditionally been attributed to tissue non-specific alkaline phosphatase (TNAP). However, evidence exists to suggest the presence of other Pi generating phosphatases in bone, with the most compelling being that initial bone mineralisation events in newborn TNAP knockout mice appear to be normal, although abnormalities of the skeleton and dentition appear later. PHOSPHO1 is a phosphatase, which belongs to the haloacid dehalogenase (HAD) superfamily of magnesium-dependent hydrolases. The work of this thesis has shown that PHOSPHO1 is able to catalyse the hydrolysis of phosphoethanolamine (PEA) and phosphocholine (PCho), which displays favourable kinetics under optimal conditions indicating that these reactions would occur *in vivo*.

Site directed mutagenesis of active site residues, along with molecular modelling, confirm this enzyme as a member of the HAD superfamily as well as implicating residues in substrate specific interactions. PHOSPHO1 protein is localised to the mineralising sites of the skeleton and cells of bone and cartilage in the mouse model. Further to this PHOSPHO1 is present in an active state within matrix vesicles, the epicentre of mineral formation. Modulation of PHOSPHO1 activity through siRNA gene knockdown studies and specific PHOSPHO1 inhibitors leads to a decrease in the mineralisation potential of cells and matrix vesicles respectively. These data further support the hypothesis that PHOSPHO1 plays a central role in matrix mineralisation, and indicates that the function of PHOSPHO1 is to sequester Pi from PEA and PCho contained within the glycerolipid membrane of matrix vesicles.

Refereed Publications

Roberts, S.J., Stewart, A.J., Sadler, P.J. and Farquharson, C. (2004) Human PHOSPHO1 exhibits high specific phosphoethanolamine and phosphocholine phosphatase activities. Biochemical Journal. 382, 59-65.

Stewart, A.J., Mukherjee, J., **Roberts, S.J.,** Lester, D. and Farquharson, C. (2005) Identification of a novel class of mammalian phosphoinositol-specific phospholipase C enzymes. International Journal of Molecular Medicine. **15,** 117-121.

Roberts, S.J, Stewart, A.J., Schmid, R., Blindauer, C.A., Bond, S.R., Sadler, P.J. and Farquharson, C. (2005) Probing the substrate specificities of human PHOSPHO1 and PHOSPHO2. Biochimica et Biophysica Acta. **1752,** 73-82.

Stewart, A.J., **Roberts, S.J.,** Seawright, E., Davey, M.G., Fleming, R.H. and Farquharson, C. (2006) The presence of PHOSPHO1 in matrix vesicles and its developmental expression prior to skeletal mineralization. Bone. **39,** 1000-1007.

Roberts, S.J., Narisawa, S., Harmey, D., Millan, J.L. and Farquharson, C. (2006) Functional evidence for a role of PHOSPHO1 in matrix vesicle mediated skeletal mineralization. Journal of Bone and Mineral Research. *In Press.*

Meeting Abstracts

Roberts, S.J., Stewart, A.J., Sadler, P.J. and Farquharson, C. (2004) Human PHOSPHO1 displays high specific phosphoethanolamine and phosphocholine phosphatase activities: A means of generating inorganic phosphate in mineralising cells. Journal of Bone and Mineral Research **19,** 1041-1041.

Stewart, A.J., **Roberts, S.J.** and Farquharson, C. (2004) Expression of PHOSPHO1 during embryonic development: Implications for skeletal mineralization. Journal of Bone and Mineral Research **19,** S60-S60 Suppl. 1.

Roberts, S.J., Harmey, D., Sadler, P.J., Millan, J.L. and Farquharson, C. (2005) Identification of active PHOSPHO1 within matrix vesicles: support for a role in hydroxyapatite crystal formation. Bone **36,** S168-S169 Suppl. 2.

Roberts, S.J., Harmey, D., Sadler, P.J., Millan, J.L. and Farquharson, C. (2005) Osteoblast and chondrocyte matrix vesicles contain PHOSPHO1: evidence for its role in mineral formation. Journal of Bone and Mineral Research **20,** 1294-1294.

Roberts, S.J., Stewart, A.J., Seawright, E, Davey, M.G., Fleming, R.H. and Farquharson, C. (2006) The developmental expression of PHOSPHO1 prior to skeletal mineralisation and its presence within matrix vesicles. Journal of Bone and Mineral Research **21,** 1166-1166.

Roberts, S.J., Narisawa, S., Harmey, D., Millan, J.L. and Farquharson, C. (2006) Discovery of novel small molecule inhibitors of PHOSPHO1 and evidence for its involvement in bone mineralization. Journal of Bone and Mineral Research **21,** S333-S333 Suppl. 1.

Chapter 1 Introduction/Literature Review

Chapter 2 Materials and Methods

Chapter 6 Functional Analysis of Mammalian PHOSPHO1

Chapter 7 Discovery and Characterisation of PHOSPHO1 Inhibitors

AA	Ascorbic acid 2-phosphate
Ab	Antibody(ies)
ALP	Alkaline phosphates
AMP	Adenosine monophosphate
AMPase	AMP phosphatise
ANK	Ankylosis
ANOVA	Analysis of variance
ATP	Adenosine 5'-triphosphate
BAP	Brain alkaline phosphatise
BMP	Bone morphogenic protein
bp	Base pair (s)
BSA	Bovine serum albumin
BSP	Bone sialoprotein
CAPS	3-(Cyclohexylamino)-1-propanesulfonic acid
Cbfa1	Core binding factor a-1
cDNA	Complementary DNA
CDP-Cho	Cytosine diphosphate-choline
CDP-EA	Cytosine diphosphate-ethanolamine
CDS	Coding sequence
CMP	Cytidine monophosphate
CPC	Cetylpyridinium chloride
CPPD	Calcium pyrophosphate dihydrate deposition disease
Ct	Threshold cycle
CTP	Cytidine 5'-triphosphate
Dkk1	Dikkopf 1
DMEM	Dulbecco's modified Eagle's medium
DMSO	Dimethylsulfoxide
DNA	Deoxyribonucleic acid
DNase	Deoxyribonuclease

dNTP	Deoxyribonucleoasid triphosphate
Dsh	Dishevelled
DTT	Dithiothreitol
EDTA	Ethylenediaminetetraacetic acid
ES	Embryonic stem
EST	Expressed sequence tag
EtBr	Ethidium bromide
FBS	Foetal bovine serum
FCS	Foetal calf serum
FGF	Fibroblast growth factor
FITC	Fluorescein isothiocyanate
Frz	Frizzled
GFP	Green fluorescent protein
GM-CSF	Granulocyte- macrophage colony stimulating factor
GPI	Glycosylphosphatidylinisotol
GSK3β	Glycogen. synthase kinase 3β
HA	Hydroxyapatite
HAg	Hemagglutinin
HAD	Haloacid dehalogenase
HBSS	Hanks' balanced salt solution
IGF	Insulin-like growth factor
IMAC	Immobilised Metal ion Affinity Chromatography
kb	Kilobase (s) or 1000bp
kDa	Kilodalton (s)
KEGG	Kyoto Encyclopedia of Genes and Genomes
KLH	Keyhole limpet hemocyanin
LB	Lysogeny broth
LEF	Lymphoid enhancer factor
MALDI-TOF	Matrix Assisted Laser Desorption Ionization Time-of-flight

M-CSF	Macrophage colony stimulating factor
MEM	Minimum essential medium
MES	2-(N-Morpholino)ethanesulfonic acid
MESG	2-amino-6-mercapto-7-methylpurine ribonucleoside
MGP	Matrix gla protein
MOPS	4-Morpholinepropanesulfonic acid
mRNA	Messenger RNA
MV	Matrix vesicle
MW	Molecular weight
Ni-NTA	Nickel-nitrilotriacetic acid
NPP1	Nucleotide pyrophosphatase phosphodiesterase 1
OCN	Osteocalcin
O-CPC	O-cresolpthalein complexone
OD	Optical density
oligo	Oligodeoxyribonucleotide
OPN	Osteopontin
OSF2	Osteoblast-specific factor-2
P5P	Pyridoxal 5-phosphate
PAGE	Polyacrylamide gel electrophoresis
PBS	Phosphate-buffered saline
PCho	Phosphocholine
PCR	Polymerase chain reaction
PEA	Phosphoethanolamine
PFA	Paraformaldehyde
PGK	Phosphoglycerate kinase
Pi	Inorganic phosphate
pNPP	Para-nitrophenyl phosphate
PPi	Inorganic pyrophosphate
PPiase	PPi phosphates

PSP	Phosphoserine phosphatise
PST	Proline-serine-threonine
PTH	Parathyroid hormone
qPCR	Quantitative PCR
RA	Retinoic acid
RGD	Arginyl-glycyl-aspartic acid
RISC	RNA induced silencing complex
RNA	Ribonucleic acid
RNase	Ribonuclease
RT-PCR	Reverse transcription PCR
SD	Standard deviation
SDS	Sodium dodecyle sulfate
SEM	Standard error of the mean
shRNA	short hairpin RNA
siRNA	Short interfering RNA
SOC	Super optimal media with catabolite repression
SPARC	Secreted protein acidic and rich in cysteine (osteonectin)
SURE	Stops unwanted recombination events
SV40	Simian virus 40
TAE	Tris-Acetate EDTA
TBE	Tris-Borate EDTA
TBS	Tris-Buffered Saline
TBST	Tris-Buffered Saline with 0.1% Tween20
TGF- β	Transforming growth factor β
TNAP	Tissue non-specific alkaline phosphatise
TRAP	Tartrate resistant acid phosphatise
Tris	Tris (hydroxymethyl)aminomethane
VEGF	Vascular endothelial growth factor
βGP	β-Glycerophosphate

CHAPTER 1

INTRODUCTION/LITERATURE REVIEW

Chapter Contents

Preface

The biochemistry surrounding bone formation is relatively poorly understood with proteins that contribute to the initial events of bone formation being suggested through hypothesis and speculation. Indeed PHOSPHO1 is a completely novel protein which is concentrated at sites of bone formation. This protein could conceivably be one of the missing links in unravelling the mechanisms by which bones grow and develop. It is amazing that a process such as growth is so poorly understood; yes we know that the length of your bones determines your final height but the molecular and biochemical processes surrounding growth remains to leave biologists scratching their heads. Understanding these mechanisms will give rise to novel strategies aimed at therapeutics for bone and soft tissue abnormalities that include diseases of great public health concern.

1.1 Skeleton

The skeleton is a highly complex organ with a range of functions spanning from support and locomotion to ion homeostasis. The skeleton itself is comprised of two different tissues – cartilage and bone (Karsenty, 2003). The bones, which form the skeletal frame, are held together by tendons thus providing a scaffold to which muscles can attach. The protective role that the skeleton provides cannot be understated with the most important organs such as the brain and lungs/heart being shielded from physical forces by the skull and ribcage, respectively. In addition to this the skeleton has an important role to play in ion homeostasis with large amounts of calcium and phosphate stored as hydroxyapatite crystals. Phosphate homeostasis is highly important as phosphate forms a major component of all glycolytic compounds

such as ATP and creatine phosphate due to the intrinsic high energy nature of the phosphate bond, as well as being used as both an extracellular and intracellular pH buffering system. Calcium also has many important roles including acting as a co-factor for cellular, enzyme mediated reactions, secondary messengers and also regulating blood clotting. Disruption of phosphate or calcium homeostasis can lead to hypocalcaemia, osteomalacia and rickets or hypercalcaemia.

1.2 Bone

Two types of bone structure exist; cortical (compact) and cancellous (trabecular) bones. Cortical bone makes up approximately 80% of the total skeletal mass (Sambrook *et al,* 1993). This bone type is also known as compact bone due to its unporous (2-5%), dense and highly organised nature. It is located along the shafts of long bones (figure 1.1A), such as the tibia and ulna and forms the primary constituent of flat bones such as the skull. Cortical bone intrinsically has a high resistance to tensile forces due to its compact structure (Skedros *et al,* 1996), which is particularly advantageous in central regions of long bones where bending is likely. Compact bones have very few internal spaces, those that do exist are arranged in structures called osteons with their Haversian canals and central blood capillaries (Havers, 1691). Between each osteon interstitial lamellae are found as shown in figure 1.1C. Lamellar bone is made up from parallel deposits of mineralised bone, the orientation of which gives the bone a complex rotated plywood-like structure and allows the formation of a very strong tissue (Weiner *et al,* 1999).

Cancellous bone, represents around 20% of the total skeletal mass. Cancellous, otherwise known as trabecular or spongy, bone is less dense (porosity

50-90%), more elastic and has a higher turnover rate than cortical bone. This bone is arranged as a scaffold of trabeculae found within the epiphyseal space of long bones as shown in figure 1.1B. Trabecular bone is also found within bones of the skull, ribs and spine. The main function of trabecular bone is to allow bones to withstand compressive forces felt during movement. For example the force felt during weight bearing on the proximal femur is redistributed by the trabecular bone to the cortical bone of the diaphysis thus minimising fracture risk (Sommerfeldt and Rubin, 2001).

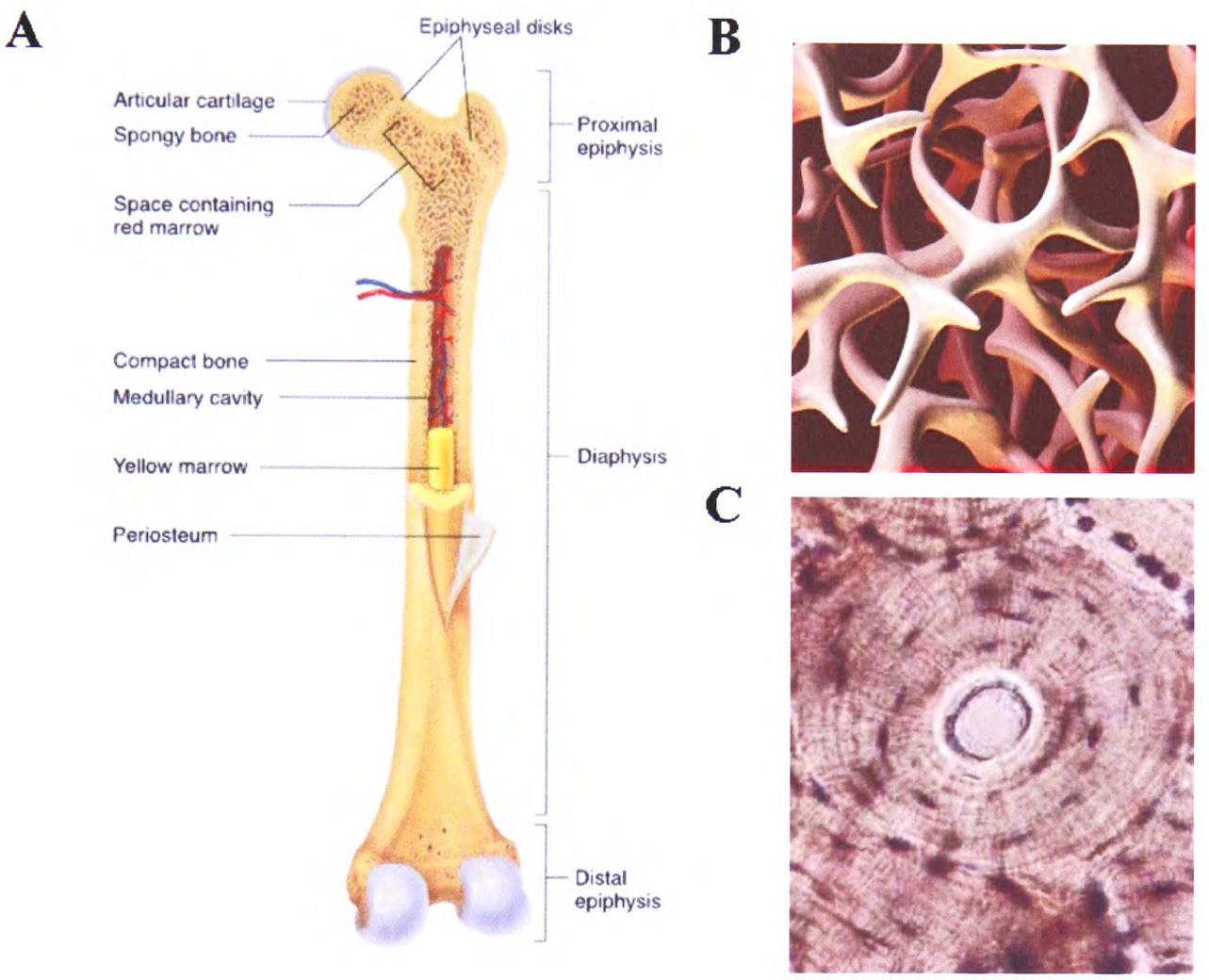

Figure 1.1 Structure and components of long bone. (**A**) The medullary cavity is shown which houses the bone marrow. In addition the spongy or trabecular bone is shown (within the epiphysis) (www.sirinet.net/~jgjohnso/skeletonorg.html). A 3D representation of structure and organisation of trabecular bone is shown in (**B**). Note the organisation of the trabeculae to allow the resistance of compressive forces by filling the epiphyseal space (www.gcarlson.com/anatomical_trabecularbone.htm). (**C**) Structure of compact bone found at the diaphyseal region of long bones. Note the unporous nature of this bone type when compared to trabecular bone with laminar sheets making up the plywood like structure. The central region is the osteon with a central Haversian canal and blood capillary (www.histology-world.com/audioslides/bone.htm).

As stated previously mineralised bone is characterised by vast amounts of hydroxyapatite (calcium phosphate) $Ca_{10}(PO_4)_6(OH)_2$, formed as a result of calcium and inorganic phosphate (Pi) precipitation. This mineral forms around 70% of the total bone mass and the majority of the inorganic content. The mineral crystals are deposited along, and in close relation to bone collagen fibrils. A balanced diet is essential for a healthy skeleton as calcium and phosphate are derived from nutritional sources, however phosphate can also be produced through the actions of enzymes such as alkaline phosphatase. Vitamin D metabolites and parathyroid hormone (PTH) are key mediators of calcium regulation, and lack of the former or excess of the latter leads to bone mineral depletion.

1.3 Bone Cells

Bone contains three main cell types osteoblasts, osteoclasts and osteocytes. Osteocytes are terminally differentiated osteoblasts, which are immobilised within mature bone. Osteoblasts are responsible for bone formation and osteoclasts for bone resorption thus these two cell types function in a synchronised manner to regulate bone turnover.

1.3.1 Osteoblasts

Osteoblasts are derived from multipotent mesenchymal stem cells (stromal stem cells) found in the bone marrow and have been described as complex fibroblasts, other cell types that can descend from this stem cell include chondrocytes (cartilage cells) and adipocytes (fat cells) (Ducy *et al,* 2000; Aubin *et al,* 2002). Morphologically osteoblasts are cuboidal in shape and are found very close to the

bone surface and along with their precursors form a very tight layer of cells. The gene expression profile of the osteoblast is very similar to that of a fibroblast with very few bone specific transcripts being produced. The main difference in cell function is that osteoblasts have the ability to form an extracellular matrix (osteoid) which they can subsequently mineralise (Ducy *et al,* 2000). The un-mineralised matrix is formed mainly from collagen type 1 (approximately 94%) which is laid down early in bone formation, with the remainder being taken up with embedded proteins such as osteocalcin, osteonectin, osteopontin and bone sialoprotein (Sommerfeldt and Rubin, 2001). This stage of matrix production is under strict control of growth factors such as fibroblast growth factor (FGF) and insulin like growth factor (IGF). IGF-I and IGF-II can stimulate the production of type I collagen and decrease its degradation though the inhibition of collagenase expression (McCarthy *et al*, 1989). FGF functions in a complex manner, signalling through the FGF receptor can cause inhibition of matrix development through the down regulation of collagen type I expression and also stimulation of osteoblastic precursors (Hurley and Florkiewicz, 1996). It was originally thought that the osteoblast specific transcripts were restricted to Runx2, which is a gene transcription factor and osteocalcin, which is a secreted protein with the ability to inhibit osteoblastic function (Ducy *et al,* 1996, 1997), however more recently several other osteoblast specific genes including osterix have been described.

Runx2, otherwise known as osteoblast specific factor-2 (OSF2) or core binding factor alpha1 (Cbfa1), has the characteristics of a differentiation factor, which functions by pushing the cell from a mesenchymal stem cell to one with an osteoblast phenotype. During embryonic development Runx2 expression is limited to

cells which are intended to become osteoblasts (Ducy *et al,* 1997). In addition, the expression of this transcription factor *in vivo* inhibits the differentiation of mesenchymal cells into either adipocytes or chondrocytes (Komori, 2006). The Runx proteins are homologues of Drosophila gene products known as Runt (Gergen and Wieschaus 1985), with particularly high identity within their 128 amino acid DNA binding domain motif known as the Runt domain (Kagoshima *et al,* 1993). In addition, a C-terminal proline-serine-threonine-rich (PST) domain is present within all Runt proteins and is thought to act as the transcription activation domain (Thirunavukkarasu *et al,* 1998). This protein only binds to DNA in its monomeric form, which differs from other members of the Runt family. This is directly due to an extra domain known as the AD2 or QA domain. In total three novel domains are present in the Runx protein compared with other members of the family thus perhaps accounting for its osteoblast specific functions (Thirunavukkarasu *et al,* 1998). Runx2 knockout mice (*Runx*$^{-/-}$) display no bone formation (either endochondral or intramembranous) due to the lack of differentiated osteoblasts (Komori *et al*, 1997).

Osterix is another osteoblast specific transcription factor which belongs to the SP family and contains three zinc finger, DNA binding domains. Studies on this protein using a knockout mouse model revealed that *Osterix*$^{-/-}$ animals had no osteoblasts thus identifying its function as a key transcription factor in osteoblast differentiation (Nakashima *et al*, 2002). It is known that osterix activates gene transcription downstream of Runx2 as Runx2 is expressed in mesenchymal stem cells of *Osterix*$^{-/-}$ mice but osterix is not expressed in these cells of *Runx2*$^{-/-}$ mice. Overexpression of osterix in mesenchymal stem cells causes an increase in cellular

proliferation, alkaline phosphatase activity, and ability to form bone nodules further indicating its importance in osteoblast differentiation (Tu *et al*, 2006).

A further signalling pathway which directs differentiation into an osteoblast phenotype is the canonical Wnt signalling pathway. This pathway is involved in the differentiation of mesenchymal stem cells into the cells of the skeletal system, stimulation of which is a positive regulator of osteoblastic differentiation. This pathway induces cellular differentiation and a post mitotic state by increasing the intracellular level of non-phosphorylated (stable) β-catenin through the inhibition of glycogen synthase kinase 3 β (GSK3 β) thus promoting the transcription of cell specific genes. A natural inhibitor of this pathway Dickkopf -1 (Dkk1), inhibits the differentiation of mesenchymal cells into specific cell types by the down regulation of nuclear β-catenin and thus gene transcription and also cytoskeletal β-catenin inhibiting the formation of adherens junctions, which is a key regulator of mesenchymal stem cell differentiation (Gregory *et al*, 2003).

The Wnt pathway as shown in figure 1.2 functions through the binding of the Wnt ligand to a receptor complex consisting of the transmembrane protein frizzled (Frz) and lipoprotein-related protein 5 and 6 (LRP-5/6). Stimulation of Frz induces the recruitment of the cytoplasmic bridging molecule, disheveled (Dsh), which acts to inhibit glycogen synthetase kinase 3β (GSK3β). The function of GSK3β is to phosphorylate β-catenin which induces its degradation through the ubiquitin mediated pathway, inhibition of which causes an increase in intracellular β-catenin which acts in the nucleus causing the activation of the lymphoid enhancer factor (LEF)/TCF family of DNA-binding proteins resulting in LEF/TCF-mediated transcription (Huelsken and Birchmeier, 2001). This pathway is inhibited naturally

through the binding of Dkk1 to the LRP-5/6 thus antagonising the action of the Wnt ligand. Simulation of the Wnt pathway through GSK3β inhibition results in the upregulation of bone specific transcripts such as osteopontin, collagen type I and V, osteocalcin, alkaline phosphatase and Runx2 (Kulkarni *et al*, 2006). In addition to this mesenchymal stem cells from *β-catenin*$^{-/-}$ mice maintain their ability to differentiate into chondrocytes, indicating that this pathway is essential for osteoblastic differentiation but not to all cell types of the mesenchymal lineage (Hill *et al,* 2005). Runx2 and not osterix is expressed in *β-catenin*$^{-/-}$ mice suggesting that β-catenin functions on an osteoblast progenitor cell during mesenchymal differentiation. Thus Runx2 directs mesenchymal stem cells to a preosteoblast phenotype and osterix and β-catenin function to promote differentiation into an immature osteoblast (Komori, 2006).

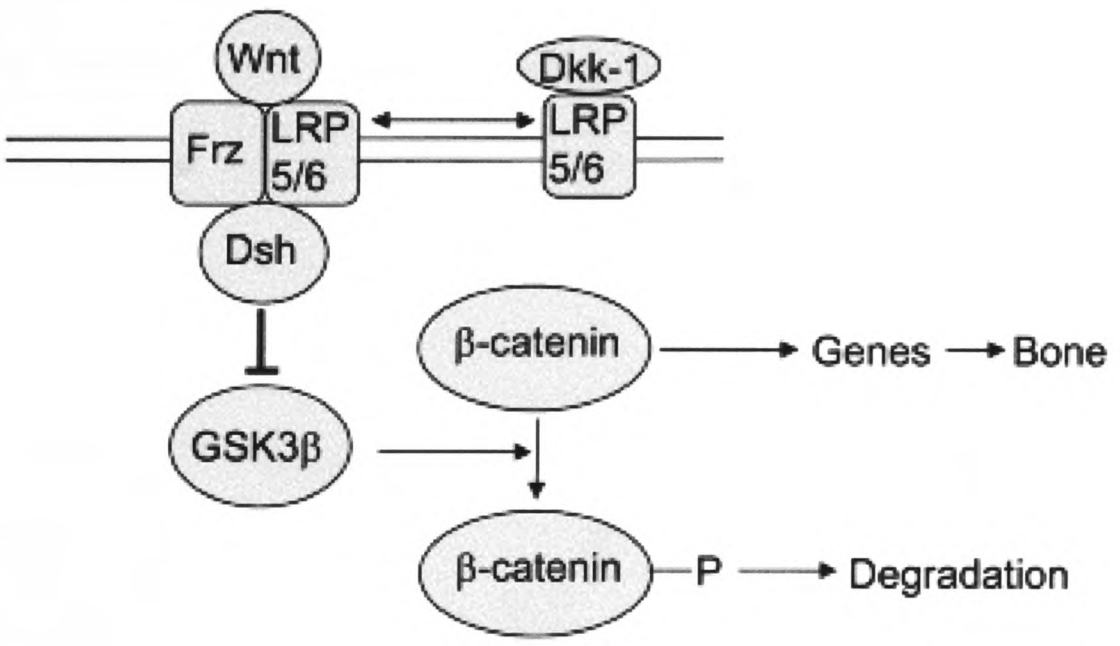

Figure 1.2 Major components of the canonical Wnt pathway. Stimulation of the pathway causes the inhibition of GSK3β thus resulting in an increase of un-phosphorylated (stable) β-catenin which results in gene transcription. The inhibitor Dkk1 inhibits this pathway causing GSK3β to phosphorylate β-catenin thus targeting it for ubiquitin mediated degradation (Gregory *et al*, 2003).

1.3.2 Osteoclasts

Osteoclasts are multi-nucleated cells, derived from haematopoietic stem cells, which resorb mineralised bone at sites known as Howships lacunae (Sommerfeldt and Rubin, 2001). This is an essential process (pathway shown in figure 1.3) as it allows bone repair as well as allowing sequestration of calcium into the blood to maintain ion homeostasis. Bone modelling and re-modelling is a crucial event in skeletal development and repair which is strictly controlled by osteoclasts. Defects in these processes lead to diseases such as hypercalcemia of malignancy and postmenopausal osteoporosis where an increase in bone resorption is the main pathological episode (Vaananen *et al,* 2000). Osteoclasts are closely related to macrophages and dendritic cells with only the final stage of differentiation altering for each cell type. This differentiation is dependent on whether the cell is stimulated by exposure to a particular receptor activator of NF-kB ligand i.e. osteoclast differentiation factor, macrophage colony-stimulating factor (M-CSF) or granulocyte-macrophage colony-stimulating factor (GMCSF) (Vaananen *et al,* 2000).

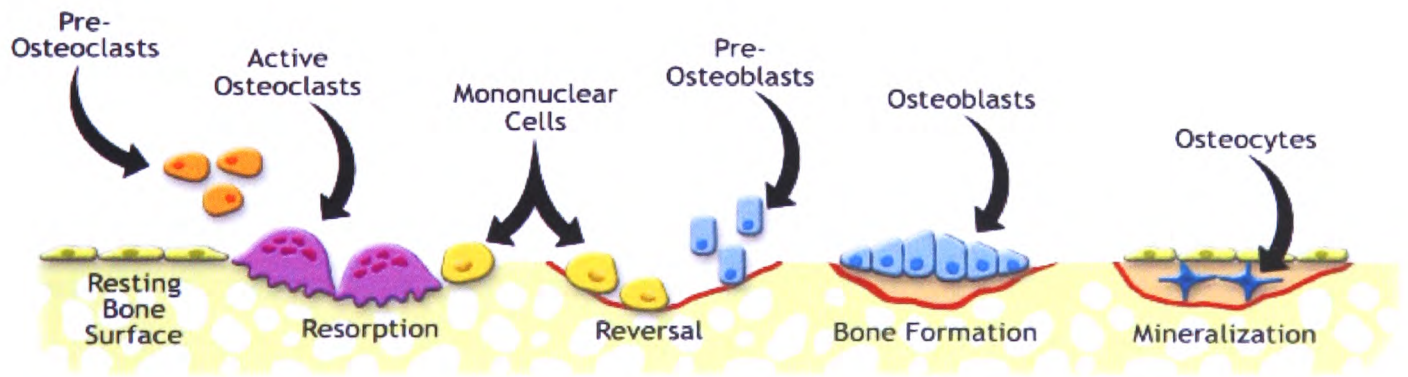

Figure 1.3 The bone remodelling cycle showing the interplay between all the major cell types. Osteoclasts create a cavity at the remodelling site through the secretion of enzymes and acids, osteoblasts are then recruited to this site where they lay down a matrix which is subsequently mineralised. Osteocytes are embedded in the bone and are thought to be involved in mechano-sensing (http://www.umich.edu/news/Releases/2005/Feb05/bone.html).

The osteoclast can degrade both the inorganic and the organic components of bone matrix. To initiate resorption of bone the osteoclast is firstly recruited to the site of damage by cytokines such as M-CSF and vascular endothelial growth factor (VEGF) (Niida, 1999). Following recruitment, the osteoclast attaches to the resorption site through a membrane domain called the sealing zone (Vaananen *et al,* 2000). It has been hypothesised that integrins play a vital role in this stage of the resorption, with at least four being expressed in osteoclasts (αvβ3, αvβ5, α2β1, αvβ1) (Nesbitt *et al,* 1993). It is unclear how these integrins help coordinate bone resorption however it is thought that they may bind to collagen type I and also matrix proteins such as osteopontin (OPN) (Horton *et al,* 1995; Helfrich *et al,* 1996). Adhesion to the bone surface causes the osteoclast to become polarised and form specific membrane domains known as the ruffled border, a secretory domain and a basolateral membrane. The ruffled border is formed by the fusion of intracellular lysosomal vesicles with the membrane region in contact with the bone. This initiates the secretion of hydrochloric acid by the vacuolar H^+-ATPase (proton pump), along with this acid proteases are also secreted. At this stage the plasma membrane in contact with the matrix becomes convoluted due to an increase in membrane surface area thus giving it a ruffled appearance (Mulari *et al,* 2003). Secreted enzymes, such as matrix metalloproteases and tartrate resistant acid phosphatase (TRAP), cause the breakdown of the extracellular matrix thus allowing the release of hydroxyapatite crystal, which is subsequently dissolved due to the high pH of the secreted acid. The digested bone matrix is phagocytosed and degradation products such as the collagen fragments, along with TRAP, are then passed through the secretory domain in the basolateral membrane. Thus, the amount of TRAP released into the circulation

should reflect the rate of bone resorption and is hence used as a diagnostic marker of bone resorption (Mostov and Werb, 1997; Halleen and Ranta, 2001).

1.4 Cartilage

Cartilage is a tough, elastic and flexible connective tissue which has many pre and postnatal functions and is found in the body in three main types. Hyaline, or articular cartilage, functions to disperse forces on joints caused by movement, acts as a template for long bone growth, and is involved in the repair of fractured bones (Shum and Nuckolls, 2001). Within this type of cartilage, chondrocytes (cartilage cells) are embedded in a matrix, composed mainly of collagen type II and proteoglycans. A second type, elastic cartilage gives support to external structures, and is composed of chondrocytes embedded in a matrix of collagen and elastic fibres. Fibrocartilage aids in transferring loads between tendons and bone. It consists of an outer layer of collagen and fibroblasts that provide support and an inner layer of chondrocytes that synthesise type II collagen fibres. Surrounding all cartilage, bar hyaline cartilage in joints, is a dense layer of fibrous connective tissue, known as the perichondrium, which is closely involved with the ability of the chondrocytes to produce the aforementioned matrix (Colnot *et al,* 2004).

1.4.1 Chondrocytes

Chondrocytes are derived from the same progenitor cells as osteoblasts and, in many manners, function very similarly. Terminal differentiation of chondrocytes gives rise to the three different types of cartilage, as discussed earlier. The actual phenotype of the cartilage is very much under the control of various transcription

factors, DNA binding proteins and adhesion molecules (Shum and Nuckolls, 2001). Sox9 is a transcription factor, which is expressed in prechondrocytic, and chondrocytic cells during embryonic development. Interestingly its expression mirrors that of collagen type II indicating a possible involvement in chondrocyte development. Indeed cells lacking Sox9 fail to differentiate to a chondrocyte phenotype due to decreased activation of COL2A1 (collagen type II gene), which is an important element of differentiation (Lefebvre *et al,* 1997). This results in campomelic dischondroplasia through decreased production of collagen type II. Mesenchymal cells from *Sox9*$^{-/-}$ knockout mice cannot differentiate into chondrocytes and cartilage cannot be formed from teratomas derived from *Sox9*$^{-/-}$ embryonic stem (ES) cells. (Bi *et al,* 1999). In addition to this when Sox9 is inactivated following mesenchymal condensations during embryonic development the phenotype displayed was that of chrondodysplaysia with a severe decrease in differentiated chondrocytes (Akiyama *et al*, 2002). Sox9 is a critical transcriptional regulator of chondrocyte differentiation and in essence functions as Runx2 in osteoblasts. Additional transcription factors such as Runx2 and c-fos also seem to be involved in chondrogenesis. Runx2 although involved in osteogenesis also has a significant role in chondrogenesis with knockout mice showing over expression of type II and IX collagens, aggrecan (a proteoglycan involved in cartilage shock resistance), and chondromodulin (Inada *et al,* 1999). Interestingly *Runx2*$^{-/-}$ mice show no ossification due to the maturational arrest of osteoblasts (Komori *et al,* 1997) however chondrocytes are found indicating perhaps a more crucial role in osteoblast generation (Inada *et al,* 1999). It has however been reported that Runx2 might function synergistically with Runx3 as *Runx2*$^{-/-}$*3*$^{-/-}$ mice showed a complete

absence of chondrocyte maturation (Yoshida *et al*, 2004). C-fos is a proto-oncogene, which interferes with proteoglycan synthesis in chondrocytes and inhibits the production of an extracellular matrix and chondrocyte differentiation (Tsuji *et al,* 1996).

The chondrocytes of most importance, with regard to bone growth, are those of the growth plate, which are involved in the manufacture of a template for endochondral ossification. Within the growth plate, chondrocytes go through various stages of proliferation and differentiation, which is accompanied by a hypertrophic phenotype (increased cellular volume) (Beier *et al,* 1999). This is strictly controlled by growth factors and hormones, shown through the knockout of receptors for parathyroid hormone/parathyroid hormone-related peptide receptor (Lanske *et al,* 1996), FGF receptor 3 (Deng *et al,* 1996), transforming growth factor β (TGF-β) (Serra *et al,* 1997) and many more, all of which cause defects in bone growth. Bone morphogenic proteins, retinoic acid and steroids are also involved in the function of the growth plate. Bone morphogenic proteins are extracellular ligands which are members of the TGF-β super-family and can induce both bone and cartilage formation by signalling through serine threonine kinase receptors (Miyazono *et al,* 2000). Initial investigations on these factors noted their propensity to induce bone formation when injected subcutaneously in mice (Urist *et al*, 1965). During mesenchymal stem cell differentiation the BMP receptor antagonist, Noggin, inhibits the formation of precartilaginous condensations, the stage preceding cellular differentiation (Pizette and Niswander, 2000) and mutations in the BMP5 gene cause condensations to be abnormal or absent in short ear mice (Kingsley *et al,* 1992).

1.5 Bone Growth

Bones can grow by two distinct mechanisms; flat bones of the skull grow by intramembranous ossification while all long bones grow by endrochondral ossification. Endochondral ossification is the process whereby a mineralised cartilage template (growth plate), produced by chondrocytes is resorbed by osteoclasts and replaced with bone from osteoblasts. The growth plate is located between the epiphysis and diaphysis and is the centre for bone growth. As mentioned before, chondrocytes at varying stages of proliferation and differentiation are located in this region, with several distinct zones consisting of resting, proliferating and terminally differentiated hypertrophic cells, as shown in figure 1.4. These zones are arranged in columns with resting at one end and hypertrophic at the other in parallel to the direction of bone growth, separated by longitudinal and transverse septa consisting of collagen and proteoglycans (Farquharson, 2003). As the chondrocytes become hypertrophic and increase their size they begin to produce type X collagen and cease to produce collagen type II (Kronenberg, 2003). A further marker of chondrocyte differentiation is the expression of alkaline phosphatase, which is characteristic of cells within the hypertrophic zone (Matsuzawa and Anderson, 1971). Chondrocytes which reach this terminally differentiated state mineralise the surrounding matrix before progressing to programmed cell death or apoptosis.

Following growth plate matrix mineralisation blood vessels from the bone marrow invade the hypertrophic region; these are attracted to this site through the production of vascular endothelial growth factor by chondrocytes (Kronenberg, 2003). These vessels bring with them osteoclasts which results in compete resorption of the transverse septa along with the terminally differentiated chondrocytes and

approximately half of the longitudinal septa. This forms a scaffold for bone formation, with osteoblasts laying down an un-mineralised matrix (osteoid) consisting of collagen type I and matrix proteins such as osteocalcin. This matrix is mineralised forming a network of immature trabeculae termed the primary spongiosa which is eventually replaced with secondary spongiosa before being converted into primary cortical bone by filling of spaces between the trabeculae (Howell and Dean, 1992). This ultimately leads to the longitudinal growth of the bone. The growth plate exists as this dynamic structure of constant bone formation (distal femur in humans extends by 0.04mm/day; Farquharson, 2003) from the cartilage template until adolescence, at which time it is resorbed following a sharp increase in growth (Kronenberg, 2003).

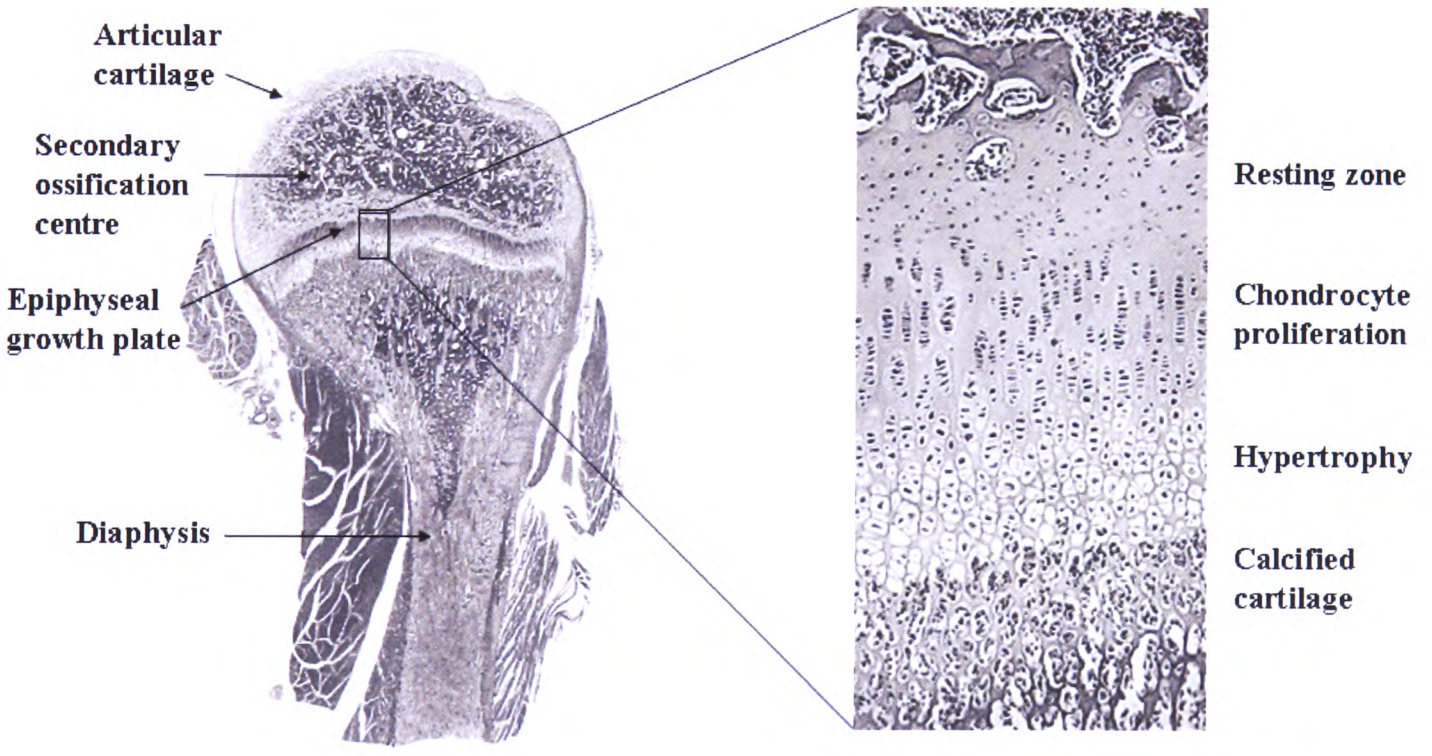

Figure 1.4 Schematic diagram showing the position of the growth plate at end of the long bone contained within the epiphysis. Chondrocytes within this region go through stages of differentiation resulting in hypertrophy and calcification (www.kumc.edu/instruction/medicine/anatomy/histoweb/bone/small/Bone002s.JPG & www.bu.edu/histology/p/02401ooa.htm)

1.6 Matrix Mineralisation

1.6.1 The History of Mineralisation

The process of mineralisation or calcification was first documented by Rudolf Virchow in 1855 upon describing pathological metastatic calcification, when he concluded that "calcium salts dissolved from bone were carried in the blood and deposited at some distant site to form calcium metastases, a process analogous to the dissemination of cells from a primary neoplasm." The initial research on calcification was based on case studies from calcification disorders. This gave rise to information regarding the extracellular nature of calcification, the crystalline form of calcium phosphate and also that the extracellular Ca^{2+} and PO_4^{3-} ions are maintained by homeostasis (Pommer, 1885 – cited in Anderson, 1992; Shipley *et al,* 1926). However perhaps the most important discovery with regard to understanding the process of mineralisation was that of alkaline phosphatase in 1923 by Robert Robison this was accompanied by his theory of local phosphatase derived Pi driving cell mediated mineralisation (Robison, 1923).

However it was not until 1970-71 that the actual mechanism of mineralisation was hypothesised. At this point it was known that the initiation of mineral crystals required a local nucleator through the discovery that the extracellular fluid at the calcification front is metastable (the concentrations of Ca and PO_4 are less than that required to allow calcium phosphate precipitation) (Howell *et al,* 1968). In addition to this Irving (1963) and Wuthier (1968) demonstrated that lipids were concentrated at the mineralisation front thus hypothesising that the local nucleator should consist of lipids or have a high lipid element. In 1970-71 pioneering work by Anderson *et al*, Matsuzawa *et al* and Ali *et al* illustrated the presence of matrix vesicles (MVs) which

were shown to be membrane derived packages found at the mineralisation front and were characterised by intense phosphatase activity.

1.6.2 The Chemistry of Hydroxyapatite

Hydroxyapatite is a double salt of tricalcium phosphate and calcium hydroxide and has theoretical calcium to phosphate ratio of 1.67:1. The calcium phosphate which makes up the inorganic constituent of bone can be divided into two separate phases, the amorphous phase which consists of tricalcium phosphate and the crystalline phase which exists as hydroxyapatite. The amphorous phase is predominately found in younger immature bones and is subsequently turned into hydroxyapatite crystal, which forms around 40% of adult bone (Narasaraju and Phebe 1996).

It was originally postulated that the major mineral constituent of bone was a very small apatite, a finding from X ray diffraction by DeJong in 1926. However it was not until the crystal structure of hydroxyapatite was first resolved in 1964 by Kay *et al* that more clues on bone mineral were identified. It was found that the structure of hydroxyapatite consisted of a hexagonal arrangement of calcium and phosphate that surrounded a column of monovalent hydroxide. When these findings were compared with X ray diffraction patterns of apatite found in bones it was discovered that teeth and bone did actually contain natural hydroxyapatite (Eanes and Posner, 1970). The crystal lattice of hydroxyapatite is formed from the ions Ca^{2+}, PO_4^{3-}, and OH^- with their arrangement in the unit cell reflecting two phases which are a mirror image of each other, with each cell measuring 9.432 A by 6.881 A (Posner *et al,* 1958). The needle like crystals of hydroxyapatite reach a length of up

to 300 Å in bone tissue (Durning, 1958). The crystalline structure of hydroxyapatite lends itself to isomorphous substitution, where an ion can be replaced within the structure without disrupting the structure itself (Narasaraju and Phebe 1996). These substitutions include the replacement of OH^- with F^- (Narasaraja, 1972), and can provide an explanation of the integration of carbonate ions in both bones and teeth.

1.6.3 The Mineralisation Process

1.6.3.1 The Role of Matrix Vesicles (MVs)

Matrix mineralisation is a controlled process exhibited by both osteoblasts and mineralising chondrocytes of the growth plate. It is widely regarded that the initial stages of mineral formation occurs within the previously described packages known as MVs. MVs bud from distinct areas of the membrane on the surface of all mineralising cells, these areas usually lie adjacent to the matrix which will be mineralised. The region of the hypertrophic chondrocyte that the MVs bleb from is the lateral membrane that lies adjacent to the longitudinal septal matrix. Developing bone MVs are restricted to the freshly formed osteoid that is located at the basal plasma membrane of mineralising osteoblasts (Morris *et al*, 1992). Inside the MV lumen, calcium phosphate accumulates within the matrix vesicle sap until sufficient amounts are present for precipitation to occur. This is then converted to an intermediate, octa-calcium phosphate, crystals of which are transformed into the less soluble hydroxyapatite (Sauer and Wuthier, 1988). The first hydroxyapatite crystals are visible by EM and are often found closely aligned to the MVs trilaminar membrane as seen in figure 1.5 (Anderson, 1995). Calcium accumulation is controlled by Ca^{2+}-binding molecules such as annexin I and phosphatidylserine (Wu

et al, 1995; Anderson, 2003). Pi accumulation is associated with the action of alkaline and acid phosphatases (Wu *et al,* 1995; Anderson 2003). The most abundant of these being tissue non-specific alkaline phosphatase (TNAP), an isoenzyme of alkaline phosphatase expressed in bone, liver and kidney (Anderson, 1996). It is thought that the mineralisation process is divided into two phases; phase one concerns the intravesicular precipitation of calcium phosphate and the initial production of hydroxyapatite crystals. This phase is predominantly regulated by enzymes and the membrane embedded proteins such as annexin. Phase two occurs when the crystal grows to an extent that it pierces the vesicle membrane, causing it to collapse, allowing the egress of mineral into the extracellular space. This mineral serves as a template for the epitaxial proliferation of the HA crystal (Anderson, 1995). The crystal, at this point, proliferates radially around the edge of the matrix vesicle to form a sphere or spherule of hydroxyapatite, these continue to grow until they fuse forming a mineralisation front. The rate of mineral growth at this stage is dependent upon the ionic conditions of the extracellular fluid (Ca^{2+} and Pi), the pH and also presence of inhibitory molecules such as inorganic pyrophosphate (PPi), anionic proteoglycans and calcium binding noncollagenous proteins (Bohn *et al*, 1984; Dziewiatkowski and Majznerski, 1985; Campo and Romano, 1986). Three molecules present in osteoblasts have so far been identified as affecting the controlled deposition of bone mineral by regulating the extracellular levels of PP_i i.e., tissue-non-specific alkaline phosphatase (TNAP); NPP1 (a nucleotide pyrophosphatase/phosphodiesterase isozyme) and the ANK gene product (which forms a PPi channel on the surface of mineralising cells). Hydroxyapatite crystals form structures around the triple helix of the collagen fibril, which has been

described as a "rotating plywood structure" by Anderson (1995) and has been attributed to the reason why mineralised bone matrix has both hard and flexible properties.

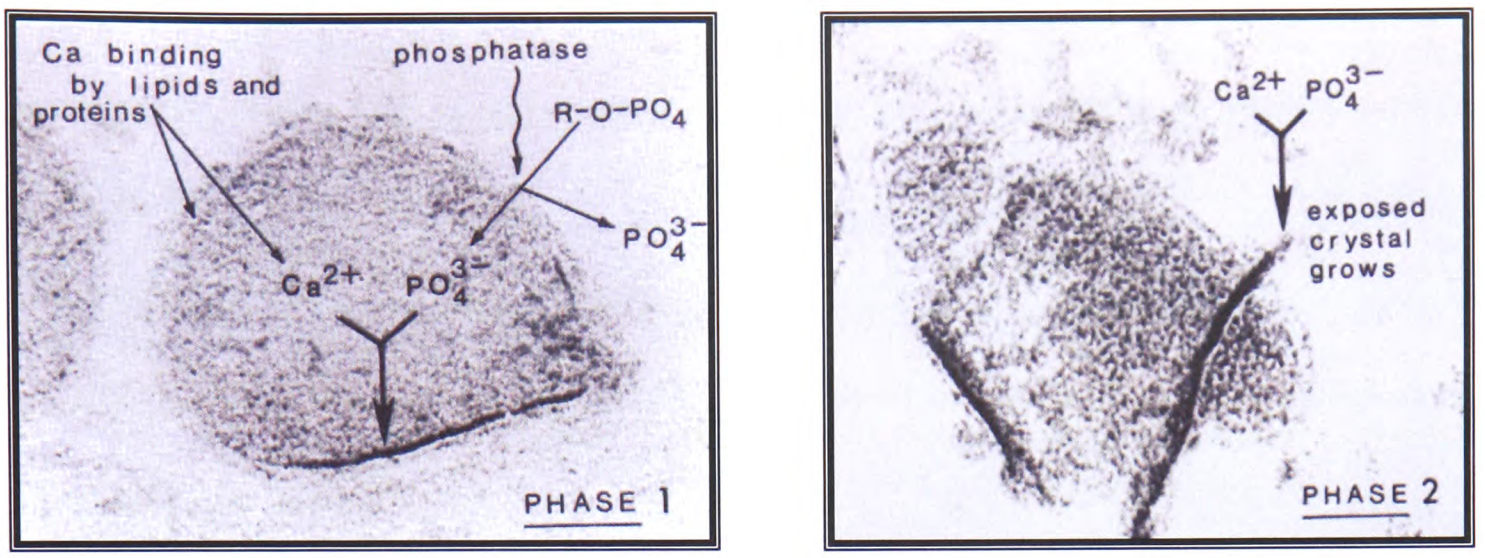

Figure 1.5 Electron micrographs showing the process of mineral formation. Note the two phases; phase 1 is very much enzymatically controlled, whereas phase 2 is more a biochemical reaction (Anderson, 1995).

1.6.3.2 Apoptosis and Apoptotic Bodies

Following growth plate cartilage mineralisation hypertrophic chondrocytes undergo programmed cell death, or apoptosis, leaving behind a mineralised cartilage-bone template. During the process of chondrocytic apoptosis the cell phenotype and morphology undergoes rapid change beginning with DNA fragmentation, nuclear alterations and chromatin condensations. This progresses to the loss of membrane stability which is preceded by the exteriorisation of phosphatidylserine, resulting in the release of phospholipid membrane fragments (Kirsch *et al*, 2003). These membrane fragments progress to form apoptotic bodies which characterise the end point of cellular death (Zhang *et al,* 1998). This chondrocyte apoptotic process also occurs in articular chondrocytes, which do not normally adopt a hypertrophic phenotype, as found in osteoarthritic cartilage. Interestingly these areas are

characterised by pathological mineralisation leading to the theory that apoptosis is an important step in the mineralisation process (Hashimoto *et al,* 1998). In addition, apoptotic bodies can be induced to mineralise *in vitro* though a similar mechanism to MVs (Proudfoot *et al,* 2000), this initially led to the hypothesis that MVs were closely related to apoptotic bodies and perhaps apoptosis mediated matrix vesicle release. This is however not the case as matrix vesicle production precedes the apoptotic process and mineralisation of the growth plate cartilage occurs in a wider region than that of apoptosis (Kirsch *et al*, 2003). Also several structural differences exist between MVs and apoptotic bodies including, particle size (MVs are bigger, as shown in figure 1.6), however perhaps more importantly MVs contain all of the necessary machinery to create an environment conducive to mineralisation (alkaline phosphatase activity and annexins) whereas apoptotic bodies do not (Kirsch *et al*, 2003). It is more likely therefore that mineralisation can occur upon apoptotic bodies due to the capture of calcium during the exteriorisation of phosphatidylserine, this is in concordance with the findings that detergent treatment of apoptotic bodies causes inhibition of calcium uptake through membrane solubilisation (Proudfoot *et al*, 2000), however an identical treatment of MVs only serves to release the mineral from the lumen where it can continue to grow as per phase 2 of crystal growth (Kirsch *et al*, 1994). These findings indicate that mineral is produced on the outer membrane of apoptotic bodies whereas it is produced in the lumen of MVs (Anderson, 1995). It is not clear what the precise function of these apoptotic bodies are in growth plate cartilage as mineralisation of this area is mediated before apoptosis occurs, through the production of MVs. At the point of apoptosis a vascular network is present thus it is possible these bodies will be phagocytosed

along with cellular debris by macrophages. However in areas where vascularisation is not present, such as articular cartilage, it is possible that this mechanism mediates pathological calcification (Kirsch *et al*, 1994).

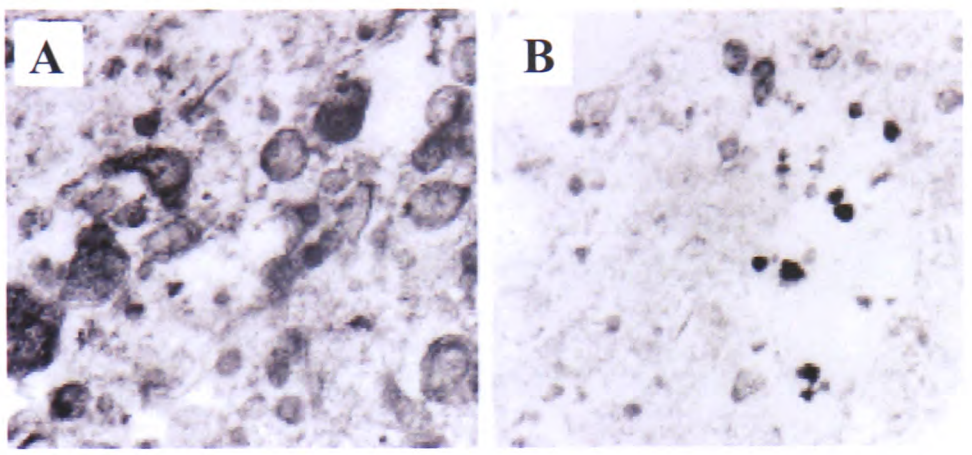

Figure 1.6 Comparison of MVs and apoptotic bodies by electron microscopy. From (**A**) Chondrocytes induced to release MVs by the addition of retinoic acid and (**B**) apoptotic chondrocytes. MVs from A measure approximately 200 to 500 mM whereas the apoptotic bodies from C were approximately 100 to 200nM (Adapted from Kirsch *et al*, 2003).

1.6.4 Regulatory Factors of Matrix Mineralisation

1.6.4.1 Tissue Non-Specific Alkaline Phosphatase

TNAP, an isoenzyme of alkaline phosphatise, is the only tissue-nonrestricted isozyme of a family of four homologous alkaline phosphatase genes (EC 3.1.3.1). TNAP is a dimeric ecto-enzyme which is attached to the cell membrane via a glycosylphosphatidylinisotol anchor (GPI) and also to collagen through a crown region (shown in figure 1.7) and has been has been shown to play a pivotal role in matrix mineralisation. This is clear as deficiency in this enzyme leads to hypomineralisation (hypophosphatasia), manifesting itself as rickets in children and osteomalacia in adults (Anderson *et al,* 2004). The severity of hypophosphatasia is variable and modulated by the nature of the TNAP mutation (Henthorn *et al*, 1992; Shibata *et al*, 1998; Zurutuza *et al*, 1999). Unlike common types of rickets and

osteomalacia the serum levels of calcium and Pi are not subnormal in hypophosphatasia. The clinical severity in hypophosphatasia patients varies widely. The different syndromes, listed from the most severe to the mildest forms, are: perinatal hypophosphatasia, infantile hypophosphatasia, childhood hypophosphatasia, adult hypophosphatasia, odontohypophosphatasia and pseudohypophosphatasia (Whyte, 1995). The symptoms of these diseases range from complete absence of a mineralised skeleton and stillbirth to spontaneous fractures and premature loss of teeth in adult life. Inactivation of the mouse TNAP gene mimics the infantile form of human hypophosphatasia (Narisawa *et al*, 1997; Fedde *et al*, 1999).

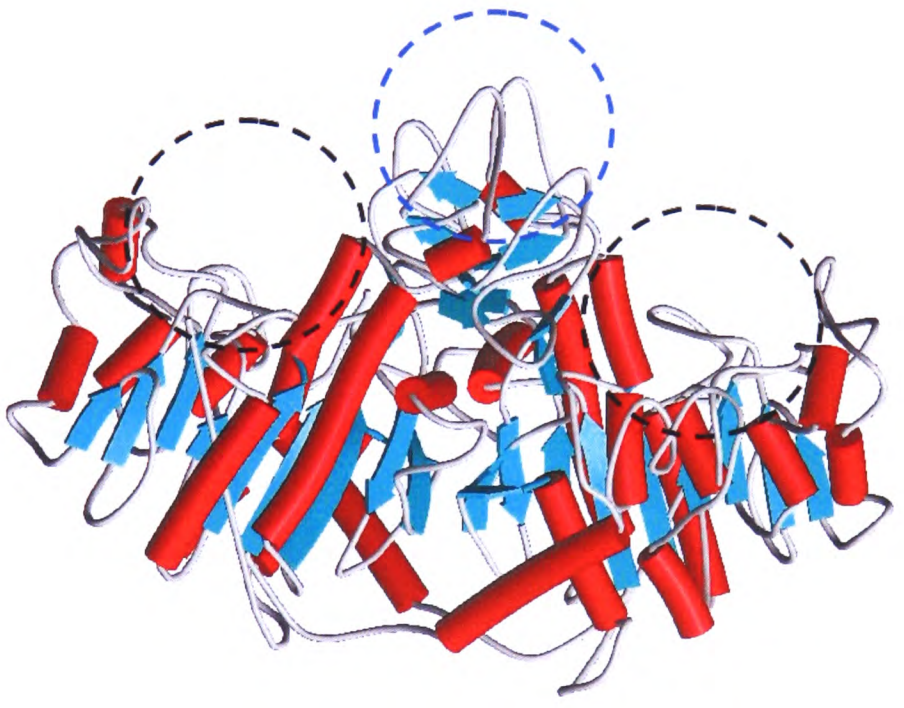

Figure 1.7 Structural model of human TNAP. The model is based on the crystal structure of human placental alkaline phosphatase (shares 74% identity). Black circles depict the active sites of the enzyme and the blue circle depicts the 'crown' or collagen binding domain (Mornet *et al,* 2001).

As seen in figure 1.8A TNAP is localised on the outer membrane of hypertrophic chondrocytes and MVs. It is also found on the surface of mineralising osteoblasts and MVs derived from this cell type. TNAP is more concentrated on the surface of MVs compared to their parent cells, the mechanism by which this occurs, however is unknown. It has been advocated that the role of TNAP in bone formation is to generate the Pi needed to facilitate calcium phosphate precipitation and therefore hydroxyapatite deposition, however this is not the whole story regarding TNAP function (Robison, 1923; Majeska and Wuthier, 1975). Perhaps the most important role that TNAP plays in mineralisation is by hydrolysing PPi, its natural substrate since PPi is a potent inhibitor of hydroxyapatite crystal formation, elimination of the molecule from mineralising sites is critical to the mineralisation process. This has in part been proven by examination of TNAP knockout mice where hypomineralisation of the skeleton is evident. Electron microscopic analysis of MVs from TNAP-deficient mice, demonstrate that crystals of calcium phosphate are present within the vesicle lumen (as shown in figures 1.8B and C), however extravesicular crystal propagation is retarded (Anderson *et al*, 1997; 2004). Indeed it has recently been hypothesised that the actual function of TNAP is to decrease the PPi/Pi ratio thus forming an environment conductive for hydroxyapatite deposition. This hypothesis has been formed due to the finding that TNAP knockout mice have an abnormally high bone PPi concentration whereas the Pi concentration remains constant (Harmey *et al,* 2004). It has previously been hypothesised that TNAP can also function as a Pi transporter (Farley *et al,* 1980) due to its apparent affinity for free phosphate however more recently the specific Pi transporters Pit-1 and Pit-2

have been attributed to Pi handling in osteogenic cells (Montessuit *et al,* 1991; Palmer *et al,* 1997).

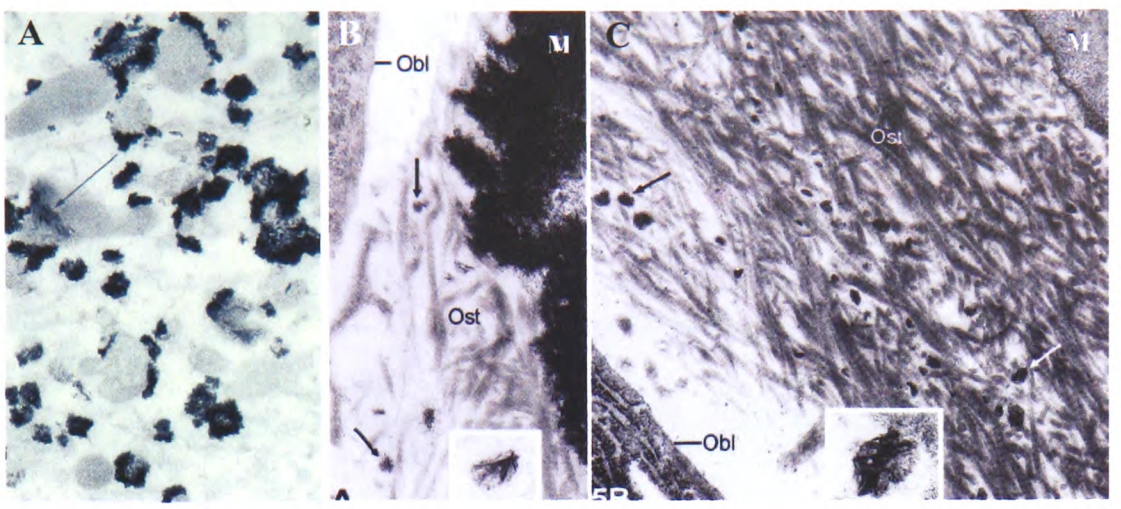

Figure 1.8 (**A**) MVs of hypertrophic growth plate chondrocytes, which have been stained for alkaline phosphatase. Black colouration denotes areas of alkaline phosphatase activity (Anderson, 1995). Analysis of uncalcified osteoid layers from wildtype mice (**B**) and osteoid layer in TNAP-deficient tibial metaphyseal bone (**C**). MVs are visible (indicated by **arrows** and shown at higher magnification in inserts) in both bone sections. Note both contain apatite like needles M, mineralized bone matrix; Obl, osteoblast; Ost, osteoid. (Anderson *et al*, 2004)

1.6.4.2 Clues from NPP1 and Ank

Further studies with NPP1 and TNAP double knockout animals provides insights into TNAP function. NPP1 or PC1 (plasma cell membrane glycoprotein 1) as it is alternatively known is a membrane protein that acts as a phosphodiesterase (pyrophosphatase) and is an isozyme of the NPP family of pyrophosphatases (Oda *et al*, 1991). Two other members, autotoxin (NPP2) is secreted and B10 (NPP3) is found within intracellular compartments, with all three being found within mineralising tissues (Bachner *et al*, 1999; Bollen *et al*, 2000). NPP1 has a large extracellular domain that contains the catalytic site and one or possibly two calcium-binding motifs (Belli *et al*, 1994). The main function of this enzyme is to cleave nucleotide tri phosphates (NTP's) to produce pyrophosphate (most commonly CTP to CMP and PPi) thus functioning to increase both intra and extracellular

concentrations of PPi. NPPs have been implicated in several cellular pathways including bone mineralisation, cell signalling by insulin and nucleotides and cell differentiation and motility (Bollen *et al*, 2000). NPP1 localisation mirrors that of TNAP, with high concentrations being found on the surface of osteoblasts and chondrocytes as well as MVs derived from these cell types (Johnson *et al*, 1999). The main role of NPP1 seems to be its mineralisation inhibiting properties through the production of the mineralisation inhibitor PPi. This has been shown in osteoblasts engineered to over express NPP1, the result of which is an elevated intravesicular concentration of PPi accompanied by a decrease in hydroxyapatite precipitation (Johnson *et al*, 1999). NPP1 knockout mice, however are characterised by hypermineralisation defects such as mineralisation of the posterior longitudinal ligament of the spine diffuse idiopathic skeletal hyperostosis, ankylosing spinal hyperostosis and pathological soft-tissue ossification, including arterial calcification (Okawa *et al*, 1998; Sali *et al*, 2000). Conversely when NPP1 expression is elevated, MV-mediated calcium pyrophosphate dihydrate (CPPD) matrix calcification of the knee meniscal cartilage during aging is observed (Johnson *et al*, 2001; Masuda *et al*, 2001). This pathological CPPD precipitation has also been observed in association with TNAP deficiency which, as with elevated NPP1 levels is characterised by high PPi concentrations. When TNAP was knocked out alone, PPi would build up within the matrix thus inhibiting crystal formation, however when NPP1 and TNAP were knocked out in tandem a normally mineralised skeleton was seen at birth (Hessle *et al,* 2002). A schematic pathway is shown in figure 1.9. Thus these two enzymes have an antagonistic effect on each other and loss of TNAP can be corrected by knocking out NPP1 thus decreasing the production of PPi. Interestingly PPi negatively

regulates both NPP1 and ankylosis protein (ANK) which also plays a central role in PPi homeostasis through the mediation of intracellular and extracellular PPi levels.

The *ank* gene encodes a protein containing 492 amino acids with a molecular mass of 54.3 kD. The protein contains three N-linked glycosylation sites and multiple potential phosphorylation sites (Ho *et al*, 2000). ANK functions as a transmembrane PPi channel allowing intracellular PPi to traverse the membrane into the extracellular space (Nurnberg *et al*, 2001). ANK is expressed in many tissues, however its expression seems to be upregulated in osteoblasts and chondrocytes where the protein is abundant in the cellular membrane (Sohn *et al*, 2002), it is however not present upon the surface of MVs (Harmey *et al*, 2004). Mice lacking the ANK protein are characterised by pathological calcification of articular cartilage and the synovial fluid surrounding these regions (Hakim *et al*, 1984). These mice mimic severe arthritic diseases including ectopic calcification, cartilage erosion and vertebral fusion (Sampson, 1988; Johnson *et al*, 2005).

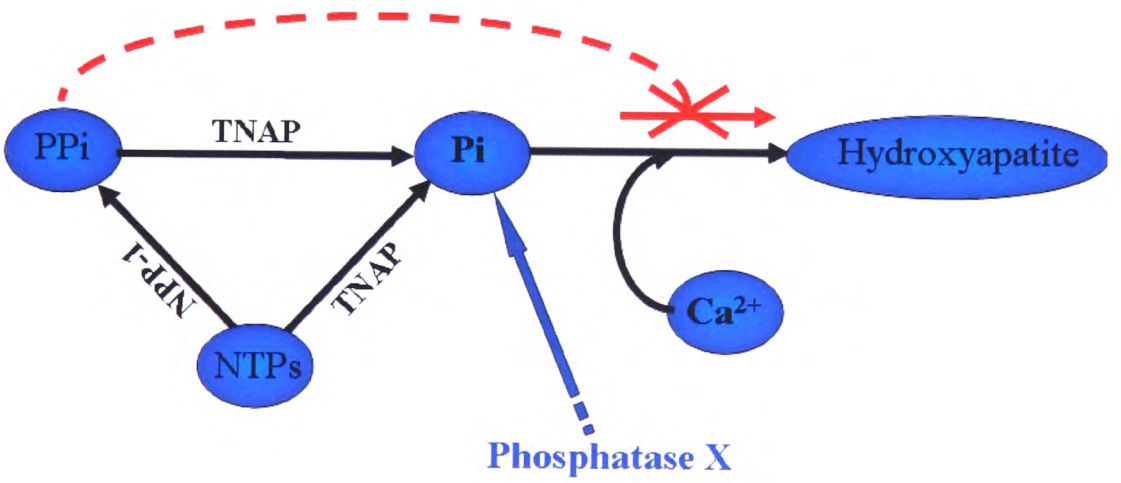

Figure 1.9 Schematic diagram showing how TNAP and NPP-1 work in tandem to allow mineralisation, however if both these enzymes are knocked out mineralisation still occurs giving rise to the potential for additional phosphatases.

An interesting finding from these studies is that the Pi to allow mineralisation of the double knockout skeleton must be produced or sourced from another location hinting that TNAP is not the only enzyme supplying Pi for mineralisation. Indeed, recently it has been suggested that other phosphatases contributing to the Pi pool are present (Anderson *et al,* 2004).

1.6.4.3 Other Phosphatases Contributing to Pi Accumulation

MVs contain many other phosphatases which have the potential to raise the intravesicular concentration of Pi to allow the initiation of mineralisation. Adenosine monophosphoesterase (AMPase) is one such phosphatase which is enriched in MVs (Ali *et al*, 1970). Interestingly it has recently been shown that adenosine monophosphate (AMP) can induce, and indeed was one of the best substrates for the deposition of calcium phosphate within isolated rat MVs (Garimella *et al*, 2004). In addition to this inorganic pyrophosphatase (PPiase) has also been shown to be concentrated within matrix vesicle preparations, this enzyme functions in a similar fashion to TNAP by hydrolysing the mineralisation inhibitor PPi (Ali *et al*, 1970). It is however not known what the relative contribution is of TNAP vs PPiase in contributing Pi for calcium phosphate precipitation. Another phosphatase known to be present within MVs is ATPases (Matsuzawa and Anderson, 1971), it has also been shown that ATP hydrolysis increases the potential for MVs to mineralise *in vitro* (Hsu and Anderson, 1996). However, much evidence to suggest that this enzyme is not responsible for the induction of mineralisation *in vivo* is present. Perhaps the most compelling of this evidence comes from the analysis of the action of matrix vesicle ATPase and its hydrolysis products. This enzyme acts as a tri phosphate pyrophosphatase, producing AMP and the mineralisation inhibitor PPi

(Hsu, 1983), and as stated previously AMP is a potent inducer of mineralisation. In addition when using ATP as a substrate for *in vitro* MV calcification the mineral formed is mostly calcium pyrophosphate dihydrate, which is of a non-crystaline nature (Derfus *et al*, 1995). This would suggest that the role of ATPases are in fact to modulate the mineralisation process through the production of PPi.

1.6.4.4 Osteopontin

Osteopontin (OPN) is a negatively charged, acidic and hydrophilic protein of around 300 amino acids (44KDa) in size (Mazzali *et al*, 2002). It is secreted by both osteoblasts and osteoclasts, but not exclusively, and mediates the attachment of cells to hydroxyapatite crystals through polyaspartic acid motifs as well as arginine-glycine-aspartic acid (RGD) motifs (Young *et al*, 1990). Osteopontin also potentially contains calcium binding motifs and two heparin binding domains thus perhaps accounting for its affinity for hydroxyapatite (Prince, 1989). In addition to this it is also thought that it can attach to collagen through transglutamination (Beninati *et al*, 1994). OPN was first recognised in bone matrix by Franzen and Heinegard in 1985 and at that time it was called bone sialoprotein 1. A specific function for this gene product is not known, which is in part due to $Opn^{-/-}$ mice displaying a normal skeleton with the only phenotypic differences being greater crystal size and crystallinity (Boskey *et al*, 2002). These mice however, when challenged with parathyroid hormone, which signals indirectly via osteoblasts for osteoclast differentiation through production of RANKL and therefore bone resorption, show an impaired response (Ihara *et al*, 2001).

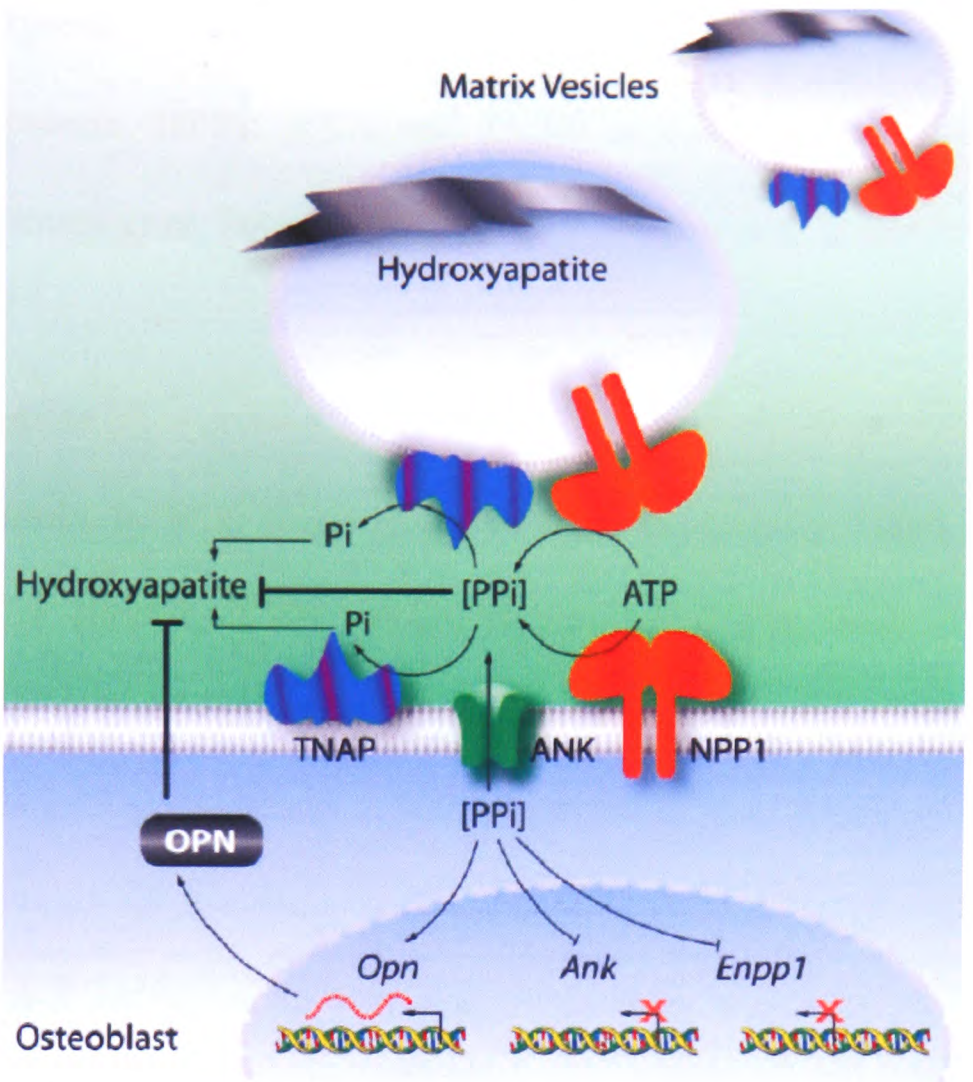

Figure 1.10 The roles of TNAP, ANK, NPP1, PPi and OPN in the mineralisation process. The role of NPP1 and ANK is to raise the extracellular PPi pool whereas TNAP depletes it thus eliminating it from sites of mineralisation. PPi is also a regulator of transcription from the NPP1 (*Enpp1*) and *Ank* genes thus a negative feedback loop is present to mediate transcription. In addition to this PPi induces OPN transcription which further inhibits mineralisation. Thus when TNAP is not functional PPi serves to inhibit mineralisation both directly and through the production of OPN causing hypomineralisation (Harmey *et al,* 2004).

Osteopontin is thought to be involved in the mineralisation process through inhibition of formation and more importantly the propagation of hydroxyapatite crystals (Hunter *et al*, 1996). This inhibition of crystal growth is thought to involve both carboxylate and phosphate groups on the protein, the poly-aspartic acid motif may also play an important role in the inhibition of mineralisation (Hunter *et al*, 1994). Other functions of OPN include inhibition of apoptosis, stimulation of cellular attachment and migration in tumour formation, wound healing and modulation of immune responses (Xuan *et al*, 1995; Rollo and Denhardt, 1996; Noti, 2000).

Osteopontin expression is also promoted in the presence of PPi, thus providing a link between this protein, NPP1, ANK and TNAP in mineralising cells, as shown in figure 1.10 (Harmey *et al*, 2004).

1.6.4.5 Osteocalcin

Osteocalcin, or BGP (bone gla protein), is exclusively found in bone tissue, and accounts for 10-20% of the non-collagenous protein in bone. This protein has been the subject of investigation by knockout mouse technology, and functionally it was found to be able to negatively regulate bone formation. Newborn knockout mice have a normal bone phenotype at birth but after a period of 6 months an increased bone density and thickness is observed. This was hypothesised to be due to osteoblasts depositing more bone matrix than those of wild-type mice, which led to the conclusion that osteocalcin was a negative regulator of bone formation (Wolf, 1996). Osteocalcins' regulatory function is due to the structure of the protein; it consists of a single chain approximately 50 amino acids in length and contains three vitamin K-dependent gamma-carboxyglutamic acid residues (GLA). These are closely involved in its ability to bind both calcium and hydroxyapatite, shown in figure 1.11. This protein is largely unstructured when calcium is not present, however when calcium is in the vicinity of the protein it is transformed into a folded state (Hoang *et al,* 2003). This allows calcium sequestering thus inhibiting mineral formation and matrix mineralisation (Chenu *et al,* 1994). In addition to osteocalcins ability to regulate bone formation it has also been implicated in bone remodelling by acting as a chemo-attractant for monocytes which are part of the osteoclast cell linage (Malone *et al,* 1982).

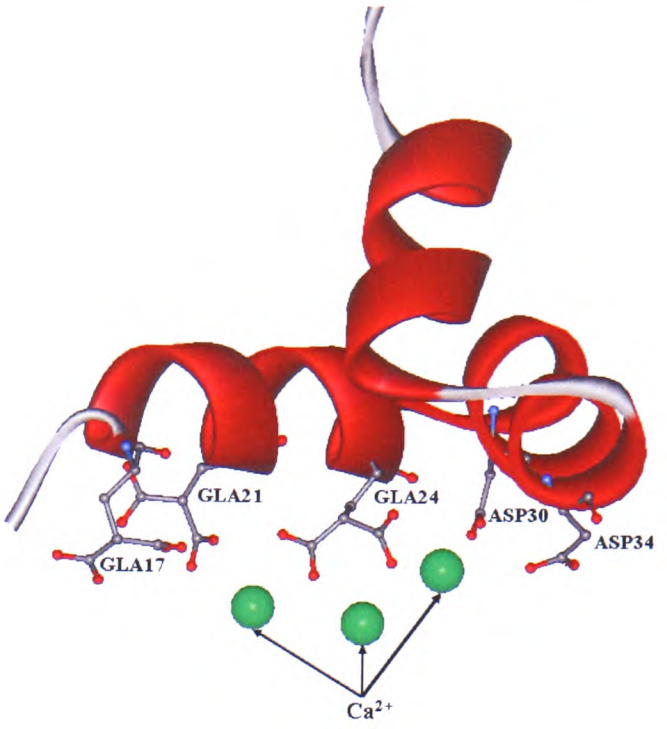

Figure 1.11 Structure of porcine osteocalcin showing the residues involved in calcium binding. Each osteocalcin molecule can co-ordinate to calcium ions sequestered in a hydroxyapatite crystal lattice thus attributing to its affinity of mineralised bone matrix.

1.6.4.6 Matrix Gla Protein (MGP)

Matrix gla protein (MGP) was originally isolated from bone by Price *et al* in 1983 and like osteocalcin contains 5 vitamin K dependent γ-carboxyglutamic acid (GLA) residues (Price and Williamson, 1985). MGP is a 14-kD extracellular matrix protein which, although expressed in many tissues only appreciably accumulates in the matrix of bone, cartilage, and dentin (Hale *et al*, 1988). As with osteocalcin, the GLA residues found within this protein function to promote the binding of hydroxyapatite through their affinity to calcium ions. Due to this the protein is closely associated to the mineralisation process, indeed mice lacking this gene product are severely compromised and fatality is observed within two months. This is primarily due to the presence of arterial calcification, through the action of chondrocytes, which leads to the rupture of blood vessels (Luo *et al*, 1997). The chondrocytes, which have replaced the smooth muscle cells that normally reside in this region, undergo the process of enochondral ossification, hence it is likely that MGP also plays a pivotal role in the mediation of cell differentiation. In addition to this pathological calcification of the growth plate is also observed which leads to fractures and osteopenia, thus it has been hypothesised that this primary function of

this protein is to inhibit or, in the case of the growth plate, modulate the mineralisation process (Luo *et al*, 1997). This hypothesis has been furthered through the demonstration that overexpression of MGP in hypertrophic chondrocytes reduces their mineralisation potential (Newman *et al*, 2001). The human disease Keutel syndrome is triggered by mutations in the MGP gene, and is characterised by excessive cartilage calcification (Munroe *et al*, 1999).

1.6.4.7 Osteonectin

Osteonectin, otherwise known as SPARC (secreted protein acidic and rich in cysteine) or BM-40 is an osteoblast expressed, phosphorylated glycoprotein of approximately 32KDa (Termine *et al*, 1981). Osteonectin is known as a matricellular protein as it does not function as a structural component of matrix but does act as regulator of cell behaviour and can account for up to 15% of non collagenous protein in bone (Bradshaw and Sage, 2001). This protein has been implicated in many cellular pathways in nonskeletal systems including the stimulation of metalloproteinase expression, modulation of angiogenesis and inhibition of cell proliferation. It can also inhibit the function of growth factors such as platelet-derived growth factor, TGFß, and vascular endothelial growth factor (Bradshaw and Sage, 2001). Its precise function in bone remains unclear, however osteonectin null mice display an imbalance in bone turnover. This primarily affects trabecular bone where a decrease in both osteoblast and osteoclast numbers are present, this results in a negative effect on bone mass (Delaney *et al*, 2000). It is thought that this is directly due to osteopontin acting as matrix embedded differentiation factor for osteogenesis (Delany *et al*, 2003).

Osteonectin can bind collagen within the matrix and when complexed can bind apatite. It has therefore been hypothesised that this protein may initiate mineralisation in normal bone by acting as a local nucleator for hydroxyapatite formation (Termine *et al*, 1981). Human osteonectin is found on chromosome five and spans 10 exons containing domains attributing to its calcium binding characteristic. The two domains involved in calcium binding are the N-terminal acidic region containing clusters rich in glutamic acid residues and the EF-hand domains which are helices connected with a calcium binding loop. The N terminal region is negatively charged thus attributing to its affinity for Ca^{2+} whereas the helices of the EF hand domain are co-ordinated to allow calcium binding, as found in other intracellular binding proteins such as calmodulin. When the protein is fully loaded with several Ca^{2+} ions a structural change is educed resulting in an increased helix content of the protein (Engel *et al*, 1987). It has also been reported that osteonectin has the ability to inhibit hydroxyapatite crystal growth *in vitro* (Romberg *et al*, 1986).

1.6.4.8 Bone Sialoprotein

Bone sialoprotein (BSP-II) is one of the major phosphorylated proteins in bone and protein localisation reflects sites of mineralisation. These sites are associated with both chondrocytes and osteoblasts and have been linked to an involvement in hydroxyapatite crystal formation (Chen *et al*, 1991). BSP-II is highly glycosylated and has a molecular weight of approximately 57KDa and contains approximately 50% carbohydrate (small O-linked oligosaccharides) with around 15% sialic acid (Fisher *et al*, 1983). The protein also contains a RGD cell attachment

sequence, three regions of acidic amino acids (glutamic acid) and three regions of tyrosine residues throughout its sequence (Fisher *et al,* 1990). The tyrosine residues are likely to undergo sulphation, however the importance of this process is yet unknown.

BSP-II has been shown to act as a local nucleator for hydroxyapatite production (Hunter and Goldberg, 1994). It is thought that this function is due to glutamic acid rich sequences as polypeptides of L-Glu induced the formation of hydroxyapatite similar to that seen with bone sialoprotein (Hunter and Goldberg, 1994). It has been suggested in this study that this nucleation of hydroxyapatite growth may be directly due to the specific conformation of the helical polyglutamate stretches in the bone sialoprotein at mineralisation sites. In addition it has been reported that in a case of bovine osteoporosis a significant reduction in BSP-II is present within the bone matrix thus strengthening its role in mineral formation (Fisher *et al*, 1990).

1.6.4.8 Potential Mediators of Mineralisation - PHOSPHO1?

Although the eradication of the potent mineralisation inhibitor, PPi has been shown to be of utmost importance for the propagation of hydroxyapatite crystals, examination of MVs from TNAP knockout mice by electron microscopy indicate that they contain mineral (figure 1.8C) (Anderson *et al,* 2004). As TNAP is localised on the outer leaflet of the MV thus controlling the extra-vesicular PPi/Pi ratio it would have no influence on the mineralisation occurring in the vesicle lumen. Although other phosphatase enzymes have been identified within MV's their relevance to the mineralisation process remains to be questioned. Undoubtedly

enzymes causing the hydrolysis of intra-vesicular PPi or elevating Pi thus creating an environment permissive for hydroxyapatite formation are present. It has been suggested that PHOSPHO1, a novel enzyme thought to belong to the haloacid dehalogenase superfamily of hydrolases could be involved in this stage of mineralisation.

1.7 On the Origin of PHOSPHO1

PHOSPHO1, or 3X11A as it was originally known, was discovered at the Roslin Institute during a scheme of work that was attempting to characterise the gene expression profile of both proliferating and hypertrophic chondrocytes. In particular it was trying to identify factors that may regulate chondrocyte differentiation and/or matrix resorption. By separating chondrocytes into populations depending on their stage of differentiation a novel transcript that was highly expressed in differentiated chondrocytes was identified. Analysis of gene expression by RT-PCR showed that this phosphatase was up regulated 5-fold during terminal differentiation of chondrocytes and expressed around 100-fold higher in growth plate chondrocytes compared to various non-skeletal tissues including heart, lung and brain (figure 1.12A) (Houston *et al,* 1999). Upon sequence analysis three motifs were identified which were found to be conserved at the active sites of members of the haloacid dehalogenase (HAD) superfamily. The HAD superfamily is a group of magnesium-dependent hydrolases, including dehalogenases, P-type ATPases, phosphatases and phosphomutases (Aravind *et al,* 1998; Collet *et al,* 1998). Following analysis of the active site motifs it was suggested that this protein was a phosphatase and it has subsequently been shown to have the ability to cleave p-nitrophenyl phosphate

(pNPP) (Farquharson *et al*, 2002). PHOSPHO1 is also expressed in human osteoblast-like cells (SaOS-2) along with TNAP, but not in the MG-63 cell line (figure 1.12B). This finding furthers the initial hypothesis that PHOSPHO1 is involved and perhaps critical to the mineralisation process as SaOS-2 cells are widely regarded as a good model cell type for a well differentiated osteoblast, through expression of TNAP and the ability to form a mineralised matrix in culture (McQuillan *et al,* 1995). Conversely MG-63 cells do not have the ability to form a mineralised matrix and do not express TNAP (Houston *et al,* 2004).

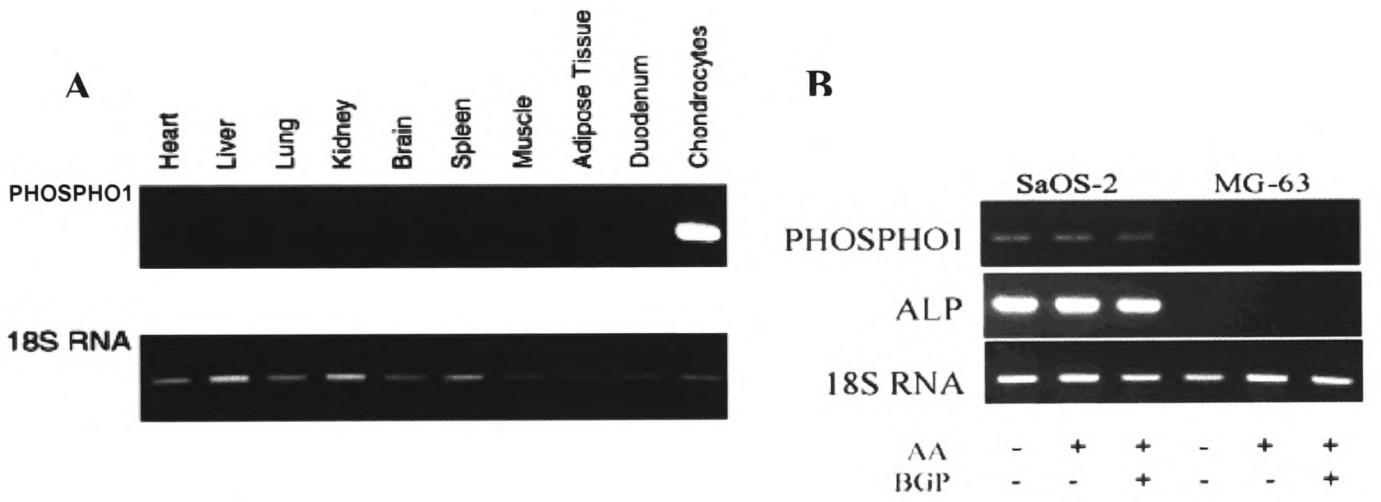

Figure 1.12 (**A**) Semi-quantitative PCR showing expression of PHOSPHO1 is approximately 100 times more in chondrocytes than in other soft tissues. (Houston *et al,* 1999) (**B**) Semi quantitative PCR showing PHOSPHO1 expression in SaOS-2 cells (do mineralise) and MG-63 cells (don't mineralise) (Houston *et al,* 2004).

The initial study on PHOSPHO1 gene expression profile was done in chickens, however since then EST sequence database entries have been identified corresponding to human and murine PHOSPHO1 which have been subsequently amplified and cloned (Houston *et al,* 2002). These transcripts have a 94% identity to each other and are 62% identical to chick PHOSPHO1.

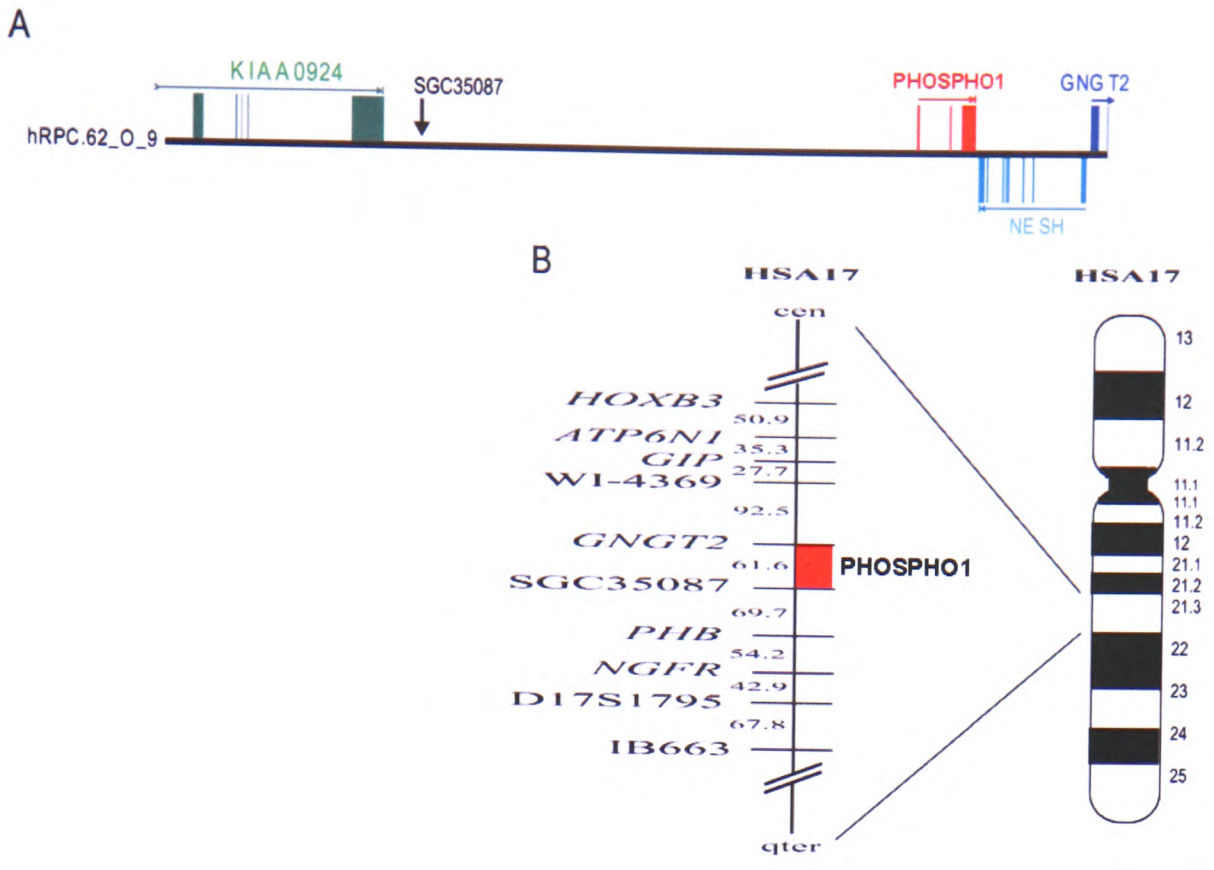

Figure 1.13 Genetic Organisation and chromosomal localisation of human PHOSPHO1. (**A**) Organisation of PHOSPHO1 and neighbouring genes. Arrows depict the direction of transcription. (**B**) Chromosomal localisation of PHOSPHO1, which maps between GNGT2 and SGC35087 on HSA17.

The human and murine PHOSPHO1 genes lie within approximately 7.4Kb regions on HSA17q21.32 and distal MMU11 respectively and are flanked by the ACLY and GH1 loci, and which exhibit conservation of synteny with part of GGA27. Using genetic linkage analysis, chick PHOSPHO1 was mapped to the syntenic region on GGA27 (Houston *et al,* 2002). This strongly suggests that the PHOSPHO1 loci on HSA17 and MMU11 are orthologous to the PHOSPHO1 gene originally identified in the chick. Figure 1.13 shows the genomic organisation of PHOSPHO1 including its flanking genes, in addition the chromosomal localisation of this gene is also displayed.

1.7.1 PHOSPHO1 Localisation

PHOSPHO1 protein has been localised to all regions of mineralising bone and cartilage in the avian model (Houston *et al*, 2004). As seen in figure 1.14A, PHOSPHO1 is found in early hypertrophic chondrocytes, which are the sites of the first stages of hydroxyapatite mineral production. It is not found in the hypertrophic chondrocytes suggesting that PHOSPHO1 is required for the initiation of mineralisation but not for its maintenance. The perichondral ring, as shown in figure 1.14B, is also intensely stained for the presence of PHOSPHO1. The function of the mineralised perichondral ring is to provide protection to the growth plate. PHOSPHO1 protein was also identified, in both cortical and trabecular bone. As shown in figure 1.14C strong PHOSPHO1 staining is evident in the periosteum and on the mineralising surfaces of the primary osteons, upon analysis of diaphyseal cross sections. Houston and colleagues (2004) reported that the staining within the periosteum was limited to the osteoid with fibroblast or osteogenic layers found to be PHOSPHO1 negative, however these cellular layers would also be found negative for mineralisation. PHOSPHO1 was also localised to the surfaces of 17 day old embryonic calvaria, osteoid found on both the intramembranous and periosteal bone surfaces stained positively for PHOSPHO1 (figure 1.14D). The investigators also reported its presence on the surfaces of mature trabecular bone. No PHOSPHO1 staining was found on the surface of cartilage spicules directly distal to the growth plate, interestingly this area is characterised by an absence of osteoid and mineralisation. All soft tissues examined for PHOSPHO1 localisation were negative further strengthening the hypothesis that PHOSPHO1 plays an important role in bone and cartilage mineralisation.

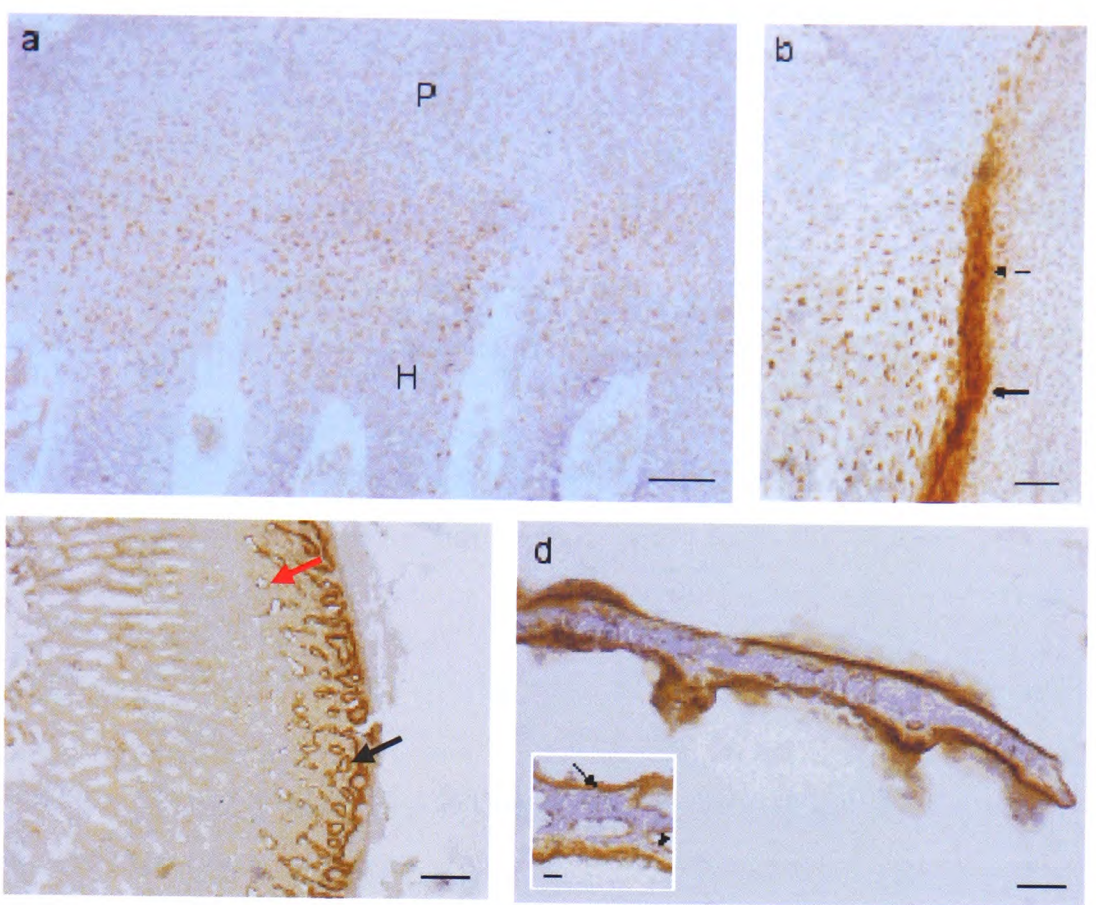

Figure 1.14 Immunocytochemistry of growth plate cartilage and bone showing regions of PHOSPHO1 localisation. Protein localisation is identified through areas of intense brown colourisation. (**A**) localisation of PHOSPHO1 within chondrocytes of the growth plate, note intense staining of those with a pre-hypertrophic phenotype (**B**) PHOSPHO1 staining of the perichondrol ring as indicated by arrows. (**C**) PHOSPHO1 staining of diaphyseal cross section, note intense staining of infilling osteons (black arrow) whereas closed osteons are negative (red arrow) (**D**) Staining of embryonic calvaria showing positive staining on all mineralising surfaces (*Inset*: staining of the periosteal (black arrows) and intramembranous (grey arrows) bone surfaces (Houston *et al*, 2004).

In addition to the protein localisation studies, PHOSPHO1 transcript has also been localised in developing embryonic bones of the chick by in situ hybridisation (Stewart *et al,* 2006). In this study the transcript of PHOSPHO1 has been found to be expressed at sites destined for mineralisation as shown in figure 1.15. Interestingly the transcript is present at these sites prior to overt signs of mineralisation thus

furthering the theory that perhaps PHOSPHO1 is involved in the initial stages of mineralisation, which as discussed previously are TNAP independent.

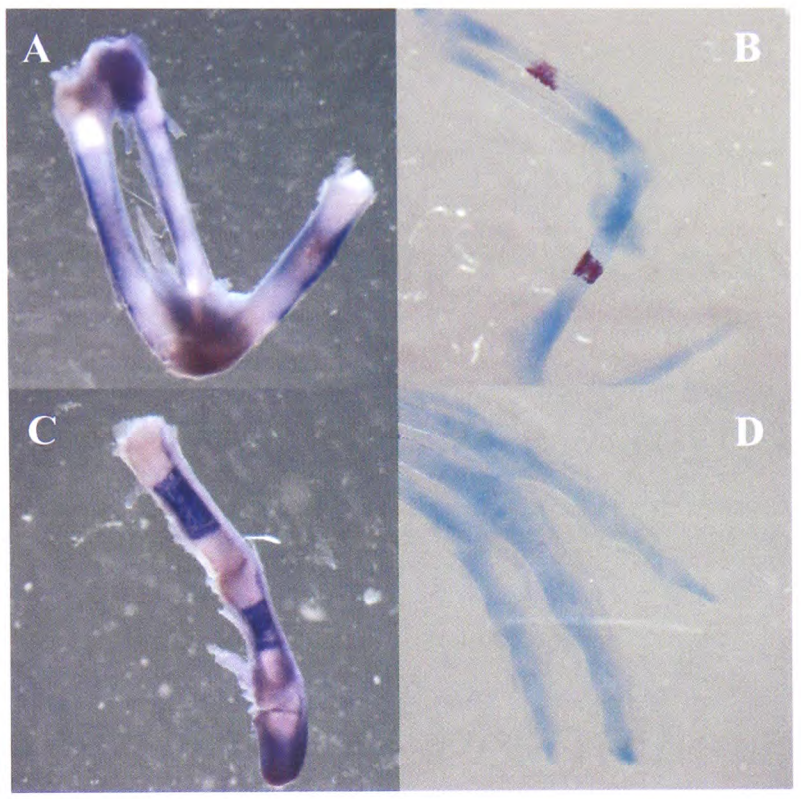

Figure 1.15 Comparison of PHOSPHO1 expression with mineral deposition as assigned by alizarin red staining. (**A**) PHOSPHO1 transcript localisation in a day 10 embryonic front limb, when compared to an alcian blue/alizarin red stained limb (**B**) it is evident that PHOSPHO1 is spread throughout the shaft that is destined for mineralisation, which contrasts with the more restricted distribution of mineral. (**C**) PHOSPHO1 transcript is present only in the diaphysis of the hind limb phalange, however no mineralisation is present in these bones, as shown by the absence of alizarin red staining (**D**). (Stewart *et al*, 2006)

1.7.2 Molecular Modelling of PHOSPHO1

A homology model has been constructed of human PHOSPHO1 based upon the crystal structure of phosphoserine phosphatase (PSP) from *Methanococcus jannaschii* to which it shares approximately 20% identity (Stewart *et al,* 2003). In the PHOSPHO1 model, amino acid side-chains involved in magnesium binding and PSP catalysis are conserved between the template and PHOSPHO1. However, residues involved in substrate-specific interactions are not. This suggests that PHOSPHO1 is not a member of the phosphoserine phosphatase subfamily but belongs to a novel, closely related enzyme group within the HAD superfamily. The residues which facilitate hydrolysis of the phosphate group (Gly100, Lys144 and Asn170) (Wang *et al*, 2002) are fully conserved in PHOSPHO1 with the exception of Gly100, which is replaced with Asp123. In addition three Asp residues (11, 13 and 167) involved in catalysis are also conserved between the two proteins (Stewart *et al*, 2003). This implies that the catalytic site in PHOSPHO1 is very closely related to that of PSP thus suggesting that phosphocompound hydrolysis by PHOSPHO1 occurs by the stepwise Mg^{2+}-dependent mechanism, as with PSP. Analysis, however, of the binding pocket of PSP compared to PHOSPHO1 reveals that PHOSPHO1 is likely to be able to hydrolyse larger substrates than PSP due to alterations in amino acid composition (Stewart *et al,* 2003). A diagrammatic representation of the PHOSPHO1 active site is shown in figure 1.16.

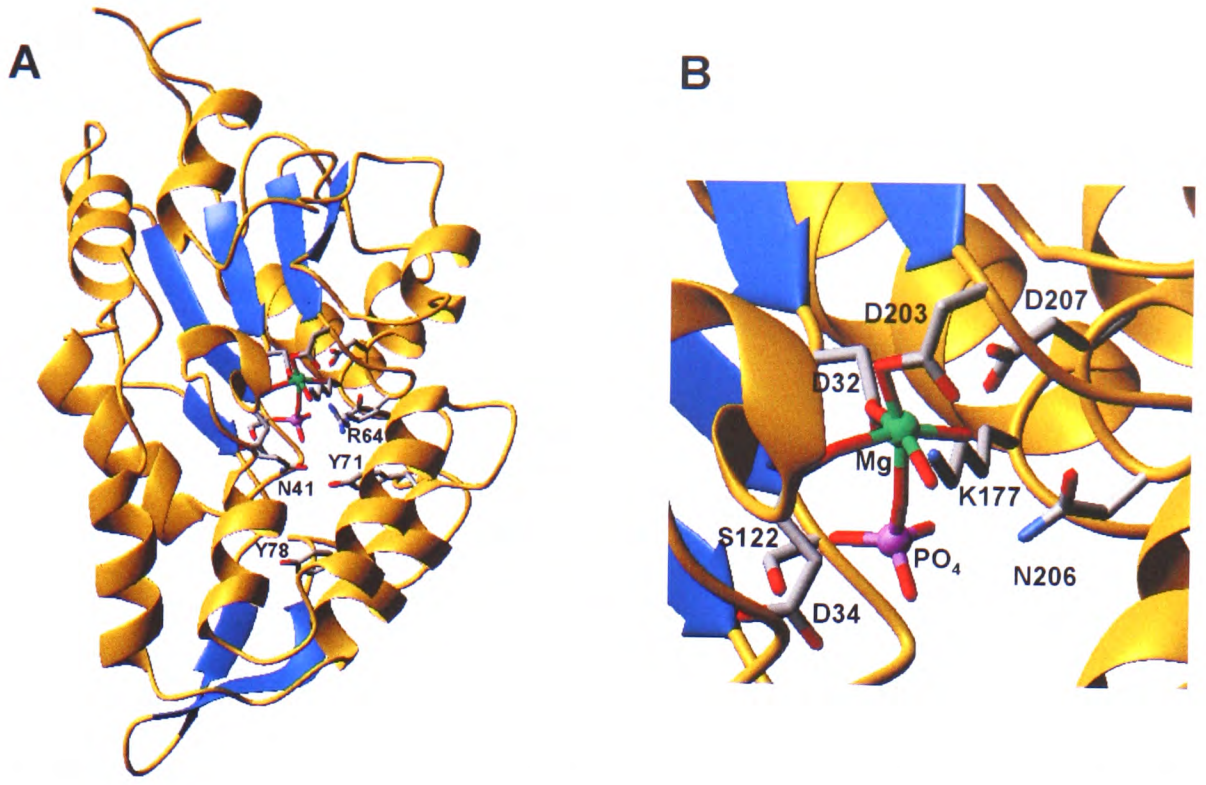

Figure 1.16 (**A**) Ribbon diagram of the human PHOSPHO1 model (**B**) Active site/binding pocket of PHOSPHO1 showing the conserved amino acids involved in Mg^{2+} binding (Stewart *et al,* 2003).

1.8 Aims and Strategy

The main aim this project was to characterise, as fully as possible, mammalian PHOSPHO1, a phosphatase belonging to the haloacid dehalogenase superfamily. This will take the take the form of a both biochemical and a cellular/molecular study. The purpose of the biochemical study is to investigate possible substrates for the enzyme and hence implicate PHOSPHO1 in certain cellular pathways. I intend to define the substrate of PHOSPHO1 by generating the recombinant human protein and utilising it in a biochemical *in vitro* assay.

PHOSPHO1 is obviously linked closely to the mineralisation process due its presence at every mineralising surface and therefore perhaps the most likely cellular pathway that it could be involved with is the generation of phosphate for hydroxyapatite production. For this to be true the enzyme would have to be

associated with MVs in a similar fashion to TNAP as these are widely regarded as the sites of mineral initiation and the only part of hydroxyapatite deposition that is enzyme restricted. This recombinant protein produced will be used for the production of an antibody to allow the immunolocalisation of PHOSPHO1.

To assign function I intend to both over express PHOSPHO1 and attempt to knock down gene transcription in cell lines. The overexpession work will take the form of driving the expression of human PHOSPHO1 in a non-mineralising cell to investigate whether this protein is potent enough to induce mineralisation. To knock PHOSPHO1 expression down I will attempt to use short hairpin (sh)RNA vectors to stably transfect both chondrocytes and osteoblasts to investigate gene function in each of these cell types.

I also intend to modulate protein activity; however this is more difficult to do than genetically manipulating cells to modify gene expression. To tackle this aim I intend to find small molecule inhibitors of PHOSPHO1 and investigate their effect on the mineralisation process *in vitro*. This will be achieved by high throughput chemical screening of compounds and assessing their effect of PHOSPHO1 mediated hydrolysis of phosphoesters.

CHAPTER 2

MATERIALS AND METHODS

Chapter Contents

2.1 Reagents and Solutions

2.1.1 Materials

All chemicals were purchased from Sigma Aldrich (Dorset, UK) unless otherwise stated. PCR oligonucleotides were purchased from MWG Biotech (Ebersberg, Germany), shRNA oligonucleotides were purchased from Sigma-Genosys (Haverhill, UK). Antibodies that were used in this study are detailed in appendix 4.

2.1.2 Buffer Recipes

Cell Culture Buffers

Phosphate Buffered Saline (PBS)

140 mM NaCl, 2.5 mM KCl, 10 mM Na_2HPO_4, 1.8 mM KH_2PO_4

Cell Freezing Buffer

60% DMEM, 30% FBS, 10% Dimethyl sulfoxide (DMSO)

Hanks Buffered Saline Solution (HBSS)

1.26 mM $CaCl_2$, 0.493 mM $MgCl_2$, 0.407 mM $MgSO_4$, 5.33 mM KCl, 0.441 mM KH_2PO_4, 4.17 mM $NaHCO_3$, 137.93 mM NaCl, 0.338 mM Na_2HPO_4, 5.56 mM D-Glucose

Bacterial Culture

Lysogeny Broth (LB) media

1% bacto-tryptone, 0.5% bacto-yeast extract, 150 mM NaCl, adjusted to pH 7.5

LB agar

LB supplemented with 1.5% bactoagar

Super Optimal Broth with Catobolite repression (SOC) Media

2% bacto-tryptone, 0.5% bacto-yeast extract, 10 mM NaCl, 2.5 mM KCl, 10 mM $MgCl_2$, 10 mM $MgSO_4$, 20 mM glucose

Gel Electrophoresis

Tris-Acteric Acid-EDTA (TAE)

40 mM Tris, 1 mM EDTA, 0.1 % Acetic Acid

Tris-Boric Acid-EDTA (TBE)

(90 mM Tris, 2 mM EDTA, 90 mM boric acid

Agarose Gel Loading Buffer

1.2 mM bromophenol blue, 50% (w/v) glycerol, 10% (v/v) 10x TBE

Qiagen Kit Buffer Compositions

Re-suspension Buffer P1

50 mM Tris-HCl, pH 8.0; 10 mM EDTA; 100 µg/ml RNase A

Bacterial Lysis BufferP2

200 mM NaOH, 1% SDS

Elution Buffer EB

10 mM Tris-HCl, pH 8.5

Neutralisation Buffer P3

3 M Potassium Acetate, pH 5.5

Equilibration Buffer QBT

750 mM NaCl; 50 mM 3-[N-morpholino] propanesulfonic acid (MOPS), pH 7.0; 15% isopropanol (v/v); 0.15% Triton X-100 (v/v)

Column Wash Buffer QC

1M NaCl, 50 mM MOPS pH7.0, 15% isopropanol (v/v) and 0.15% Triton X-100 (v/v)

Elution Buffer QN

1.6 M NaCl, 50 mM MOPS, pH 7.0, 15 % isopropanol (v/v)

DNA Re-suspension Buffer TE

10 mM Tris HCl, pH 8.0, 1 mM EDTA

PolyAcrylamide Gel Running and Staining Buffers

MOPS Running Buffer

50 mM MOPS pH 7.7, 50 mM Tris, 0.1% SDS, 1 mM EDTA

NuPAGE Transfer Buffer

25 mM Bicine pH 7.2 , 25 mM Bis-tris , 1 mM EDTA, 0.05 mM Chlorobutanol

LDS Sample Buffer

10% Glycerol, 141 mM Tris Base, 106 mM Tris HCl, 2% LDS, 0.51 mM EDTA, 0.22 mM SERVA® Blue G250, 0.175 mM Phenol Red, pH 8.5

Coomassie Stain Solution

50% (v/v) methanol, 10% (v/v) acetic acid, 1.5 mM coomassie brilliant blue

Coomassie Fixing Solution

50% (v/v) ethanol, 10% (v/v) acetic acid

Coomassie De-stain Solution

50% (v/v) methanol, 5% (v/v) acetic acid

Silver Stain Developing Solution

0.003% (w/v) citric acid, 0.012% (v/v) formaldehyde

Silver Stain Staining Solution

175 mM $AgNO_3$, 780 mM NH_4OH 0.36% (v/v) NaOH

Western Blotting

Tris-Bufferd Saline with Tween 20 (TBST)

10 mM Tris HCl pH8.0, 150 mM NaCl, 0.1% Tween-20

Blocking Solution

5% (w/v) dried milk protein (Marvel) in TBST

Immobilised Metal Chromatography Buffers

NiNTA Lysis Buffer

20 mM Tris-HCl pH 8.0, 500 mM NaCl, 10 mM imidazole and 1.6 mg/ml of Complete® protease inhibitor cocktail

NiNTA Wash Buffer

20 mM Tris-HCl pH 8.0, 500 mM NaCl, 20 mM imidazole

NiNTA Elution Buffer

20 mM Tris-HCl pH 8.0, 500 mM NaCl, 250 mM imidazole

Biochemical Assay Buffers

Calcification Buffer

50 mM Tris-HCl pH 7.6, 1mM $MgCl_2$, 85mM NaCl, 15mM KCl, 2.2 mM $CaCl_2$, 1.6 mM KH_2PO_4, 10mM $NaHCO_3$

Tris-Buffered Saline (TBS)

10 mM Tris HCl pH7.2, 500 mM NaCl

2.2 Cell Culture

2.2.1 Cell Culture Reagents

Dulbecco's Modified Eagle Medium (DMEM), containing 4500g/L glucose and L-glutamine, was purchased from Gibco (Gibco BRL, Paisley, UK). All tissue culture reagents were prepared in a sterile category 2 hood. DMEM was supplemented with 0.5% of the broad spectrum antibiotic gentomycin (Gibco) and 10% heat inactivated foetal bovine serum (FBS) (Gibco) before use. All media was filter-sterilised through a 0.22 μM filter and stored at 4°C.

2.2.2 Cell Lines and Primary Cells

For over expression and knockdown experiments SaOS-2 and SW1353 cells were used. SaOS-2 cells were obtained from the European Collection of Cell Cultures (Sailsbury, Wiltshire, UK), while SW1353 cells were a kind gift from Dr Simon Tew, University of Manchester. HeLa cells were obtained from European Collection of Cell Cultures (Sailsbury, Wiltshire, UK). MLOA5 cells were a kind gift from Lynda F Bonewald, University of Missouri-Kansas City. Primary chick chondrocytes were extracted from 3-week-old broiler chicks (as described in 2.2.7). Primary mouse TNAP null/heterozygous/wild type calvarial osteoblasts were a kind gift from Professor JL Millan, Burnham Institute, La Jolla, CA.

2.2.3 Maintenance and Passaging of Cells

Adherent cells were passaged (split) by trypsinisation at sub-confluence. The cell culture media was removed and the monolayer washed with sterile phosphate buffered saline (PBS), the cells were then covered with trypsin/EDTA solution and

EDINBURGH UNIV. EDINBURGH

incubated at 37 °C until cells become detached. Growth media containing serum was then added to the cell suspension to neutralise the trypsin, this was pipetted repeatedly to create a single cell solution and split into fresh flasks. The ratio each cell line was split at differed, however it was usually between 1:3 and 1:8. The cells were then allowed to attach to the plastic and propagate in 37°C, humidified incubator in the presence of 5% CO_2.

2.2.4 Freezing/Thawing cells

To freeze cells a monolayer was stripped as described in 2.2.3 and counted. The cells were centrifuged at 2000 rpm for 5 minutes and resuspended in the appropriate volume of cell freezing buffer to give a cell concentration of between 2-4 x 10^6 cells per ml. The cells within a cryovial (Corning, Surrey, UK) were then transferred to a temperature of -80°C for between 4-7 days and then to -150°C for longer term storage.

Cells were thawed at 37°C and added drop wise to 10ml complete media. The cell suspension was then mixed and spun at 2000 rpm for 5 minutes to remove the DMSO. The cell pellet was resuspended in complete media and transferred to a T75 tissue culture flask.

2.2.5 Cell Counts

To allow accurate plating density the cells were counted using an Improved Neubauer haemocytometer. This device has a counting chamber that is 0.1 mm deep and divided into nine large squares. Following trypsinisation an aliquot of diluted cells was mixed with trypan blue to allow quick detection of viable cells under the

microscope. The viable cells in four of the large squares were counted and an average taken. That figure was then multiplied 10^4 (as one square = 0.1 µl) and then by the appropriate dilution factor to get number of cells/ml.

2.2.6 Transfection of Mammalian Cells with Vector DNA

SW1353/SaOS-2/Hela cells were seeded in T25 flasks in complete DMEM so as to reach approximately 70% confluence the following day. For each T25 to be transfected 100 µl Opti-MEM (Gibco) serum free medium was placed into a sterile tube, 3 µl GeneJuice (Novagen, Madison, USA) was then added drop-wise directly to the serum-free medium and vortexed. The solution was incubated at room temperature for 5 min. 1 µg of plasmid DNA was added to GeneJuice/serum-free medium mixture for each T25 to be transfected and mixed. The GeneJuice/DNA mixture was incubated at room temperature for 15 min. The entire volume of GeneJuice/DNA mixture was added drop-wise to the cells in complete growth medium (4ml). The flask was rocked to ensure good distribution of the genejuice/DNA complexes. The cells were incubated for 24 h at 37°C (5% CO_2) before the growth medium was removed and replaced with fresh DMEM. At this point selective pressure with the appropriate antibiotic (G418 or Puromycin) was put on the cells and cultured. Cell growth was observed every day and medium changed with selection drug every 2 days. The stable line was usually produced after 4 weeks of selection pressure.

2.2.7 Isolation of Chondrocytes and Matrix Vesicles from Chick Growth Plate Cartilage

Under sterile conditions, growth plate cartilage from 3-week-old broiler chickens was collected and diced. Matrix vesicles were released from this according to the collagenase method as previously described (McLean *et al*, 1987). With the following adjustments; diced cartilage was incubated at 37 °C in Hanks buffered saline solution (HBSS) (Gibco) containing 0.1% trypsin type II at a ratio of 0.2g tissue/ml solution for 30mins. The cartilage was then washed in fresh HBSS and incubated in 0.07% collagenase (Worthington, type II) for three hrs with constant agitation at 37 °C. The partially digested tissue was passed through a 40 μM sieve to remove mineral and undigested material. The flow through was checked for the presence of chondrocytes by microscopy. Chondrocytes and matrix vesicles were harvested from the digest by differential centrifugation. Briefly, the digest was spun for 30 min at 1500 g to collect chondrocytes, then at 30,000g to remove sub – cellular debris and finally at 250,000g to pellet matrix vesicles. Isolated chondrocytes were seeded in T25 flasks at an initial density of $1x10^6$ cells/cm^2 in DMEM containing 10% FBS. Following cellular attachment the cells were treated with 50 μg/ml ascorbic acid 2-phosphate (AA) and 10 mM β-glycerophosphate (βGP) to induce matrix mineralisation. A media only control was always included. Cells reached confluence in approximately seven days.

2.2.8 Isolation of Matrix Vesicles from Cultured Chick Chondrocytes

The cell monolayer was washed with HBSS, and then incubated at 37°C in the presence of 0.1% trypsin type II in HBSS for 30min. This was removed, cells

washed and a 0.07% collagenase (Worthington, type II) solution added, This was allowed to incubate at 37°C for 10 minutes before scraping into a universal container and incubating for a further 90 minutes at 37°C. The cell suspension was subjected to differential centrifugation as described in 2.2.7 to isolate both cells and matrix vesicles.

2.2.9 Staining of Cell Monolayers

2.2.9.1 Alizarin Red Staining

This stain is used to detect the presence of calcium deposits on cell monolayers and hence is ideal for the detection of hydroxyapatite (calcium phosphate) deposits. Calcium forms an alizarin red S-calcium complex in a chelation reaction thus areas containing calcium deposits stain red. The growth media was removed from the cell monolayer and the cells washed 3x with PBS. The monolayer was then fixed in 2% para-formaldehyde (PFA) for 15 minutes at 4°C, washed in PBS and stored in PBS until required at 4°C. A solution of 2% Alizarin-S stain was made in H_2O and pH set at 4.2 with NaOH, this is critical to the staining procedure. The monolayer was overlaid with the stain for 5 minutes with constant agitation and repeatedly washed with distilled H_2O until no stain was present in the wash. To quantify dye incorporation the dye was leached from the monolayer by the addition of a 10% cetylpyridinium chloride (CPC) solution for 5 minutes (or until all of dye had been drawn from the monolayer). The OD of the dye solution was then measured at 570nm, calibrating the spectrophotometer to 10% CPC.

2.2.9.2 Von Kossa Staining

This stain is used to detect the presence of calcium salt deposits in cell monolayers. It utilises silver nitrate in the staining solution (silver ion carries a positive charge) binding with the anionic (negative charge) region of the salt (in this case phosphate). As the major calcium salt found in mineralising cells is calcium phosphate this stain will show regions where crystals of calcium phosphate (hydroxyapatite) are present. The growth media was removed from the cell monolayer and the cells washed 3x with distilled H_2O. The cell monolayer was then immersed in 5% silver nitrate for 30 minutes under strong light, this actively reduces the calcium and replaces it with silver thus creating black deposits. The monolayer was then washed 3x in distilled H_2O and incubated with 2.5% sodium thiosulphate for 5 minutes to remove unreacted silver ions. The monolayer was then stored under distilled H_2O until a digital image was taken.

2.2.9.3 Alkaline Phosphatase

This procedure is a simultaneous coupling azo dye method utilising sodium α-naphthyl phosphate as substrate for alkaline phosphatase in the presence of fast blue RR (a diazonium salt). When the α-naphthyl phosphate is hydrolysed by alkaline phosphatase the α-naphthyl couples with the diazonium salt, forming an insoluble, visible pigment at sites of phosphatase activity. The growth media was removed from the monolayer and the cells washed 3x with distilled H_2O. The cells were then overlaid with 2 nM α-naphthyl acid phosphate, 2 mM $MgCl_2$, 1mg/ml fast blue RR in 0.1M barbitone buffer pH9.4 (set with HCl) and incubated at 37°C for 6

minutes. The cells were then rinsed with ice cold 0.1M acetic acid to stop the reaction and washed 3x in distilled H_2O.

2.3 DNA Methods

2.3.1 Transformation of Competent Bacteria

Three stains of *Escherichia coli* (*E. coli*) were used in this study, JM109 (Stratagene, the Netherlands) for routine cloning, TOP10 (Invitrogen, Paisley, UK) for protein expression, and SURE-2 (Stratagene, the Netherlands) cells for pSUPER cloning. SURE-2 (**S**tops **U**nwanted **R**ecombination **E**vents) were selected due to the homologous regions of the pSUPER plasmid having a propensity for recombination, when using JM109 this phenomenon is observed. The transformation procedures for all three are very similar, the main differences are the length of heat shock. When using SURE-2 cells and JM109 cells, 2 µl and 0.8 µl β-mercaptoethanol was added respectively to 100 µl of cells and was incubated on ice for 10 minutes (Note this step was not necessary with TOP10 cells). Approximately 20ng of plasmid DNA was added to the cells, mixed and allowed to incubate on ice for 30 minutes. Both JM109 and TOP10 cells were subjected to heat shock at 42°C for 30 seconds, whereas for SURE-2 cells this was 45 seconds thereafter the cells were returned to ice for 2 minutes. 900 µl SOC (**S**uper **O**ptimal Broth with **C**atobolite repression; Hanahan, 1983) media (Invitrogen, Paisley, UK) was added to the cells and incubated at 37°C for 1 hr with constant agitation. Aliquots of the transformation mixture were spread on LB (**L**ysogeny **B**roth; Bertani, 2004) agar plates containing 100 µg/ml ampicillin and incubated overnight at 37°C.

2.3.2 Liquid Culture of Bacterial Clones

Individual colonies were picked from the agar plates of transformed bacteria into a 10ml LB culture media containing 100 μg/ml ampicillin. This was incubated overnight at 37°C with constant agitation. 2ml of the bacterial culture was spun at 6,000g and pelleted bacteria resuspended in 1ml LB containing 50% glycerol. These glycerol stocks were stored at -20°C until required.

2.3.3 Minipreparation of Plasmid DNA

The remaining 8ml of bacterial culture was used for plasmid DNA production utilising the Qiagen miniprep spin kit (West Sussex, UK). Briefly the 8ml of culture was spun at 6,000 rpm for 15 minutes and resuspended in 250 μl buffer P1. The cells were then lysed by addition of 250 μl buffer P2, and incubated at room temperature for 5 minutes. The genomic DNA and proteins were precipitated from the lysate by addition of 350 μl buffer N3 and centrifuged at 13,000 rpm for 15 minutes to clear the lysate. The supernatant was centrifuged through a Qiagen column containing a silica membrane to selectively adsorb plasmid DNA in the high salt buffer. The membrane was the washed with buffer PE and plasmid DNA eluted by centrifugation at 13,000 rpm with 50 μl buffer EB or distilled water.

2.3.4 Endofree Maxipreparation (Qiagen) of Plasmid DNA

Endofree Maxi Prep kits remove endotoxin generated from gram-negative bacteria such as *E. coli*. Endotoxin-free DNA improves the efficiency of transfection into sensitive or immunologically active cells. A 10ml liquid culture was set up as detailed above and grown for 9 hrs at 37°C with vigorous shaking (~300 rpm). The

10ml *E. coli* culture was then transferred into a flask containing 200ml LB (with 100 µg/ml ampicillin) and grown overnight at 37°C with vigorous shaking (~300 rpm). The bacterial cells were harvested by centrifugation at 6000 x *g* for 15 min at 4°C. The supernatant was removed and bacterial pellet resuspended in 10ml buffer P1, the cells were then lysed through addition of 10 ml buffer P2 which was mixed thoroughly by inverting and incubated at room temperature for 5 minutes. The genomic DNA, proteins, cell debris, and SDS were precipitated by addition of 10 ml chilled buffer P3, which was mixed by inverting 4–6 times. The lysate was poured into the barrel of the QIAfilter cartridge and incubated at room temperature for 10 min. The lysate was then passed into a sterile tube and 2.5 ml buffer ER was added to remove endotoxin and incubated on ice for 30 minutes. The filtered lysate was then applied to a QIAGEN-tip equilibrated with buffer QBT and allowed to enter the resin by gravity flow. The QIAGEN-tip was washed with 2 x 30 ml buffer QC. The DNA was eluted by addition of 15 ml buffer QN and precipitated through the addition of 0.7 volumes of room temperature isopropanol. This was mixed and centrifuged at 15,000 x *g* for 30 min at 4°C to pellet the plasmid DNA. The supernatant was decanted and pellet washed with 5 ml of endotoxin-free 70% ethanol and centrifuged at 15,000 x *g* for a further 10 min. The supernatant was decanted and the pellet left to air dry for 10 min. The DNA pellet was then re-dissolved in 100 µl endotoxin-free buffer TE and stored at -20°C until required.

2.3.5 Agarose Gel Electrophoresis

DNA fragments were separated by horizontal agarose gel electrophoresis. Agarose concentrations from 0.75% to 2% were used depending on fragment size

(higher concentrations for smaller fragments). The gels were produced by dissolving powdered agarose in TBE buffer by heating to the point of boiling. Ethidium bromide (EtBr) was added to a final concentration of 0.5µg/ml to allow visualisation of the DNA under UV light. The gel was then poured into a cassette with slot former and allowed to set. The DNA samples were mixed with loading buffer and loaded onto the submerged gel. The fragments were separated according to size by applying a voltage of 100V across the gel for 1-2 hrs. DNA bands were visualised using a UV transilluminator and photographed using attached camera.

2.3.6 Isolation of DNA Fragments from Agarose gel

DNA was separated as detailed in section 2.3.5. The DNA band was visualised over UV light (due to EtBr intercalation) and excised using a scalpel blade, taking care to trim all unstained gel from the slice. The agarose gel slice was weighed and then subjected to the DNA extraction protocol set out in the Quiquick gel extraction kit (Qiagen). Briefly 300 µl of QG buffer was added per 100mg of agarose and heated to 50°C for 10 minutes to dissolve the gel. 100 µl isopropanol per 100mg agarose was added to the mixture to help increase the DNA yield. The mixture was then applied to a spin column and centrifuged at 13,000 rpm for 1 minute. This allows the DNA to bind to the silica membrane of the column. The DNA was then washed with 750 µl wash buffer (PE) by applying it to the spin column and centrifuging at 13,000 rpm for 1 minute. The empty spin column was then spun for an additional minute to remove traces of ethanol. The DNA was eluted by the addition of 50 µl buffer EB or nuclease free H_2O and centrifuging at 13,000 rpm for 1 minute. The DNA was stored at -20°C until needed.

2.3.7 Quantification of DNA Concentration

DNA concentration was calculated by UV spectroscopy. Readings were taken at 260nm and 280nm. The concentration of DNA was automatically calculated by the biowave reader using the following equation: A_{260} x 50 x dilution factor. The ratio of: A_{260}/ A_{280} gives an indication to how pure the DNA is, proteins have an absorbance at around A_{280} therefore the lower the number the less pure the DNA prep is.

2.3.8 Restriction Endonuclease Digestion of DNA

Digestion of DNA using restriction endonucleases was carried out both as a diagnostic tool and to allow the formation of a DNA fragment to engineer into other DNA i.e. plasmids. Roche restriction endonucleases were used for this process along with their optimised buffer. A typical 20 µl digest would contain 1 µg DNA, 1 unit of the restriction enzyme, 2 µl 10x reaction buffer, the volume was made up with distilled H_2O. The restriction reaction was carried out at 37°C for 1-2 hrs. If a double digest is to be carried out the manufacturers technical data was consulted to find a suitable reaction buffer that both enzymes are able to operate in. Usually 1 unit of each enzyme would be used per 1 µg of DNA in a 20µl reaction.

2.3.9 DNA Ligation into Linearised Vectors

2.3.9.1 Ligation into the pBAD-TOPO Vector

The pBAD-TOPO vector (Invitrogen, appendix 1) is an expression vector which utilises topoisomerase technology to allow direct cloning of PCR fragments in front of an arabinose inducible bacterial promoter. Taq polymerase has a non-template-dependent terminal transferase activity that adds a single deoxyadenosine

(A) to the 3′ ends of PCR products. This allows ligation directly to overhanging 3′ deoxythymidine (T) residues at the cloning site of the vector. The covalently bound topoisomerase 1 enzyme allows the PCR product to be ligated without the enzyme DNA ligase. 100ng of PCR product was mixed with 1 µl vector and 1 µl salt solution, this was incubated at room temperature for 5 minutes. This ligation mixture was used directly for transformation of competent cells.

2.3.9.2 Ligation into Vectors Linerarised by Restriction Digestion

The vector of choice was linerarised by restriction enzyme digestion using enzyme sites contained within the vector multiple cloning site. The insert will also have complimentary sites at either terminus making "sticky ends" for ligation. A molar ratio of 3:1 insert to plasmid was used for all ligations of this nature. The Roche rapid ligation kit was used and manufacturers instructions followed. Briefly both insert and vector were diluted in DNA dilution buffer so that the final volume equalled 10 µl, reaction buffer (10 µl) was then added and mixed. Finally 1 µl DNA ligase was added to the reaction which was incubated at room temperature for 15 minutes. This ligation mixture was used directly for transformation of competent cells.

2.3.10 DNA Sequencing

DNA sequencing was carried out commercially at either ARK Genomics (Roslin) or through the DNA sequencing facility at Dundee University.

2.4 RNA Methods

2.4.1 Isolation of Total RNA from Cells and Tissues

Ultraspec RNA isolation reagent was used to isolate RNA from both cell monolayers and tissues. When isolating RNA from a cell monolayer the cells were scraped directly in ultraspec (1ml per $25cm^2$) and transferred to a nuclease free universal. Similarly for tissue the dissected organ was immersed in ultraspec (approx 1ml/g tissue). The tissue/cells were homogenised using an electric homogeniser in five 10-second bursts. The universal was returned to ice between each of the bursts to prevent heat build up. The homogenised lysate was then passed though a 25G needle ten times to ensure the production of a uniform lysate. Chloroform (200 µl per ml) was added and vortexed for 15 seconds, the sample was then incubated on ice for 5 minutes, before centrifuging at 12,000g (4°C) for 15 minutes; this separates the sample into two phases – the upper, aqueous phase and the lower organic phase. The RNA is contained in the aqueous phase and proteins/DNA in the organic phase. The aqueous phase was removed and transferred to a sterile tube, and 0.5x the volume of isopropanol added to the RNA. 50 µl RNA Tack resin was added to the RNA and vortexed for 30 seconds. The mixture was spun for 1 minute at 12,000g and supernatant discarded. The pellet was then washed twice with 75% ethanol by serial vortexing and centrifugation. The pellet was then left to air dry for 30 minutes. The RNA was eluted from the resin pellet by the addition of 100 µl nuclease free H_2O.

2.4.2 DNase Treatment of RNA

To each 100 µl of RNA, 10 µl 10x DNase 1 Buffer (Ambion, Huntingdon, UK) was added along with 2.5 µl RNase inhibitors (Promega, Southampton, UK).

This was vortexed before 5 µl DNase (Ambion) was added. The RNA was mixed and incubated at 37°C for 60 minutes. The DNase was inactivated using 0.2 x the volume of inactivation reagent (Ambion).

2.4.3 Reverse Transcription Polymerase Chain Reaction (RT PCR)

Reverse transcriptase is a RNA-dependent DNA polymerase which is encoded by retroviruses. Their viral function is to copy the viral RNA genome into DNA prior to its integration into host cells. This can be exploited to allow production of DNA (cDNA) from any RNA template and is known as reverse transcription PCR.

The SUPERSCRIPT - First Strand synthesis system for RT-PCR was used for reverse transcription (Invitrogen) along with Oligo dT (Roche, East Sussex, UK). 5 µg RNA sample and 500 ng Oligo dT were mixed and incubated at 70°C for 10 min to denature the RNA, this was subsequently incubated on ice for 1 minute. 2 µl 10 x RT buffer, 2 mM $MgCl_2$, 10 mM DTT and 0.5 mM dNTP's were added to each RNA sample and mixed, finally 200units (u) Superscript enzyme was added and mixed. The following PCR cycle was used; 25°C for 10 min, 42°C for 50 min and 70°C for 15 min for annealing, elongation and termination respectively. The cDNA was stored at -20°C until required.

2.4.4 Polymerase Chain Reaction (PCR)

PCR was performed on either cDNA produced from reverse transcription or on genomic DNA, as a diagnostic tool or to allow the amplification of a gene for functional studies. In a typical 50 µl PCR reaction the following quantities of reactants were used; 0.2 mM dNTP mix (Promega), 5 µl 10x PCR Buffer (Roche), 5

units Taq polymerase (Roche), 0.5 µM of the forward and reverse primers, 4 µl DNA (at appropriate concentration) and nuclease free H_2O up to 50 µl. This was then cycled in a ThermoHybaid Px2 Thermal Cycler under the following conditions: 94°C for 5 minutes for one cycle, thirty cycles of 94°C for 30 seconds 55-60°C (depending on the melting temperature of the primers) for 30 seconds and 72°C for 1 minute and finally one step of 72°C for 10 minutes. The PCR products were then run on an agarose gel, as outlined in section 2.3.5.

2.4.5 Real Time (Quantitative) Polymerase Chain Reaction (qPCR)

Tissues from several mice were pooled and RNA was isolated by phenol/chloroform extraction and used directly in a quantitative RT-PCR reaction The Brilliant® SYBR® Green QRT-PCR Master Mix Kit (Stratagene) method was utilised to allow quantification by fluorescence during the PCR reaction. Briefly 25 µl SYBR green mastermix was added to 10 ng RNA along with 0.2 µM forward and reverse primers for *Phospho1* (forward: GACAATGAGCGGGTGTTTTC reverse: GGGGATGGTCTCGTAGACAG). The RT-PCR reaction was cycled in a Perkin-Elmer Applied Biosystems Prism 7700 sequence detector as follows: 50°C for 30 minutes (RT step), 95°C for 10 minutes, 40 cycles of 95°C for 30 seconds 57°C for 30 seconds and 72°C for 1 minute. Each tissue sample was tested in triplicate and compared to 18S RNA (classic II primers; Ambion) as an external control which allowed normalisation of results. An identical PCR was carried out on a dilution series of RNA using both gene of interest and external to allow estimation of PCR efficiency.

The raw data is in the form of a C_t value which is the cycle number at which the fluorescence in the tube passed above a predefined threshold. This C_t value is used in the calculations to show relative differences in gene expression in different samples. Briefly the difference in C_t values between the gene of interest and the control was calculated and used to determine relative quantification by expressing the values as $2^{-\triangle CT}$.

2.5 Protein Methods

2.5.1 SDS Polyacrylamide Gel Electrophoresis

Mammalian cells and MVs were disrupted by sonication in PBS containing 1.6 mg/ml of Complete® protease inhibitor cocktail (Roche). Proteins were separated according to weight on Novex Bis-Tris gels (Invitrogen) based on the discontinuous method of Laemmli (1970). The comb was removed from the pre-cast gel and the wells rinsed with distilled water. This gel was then placed in to a tank filled with 1x MOPS running buffer (Invitrogen), the central portion of buffer contained an anti-oxidant to help keep reduced proteins in a reduced state.

Protein samples in 1x LDS sample buffer (containing DTT reducing agent) were heated to 70°C for 15 minutes and cooled on ice. The samples were then centrifuged at 13,000 rpm for 30 seconds. The samples (containing approximately 50 µg lysate protein or 50 ng purified protein) were loaded onto the gel, a pre-stained molecular weight marker (See Blue plus 2; Invitrogen) was also loaded into one of the wells. The gel was run at 200V for 60 minutes.

2.5.2 Coomassie Staining of Polyacrylamide Gel

The gel was removed from its cassette and immersed in fixing solution for approximately 60 minutes. The gel was then immersed in Coomassie Blue staining solution for 60 minutes which served to stain the entire gel blue. This was subsequently destained by washing overnight in 500ml destain solution in a sealed container at room temperature. This allowed the visualisation of protein as a blue band on the gel, however this technique is only sensitive down to 50ng/band and therefore other detection systems were used.

2.5.3 Silver Staining of Polyacrylamide Gel

To allow the detection of less protein in a direct method, a silver staining protocol is used which is sensitive down to approximately 10ng/band. The gel was removed from its cassette and immersed in 7% acetic acid for 7 minutes. The gel was then immersed in two changes of 200ml 50% methanol for 20 minutes, followed by two rinses in 200ml distilled water for 10 minutes. The gel was then submerged in staining solution for 15 minutes and rinsed twice in 200ml distilled water for 5 minutes. The gel was subsequently immersed in developing solution for a maximum of 15 minutes, or until bands become visible. The development was stopped by rinsing the gel in 3 changes of distilled water.

2.5.4 Western Blotting

The gel was removed from the cassette and immersed in transfer buffer. The nitrocellulose membrane that the proteins would be transferred to was washed in transfer buffer along with two 3M papers, cut slightly larger than the gel, and four

foam pads. The nitrocellulose was laid on top of the gel and sandwiched between the two 3M papers, ensuring exclusion of any air bubbles. This sandwich was placed in the X-blot module (Invitrogen) between the four foam pads. The module was then clamped onto the gel tank and topped up with transfer buffer. The proteins in the gel were electro blotted on to the nitrocellulose at 30V for 90 minutes. The nitrocellulose was then blocked overnight in 5% milk protein (Marvel) in TBST (blocking solution) at 4°C to reduce non-specific antibody binding. The primary antibody was added at an appropriate dilution in blocking solution and incubated at room temperature, with gentle agitation, for 90 minutes. Antiserum was usually used at a 1:500 dilution whereas with commercial antibodies a dilution of 1:2000 was used. The nitrocellulose was subsequently washed 3 times in 50ml TBST to remove any un/loosely bound antibody. The blot was then incubated for 60 minutes with a 1:2000 dilution of anti-IgG-peroxidase (specificity dependent on primary antibody) (DAKO, Denmark) diluted 1:2,000 in blocking solution. The blots were then washed 3 times in 50ml TBST. The immune complexes were then visualised by enhanced chemiluminescence (ECL) (Amersham, Buckinghamshire, UK). This kit operates using an acridan-based substrate which when in close proximity to peroxidase releases light. The position of the immune complexes were visualised by exposure of the membrane to ECL film (Amersham), which was subsequently developed in a Kodak automatic developer. Alternatively, in place of ECL, the immune complexes were visualised by incubation in a solution containing 25 mM Tris-HCl, pH 7.2, 75 mM NaCl, 0.25 mg/ml diaminobenzidine (DAB), 0.1 mg/ml $CoCl_2$, 0.15 mg/ml urea hydrogen peroxide, which can be visualised directly.

To assess equal loading the proteins on the blot were stained with India ink after alkali pre-treatment, as described by Sutherland and Skerrit (1986). Briefly the membranes were washed in TBST before incubation with 0.2M NaOH for 5 minutes. The membrane was then submerged in 10% India ink solution for 120 minutes and finally washed repeatedly in TBST until only the protein bands were visible.

2.5.5 Expression of Recombinant Proteins

2.5.5.1 Fermentation Method

For large scale protein production (50mg) a 100ml starter culture of *E. coli* containing the expression vector was grown to an OD of 1 in LB at 37°C thus ensuring the cells were still in the protein producing, log phase of growth. This starter culture was spiked into 10 L LB (containing 100 µg/ml ampicillin) within the fermentation vessel and grown at 37°C till an OD of 0.8 was reached. Recombinant protein expression was induced by treatment with 0.1% (w/v) L-arabinose for 4 h. The culture was continuously aerated throughout fermentation. Bacteria were harvested by centrifugation at 6500g and were resuspended in Ni-NTA lysis buffer containing 1.6 mg/ml of Complete® protease inhibitor cocktail (Roche), and mechanically lysed using a French press (16,000 psi, 16°C). A clarified lysate was prepared by centrifugation at 20,000 g for 1 h. The clarified lysate, which contained the recombinant protein, was stored at -20°C until required.

2.5.5.2 Shake-Flask Method

For small scale protein production (1mg) a 10ml starter culture of *E. coli* containing the expression vector was grown overnight at 37°C in LB. The 10 ml starter culture was spiked into 1L LB containing 100 µg/ml ampicillin and grown to

an OD of 0.8 at 37°C. Recombinant protein expression was induced by treatment with 0.1% (w/v) L-arabinose for 4 hrs. Bacteria were harvested by centrifugation at 6500g for 15 minutes and were lysed in CellLytic™ B-II lysis reagent containing 1.6 mg/ml of Complete® protease inhibitor cocktail (Roche), 50 mg/ml lysozyme, 5 µg/ml DNase I, 500 mM NaCl and 10 mM imidazole. Clarified lysates were prepared by centrifugation at 20,000 g for 1 h. The clarified lysate was stored at -20°C until required.

2.5.6 Immobilised Metal Affinity Chromatography (IMAC)

Affinity chromatography was used to allow purification of recombinant protein via a 6 His-tag at the C-terminus of the protein. The method of choice utilised Ni-NTA agarose (Qiagen) which uses a captured Ni ion to bind the 6 His tag of the recombinant protein. A 5 ml Ni-NTA-agarose column was equilibrated with 10 ml of Ni-NTA lysis buffer. Following equilibration, a 20 ml aliquot of the clarified lysate was applied to the column. The column was then washed with 50 ml of Ni-NTA wash buffer and eluted in 5 ml fractions each by addition of a single column volume Ni-NTA elution buffer. The fraction containing the pure recombinant protein was then dialysed three times in TBS, pH 7.2 (5 L, 4°C, 24 h) and stored at 4°C prior to use.

2.5.7 Circular Dichroism

The secondary structure of the mutant recombinant proteins were compared to that of wild type using circular dichroism (CD) to confirm that in each case, the mutation(s) had not affected the overall fold of the enzyme. CD spectra were

recorded on a JASCO J-600 spectropolarimeter by using 0.5 mg/ml solutions of protein in 20 mM potassium phosphate, pH 7.2, 130 mM sodium sulphate. Far-UV CD spectra (260 to 200 nm) were obtained using a cylindrical quartz cell with a path length of 0.02 cm. Spectra of the mutant proteins were directly compared with that of the wild type to identify structural differences.

2.5.8 Antibody Production and Purification

2.5.8.1 Antibody Production

Antibodies were raised against the recombinant human PHOSPHO1 protein and to a peptide corresponding to the C terminal region of human PHOSPHO1 [Cys + 225-239] with the sequence H-C-G-Y-P-M-H-R-L-I-Q-E-A-Q-K-A-E-OH, which is identical in both human and mouse proteins. The peptide was produced and conjugated to KLH commercially by AFFINITI Research Products Ltd, Exeter, UK by a maleimido based coupling procedure via the N-terminal cysteine sulphydryl moiety to afford N-terminally conjugated peptides. The recombinant protein was prepared and purified as outlined in 2.5.5.1 and 2.5.6, which was subsequently dialysed three times into PBS (5 L, 4°C, 24 h).

The immunisation for the recombinant protein antibody was carried out by the Scottish National Blood Transfusion Service, Midlothian, UK, and involved four sequential immunisations of 100 μg recombinant protein into a New Zealand white rabbit at monthly intervals. The first was in Freund's complete adjuvant and the final three in Freund's incomplete adjuvant. Serum was obtained 1 week after the final immunisation and stored at -20°C until required.

The production of the peptide antibody was carried out by AFFINITI Research Products Ltd. The peptide conjugates were emulsified in Freund's incomplete and complete adjuvant and injected at multiple sites on the hindquarters/flanks of a New Zealand white rabbit at 100 μg/mL at two week intervals for fourteen weeks. Pre-immune serum was collected from each animal prior to the commencement of immunisation. Serum was collected 1 week after the final immunisation and stored at -20°C until required.

2.5.8.2 Antibody Purification

Affinity purified anti-PHOSPHO1 antibodies were prepared using recPHOSPHO1 immobilised on nitrocellulose as an affinity matrix. The matrix was prepared by electrophoresing 100 μg recPHOSPHO1 on a 10% preparative NuPAGE minigel (1 mm x 2D) and transferring the protein onto a nitrocellulose membrane (as described in 2.5.1 and 2.5.4). The PHOSPHO1 band was visualised by in situ derivatisation with fluorescein isothiocyanate (FITC) (Houston *et al*, 1989). Briefly the nitrocellulose membrane was immersed in a 100μg/ml solution of FITC in 100 mM sodium carbonate buffer (pH 9.5) for 5 minutes. A single orange band relating to the recombinant protein was visible which fluoresces under UV light. The membrane was then blocked with 5% milk protein (Marvel) in PBS overnight at 4°C.

The PHOSPHO1 band was excised under UV light, cut into approximately 2 mm x 2 mm squares, washed several times in PBS and stored in PBS at 4°C until required. Purified anti-PHOSPHO1 antibody was prepared by incubating the PHOSPHO1 affinity matrix with 2 ml of antiserum diluted 4-fold in PBS, for 2 h at RT. The matrix was washed extensively with PBS and the antibody eluted by

incubation in 0.5 ml 0.2 M glycine-HCl, pH 2.5 for 20 min at RT. The purified antibody was immediately neutralised using 1.5 M Tris-HCl pH 8.8 and stored at 4°C until use.

2.5.9 Protein Concentration Determination – Bradford Assay

The Bio-Rad protein assay kit used is based on the method described by Bradford (Bradford, 1976). The Bradford protein assay is a simple procedure for determination of protein concentrations in solutions and utilises the change in absorbance of Coomassie Blue upon binding to protein. The Bradford protein assay is not sensitive to interference by chemicals in the lysis buffer, however high concentrations of detergent do cause anomalies in results. The method employed uses gamma-globulin as a standard. Nine standards of gamma globulin were prepared ranging from 10 µg/ml to 90 µg/ml. 160 µl of each standard was pipetted in duplicate into a 96 well plate along with a buffer blank. The protein that was to be measured was diluted in the same buffer as gamma-globulin and also added to the individual wells in duplicate. 40 µl of dye reagent concentrate (Bio-Rad, Herts, UK) was added to each well and mixed. The plate was incubated at room temperature for 5 minutes and absorbance's read at 595 nm. The absorbencies of the samples were compared to a standard curve generated from the absorbencies from the standards.

2.6 Biochemical Methods

2.6.1 Malachite Green Phosphatase Assay

The standard discontinuous colorimetric assay used was based on that of Baykov *et al,* (1988). The reactions were measured in 96-well plates containing 200 µl of 25% (w/v) glycerol, 20 mM TBS, pH 7.2, 25 µg/ml BSA, 2.5 mM substrate, 2

mM of the corresponding divalent metal chloride salt and appropriate mass of purified recombinant PHOSPHO1. For investigation of the effect of pH on PHOSPHO1 activity, 20 mM MES (2-(N-Morpholino)ethanesulfonic acid) was used to obtain pH values between 5.0 and 6.7 and 20 mM CAPS (3-(Cyclohexylamino)-1-propanesulfonic acid) for pH 9.0, in place of TBS. The ionic strength of each buffer was adjusted to that of 20 mM TBS by addition of NaCl. Standard solutions containing known concentrations of KH_2PO_4 were included in each plate. Reactions were allowed to proceed for 15 min at 37°C then stopped by the addition of 50 µl of 3.75 M sulphuric acid containing 3% ammonium molybdate, 0.2% Tween 20 and 0.12 % malachite green. The absorbance of each well at 630 nm was measured and the specific activity was calculated in units of activity per mg of enzyme, where 1 unit of activity represents the hydrolysis of 1 nmol of phosphate per min.

2.6.2 Purine Nucleoside Phosphorylase (PNPase)-Coupled Phosphatase Assay

The continuous spectrophotometric assay was performed using the EnzChek® Phosphatase Assay Kit (Molecular Probes, Paisley, UK), which is based upon the purine nucleoside phosphorylase (PNPase)-coupled assay reported by Webb (1992). The reactions were measured in 96-well plates containing 25% (v/v) glycerol, 20 mM MES, pH 6.7, 500 mM NaCl, 2 mM $MgCl_2$, 0.2 units PNPase, 200 µM MESG (2-amino-6-mercapto-7-methylpurine ribonucleoside) and 144 ng of purified recombinant PHOSPHO1 at 37°C. PNPase and MESG concentrations were optimised to ensure that the phosphatase activity was rate-limiting. PHOSPHO1 substrate concentrations were varied accordingly. Absorbence values were measured continuously at 355 nm using a VICTOR HTS plate-reader.

2.6.3 Matrix Vesicle Alkaline Phosphatase (ALP) assay

To confirm that a preparation was enriched in MVs (from cartilage and cell culture) an assessment of ALP activity was carried out. The preparation was resuspended in HBSS containing 0.05% Triton-x-100 and 1.6 mg/ml of Complete® protease inhibitor cocktail (Roche), and subsequently lysed by freeze thawing 3 times. ALP was assayed for using the Thermo-line ALP reagent (Melbourne, Australia). The enzyme activity of the MV and chondrocyte lysate was determined by measuring the cleavage of 16.3 mM p-nitrophenyl phosphate (pNPP) at 405 nm at pH 10.7. Total ALP activity was expressed as nmoles pNPP hydrolysed/ min/mg protein.

2.6.4 Matrix Vesicle Calcium Uptake Assay -Calcium-O-Cresolpthalein Complexone (O-CPC) Method.

This assay involves the reaction of calcium with *O*-CPC at an alkaline pH (10-12) to produce a purple complex which can be measured at 575 ± 5 nm. The intensity of the colour is directly proportional to the concentration of calcium in the sample. The protocol to measure calcium uptake by matrix vesicles was carried out as described by Garimella *et al,* (2004). Briefly samples of MV protein were incubated in calcification buffer in the presence of 0 to 3 mM phosphoester substrate for 5.5 h at 37°C. The reaction was terminated by centrifugation at 8800g for 30 minutes to pellet both matrix vesicles and any calcium phosphate mineral formed during incubation. The pellet was then solubilised with 0.6N HCl for 24 h and used directly in for calcium quantification using the *O*-cresolpthalein complexone method (CPC Kit, Thermotrace). Briefly, 2 µl of acidified supernatant was incubated with 200 µl of detection reagent for 1 minute and the absorbance read at 570 nm. A

standard curve with calibrators of $CaCl_2$ in 0.6N HCl was also included on the microtitre plate.

2.6.5 Inhibitor Screening

The semi-automated screening utilized a Beckman Coulter dual bridge Biomek FX liquid handler, consisting of a 96 tip head bridge for full plate pipetting. The reactions were measured in 96-well plates containing 25 µl 20 mM MES-NaOH, pH 6.7, 0.01% (w/v) BSA, 0.0125% (v/v) Tween 20, 2 mM $MgCl_2$, 62.5 µM PEA, 10 µM test compound and 500 ng (0.6 µM) of purified recombinant PHOSPHO1. Substrate addition was used to initiate the reaction thus allowing for an enzyme/compound preincubation. Reactions were allowed to proceed for 60 min at room temperature then stopped by the addition of 50 µl BIOMOL green reagent. The absorbance of each well was measured at 620 nm and the inhibitory effect of each compound calculated as a percentage of 100 in relation to controls containing 1% (v/v) DMSO. Each hit was repeated manually in duplicate, a hit from the primary screen was considered if inhibition was above 40%.

2.6.6 Kinetic Characterisation of Inhibitors

The continuous phosphatase assay to determine kinetic parameters of the reactions involved monitoring the dephosphorylation of pNPP which causes an absorbance change at 405 nm. The reactions were measured in 96-well plates containing 20 mM MES-NaOH, pH 6.7, 0.01% (w/v) BSA, 0.0125% (v/v) Tween 20, 2 mM $MgCl_2$, and 1.5 µM purified recombinant PHOSPHO1 at room temperature. pNPP and inhibitor concentrations were varied accordingly.

Absorbence values were measured continuously at 405 nm using a VICTOR HTS plate-reader.

2.7 Immunohistochemistry

2.7.1 Tissue Preparation

10-day old mice were killed by cervical dislocation and tibiae were fixed in 4% paraformaldeyde in PBS for 24 h before decalcification in 0.5M EDTA (pH 8.0) for a further 24 h at 4^0C.

2.7.2 Wax Embedding

The fixed tissues were dehydrated by passaging through different concentrations of alcohol starting with 70% ethanol for 30 minutes followed by 80% and 95% ethanol for a period of two hrs each (changing alcohol after a period of 1 hr) with constant rotation. The tissues were then placed in 100% ethanol and rolled for 2 hrs, changing the alcohol after 1 hr. The tissue specimens were transferred into a wax embedding cassette lined with filter paper and placed in xylene and rolled for 2 hrs. The cassettes were then transferred to wax at 60°C for 2 hrs allowing wax infiltration of the tissues. The tissue was then embedded into plastic moulds using an embedding machine.

2.7.3 Tissue Sectioning

Paraffin embedded tissues were sectioned, using a microtome, into 6 μM thick sections and floated out in a 50°C water bath. The sections were then floated

onto poly-lysine coated slides and allowed to dry in a 37°C oven. Slides were stored at room temperature until required.

2.7.4 Probing Using Protein Specific Antibodies

Paraffin sections were dewaxed in xylene and rehydrated through a graded series of alcohol solutions, antigen retrieval was achieved by heating in sodium citrate for 90 minutes at 70 °C followed by extensive washing in PBS. Endogenous peroxidases were blocked by incubating the sections with 3% hydrogen peroxide (in methanol), followed by 3 washes in PBS. Unspecific protein binding was blocked by normal goat serum (1:5) diluted in PBS for 30 min at RT. Rabbit antisera to mouse PHOSPHO1 (a generous gift from Professor Ikramuddin Aukhil, University of Florida, USA) was diluted 1:200 in PBS and incubated with the tissue section at 4°C overnight. Control sections received a similar dilution of normal rabbit serum. Following this the sections were washed in PBS, and incubated with a 1:100 dilution of goat anti rabbit IgG - peroxidase (DAKO, Cambridgeshire, UK) for 60 min at RT. DAB substrate reagent (0.06% DAB, 0.1% H_2O_2 in PBS) was incubated for 8 minutes at RT, rinsed in PBS and counterstained with Harris hematoxylin (Sigma) for 5 min. The sections were dehydrated and mounted in DePeX.

2.8 Bioinformatic Methods

2.8.1 Sequence Alignments

DNA or protein sequences were aligned using ClustalW programme available at http://www.ch.embnet.org/software/ClustalW.html. DNA sequencing results (ABI files) were assembled using STADEN at the HGMP bioinformatics centre

(http://www.hgmp.mrc.ac.uk). Protein and DNA similarity searches were done through BLAST on the NCBI site.

2.8.2 Structural Modelling and Ligand Docking of PHOSPHO1 and PHOSPHO2

The protein sequence of PHOSPHO2 was subjected to homology modelling as described previously for PHOSPHO1 (Stewart *et al*, 2003). Submitting the protein sequence of human PHOSPHO2 to the 3D-PSSM fold recognition server (Kelley *et al*, 2000) revealed the high resolution (1.8 Å) X-ray structure of phosphoserine phosphatase (*Mj*PSP) from *Methanococcus jannaschii* (PDB code: 1F5S) (Wang *et al*, 2001) as the most suitable template for homology modelling. A pairwise alignment between the target and template sequence was manually adjusted, taking into consideration multiple sequence alignments, structural alignments and the continuity of secondary structure elements. Twenty models were built using MODELLER v6.2 (Sali and Blundell, 1993), keeping the active site Mg^{2+} and its bound phosphate and water molecules in the positions found in the template. A disulfide bridge was introduced between Cys152 and Cys185, both of which are conserved within the PHOSPHO1/PHOSPHO2 multiple sequence alignment, since these residues were found in close proximity to each other in the structural model. Non-identical side-chains between template and target were optimised using SCWRL (Bower *et al*, 1997).

Hydrogen atoms and bonds between Mg^{2+} and its coordinating amino acids were introduced in SYBYL v.6.9 (Tripos Associates, St. Louis). The resulting pdb files were used as input files for FlexX (Rarey *et al*, 1996). Based on previous findings (Stewart *et al*, 2003), the active sites were defined manually, and included

the Mg^{2+} ion, the two water molecules, the residues 32, 34, 43, 60, 64, 71 and 123 for PHOSPHO1, or 8, 10, 19, 36, 40, 47 and 99 for PHOSPHO2, plus a 2.9 Å margin around these residues. Substrate starting structures (PEA, PCho, and pyridoxal-5-phosphate) were built and energy-minimised in SYBYL v6.9. As our initial homology models were necessarily generated without a substrate in the active site, it appears as if the sidechain of Arg60 (or Arg36) is trying to fill the "empty space" of the active site. Therefore, for subsequent FlexX runs, the side-chain of this residue was manually adjusted. Thirty docked structures were generated for each protein, and the best was selected based on the overall FlexX score. The resulting protein-substrate complexes were energy-minimised in SYBYL v6.9 applying 50 steps of minimisation, restricted to the substrate, the Mg^{2+} ion, and Arg60 for PHOSPHO1 or Arg36 for PHOSPHO2 and their immediate surroundings, followed by 100 steps of energy minimisation applied to the entire protein. The minimisation protocol used the Powell algorithm and an improved version of the Tripos force-field. The validity of the resulting model was assessed using PROCHECK v3.5 (Laskowsky *et al*, 1993) and WHAT IF v4.99 (Vriend, 1990), which are available on-line at the "Biotech validation suite" at http://biotech.embl-ebi.ac.uk. The validity of the approach was tested by docking phospho-L-serine into *Mj*PSP (PDB code: 1F5S). The resulting docked model corresponded well with the structure of the D11N mutant of *Mj*PSP with bound substrate (PDB code: 1L7P).

The structural modelling and ligand docking experiments were kindly carried out by Dr. Ralf Schmid (Institute of Evolutionary Biology) and Dr. Claudia A. Blindauer, (School of Chemistry), University of Edinburgh.

2.8.3 Statistical Analysis

Analysis of variance (ANOVA) was performed to determine the significance of a given result. General Linear Model analysis incorporating pair-wise comparisons using Turkeys test was used to compare groups within the ANOVA models. All data are expressed as the mean ± SD of three observations within each experiment. Statistical analysis was performed using Minitab 14. Statistical significance was accepted at $p<0.05$.

CHAPTER 3

MOLECULAR AND BIOCHEMICAL CHARACTERISATION OF HUMAN PHOSPHO1

Chapter Contents

3.1 Introduction

MV-mediated mineralisation is a process central to the formation of bone, cartilage and teeth. Inside the MV, calcium phosphate accumulates until sufficient amounts are present for precipitation to occur. This is then converted to an intermediate, octa-calcium phosphate, crystals of which are transformed into the less soluble hydroxyapatite (Sauer and Wuthier, 1988). The MV membranes then breakdown and release preformed hydroxyapatite into the extracellular fluid. Calcium accumulation is controlled by Ca^{2+}-binding molecules such as annexin I and phosphatidylserine (Wu *et al*, 1995; Anderson, 2003). P_i accumulation is associated with the action of alkaline and acid phosphatases (Roach, 1999; Nakano *et al*, 2003). The most abundant of these being TNAP, an isoenzyme of alkaline phosphatase expressed in bone, liver and kidney (Anderson, 1995). In addition to its structural role, P_i has also been shown to regulate multiple genes during osteoblast differentiation, including the immediate response gene, *Nrf2* (Beck *et al*, 2003).

Deficiency of P_i in skeletal tissue (termed hypophosphatasia) is highly variable in its clinical expression, ranging from death *in utero* with an unmineralised skeleton to premature loss of teeth (Whyte, 1994). Hypophosphatasia is usually attributed to a reduction in TNAP activity. In newborn TNAP knockout mice, bone development and mineralisation appear to be normal, although hypomineralisation and other abnormalities of the skeleton and dentition have subsequently been observed (Waymire *et al*, 1995; Narisawa *et al*, 1997; Hessle *et al*, 2002). Where failure occurs is in the propagation of the mineral from the MV to the surrounding extracellular matrix (Anderson *et al*, 1997 and 2004). Support for this concept comes from earlier work (Genge *et al*, 1988), which shows that the catalytic activity of

TNAP decreases in direct proportion to the extent that MVs induce mineral formation. TNAP is known to hydrolyse PP_i (Moss *et al*, 1967), which is a potent inhibitor of hydroxyapatite crystal formation (Meyer, 1984). Abnormalities found in TNAP knockout mice are, however, not present in TNAP/NPP1 double-knockout mice (Hessle *et al*, 2002). NPP1 encodes the enzyme, phosphodiesterase I in mineralising cells and generates PP_i from nucleotide triphosphates (Narita *et al*, 1994). Studies have also shown that TNAP can be removed from some preparations of MVs without reducing their potential to mineralise (Register *et al*, 1986), whilst specific inhibitory studies on TNAP provide additional evidence that other phosphatases are present within mineralising chondrocytes (Hsu and Anderson, 1996). These observations suggest that the primary role of TNAP in skeletal development is to hydrolyse PP_i, preventing its inhibition of mineral crystal growth. It therefore appears that TNAP is not essential, at least for the initial events leading to MV-induced mineralisation and implies that other phosphatases are involved.

PHOSPHO1 was identified which is expressed at levels approximately 100-fold higher in mineralising chondrocytes than in non-skeletal tissues (Houston *et al*, 1999). Immunolocalisation studies have since shown that PHOSPHO1 is specifically localised to mineralising regions of skeletal tissue (Houston *et al*, 2004). The amino acid sequence of PHOSPHO1 contains three peptide motifs that are conserved within the HAD superfamily of Mg^{2+}-dependent hydrolases. Human PHOSPHO1 shares approximately 30% homology at the amino acid level with the LePS2 family of phosphatases (Baldwin *et al*, 2001; Stenzel *et al*, 2003). Molecular modeling of human PHOSPHO1 based upon the crystal structure of phosphoserine phosphatase from *Methanococcus jannaschii* shows that all the characteristic features of the

catalytic site, with regard to the HAD superfamily, are preserved (Stewart *et al*, 2003). Despite these structural data, little is known about the activity and substrate specificity of PHOSPHO1.

3.2 Hypothesis

That PHOSPHO1 is able to sequester Pi from a source close to its localisation thus elevating Pi concentrations allowing for hydroxyapatite formation via calcium phosphate precipitation.

3.3 Aims

I. Characterise the human PHOSPHO1 gene and determine sequence of all predicted isoforms as identified by EST analysis.

II. To produce a recombinant human PHOSPHO1 protein. This will utilise a prokaryotic system to express a truncated form of the protein containing only the region that would be common to all predicted forms.

III. To develop an assay system by which phospho-esters can be screened to determine compounds which are permissive to phospho-hydrolysis.

IV. To study the kinetic parameters of the best compounds to allow an assessment of whether the reaction is favourable or not and hence whether it is likely to occur *in vivo*.

3.4 Materials and Methods

3.4.1 Analysis of PHOSPHO1 Splice Variants

RNA was isolated from SaOS-2 osteoblast-like cells by ultraspec extraction, as described in 2.4.1 and reverse transcribed as described in 2.4.3. PCR primers (shown in appendix 2) were designed to allow amplification of exons created through alternative splice patterns (defined by EST analysis) as shown in figure 3.1. Each transcript was amplified as described in 2.4.4 utilising a 55°C annealing temperature and 200ng cDNA. The PCR products were then electrophoresed on a 2% agarose gel as described in 2.3.5 and purified using the Qiagen QiaQuick gel extraction kit as outlined in 2.3.6. The PCR products were cloned directly into the pGEM-T-Easy vector (Promega, as shown in appendix 1) as outlined in 2.3.9.2. This plasmid is pre-linerarised and can ligate to the deoxyadenosine (A) at the 3′ ends of PCR products (as described in 2.3.9.1). The PCR product and plasmid were ligated in a 3:1 ratio using 100ng of PCR product. This mixture was used to transform JM109 competent cells as outlined in 2.3.1. Liquid cultures and plasmid minipreparations of individual clones were subsequently carried out (section 2.3.2 and 2.3.3 respectively). DNA sequencing of plasmids was carried out by the DNA sequencing facility at Dundee University.

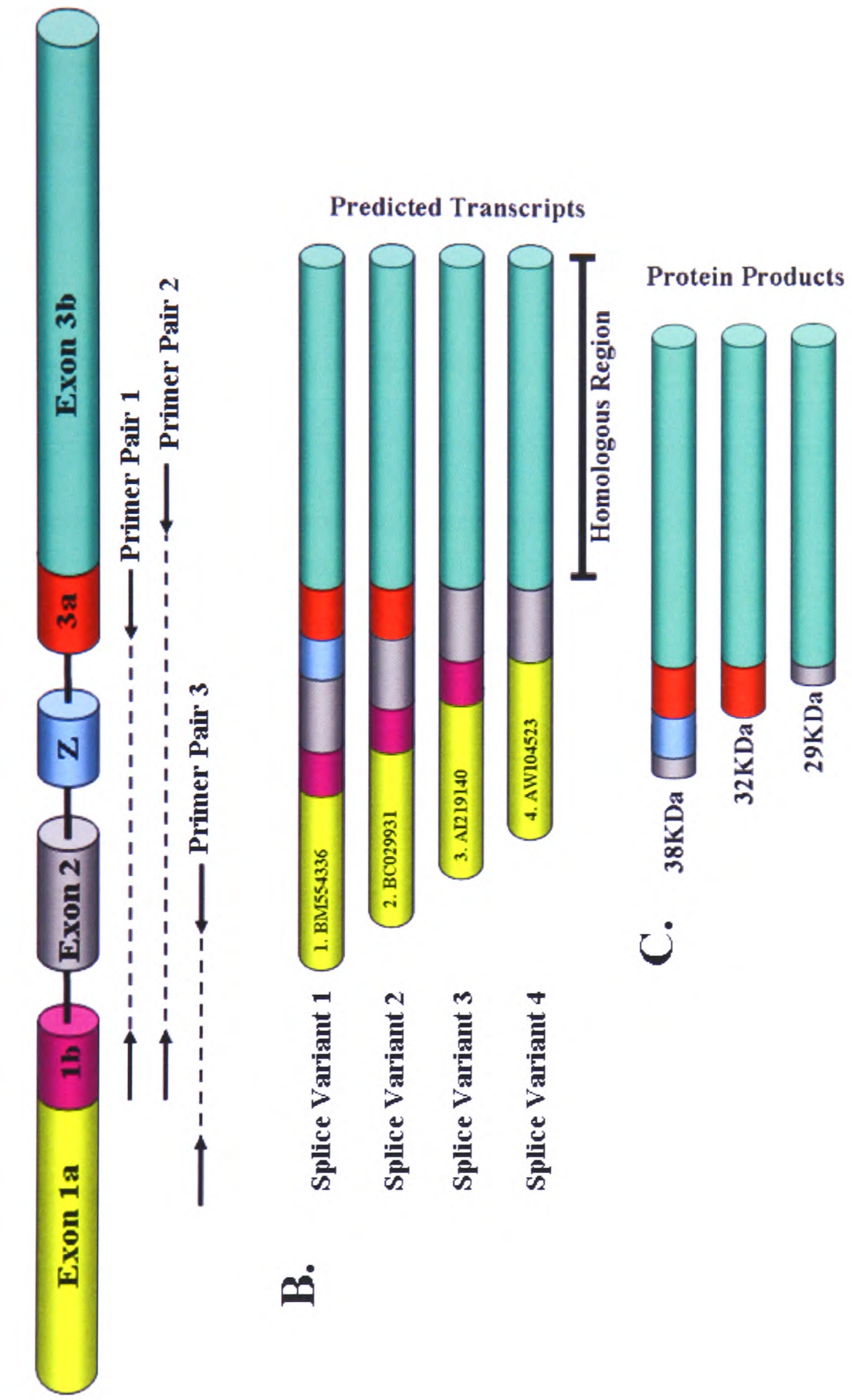

Figure 3.1 Genomic organisation of the PHOSPHO1 gene and possible splice variants. (**A**) Structure of PHOSPHO1 gene as determined by EST analysis, shown in (**B**), and position of primer sites to investigate variant expression. Each splice variant shown in (**B**) corresponds directly to the EST number shown, the newly identified exon Z is shown in blue between exon 2 and 3a (**C**) Predicted proteins from each of the four splice variants.

3.4.2 Production of Recombinant Human PHOSPHO1

RNA was isolated from SaOS-2 osteoblast-like cells by ultraspec extraction, as described in 2.4.1 and reverse transcribed as described in 2.4.3. cDNA corresponding to Met19-Cys267 of human PHOSPHO1 was amplified by PCR with the specific primers (as described in 2.4.4), hs_phos1-f1 primer (5'-ATGGCCGCGCAGGGC-3') and hs_phos1-r1 primer (5'-GCACGACTTCAGCACCTGTTGC-3'). This strategy was adopted in view of the splice variants arising from the PHOSPHO1 gene and therefore expressing a protein which contained only the region that would be common to all predicted forms. The expression plasmid of choice was the pBAD TOPO TA vector (Invitrogen, appendix 1) which is designed to express the recombinant protein fused to a V5 epitope and a 6 His-tag at the C-terminal (nucleotide and protein sequences shown in appendix 3). The cDNA fragment was ligated into the pBAD TOPO TA vector (2.3.9.1) and this used to transform TOP10 cells as described in 2.3.1. Liquid cultures and plasmid minipreparations of individual clones were subsequently carried out (section 2.3.2 and 2.3.3 respectively). A clone containing the PHOSPHO1 fragment in the correct orientation was identified by restriction digestion of plasmid minipreps as described in 2.3.8. Briefly the plasmid DNA was digested with the restriction enzymes Sph1, Pme1 and Asc1, the latter is found only within the PHOSPHO1 coding sequence (CDS). The *E. coli* containing the PHOSPHO1 expression vector were grown a 10L fermentation vessel and recombinant protein expressed by the addition of arabinose outlined in section 2.5.5.1. The recombinant protein was purified by Immobilised Metal Affinity Chromatography (IMAC) as described in 2.5.6. Briefly the NiNTA agarose utilises NTA which is a tetradentate chelating adsorbent. NTA occupies four

of the six ligand binding sites in the coordination sphere of the nickel ion, leaving two sites free to interact with the 6xHis tag, as shown in figure 3.2.

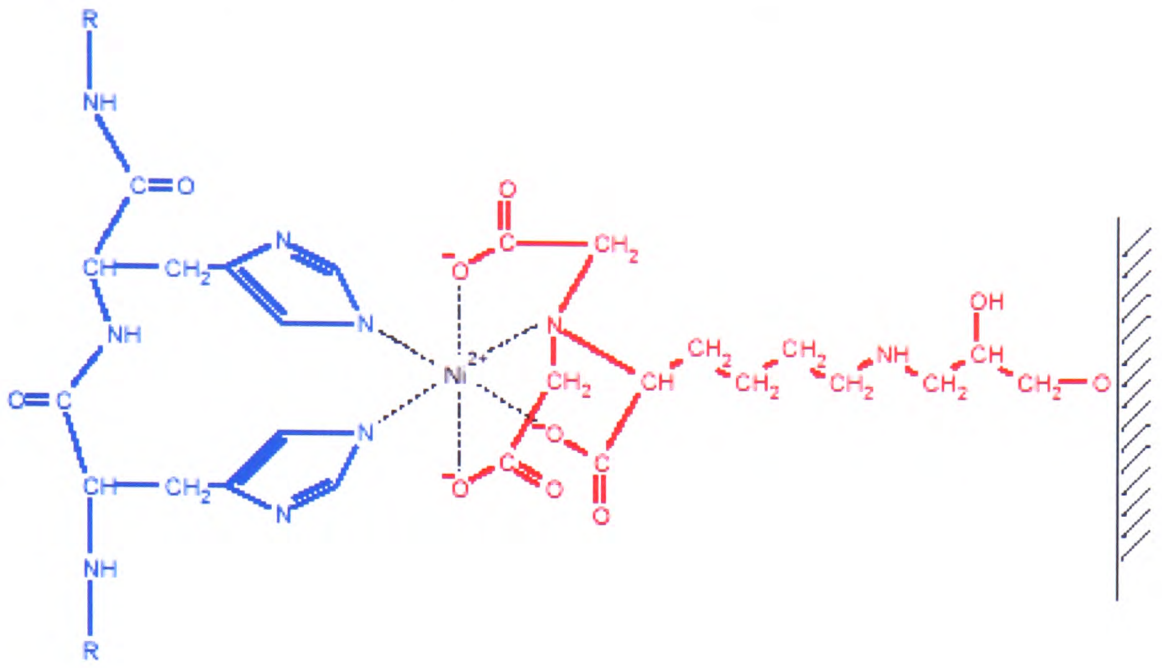

Figure 3.2 Mechanism of nitrilotriacetic acid mediated affinity chromatography. Note the ability of NTA to occupy 4 of the six binding sites in the coordination sphere thus allowing 6 His binding through the remaining two sites.

3.4.3 Western Blotting

To confirm that the purified protein was indeed PHOSPHO1 1 μg of purified protein was subjected to SDS-PAGE as described in 2.5.1, which was subsequently blotted onto nitrocellulose and used for Western blotting analysis as outlined in 2.5.4. This utilised a 1:3000 dilution of mouse monoclonal horseradish peroxidase-labeled anti-V5 antibody (Invitrogen). The immune complexes were then visualised using the DAB technique as described in 2.5.4.

3.4.4 Phosphatase Assays

The standard discontinuous colorimetric assay used was based on that of Baykov *et al,* (1988) as described in section 2.6.2 utilising 600ng of purified recombinant PHOSPHO1 per reaction. Twelve compounds were analysed for

phosphatase activity (Table 3.1); specific activities were calculated in units of activity per mg of enzyme, where 1 unit of activity represents the hydrolysis of 1 nmol of phosphate per min. A standard curve using 5 to 50 nmoles phosphate (KH_2PO4) under the conditions described in section 2.6.2 is shown in figure 3.3, a typical assay plate is shown in figure 3.4.

To analyse kinetic constants for these reactions the continuous spectrophotometric assay was performed using the EnzChek® Phosphatase Assay Kit (Molecular Probes) as described in 2.6.2 utilising 144ng of recombinant PHOSPHO1 per reaction.

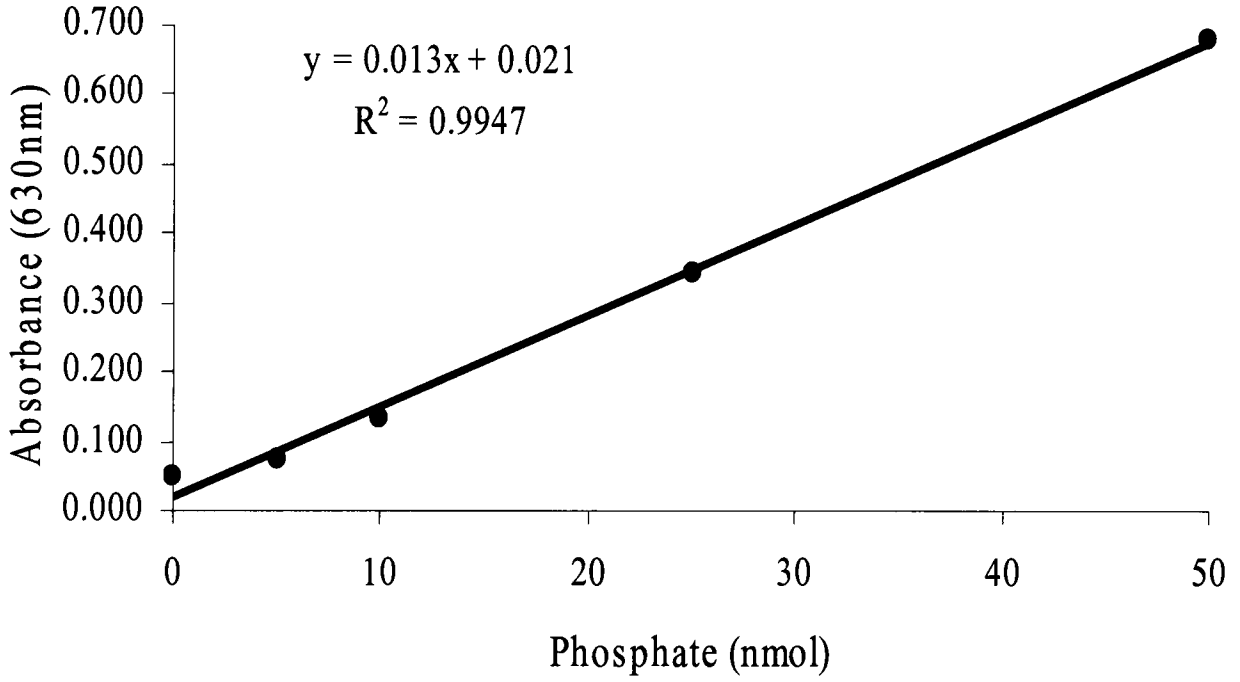

Figure 3.3 Standard curve showing linear absorbance. The reaction utilises the modified malachite green assay as described in section 2.6.2 and known concentrations of KH_2PO_4.

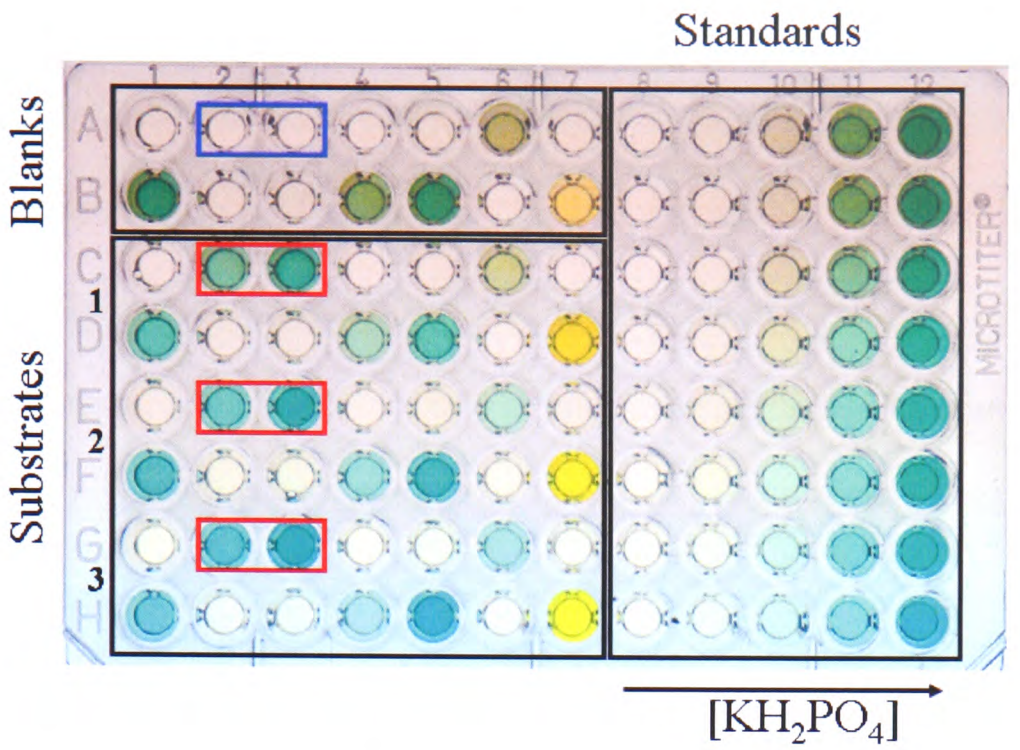

Figure 3.4 Malachite green assay plate containing blank reactions and standards. The reaction utilises the modified malachite green assay as described in section 2.6.2 and known concentrations of KH_2PO_4 as standards. The phosphate containing substrates are set up in triplicate reactions, note the presence of two 'hits' when comparing the substrates (indicted by the red boxes) to the blanks (indicted by the blue box).

3.5 Results

3.5.1 Splice Variant Analysis

Analysis of the PCR products from section 3.4.1 as shown in figure 3.5 revealed several bands which correspond directly to the expected size of certain PHOSPHO1 splice variants. Primer pair 1 should amplify both splice variant 1 and 2, however only a band of 230bp (band1, 230bp) corresponding to splice variant 2 is observed. Primer pair 2 should amplify splice variants 1 to 3 however only bands corresponding to splice variant 2 (band 2, 638bp) and splice variants 3 (band 3, 511bp) are present. To identify spice variant 4 primer pair 3 was used, the expected product sizes were 311bp (band 4) for large Exon 1 (1a and 1b) transcript and 202bp (band5) for a transcript containing exon 1a only, corresponding to splice variant 4. The sequence of each of these transcripts was determined and compared directly to

the ESTs which suggested the existence of each of these varients. This confirmed the existence of splice variants 2, 3 and 4. Interestingly analysis of the reading frames from the sequences of the EST clones reveal that only three proteins can arise from these splice variants due to the start codon arising on exon 2. The introduction of exon 3a causes this to be lost and due to a frame shift giving rise to a new start codon within exon 3a, however the introduction of exon Z causes the frame shift to be corrected thus creating a protein containing information from exon 2, Z, 3a and 3b. However as it was not possible to amplify splice varient 1, it either does not exist, or is not expressed within bone cells, thus only two potential proteins are present within bone cells (29 and 32 KDa forms).

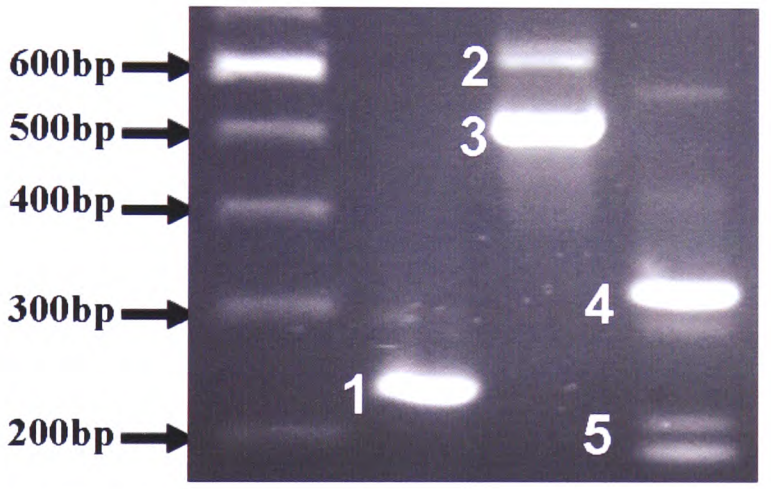

Figure 3.5 Agarose gel electrophoresis of PCR products corresponding to splice variants of human PHOSPHO1. 1 & 2 correspond to splice variant 2, 3 corresponds to splice variant 3, band 4 corresponds to variant 2 and 3, band 5 corresponds to variant 4.

3.5.2 Production of a pBAD-PHOSPHO1 Clone

pBAD-PHOSPHO1 clones were analysed for orientation in respect to the bacterial arabinose inducible promoter. As seen in figure 3.6 the clones display two different digestion patterns when digested with Sph1, Pme1 and Asc1. When in the correct orientation the clones should display DNA fragments equal to 2656bp,

1384bp and 833bp and when inverted, sizes 2656bp, 2103bp and 144bp would be present. From this is can be deduced that clone A and clone C have the PHOSPHO1 CDS in the correct orientation while clone B is inverted. All clones with PHOSPHO1 in the correct orientation were DNA sequenced and one displaying the correct sequence when compared to NM_178500 on the NCBI database used for recombinant protein production.

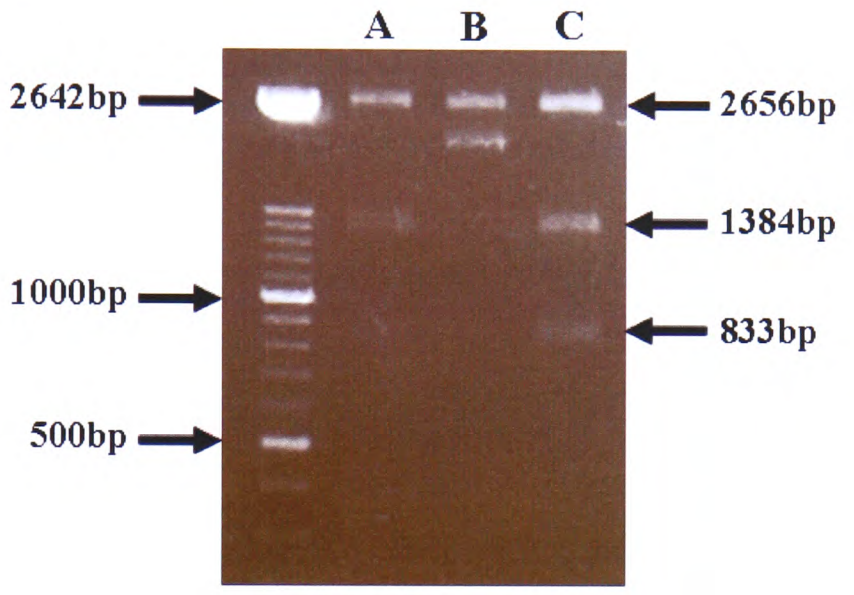

Figure 3.6 Analysis of three pBAD-PHOSPHO1 clones by restriction digestion with enzymes Sph1, Pme1 and Asc1. Clones A and C represent plasmids that have PHOSPHO1 CDS in the correct orientation.

3.5.3 Purification of Recombinant Human PHOSPHO1

Recombinant His-tagged PHOSPHO1 protein in fractions eluted from a Ni-NTA-agarose column were assayed by SDS-PAGE. Typically, fraction 2 yielded a single band of the expected mass (32 kDa) consistent with >99% purity (figure 3.7A). The final yield of protein was approximately 35 mg per 10 litres of culture. Western blotting of the purified protein yielded a band of expected size which showed the presence of the V5-epitope tag (figure 3.7B).

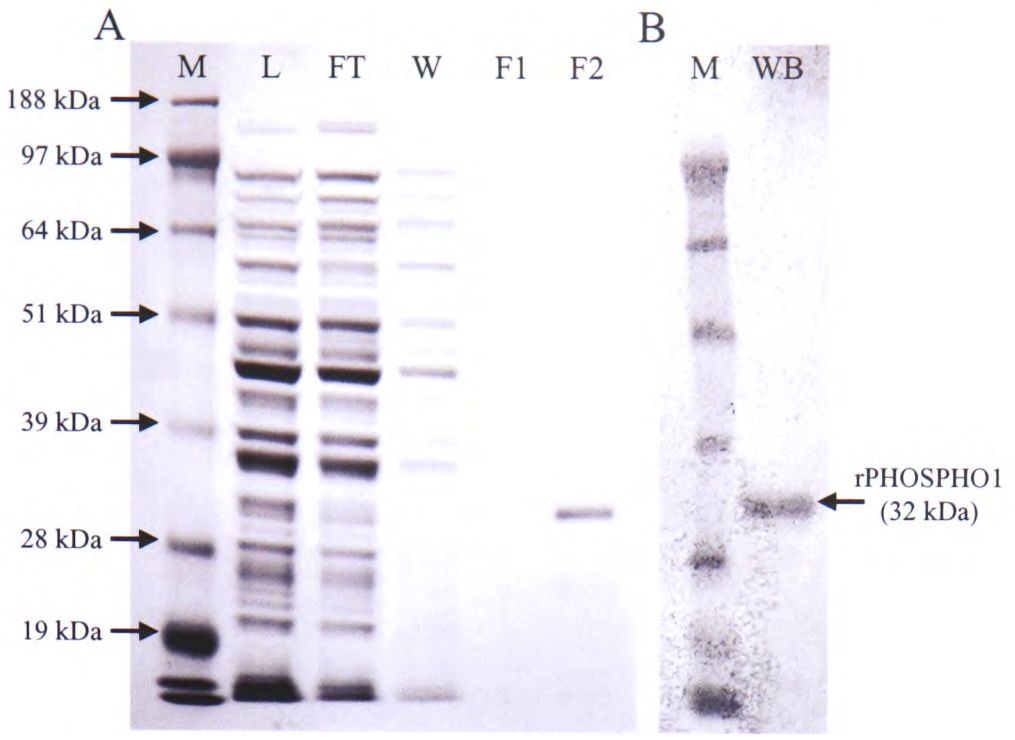

Figure 3.7 SDS-PAGE and Western analysis of purified recombinant human PHOSPHO1. (**A**), the cell lysate (L) and the flow-through (FT), wash (W) and eluted fractions 1 and 2 (F1 and F2) from each stage of Ni-NTA purification were subjected to SDS-PAGE under reducing conditions and visualised by Coomassie Blue staining. Molecular weight standards are also shown (M). (**B**), Western blot (WB) of the purified protein (1.2 μg) with anti-V5 antibody, which recognises the V5 epitope tag fused to the recombinant protein near its C-terminus.

MALDI-TOF mass spectrometry (commercial analysis at Moredun Research Institute, Functional Genomics Unit) was carried out on a purified recombinant PHOSPHO1 as a secondary method for protein identification and verification that it was indeed PHOSPHO1. The peptide masses were searched against the mascot database which returned a top score of 97 for the protein and was therefore identified as PHOSPHO1 (figure 3.8). This score is the probability mowse score for the peptides where the score is equal to -10*Log(P), where P is the probability that the observed match is a random event. Protein scores greater than 58 are significant ($p<0.05$). 13 of the identified peptides matched tryptic fragments of PHOSPHO1 spanning from the N to the C terminus of the protein.

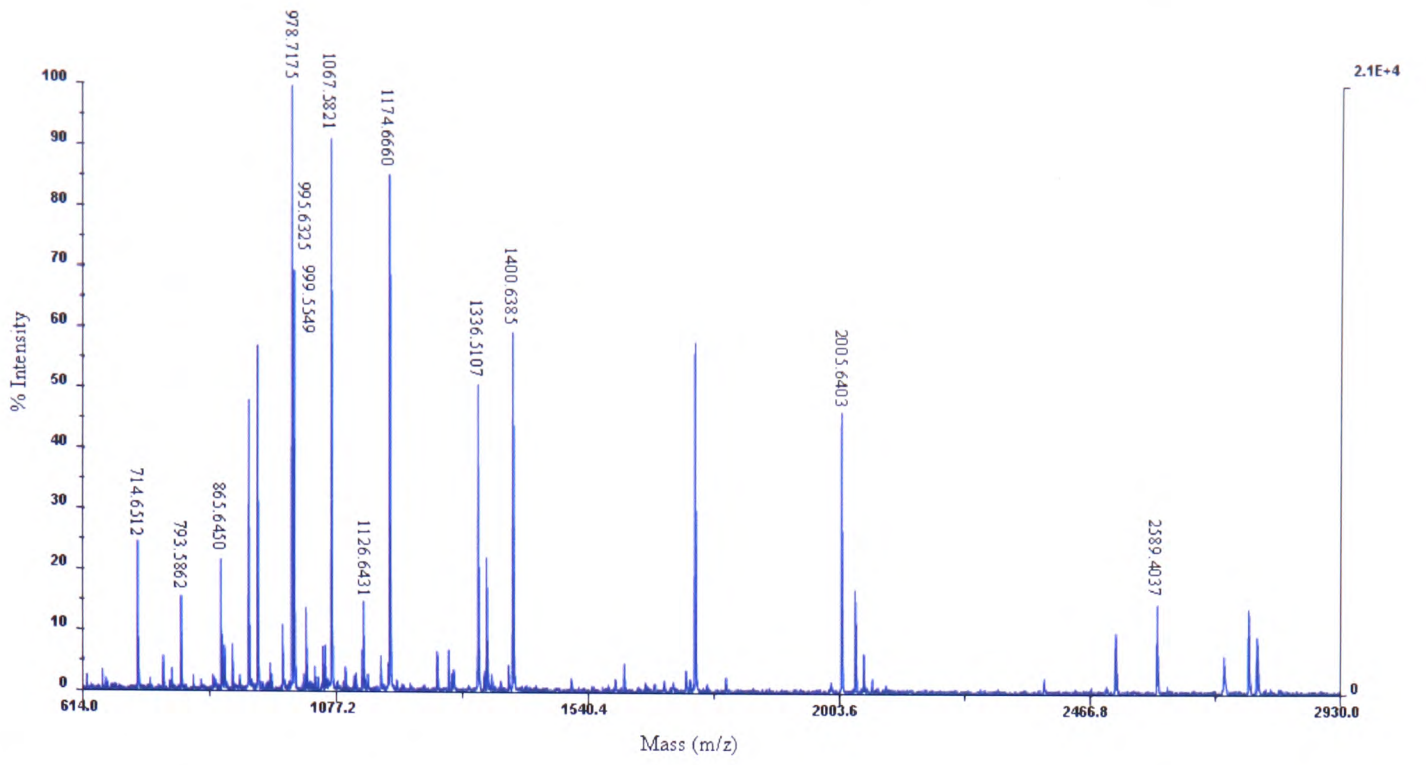

Figure 3.8 MALDI-TOF mass spectra of recombinant PHOSPHO1. All labelled peaks represent major fragments relating to tryptic peptides from the recombinant PHOSPHO1 protein (Expected peptide masses shown in appendix 5).

3.5.4 Catalytic Properties of Recombinant Human PHOSPHO1

3.5.4.1 Substrate Specificity

Twelve phosphate compounds were investigated as potential substrates for human PHOSPHO1. The resultant specific activities are shown in Table 3.1. PHOSPHO1 was found to have the highest specific activities toward phosphoethanolamine (PEA) and phosphocholine (PCho), with PEA being hydrolysed approximately 1.5 times faster than PCho. Six of the potential substrates tested (pyrophosphate, phospho-L-serine, glycerone phosphate, fructose-6-phosphate, phospho-L-tyrosine and ATP) yielded no detectable phosphatase activity.

Compound		Specific activity (units/mg)
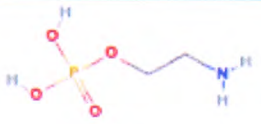	Phosphoethanolamine	4,600 ± 582
	Phosphocholine	2,980 ± 335
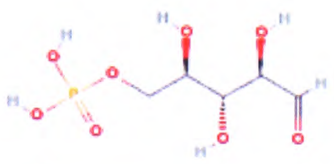	Ribose-5-phosphate	74.8 ± 6.2
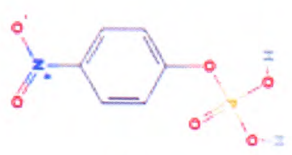	*p*-Nitrophenyl phosphate	64.5 ± 36.6
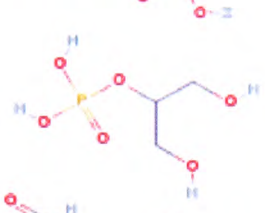	β-Glycerol phosphate	39.6 ± 6.2
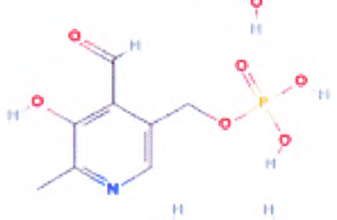	Pyridoxal-5-phosphate	17.6 ± 12.4
	Pyrophosphate	< 0.1
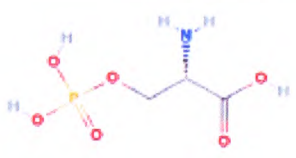	Phospho-L-serine	< 0.1
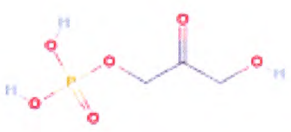	Glycerone phosphate	< 0.1
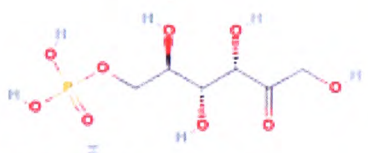	Fructose-6-phosphate	< 0.1
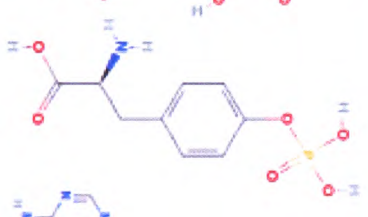	Phospho-L-tyrosine	< 0.1
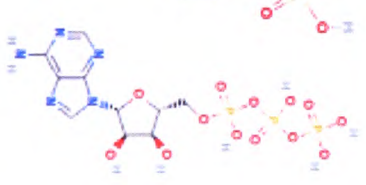	ATP	< 0.1

Table 3.1 Substrate specificity of recombinant human PHOSPHO1. Recombinant human PHOSPHO1 (3 µg/ml) was incubated with each substrate and assayed for phosphatase activity by the discontinuous assay at 37°C. The 200 µl reaction mixture contained 25% (v/v) glycerol, 20 mM TBS, pH 7.2, 25 µg/ml BSA, 2.5 mM substrate and 2 mM $MgCl_2$. The results are the averages of triplicate assays.

3.5.4.2 Magnesium and pH Optimum

The concentration of $MgCl_2$ was varied between 2 μM and 200 mM and activity was found to be maximum at 2 mM $MgCl_2$. In the presence of 2 mM Mg^{2+} at 37°C, the recombinant enzyme exhibited a pH optimum around 6.7 for both PEA and PCho (figure 3.9). High catalytic activity (greater than 70% of maximum) was observed between pH 6.0 and 7.2. This high level of activity extends up to at least pH 7.5 for PEA but begins to decline significantly for PCho after pH 7.2.

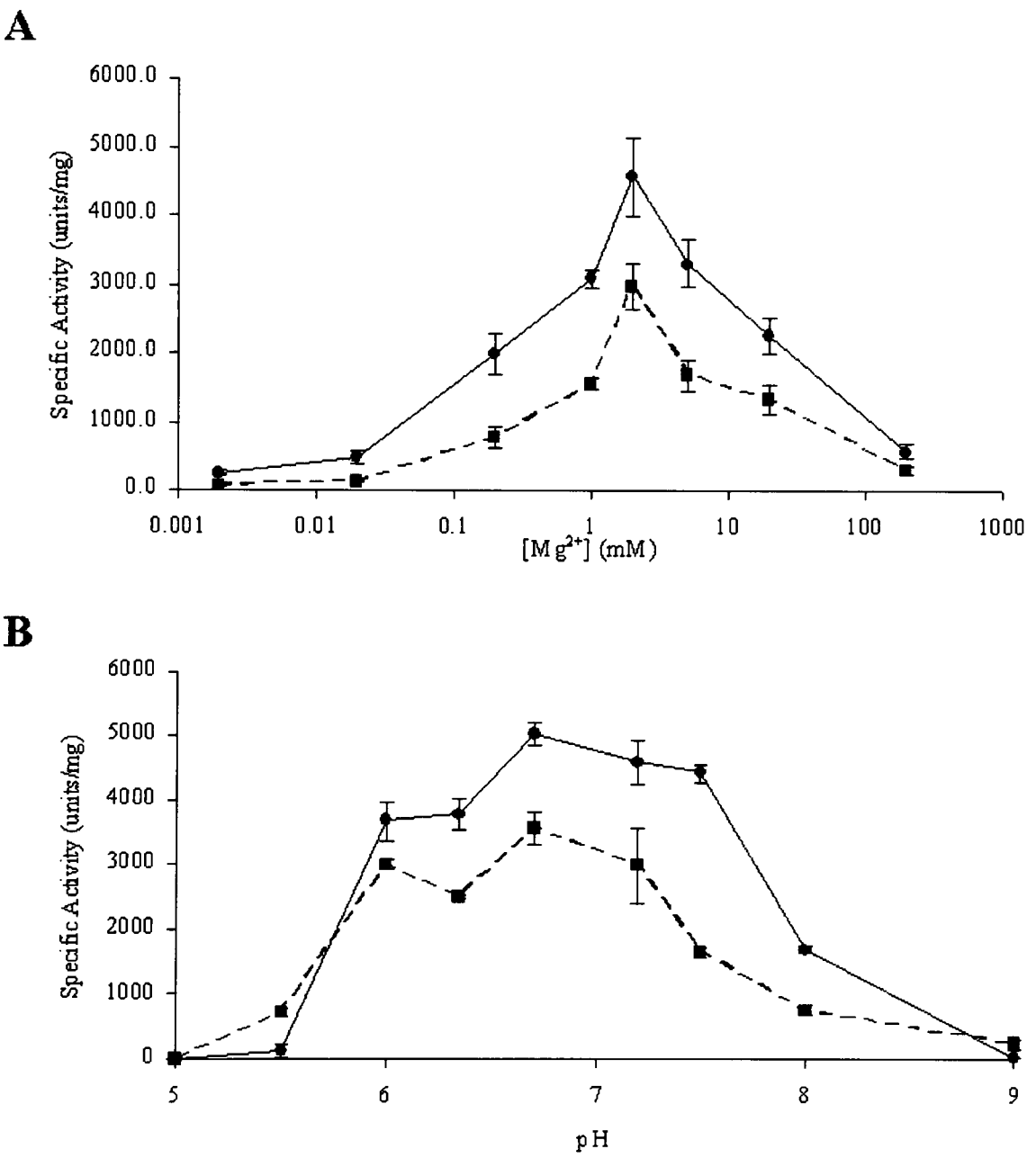

Figure 3.9 Determination of the optimum conditions for activity of recombinant PHOSPHO1. Enzymatic activity was measured in the presence of 3 μg/ml enzyme concentration (**A**) dependence of apoenzyme activation by Mg^{2+} for PEA (solid line) and PCho (dashed line); (**B**) the optimum pH was measured utilising buffers spanning pH 5 to 9, enzyme activity was measured using the discontinuous assay in the presence of 2 mM Mg^{2+}, for PEA (solid line) and PCho (dashed line).

3.5.4.3 Kinetic Constant Determination

The kinetic constants of recombinant PHOSPHO1 were determined for PEA and PCho using the continuous coupled assay in the presence of 2 mM Mg^{2+} at 37°C (pH6.7). The enzyme exhibited Michaelis-Menten kinetics for both substrates (Hill coefficients = 1.00). A plot of reaction rate versus substrate concentration for PEA and PCho and also Lineweaver-Burke plots, allowing the calculation of K_m and V_{max} values, are shown in figure 3.10 for PEA and 3.11 for PCho. PHOSPHO1 displayed an apparent K_m of 3.0 μM and a k_{cat} of 2.27 s^{-1} for PEA, and a K_m of 11.4 μM and a k_{cat} of 1.98 s^{-1} for PCho.

3.5.4.4 Requirement for Metals

To investigate the requirement of metal ions for the recombinant enzyme, the purified enzyme solution was extensively dialysed against metal-free buffer to remove any weakly bound metal ions. The effect of different metal ions on the hydrolysis of PEA and PCho was assessed by addition of 2 mM concentrations of various metal salts. As controls, reactions were also carried out in buffers without added metal ions. The results are shown in figure 3.12.

The phosphatase activity was approximately 80-fold higher for both substrates in the presence of Mg^{2+} compared to the metal-free control. Co^{2+}, Mn^{2+} and Ni^{2+} also stimulated activity but to a lesser extent than Mg^{2+}, whereas the presence of Ca^{2+} and Zn^{2+} had no apparent effect on activity compared to the control ($Mg^{2+} > Co^{2+} > Mn^{2+} > Ni^{2+} > Ca^{2+} = Zn^{2+}$ = no metal). Interestingly, PHOSPHO1 has a higher activity toward PCho than to PEA in the presence of Co^{2+} and Mn^{2+}. This is

most likely to be due to an allosteric effect caused by a difference in the metal-binding properties of each enzyme-substrate complex.

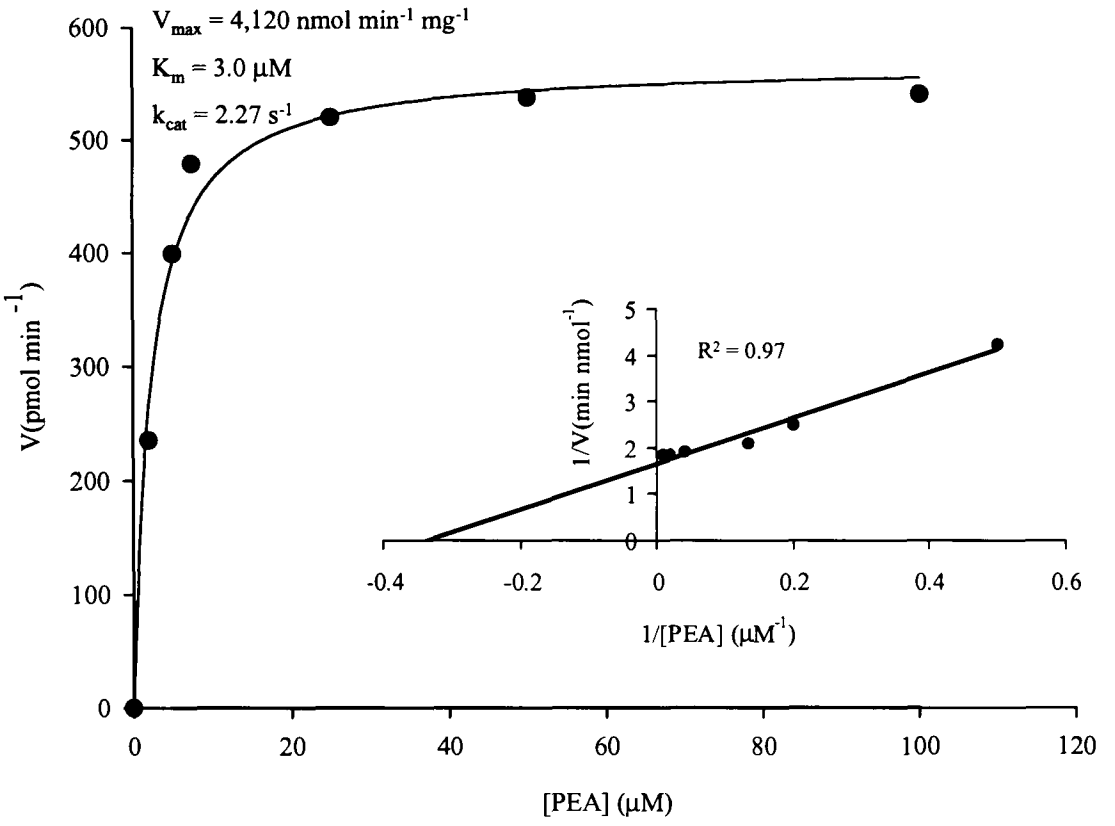

Figure 3.11 Kinetic analysis of substrate hydrolysis catalysed by recombinant PHOSPHO1. Kinetic activity towards **(A)** phosphoethanolamine and **(B)** phosphocholine, measured using the continuous assay as described in 2.6.2. Shown are the reaction velocities (V) as a function of substrate concentration. *Insets*, Lineweaver-Burke plots from which K_m and V_{max} values were calculated, k_{cat} = V_{max}/[PHOSPHO1].

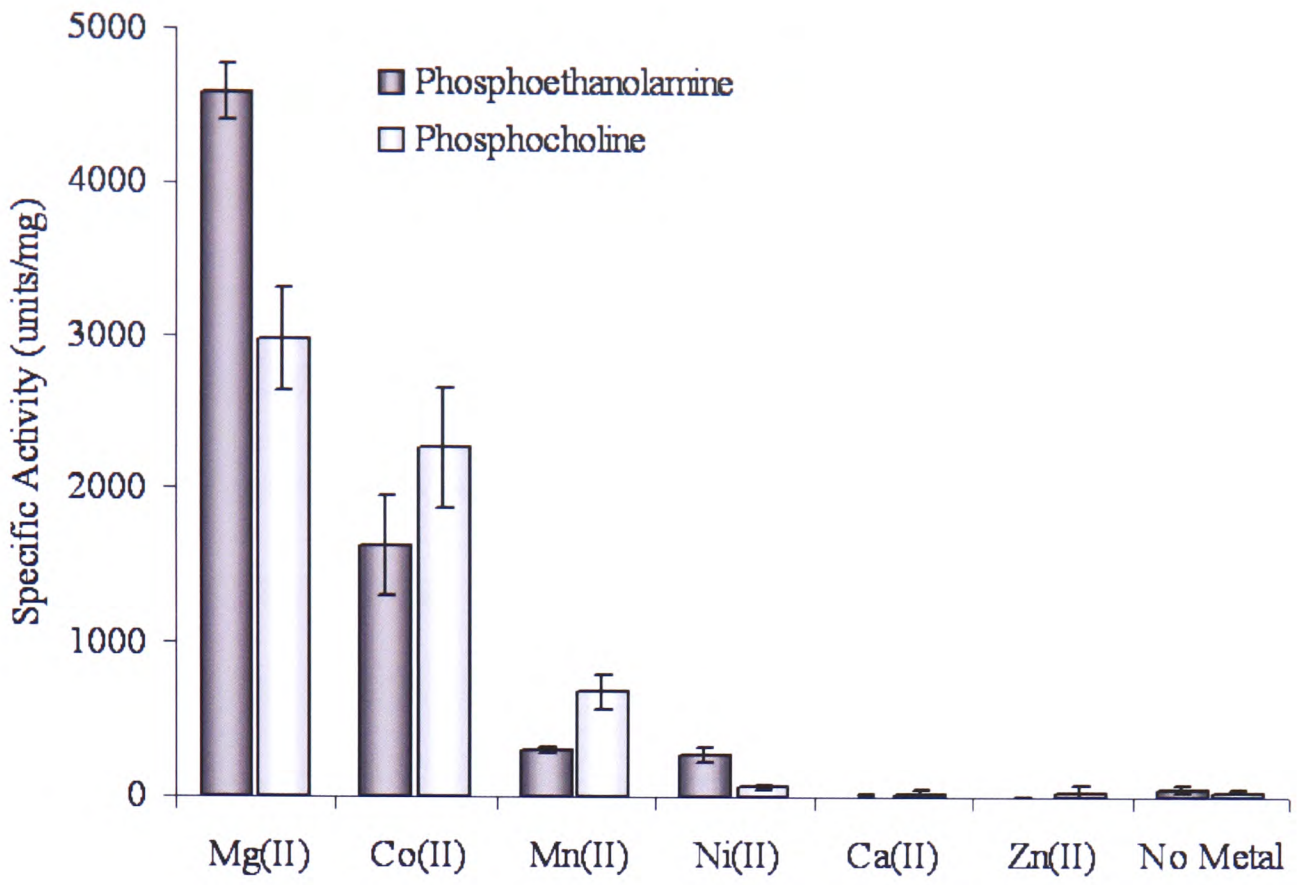

Figure 3.12 Metal requirement for activity of recombinant PHOSPHO1. Enzyme activity toward PEA (shaded boxes) and PCho (white boxes) was measured in the presence of the indicated metal ions (final concentration 2 mM). *No metal*, the activity of the apoenzyme was measured in the absence of added metals.

3.5 Discussion

The characterisation of the human PHOSPHO1 gene reveals five splice variants from which 3 proteins with alternative N terminal regions can be produced. This is not uncommon within the haloacid dehalogenase superfamily, in fact H^+-K^+-ATPases show a somewhat similar splicing pattern with alternative transcriptional initiation and mRNA splicing giving rise to distinct N-terminal variants of the HKalpha2 subunit (Kone and Higham, 1998). The splice variants of PHOSPHO1 only differ in the N terminal region thus these variants are perhaps encoding PHOSPHO1 proteins with slightly different functions within or outside the cell. In

fact when the variant with the 3a Exon is analysed with the SignalP package it has a relatively strong secretory domain hinting that this form is either being secreted or in some way signalled to somewhere in the cell. All three domains within the PHOSPHO1 gene are conserved within the exon 3b thus indicating that these splice variants are all functioning against a common substrate or substrate structure, as with the example of H^+-K^+-ATPases, the N terminal alteration causes the differences in pharmacological profile but not on substrate specificity. Although ESTs are present for all 5 splice variants, hence indicting the potential for all three proteins to be expressed, only two are present in bone cells as no splice variant containing the Z exon could be amplified from SaOS-2 cell RNA. The lack of quantitative data for these two transcripts, however, mean that no hypothesis to which isoform is more predominant can be formed.

The results of the biochemical characterisation show that PHOSPHO1 has an activity which is typical of most enzymes within the HAD superfamily, with a strong Mg^{2+}-dependence and a pH optimum within the acid-to-neutral pH range (Morais *et al*, 2000; Klutts *et al*, 2003; Wu and Woodard, 2003). A high level of activity extends up to at least pH 7.5 for PEA but begins to decline significantly for PCho after pH 7.2. The pH of the extracellular fluid of growth plate cartilage is close to pH 7.6 (Howell *et al*, 1968) and so the activity of PHOSPHO1 may be restricted mainly to PEA at this region. Overall, PHOSPHO1 has a high specific activity toward PEA and PCho compared with the other phosphomonoesters investigated, which is not surprising due to the high degree of structural similarity between these two compounds. The results are highly significant for the mineralisation process in cells. Both PCho and PEA are present in mineralising cells and are the two most abundant

phosphomonoesters in cartilage (Kvam *et al*, 1992). The very low K_m values for both PEA and PCho (μM range) suggest that they would be half-saturated at levels of 3 and 11.4 μM, respectively. This indicates that under the reported conditions both substrates would be rapidly hydrolysed. These compounds are therefore likely to be natural substrates of PHOSPHO1.

The hydrolysis of PEA and PCho is known to occur *in vivo*, although the enzyme responsible has not been identified previously. It has been hypothesised that PEA is a natural substrate for TNAP (Whyte, 1994, 1995) due to an increase in its urinary excretion in patients diagnosed with hypophosphatasia (Rasmussen, 1968). However, this appears unlikely following examination of kinetic data for the TNAP-catalysed hydrolysis reaction at physiological pH, with reported high K_m values at mM concentrations (Tenenbaum and Palangio, 1987; Fedde *et al*, 1988; Muller *et al*, 1989). It is therefore possible that the genetic defect assumed to be caused by a loss of TNAP in hypophosphatasia is actually due to a loss or defect of PHOSPHO1. Although the mutation which causes this disease is mapped directly to the TNAP gene an indirect effect on PHOSPHO1 activity can not be ruled out. It is known that when TNAP is absent the components of the extracellular fluid are altered (Anderson *et al*, 2004). Brain alkaline phosphatase (BAP), an isoenzyme of TNAP, is reported to have PCho phosphatase activity (Sok, 1999). However, the specific activity of BAP toward PCho in the reported study was measured under alkaline conditions (pH 8.5) and is likely to be much lower at physiological pH. PCho hydrolysis has been studied in hamster heart and is not catalysed by alkaline phosphatase but by a separate unidentified enzyme (Hatch and Choy, 1987). It has also been shown that the hydrolysis of PEA and PCho is due to the action of an acid phosphatase in a

variety of tissues including bone and teeth (McDonald *et al*, 1980), a study which agrees well with our present finding that PHOSPHO1 displays high activity toward both substrates between pH 6.0 and 7.2.

PEA and PCho are metabolites in the cytidine 5'diphosphoethanolamine (CDP-EA) and cytidine 5'-diphosphocholine (CDP-Cho) pathways, respectively (Scheme 3.1). These are the main pathways involved in the formation of phosphatidylcholine and phosphatidylethanolamine (Walkey *et al*, 1997), which are involved in the metabolism of complex glycerolipids, GPI-anchors, prostaglandins, leukotrienes and the amino acids glycine, serine and threonine (Kanehisa, 2002). These pathways are also implicated in the pathogenesis of Alzheimer's and Huntington's disease (Ellison *et al*, 1987; Farber *et al*, 2000). Therefore the identification of a phosphatase with specificity toward PEA and PCho is highly significant. Conversely, phosphatidylethanolamine and phosphatidylcholine may be hydrolysed by phospholipase C to form PEA and PCho, respectively (van Dijk *et al*, 1997). The synthesis of phosphatidylcholine from choline by the CDP-Cho pathway in mineralising cells has previously been investigated. PCho accumulation is greatly decreased in neo-natal rat calvaria compared with the liver of the same animal (Stern and Vance, 1987). PCho concentration is usually determined by the relatively higher activity of choline kinase compared with that of phosphate cytidylyltransferase 1. However, the low PCho accumulation in mineralising compared with non-mineralising cells may be due to the upregulation of PHOSPHO1. PHOSPHO1 is highly expressed at sites of mineralisation (Houston *et al*, 2004) and as a consequence will reduce the levels of PCho and PEA in chondrocytes and osteoblasts. P_i may be scavenged from PEA and PCho during the mineralisation

process in order to generate the concentration required for hydroxyapatite crystal formation.

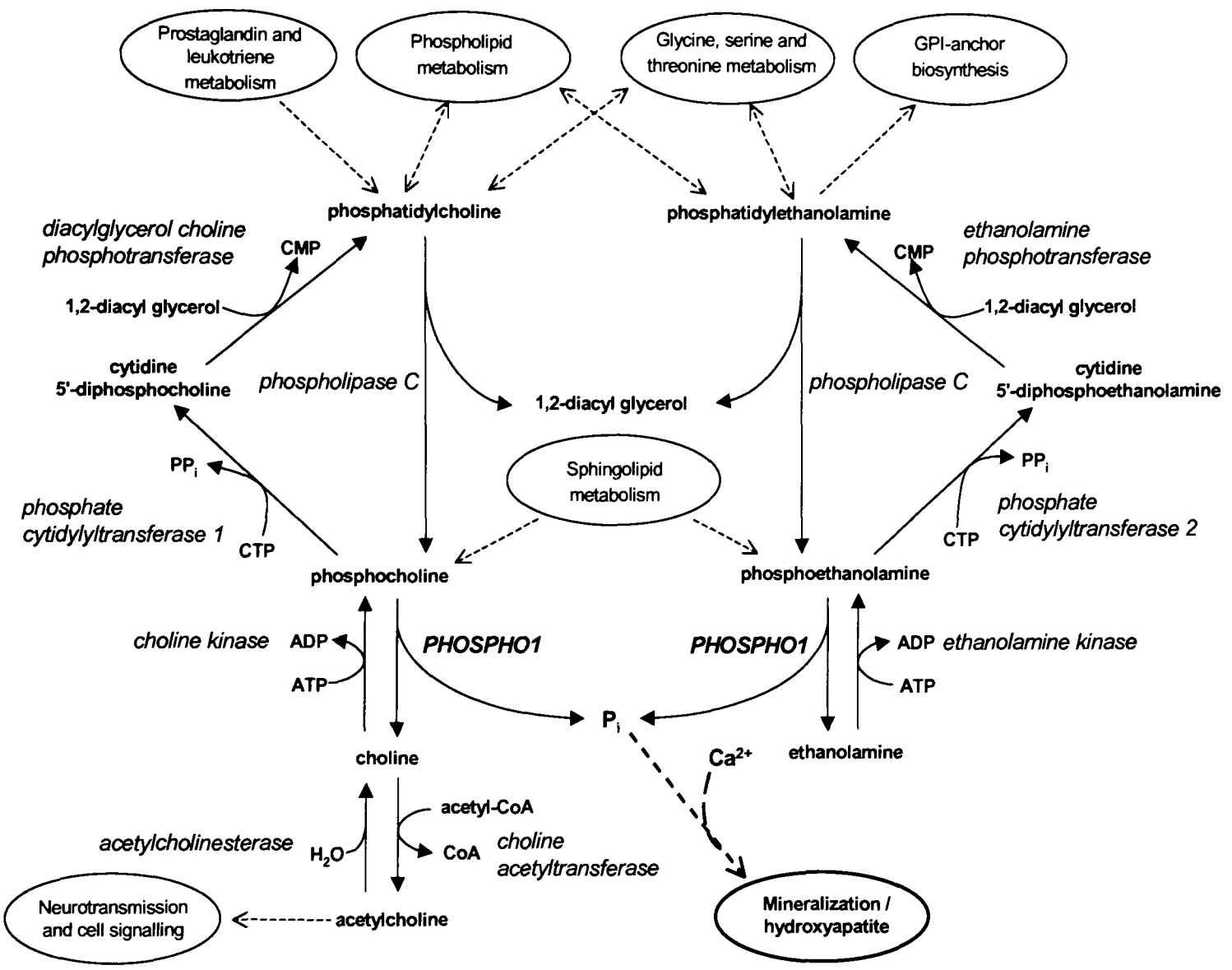

Scheme 3.1 Human PEA and PCho metabolism. Proposed metabolic pathways for the generation of PEA and PCho. The basis of the diagram is information from the Kyoto Encyclopedia of Genes and Genomes (KEGG) (Kanehisa *et al*, 2002).

The MV-membrane is a rich source of both phosphatidylethanolamine and phosphatidylcholine and may act as a pool for PEA and PCho in MVs. Wu *et al,* (2002) have found that the phosphatidylethanolamine and phosphatidylcholine composition of the MV membrane decreases during mineralisation and that 1,2-

diacyl glycerol accumulates in MVs, indicative of phospholipase C activity. However in the absence of any kinetic data relating to phosphatidylethanolamine or phosphatidylcholine degradation in MVs it is impossible to say at this time whether such a mechanism exists as a viable means of generating PEA or PCho. Ca^{2+} and P_i are present at high levels in MVs even before induction of mineral formation and are derived from cellular activity prior to MV formation (Wu *et al*, 1997). Since the ambient concentration of P_i in the extracellular fluid is close to 2 mM (Wuthier, 1977), it is doubtful that the amount of P_i released from MV lipids would be sufficient to increase the overall level of extracellular P_i. However, the local effect of this limited release may be sufficient to alter the Pi/PPi ratio thus facilitating mineral formation.

In conclusion, these results show for the first time that human PHOSPHO1 is a PEA and PCho phosphatase. PHOSPHO1 is known to be upregulated in mineralising cells, these findings therefore provide a novel means of generating P_i in mineralising cells and may have implications for the diagnosis hypophosphatasia and treatment of bone mineralisation abnormalities such as osteomalacia and pathological soft-tissue ossification, a process clinically significant in atherosclerosis and heart failure.

CHAPTER 4

PROBING THE SUBSTRATE SPECIFICITIES OF HUMAN PHOSPHO1 AND PHOSPHO2

Chapter Contents

4.1 Introduction

The discovery of PHOSPHO1 provides a close link between PEA and PCho accumulation and the generation of Pi in mineralising cells. PHOSPHO1 is therefore a potential target in the design of new therapeutics toward diseases such as osteopetrosis and craniosynostosis, which lead to skeletal abnormalities characterised by excess or premature mineral formation (Kaplan *et al*, 1991). Inhibition of PHOSPHO1 may also be of benefit in the treatment of vascular calcification, a process that shares many similarities with the mineralisation of bone and is clinically significant in atherosclerosis and heart failure (Boström, 2001).

Enzymes of the HAD superfamily catalyse the hydrolysis of C-Cl, C-OP and C-P bonds from a wide range of substrates and demonstrate great functional diversity from a single protein fold. The amino acid sequence of PHOSPHO1 contains three motifs that are conserved within the HAD superfamily. These motifs form the active site of this group of enzymes, which includes a variety of magnesium-dependent phosphatases (Ridder and Dijkstra, 1999). In motif 1, DXDX(T/V), both Asp residues coordinate to the catalytic Mg^{2+} ion, and the first Asp also forms a phospho-protein intermediate during hydrolysis (Wang *et al*, 2002). In motif 2, (S/T), the conserved serine or threonine is involved in hydrogen bonding to a phosphoryl oxygen. Motif 3, $K(X)_{18\text{-}30}(G/S)(D/S)XXX(D/N)$, is also involved in phosphoryl oxygen hydrogen bonding and coordination to the Mg^{2+} ion (Wang *et al*, 2002; Collet *et al*, 1999).

A search for homologous proteins to PHOSPHO1 revealed the sequence of PHOSPHO2, a putative human phosphatase that shares 42% sequence identity with human PHOSPHO1. Analysis of ESTs in dbEST indicate that PHOSPHO2 is

expressed in a wide range of tissues. In addition, analysis of transcript levels in chick has revealed that the transcript is present in both mineralising and soft tissues and expression is comparable in all tissues analysed as shown in figure 4.1B (Houston, unpublished data). The transcript levels do not alter depending on degree of chondrocyte differentiation and transcript is present in both SaOS-2 and MG-63 cells, which is the converse of PHOSPHO1 expression, as shown in figure 4.1. Orthologous proteins to PHOSPHO2 were also found and figure 4.2 shows a sequence alignment of PHOSPHO1 and PHOSPHO2 proteins from a number of species. Analysis of sequences with the program SignalP v3.0 (Bendtsen *et al*, 2004) suggests the absence of any signal sequences in the PHOSPHO1 or PHOSPHO2 proteins suggesting both enzymes are cytosolic. Closer inspection of the amino acid sequence of PHOSPHO2 protein revealed that all three catalytic motifs are conserved. Also conserved are Asp19 and Asp99, which correspond to two residues (Asp43 and Asp123) previously postulated to be involved in substrate-specific interactions in PHOSPHO1 (Stewart *et al*, 2003). These two residues were found to line the substrate-binding pocket in a structural model of PHOSPHO1 (as shown in figure 4.3), and are the only residues in this region that are conserved between orthologous proteins from other species, but not in PSPs, which are a closely related group of enzymes within the HAD superfamily. In contrast, in PSP with bound substrate (PDB: 1L7P; Asp11Asn mutant), Glu20, Met43, Phe49 and Arg56 have been shown to be involved in phospho-L-serine binding, and these residues are fully conserved in PSPs, but not present in PHOSPHO1 or PHOSPHO2 (Wang *et al*, 2002). These observations have led to the suggestion that PHOSPHO1 and

PHOSPHO2 might utilise the same, or highly similar substrates. If true, this would intimate functional redundancy between PHOSPHO1 and PHOSPHO2 *in vivo*.

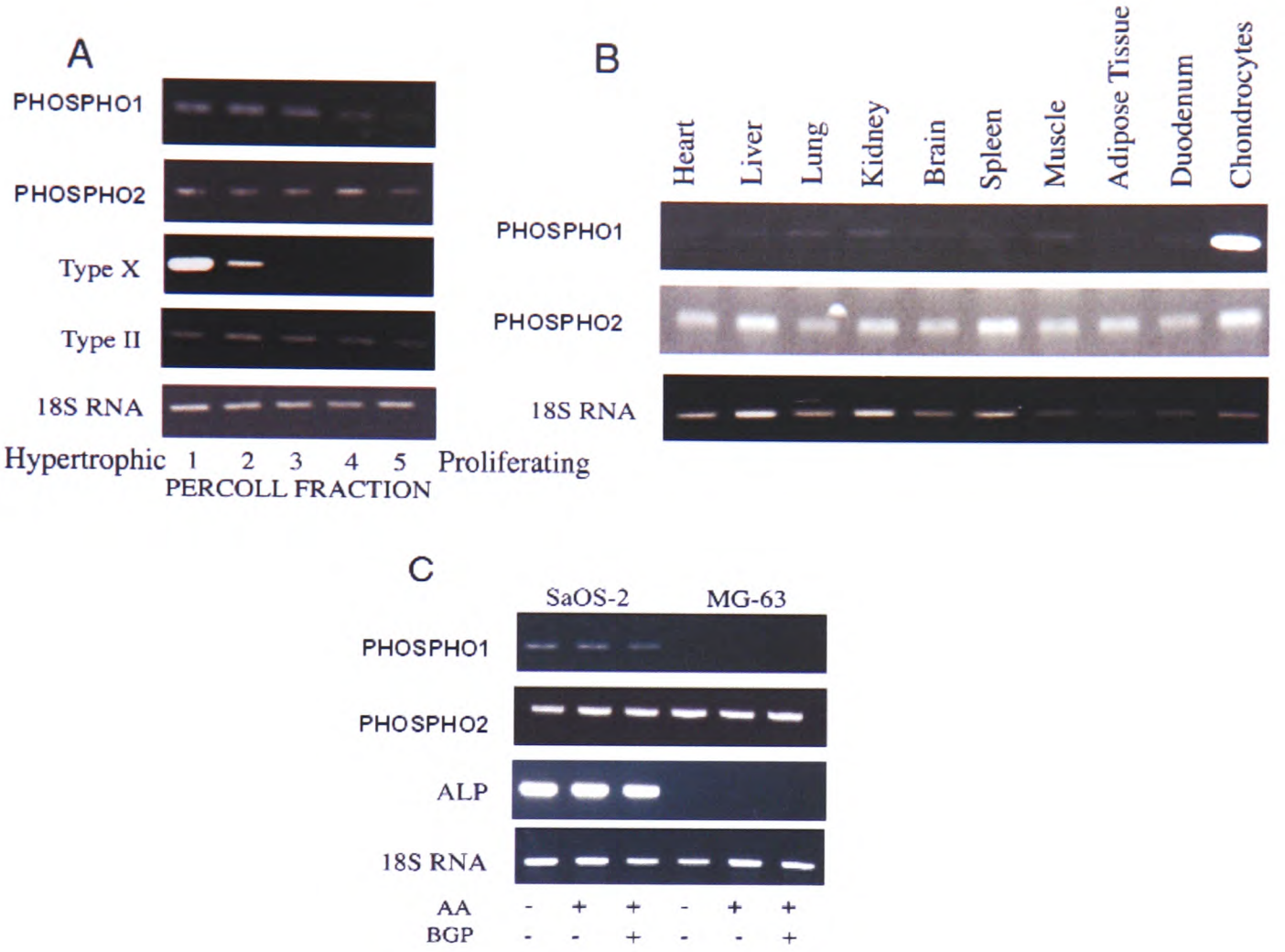

Figure 4.1 Analysis of PHOSPHO2 expression in tissues and cells. (A) Expression of PHOSPHO1, PHOSPHO2 and marker genes in growth plate chondrocytes at varying stages of differentiation (B) Expression of PHOSPHO1 and PHOSPHO2 in chick tissues (C) Expression of PHOSPHO1, PHOSPHO2 and TNAP (ALP) in the human osteoblast cell lines SaOs-2 and MG-63 (Houston *et al*, 1998 and unpublished data).

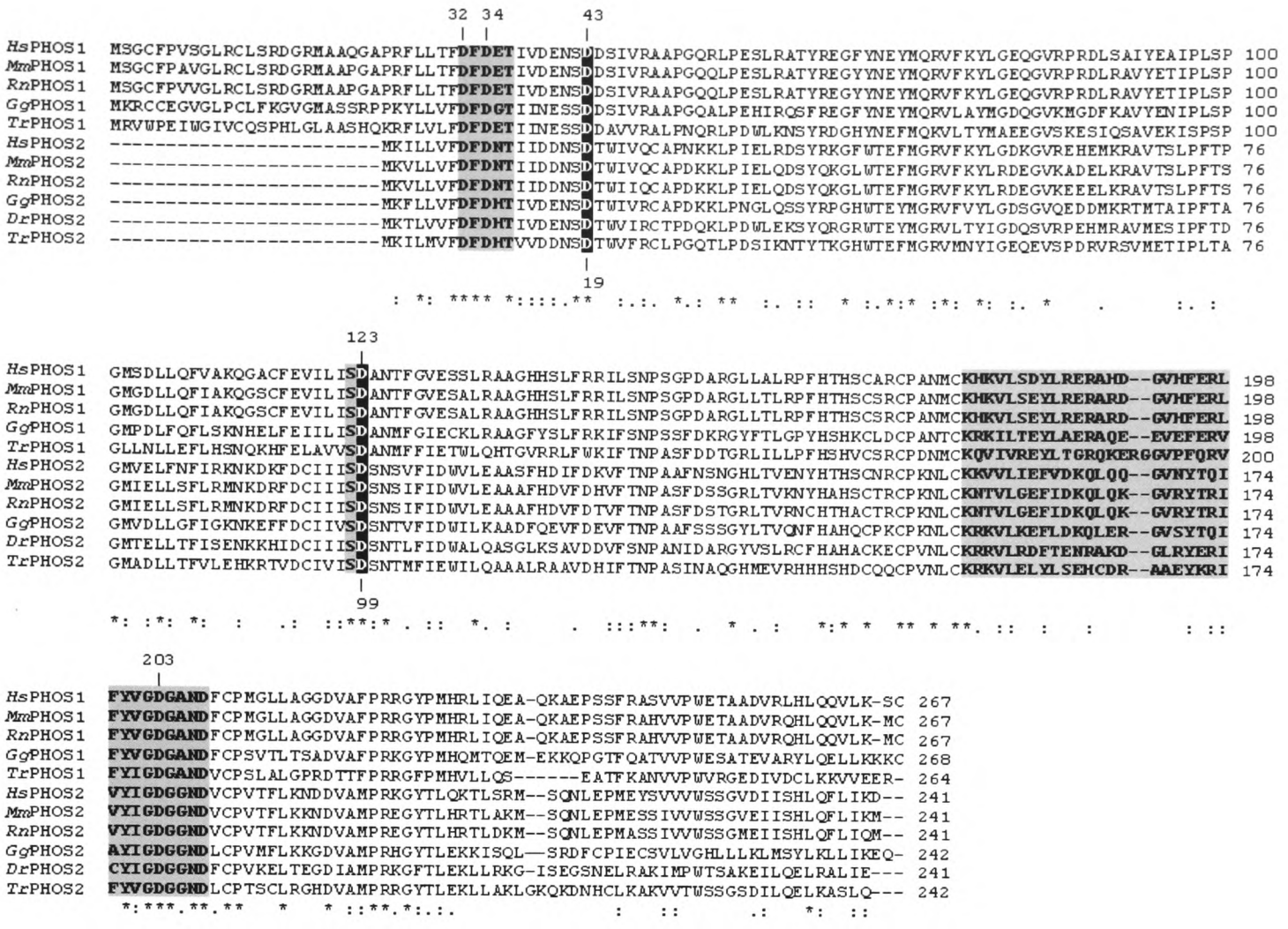

Figure 4.2 Alignment of the amino acid sequences of PHOSPHO1 with PHOSPHO2 and its homologues. The three catalytic motifs are highlighted in grey. The white on black letters denote residues which are proposed to be involved in substrate specific interactions. The following sequences are used (accession numbers are shown in parentheses): *Hs*PHOS1, human PHOSPHO1 (Q8TCT1); *Mm*PHOS1, mouse PHOSPHO1 (Q8R2H9); *Rn*PHOS1, rat PHOSPHO1; *Gg*PHOS1, chicken PHOSPHO1 (O73884); *Tr*PHOS1, puffer fish PHOSPHO1; *Hs*PHOS2, human PHOSPHO2 (Q8TCD6); *Mm*PHOS2, mouse PHOSPHO2 (Q9D9M5); *Rn*PHOS2, rat PHOSPHO2 (XP_230005); *Gg*PHOS2, chicken PHOSPHO2 (XP_422006); *Dr*PHOS2, zebrafish PHOSPHO2 (ENSDARP00000004689); *Tr*PHOS2, puffer fish PHOSPHO2 (SINFRUP00000138420). "*" = identical or conserved residues in all sequences in the alignment, ":" = indicates conserved substitutions and "." = indicates semi-conserved substitutions.

In this study site directed mutagenesis has been used to confirm PHOSPHO1 as a member of the HAD superfamily and also to ascertain the importance of Asp43 and Asp123 residues for the catalysed hydrolysis of PEA and PCho. The activity of PHOSPHO2 protein toward PEA and PCho as well as a range of other potential substrates is investigated. In addition, structural models of PHOSPHO1 and

PHOSPHO2 based upon the X-ray crystal structure of PSP from *Methanococcus jannaschii* are presented and potential enzyme-substrate interactions using *in silico* ligand docking experiments examined.

Figure 4.3 PHOSPHO1 binding site showing 4 residues targeted for mutation. Asp32 and Asp203 are critical for bond hydrolysis in the HAD superfamily, whereas Asp43 and Asp123 have been hypothesised to be involved in substrate specific interactions. The Mg^{2+} ion is coloured green and the Phosphate moiety coloured orange.

4.2 Hypothesis

That PHOSPHO2 displays a similar substrate specificity profile to PHOSPHO1 due to the conservation of the three catalytic motifs found in PHOSPHO1 and residues that have previously been implicated in substrate specific interactions. Also that D32 and D203 are essential for PHOSPHO1 mediated catalysis of PEA.

4.3 Aims

I. To produce a recombinant human PHOSPHO2 protein in an identical manner to the PHOSPHO1 protein described in chapter 3 and compare substrate specificity profile of the two enzymes

II. To create mutants of the PHOSPHO1 protein to confirm its identity as a HAD enzyme and to investigate substrate binding residues of the active site.

III. To study the kinetic parameters of the mutant PHOSPHO1 protein to allow an assessment of mutational effect.

IV. To model the PHOSPHO2 protein and compare this to the existing PHOSPHO1 model allowing an assessment of active site differences and further investigate residues essential for catalysis.

4.4 Materials and methods

4.4.1 Site-Directed Mutagenesis of Human PHOSPHO1

DNA corresponding to Met19-Cys267 of human PHOSPHO1 was amplified and cloned into the pBAD TOPO TA vector (Invitrogen) as described in chapter 3. Oligonucleotide-directed mutagenesis was used to prepare cDNAs encoding the PHOSPHO1 mutants. Mutagenesis was performed using the QuikChange Site-Directed Mutagenesis kit (Stratagene). This kit utilises PCR-based methodology using overlapping sense and antisense primers containing the desired mutation. As the primers intrinsically become part of the PCR product the mutation will be

incorporated into the product produced by PCR as described in 2.4.4. Briefly the reaction mixture used for mutagenesis contained 500ng PHOSPHO1 clone, 125 ng each primer (sequences shown in appendix 6), 1 µl dNTP mix, 2.5units Pfu Turbo DNA Polymerase. The reaction was cycled at 60 seconds at 95°C for 1 cycle, 50 seconds at 95 °C; 50 seconds at 60 °C; 300 seconds at 68 °C, for 18 cycles, followed by 420 seconds at 68 °C for one cycle. Treatment of DNA after PCR with the restriction enzyme, DpnI, selectively destroys the parental DNA while leaving the newly mutated DNA intact. This is due to the parental DNA being methylated when cloned in bacteria. The restriction enzyme DpnI will only digest methylated DNA and since PCR-amplified DNA is unmethylated it will survive the digestion process. The digest was conducted as described in 2.3.8 utilising the entire PCR reaction and 10U Dpn1 enzyme. Five mutants were prepared in this manner (D32N, D43N, D123N, D203S and a double mutant D43N/D123N). The digestion mixture (1 µl) was then used to transform TOP10 cells as described in 2.3.1. Liquid cultures and plasmid mini-preparations of individual clones were subsequently carried out (section 2.3.2 and 2.3.3 respectively). Clones containing the desired mutation(s) were identified commercially (The UK Centre for Functional Genomics in Farm Animals (ARK-Genomics), Roslin, UK) by nucleotide sequence analysis across the mutation site. The mutant proteins were expressed utilising the shake flask method as described in 2.5.5.2 and purified by Immobilised Metal Affinity Chromatography (IMAC) as described in 2.5.6. The secondary structures of the mutants were compared to that of wild type recombinant PHOSPHO1 using circular dichroism (CD) to confirm that in each case, the mutation(s) had not affected the overall fold of the enzyme. CD spectra were recorded on a JASCO J-600 spectropolarimeter by

using 0.5 mg/ml solutions of the recombinant PHOSPHO1 proteins in 20 mM potassium phosphate, pH 7.2, 130 mM sodium sulphate. CD analysis was performed by Dr Sharon Kelly, University of Glasgow.

4.4.2 Production of Recombinant PHOSPHO2 Protein

DNA corresponding to PHOSPHO2 was amplified from human genomic DNA, as the whole coding sequence was found to be on the same exon, by PCR as described in 2.4.4. The expression plasmid of choice was the pBAD TOPO TA vector (Invitrogen) as used for PHOSPHO1 and PHOSPHO1 mutant expression. The cDNA fragment was ligated into the pBAD TOPO TA vector (2.3.9.1) and this used to transform TOP10 cells as described in 2.3.1 (nucleotide and protein sequences shown in appendix 3). Liquid cultures and plasmid mini-preparations of individual clones were subsequently carried out (section 2.3.2 and 2.3.3 respectively). A clone containing the PHOSPHO2 fragment in the correct orientation was identified by restriction digestion of plasmid minipreps as described in 2.3.8. Briefly the plasmid DNA was digested with the restriction enzymes Nco1 and *HindIII* the latter is found only within the PHOSPHO2 CDS. The *E. coli* expressing the recombinant protein were grown in a 10L fermentation vessel as outlined in section 2.5.5.1. The recombinant protein was purified by Immobilised Metal Affinity Chromatography (IMAC) as described in 2.5.6.

4.4.3 Phosphatase Assays

The standard discontinuous colorimetric assay used was based on that of Baykov *et al*, (1988) as described in section 2.6.2 utilising 600ng of purified

recombinant enzyme per reaction. Buffers used were 20 mM MES, pH 6.7 for the PHOSPHO1 and mutants assays and 20 mM Tris-HCl pH 7.2 for the PHOSPHO2 experiments to allow the direct comparison with previous results. Twelve compounds were analysed for phosphatase activity by PHOSPHO2 (figure 4.8); whereas PEA and PCho were analysed for hydrolysis by PHOSPHO1 mutants. Specific activities were calculated in units of activity per mg enzyme, where 1 unit of activity equals the hydrolysis of 1 nmol phosphate/min.

To analyse kinetic constants for these reactions the continuous spectrophotometric assay was performed using the EnzChek® Phosphatase Assay Kit (Molecular Probes) as described in 2.6.2 utilising 0.65 μg of PHOSPHO1 or 9.98 μg PHOSPHO2 at 37°C. The concentration of substrate was varied from 2 μM to 100 μM for PHOSPHO1 and from 2 μM to 150 μM for PHOSPHO2.

4.4.4 Structural Modelling and Ligand Docking

The protein sequence of PHOSPHO2 was subjected to homology modelling as described previously for PHOSPHO1 (Stewart *et al*, 2003) and outlined in section 2.7.2.

4.5 Results

4.5.1 Production of pBAD-PHOSPHO2 Clone

pBAD-PHOSPHO2 clones were analysed for orientation in respect to the bacterial arabinose inducible promoter. As seen in figure 4.4 the clones display two different digestion patterns when digested with *Nco1* and *HindIII*. When in the correct orientation the clones should display bands equal to 4728 and 124bp, and

when inverted bands of 4166bp and 686bp would be present. From this is can be deduced that clone A and clone B have the PHOSPHO2 CDS in the inverted orientation while clone C and D are correct. All clones with PHOSPHO2 in the correct orientation were DNA sequenced and one displaying the correct sequence when compared to BC_022324 on the NCBI database used for recombinant protein production.

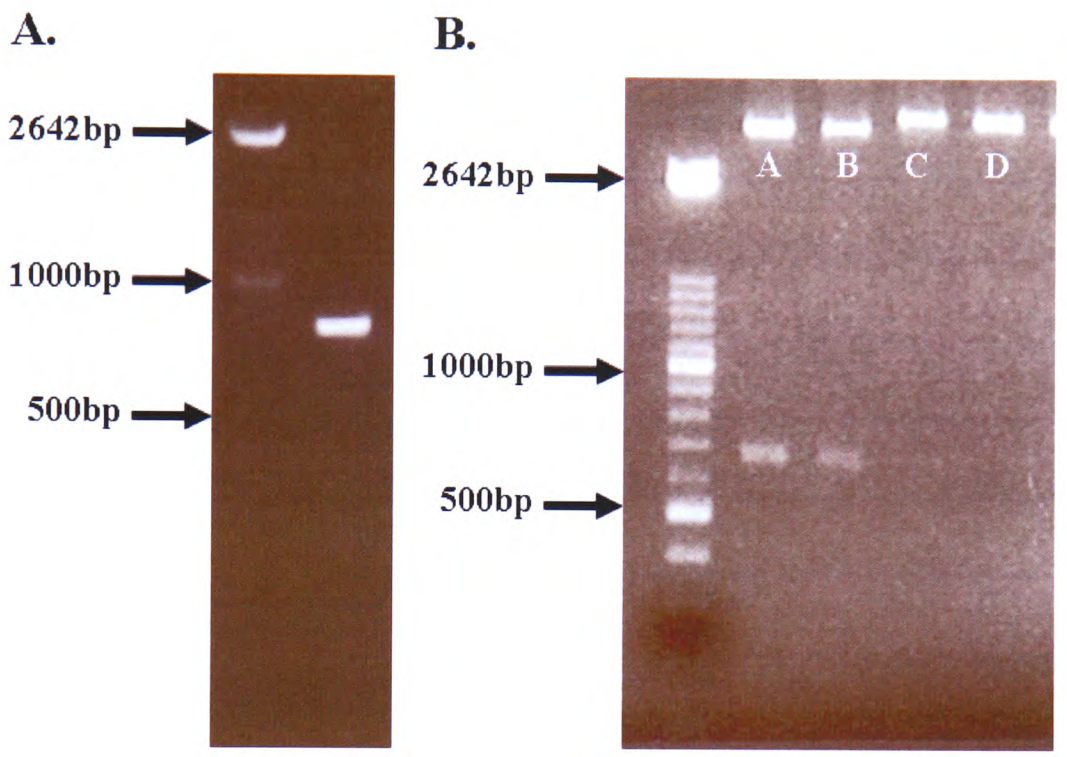

Figure 4.4 Amplification and cloning of PHOPSHO2 into pBAD-TOPO plasmid. Analysis by restriction digestion with enzymes *HindIII* and *NcoI*. (**A**) Amplification of human PHOSPHO2 CDS from genomic DNA by PCR (**B**) Identification of CDS orientation by restriction digestion, clones A and B are in the inverted orientation while clones C and D are in the correct orientation.

4.5.2 Analysis of DNA Sequence from PHOSPHO1 Mutant Clones

The pBAD-PHOSPHO1 mutant plasmids were sequenced in both directions and assembled using STADEN (HGMP). The sequences were compared at the specific point of mutation with the wild type sequence (NM_178500). As seen in figure 4.5 each of the chosen PHOSPHO1 clones contained the desired mutation.

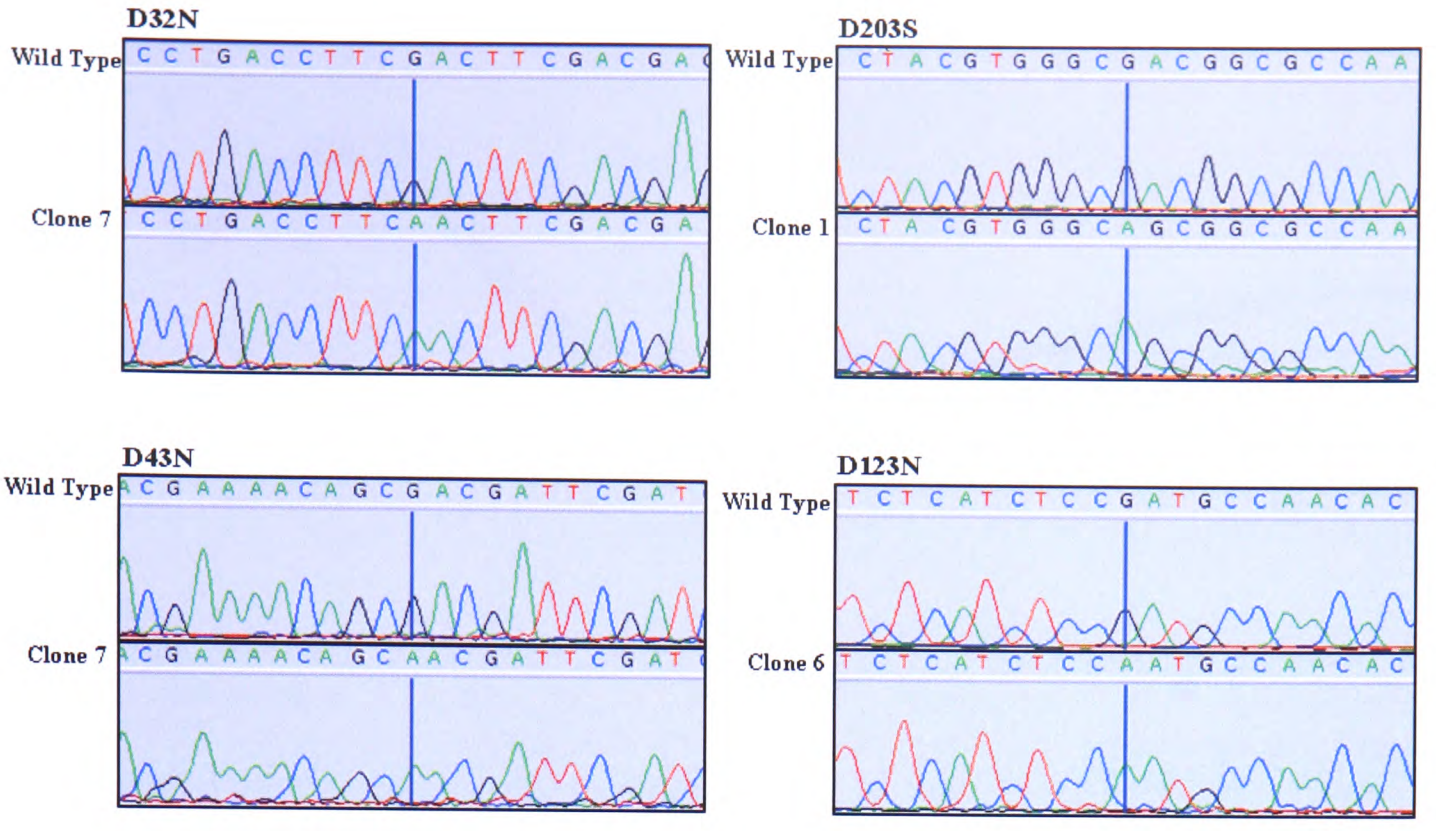

Figure 4.5 Analysis of DNA sequencing results from site directed mutagenesis of pBAD-PHOSPHO1 clones. The upper panel of each figure relates to the wildtype control sequence. As seen on each of the lower panels the mutations have been successful in the cloned plasmids.

4.5.3 Purification of Recombinant Human PHOSPHO2 and PHOSPHO1.

Recombinant His-tagged PHOSPHO proteins were eluted in fractions from a Ni-NTA-agarose column and assayed by SDS-PAGE. Typically, fraction 2 yielded a single band of the expected mass (32 kDa) consistent with >99% purity. The final yield of protein was ca. 25 mg per 10 litres of culture for the PHOSPHO2 expressed by fermentation and approximately 2mg per 1 litre for the PHOSPHO1 mutants. The mutant proteins were compared to the wild type protein by CD analysis. The spectra of the mutants were similar to the native protein showing that the mutations did not cause any significant changes in secondary structure as shown in figure 4.6.

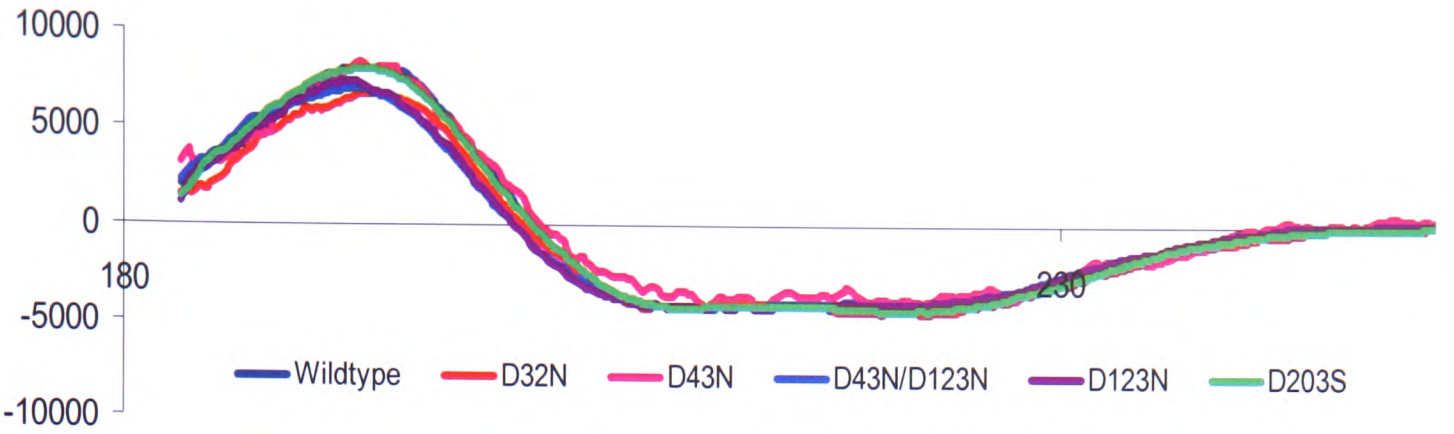

Figure 4.6 Analysis of human recombinant PHOSPHO1 mutant proteins by circular dichroism. CD spectra, in the far UV range, of human Recombinant PHOSPHO1 mutant proteins D123N (purple), D43N (pink), D123N/D43N (blue), D32N (red), D203N (green) and human recombinant wild type PHOSPHO1 (navy).

4.5.4 PEA and PCho Phosphatase Activity from PHOSPHO1 Mutants

Phosphatase activities toward PEA and PCho were assayed using the standard discontinuous assay for the five PHOSPHO1 mutants. The resultant specific activities are shown in Table 4.1. No detectable phosphatase activity was observed with either of the two active site mutations (D32N and D203S). Mutations of Asp43 (D43N) and Asp123 (D123N) dramatically decreased the reactivity toward both substrates when compared with the wild-type enzyme, the D123N mutation reduced activity ~20-fold for PEA and ~60-fold for PCho. The D43N mutation reduced activity ~60-fold for PEA, whilst no activity was observed with PCho. No activity was detected with the double mutant, D43N/D123N-PHOSPHO1, with either substrate.

The reaction with PEA catalysed by the D43N mutant was too slow to allow accurate determination of the kinetic parameters. However, the kinetic constants were determined for recombinant D123N-PHOSPHO1-catalysed hydrolysis of PEA in the presence of 2 mM Mg^{2+} at 37°C. The reaction exhibited Michaelis-Menten

kinetics. A plot of reaction rate versus PEA concentration and also a Lineweaver-Burke plot for the D123N-PHOSPHO1-catalysed reaction are shown in figure 4.7. The enzyme displayed apparent K_m, V_{max} and k_{cat} values of 9.5 μM, 175 nmol min^{-1} mg^{-1} and 0.094 s^{-1}, respectively.

Protein	Specific activity (units/mg)	
	PEA	PCho
Wild-type	4959 ± 327	2203 ± 147
D32N	< 0.1	< 0.1
D203S	< 0.1	< 0.1
D43N	92 ± 42	< 0.1
D123N	277 ± 12	40 ± 18
D43N/D123N	< 0.1	< 0.1

Table 4.1 Specific activities of recombinant human PHOSPHO1 mutants. Wild-type recombinant human PHOSPHO1 and the five mutants (3 μg/ml) were incubated with 2.5 mM PEA or PCho and assayed for phosphatase activity by the discontinuous assay at 37°C. The 200 μl reaction mixture contained 25% (w/v) glycerol, 20 mM TBS, pH 7.2, 25 μg/ml BSA, 2.5 mM substrate and 2 mM $MgCl_2$. The results are the averages of triplicate assays.

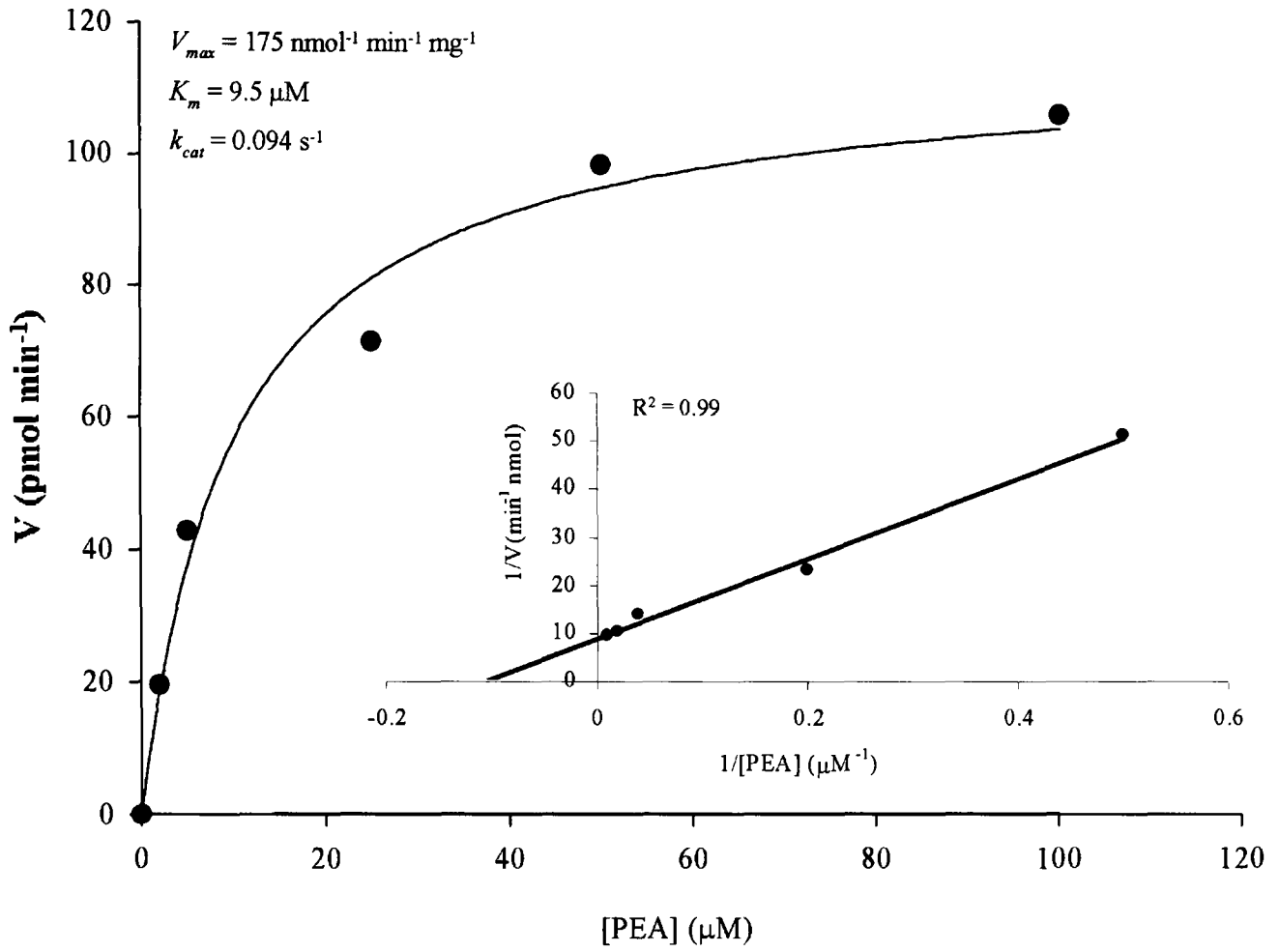

Figure 4.7 Kinetic analysis of the hydrolysis reactions catalysed by recombinant PHOSPHO1 D123N mutant. Plot of the reaction velocity (V) as a function of substrate concentration. *Inset*, Lineweaver-Burke plot from which K_m and V_{max} values were calculated. Kinetic activity toward PEA was measured using a method based upon the PNPase-coupled continuous phosphatase assay.

4.5.5 Substrate Specificity of Recombinant PHOSPHO2 Protein

Eleven phosphate compounds were investigated as potential substrates for human PHOSPHO2. A comparison of the resultant specific activities with those previously reported for human PHOSPHO1 in chapter 3 is shown in figure 4.8. Of the phosphate compounds tested, pyridoxal-5-phosphate (P5P) was hydrolysed by PHOSPHO2 with the highest specific activity (464.1 ± 19.5 units/mg), which was approximately 3 times higher than that towards ATP and phospho-L-serine. PHOSPHO2 also hydrolysed pyrophosphate, PEA, phospho-L-tyrosine, fructose-6-phosphate, *p*-nitrophenyl phosphate, β-glycerophosphate and PCho. No hydrolysis of

ribose-5-phosphate was observed in the presence of PHOSPHO2. PHOSPHO1 has previously been shown to have high specific activities toward PEA and PCho (4600 ± 582 and 2980 ± 335 units/mg, respectively). Five of the potential substrates that previously yielded no detectable phosphatase activity with PHOSPHO1 showed activity with PHOSPHO2 (pyrophosphate, phospho-L-serine, fructose-6-phosphate, phospho-L-tyrosine and ATP).

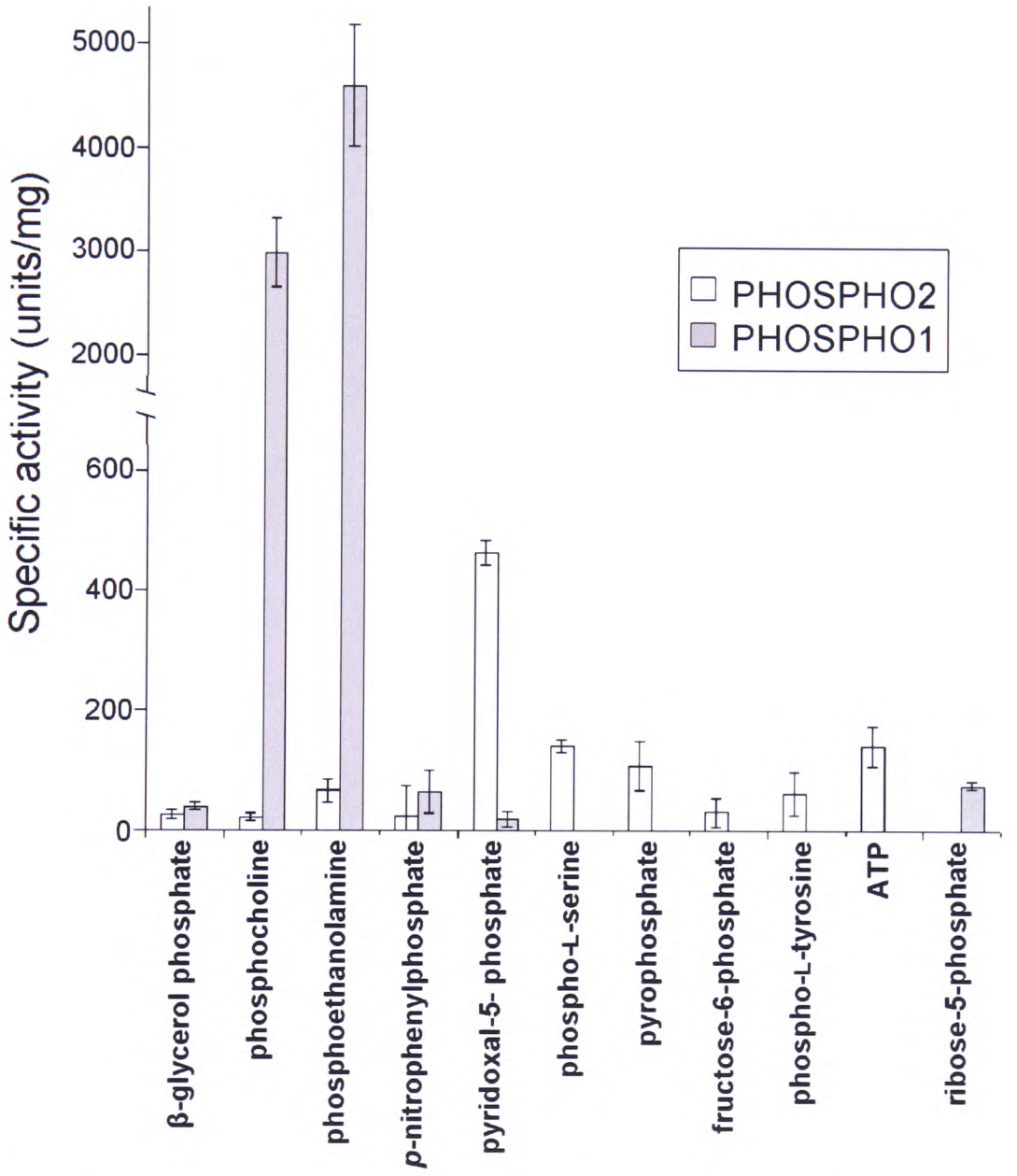

Figure 4.8 Specific activities of PHOSPHO2 and PHOSPHO1 in the presence of a range of substrates. PHOSPHO1 and PHOSPHO2 activities were determined using a discontinuous assay at 37°C. The 200 µl reaction mixture contained 25% (v/v) glycerol, 20 mM TBS, pH 7.2, 25 µg/ml BSA, 2.5 mM substrate and 2 mM $MgCl_2$. The results are the averages of triplicate assays (± SD).

Kinetic constants were determined for recombinant PHOSPHO2-catalysed hydrolysis of P5P in the presence of 2 mM Mg^{2+} at 37°C. The reaction exhibited Michaelis-Menten kinetics. A plot of reaction rate versus PEA concentration and also a Lineweaver-Burke plot for the PHOSPHO2-catalysed reaction are shown in figure 4.9. The enzyme displayed apparent K_m, V_{max} and k_{cat} values of 45.5 μM, 633.3 nmol min^{-1} mg^{-1} and 0.34 s^{-1}, respectively.

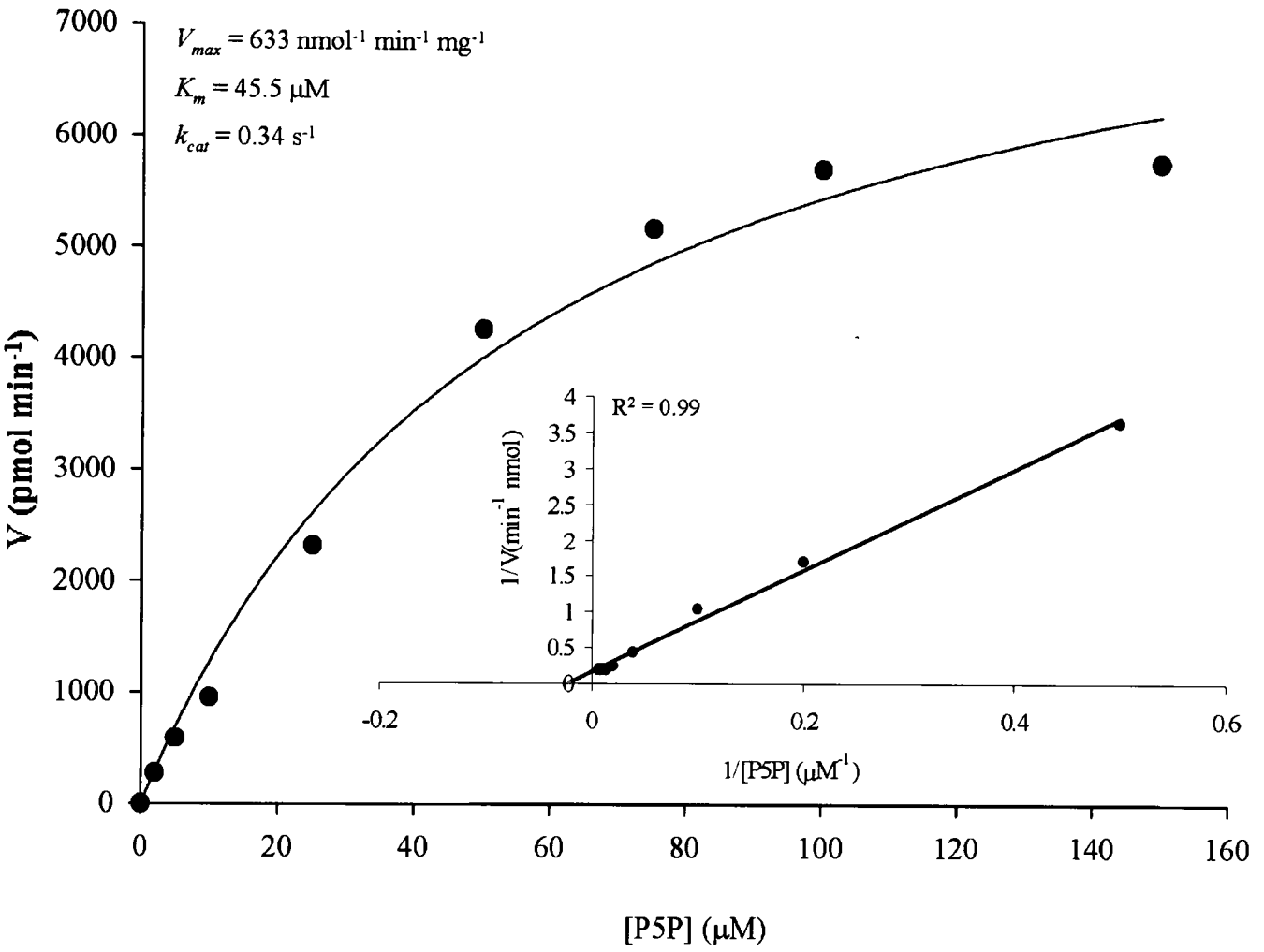

Figure 4.9 Kinetic analysis of the hydrolysis reactions catalysed by recombinant PHOSPHO2. Plot of the reaction velocity (V) as a function of substrate concentration. *Inset*, Lineweaver-Burke plot from which K_m and V_{max} values were calculated. Kinetic activity toward P5P was measured using a method based upon the PNPase-coupled continuous phosphatase assay.

4.5.6 Molecular Modelling of PHOSPHO2

4.5.6.1 Construction of a PHOSPHO2 Model

In the absence of structural data for PHOSPHO2, a three-dimensional model was built based on the X-ray crystal structure coordinates of *Mj*PSP (PDB: 1F5S). Sequence identity between *Mj*PSP and PHOSPHO1 is 19.4% whilst identity between *Mj*PSP and PHOSPHO2 is 18.0%. Despite the low sequence identity, fold recognition strongly suggests that PHOSPHO2 (and PHOSPHO1) and PSPs belong to the same fold (alignment shown in figure 4.10), therefore allowing us to build a meaningful structural model (figure 4.11). The protein model consists of two domains: the catalytic α/β domain and a four-helix-bundle. The α/β domain forms a Rossman fold structure consisting of a six-stranded parallel β-sheet, surrounded by six α-helices.

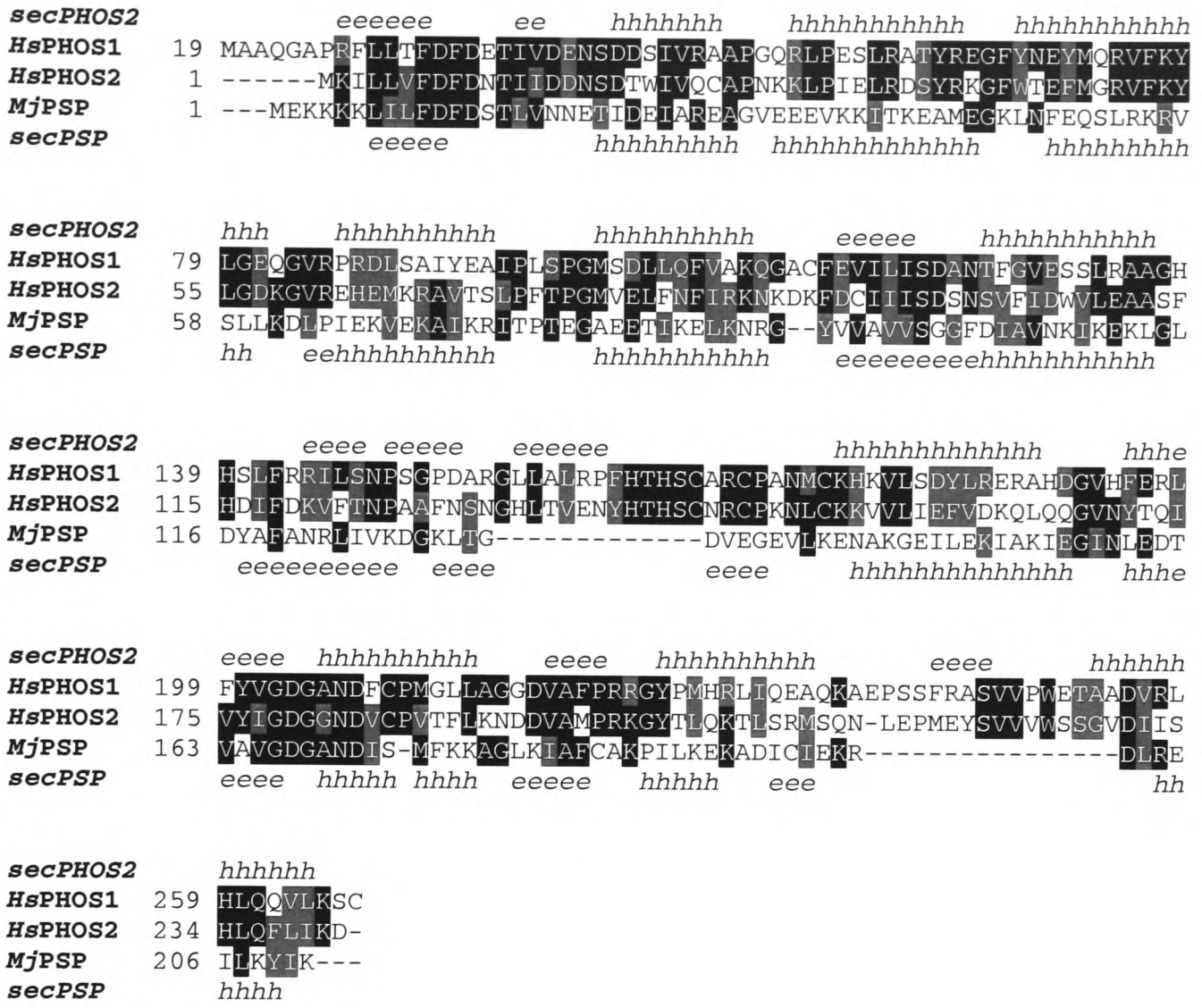

Figure 4.10 Alignment of *Hs*PHOSPHO1, *Hs*PHOSPHO2 and the scaffold protein *Mj*PSP, showing the secondary structure for PSP and secondary structure prediction for PHOSPHO2. The following sequences are used (accession numbers are shown in parentheses): *Hs*PHOS1, human PHOSPHO1 (Q8TCT1); *Hs*PHOS2, human PHOSPHO2 (Q8TCD6); *Mj*PSP, phosphoserine phosphatase from *Methanococcus jannaschii* (Q58989). Secondary structure elements for PHOSPHO2 (secPHOS2) and MjPSP (secPSP) are denoted as h = α-helix, e = β-strand. Black shading indicates identical, and grey shading highly similar amino acid residues.

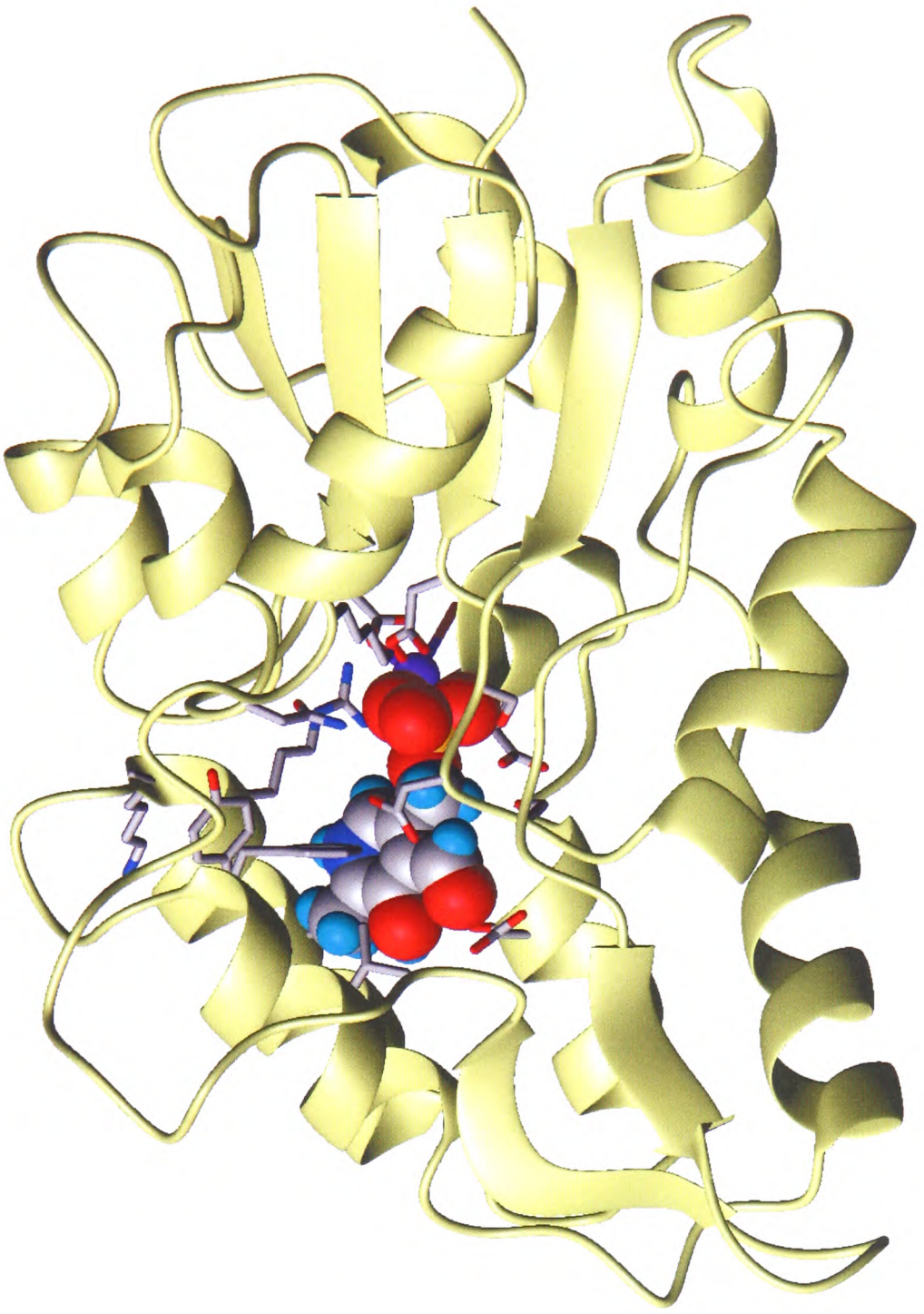

Figure 4.11 Ribbon diagram of the human PHOSPHO2 model showing the overall fold. The model is based on the crystal structure of phosphoserine phosphatase from *Methanococcus jannaschii* (*Mj*PSP; PDB code: 1L7P). P5P was modelled into the catalytic site as this was found to be the best substrate for PHOSPHO2 of those tested.

4.5.6.2 Ligand Docking

The homology models of PHOSPHO2 and PHOSPHO1 were subjected to *in silico* docking calculations, a model of PHOSPHO2 incorporating P5P as substrate is presented in figure 4.11. In this model, a hexadentate Mg^{2+} ion is bound in an octahedral geometry via three Asp residues (Asp8, Asp10 (backbone oxygen) and Asp179), O-ligands are also provided by the phosphate group of P5P and two water molecules.

Previous modelling studies of PHOSPHO1 suggested that as well as Asp43 and Asp123, two additional residues, Arg60 and Tyr71, also line the substrate-binding pocket (Stewart *et al*, 2003). A comparison of this region in both the PHOSPHO1 and PHOSPHO2 models is shown in figure 4.12. The active sites of PHOSPHO1 and PHOSPHO2 in our models are very similar. Apart from the conserved Mg^{2+}-binding site (side-chains of Asp8 and Asp179, backbone-CO of Asp10 in PHOSPHO2), and phosphate-binding site (backbone-NH of Phe9, side-chains of Ser98, Lys153 and Asn182; PHOSPHO2), residues in or close to the predicted substrate pocket are: Asn11, Asn17, Asp19, Thr20, Arg36, Tyr39, Arg40, Phe47, Tyr54, Asp99, and Ser100 in PHOSPHO2 (corresponding to Glu35, Asn41, Asp43, Asp44, Arg60, Tyr63, Arg64, Tyr71, Tyr78, Asp123 and Ala124 in PHOSPHO1 respectively).

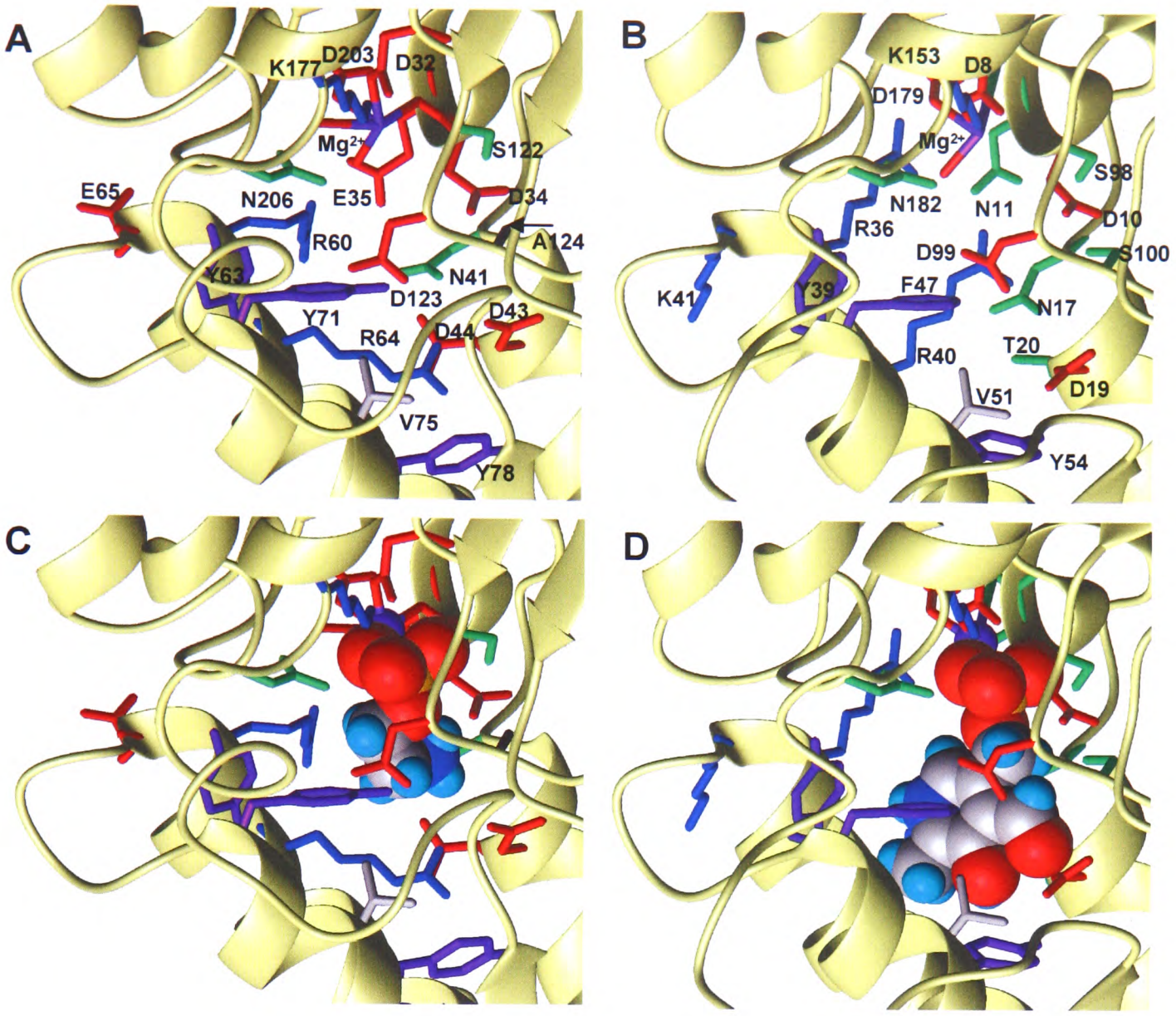

Figure 4.12 Models of the active sites of PHOSPHO1 without and with phosphoethanolamine (A and C) and PHOSPHO2 with pyridoxal-5-phosphate (B and D). Key residues around the sites likely to be involved in substrate binding and catalysis are shown. Amino acid residues are coloured according to type: negatively charged (red), positively charged (blue), hydrophilic uncharged (green), aromatic (violet), and hydrophobic (grey). Atoms of the ligands are coloured as follows: hydrogen (cyan), carbon (grey), nitrogen (blue), oxygen (red), phosphorus (orange); the magnesium ion is shown in purple.

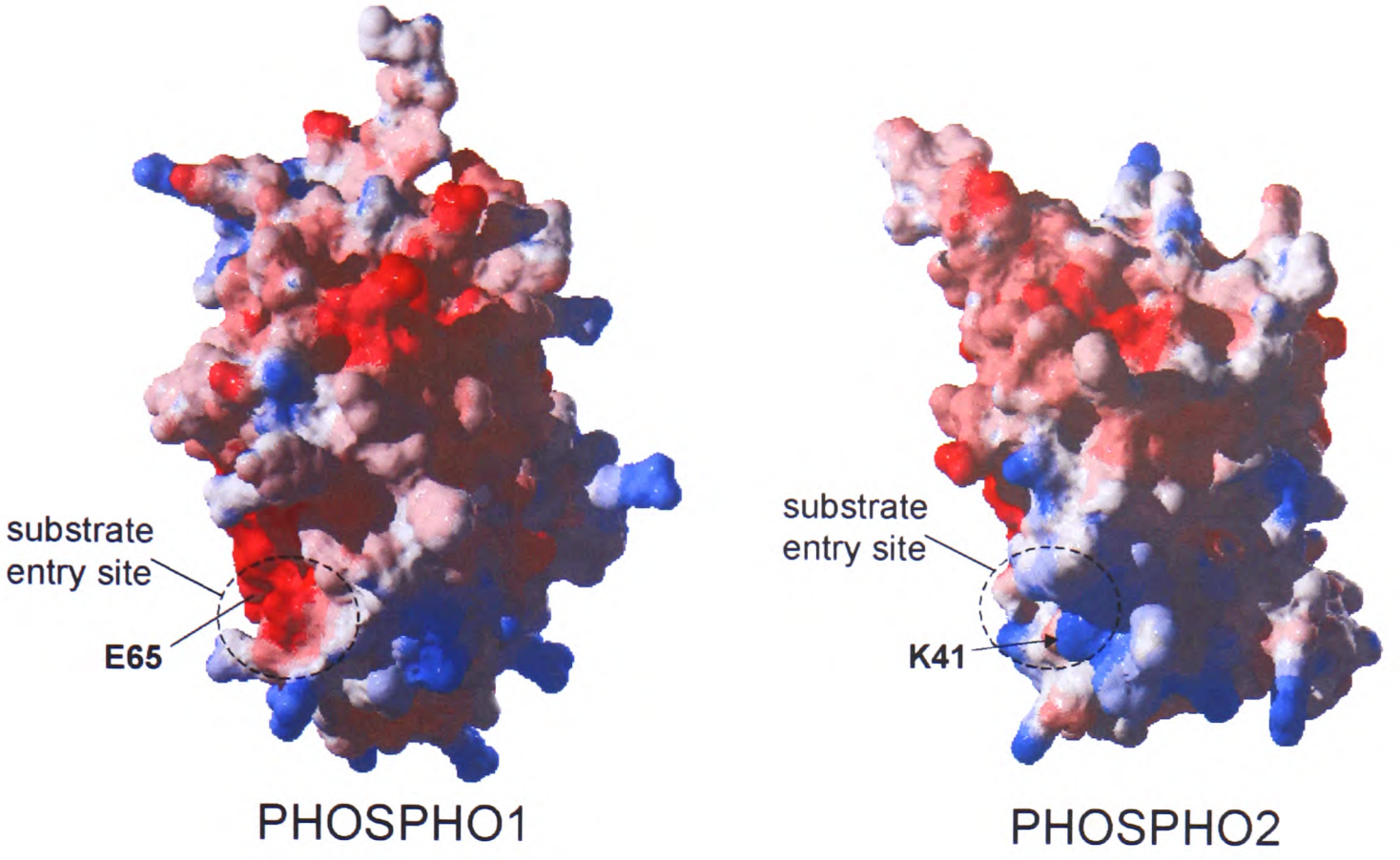

Figure 4.13 Electrostatic potential surfaces for PHOSPHO1 (left) and PHOSPHO2 (right). Negative and positive potentials on the surface of each protein are shown in red and blue, respectively. The models suggest that a large difference in potential exists between the two proteins around the entrance to their catalytic sites. The large negative charge at this region of PHOSPHO1 is partly due to Glu65, which corresponds to a positively charged Lys41 in PHOSPHO2.

4.6 Discussion

The results of chapter 3 have indicted that the natural substrates of PHOSPHO1 are likely to be PEA and PCho, both of which are positively charged. Previous molecular modelling studies implicated two negatively charged residues (Asp43 and Asp123), which line the substrate-binding pocket of PHOSPHO1, in substrate-specific interactions (Stewart *et al*, 2003). Mutation of active-site residues Asp32 (D32N) and Asp203 (D203S) of PHOSPHO1 resulted in a complete loss of activity toward PEA and PCho. This characteristic is a hallmark of the HAD superfamily of proteins (Maruyama *et al*, 1989; Clarke *et al*, 1990; Aravind *et al*, 1998; Selengut, 2001; Tootle *et al*, 2003), and confirms PHOSPHO1 as a member of

this family. PHOSPHO1 mediated hydrolysis of PEA and PCho is therefore likely to follow by the same Mg^{2+}-dependent mechanism as other HAD-like phosphatases. Scheme 4.1 illustrates how PHOSPHO1 is likely to interact with the phosphate moiety of the substrate during the reaction cycle based upon previous crystallographic studies investigating PSP-catalysed hydrolysis of phosphoserine (Wang *et al*, 2002) and the previously constructed PHOSPHO1 model (Stewart *et al*, 2003).

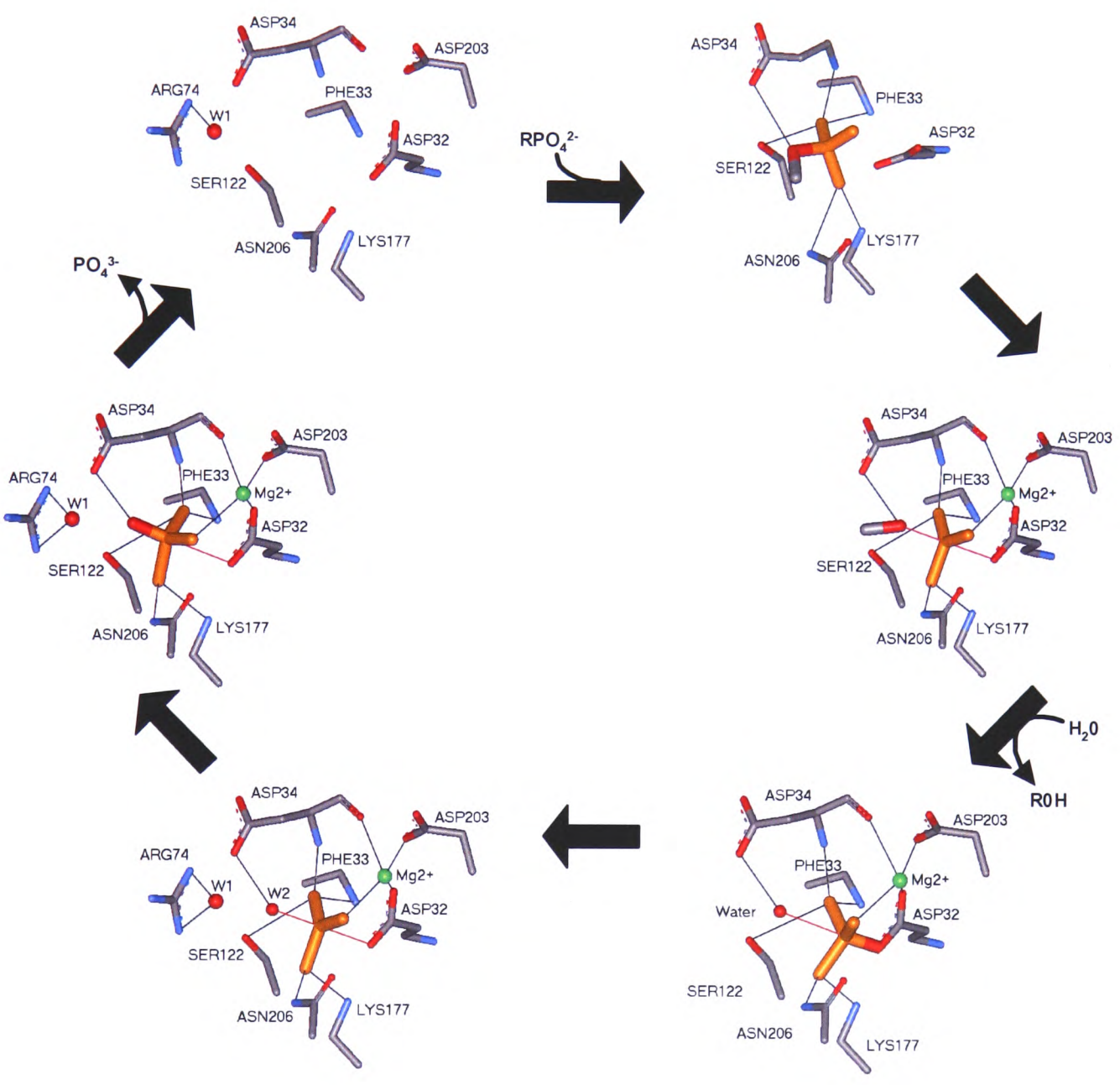

Scheme 4.1 Proposed reaction pathway of PHOSPHO1-catalysed hydrolysis based upon the molecular model of PHOSPHO1 (Stewart *et al*, 2003) and the known pathway for PSP from *Methanococcus jannaschii* (Wang *et al*, 2002) (Figure created by Stephen J. Paisey, University of Edinburgh).

Upon analysis of this scheme, it is likely that the substitutions D32N and D203S have dramatically reduced the affinity of Mg^{2+} towards the site, whilst the D32N mutation would also prevent the formation of a phospho-protein intermediate during the reaction.

The mutations D43N and D123N also greatly affected PHOSPHO1 activity towards PEA and PCho. Both mutations reduced the specific activity, by varied degrees toward PEA and PCho, with D43N having the more pronounced effect. The double mutant, D43N/D123N, exhibited no activity toward either PEA or PCho. Kinetic analysis revealed that PEA hydrolysis by the D123N mutant is reduced by a factor of 24 compared to wild type PHOSPHO1 under the same conditions. This suggests that Asp123 is important for hydrolysis of PEA. Asp123 mutation has only a moderate effect on substrate binding (reduction of K_m by a factor of ca. 3). The K_m value is, under true Michaelis-Menten conditions, an estimate of the dissociation constant of enzyme from substrate. A probable explanation for these kinetic data is that Asp123 of PHOSPHO1 does not interact directly with the substrate but plays a similar role to that of Glu20 in *Mj*PSP, which stabilises an attacking nucleophilic water molecule during phosphoserine hydrolysis and is conserved in all known PSPs (Wang *et al*, 2002). Such a role for Asp123 during the reaction would account for the relatively larger difference in V_{max} and k_{cat} values and small difference in K_m value observed between the D123N mutant and wild type enzyme. However a role for this residue stabilising the positive charge of the NH_3^+ group both in the initial complex and during catalysis cannot be eliminated. The D43N mutation has a much more dramatic effect than D123N. No activity toward PCho was observed with the D43N mutant and activity toward PEA was reduced ~60-fold compared to wild type. This

suggests that Asp43 is a more likely candidate than Asp123 to directly interact with the substrate. Such an interaction would presumably be more important for the binding of the bulkier choline moiety of PCho than the smaller ethanolamine moiety of PEA as our results suggest.

Recombinant PHOSPHO2 protein was assayed for phosphatase activity in the presence of a number of phosphomonoesters. Surprisingly, activities toward PEA and PCho were ~100 times lower for PHOSPHO2 compared to PHOSPHO1 under the same conditions. The highest activity corresponded to the hydrolysis of P5P (*ca.* 464.1 ± 19.5 nmol min^{-1} mg^{-1}). This activity is ~10-fold less than that measured for PHOSPHO1 catalysed hydrolysis of PEA under the same conditions. The relatively low K_m (*ca.* 45.5 μM) suggests that this molecule may be hydrolysed by PHOSPHO2 *in vivo*, however the existence of a more specific ligand is conceivable. It would however be likely if P5P is not the physiological substrate of PHOSPHO2, such a substrate would retain some defining features of P5P, such as a positively-charged aromatic ring.

These results show that despite the overall high level of identity (*ca.* 42%), PHOSPHO1 and PHOSPHO2 are distinct enzymes with different substrate specificities. Indeed sequence similarity in proteins with distinct functions is well documented (Orengo *et al*, 1993). Specific examples of this include spinach glycolate oxidase (EC 1.1.3.15) and yeast flavocytochrome b2 (EC 1.1.2.3). These enzymes share 37% identity but catalyse oxidoreductase reactions with distinct substrates and acceptor molecules (Lindqvist *et al,* 1991). It is however surprising that these two enzymes, which share such close similarity outwith the catalytic motifs have such different specificities.

Human PHOSPHO2 protein was modelled based on the crystal structure of *Mj*PSP to allow a better understanding of why these two proteins are functionally distinct. The model shows that the characteristic features of the catalytic site found in the HAD superfamily are all preserved. This includes all residues involved in the recognition of the phosphate group in *Mj*PSP, with the exception of Gly100 (in PSP), which is replaced by Asp99 (in PHOSPHO2). Considering that only the backbone oxygen of this residue is involved in substrate binding in PSP, the modelled catalytic site in PHOSPHO2 closely resembles the catalytic site in *Mj*PSP (Wang *et al*, 2001). The models including bound substrate molecules have been generated by *in silico* docking. The conformation shown for each substrate is just one of many possible, but is probably a reasonable representation of the general orientations of the molecules. Although no restraints were used during the docking procedure, the interactions between the phosphate group and the amino acid side-chains (Ser122, Lys177, Asn206 for PHOSPHO1 or Ser98, Lys153, and Asn182 for PHOSPHO2) agree very well with those observed in the X-ray structures of related phosphatases (Wang *et al*, 2001 and 2002; Kim *et al,* 2002). The situation is slightly more complicated for the remainder of the binding pocket, as the residues defining the "non-phosphate" moiety of the substrate-binding site are not conserved between our template and the two target proteins. Although it is therefore not possible to predict reliably the orientation of the side-chains of these residues, the models allow us to define the residues lining the binding pocket and to predict some of the interactions which may contribute to substrate specificities. In the theoretical PHOSPHO1/PEA model, the negatively charged side-chains of Asp34, Asp43, and Asp123 are all in the vicinity of the positively charged ammonium group of PEA, potentially providing both a highly

negatively charged pocket as well as H-bond acceptor atoms. These interactions are consistent with the decrease in activity for the D43N, the D123N, and the D43N/D123N mutants. Residues in or near the substrate pocket that are not highly conserved between PHOSPHO2 and PHOSPHO1 are Asn11/Glu35, Thr20/Asp44, Ser100/Ala124 and Phe47/Tyr71. Of these, only Thr20/Asp44 and Ser100/Ala124 are fully conserved within the two subfamilies. With the exception of chicken PHOSPHO1, Glu35 is also conserved within the PHOSPHO1 sub-family; PHOSPHO2 proteins carry either an Asn or a His residue at this position. In the case of Tyr71, there does not appear to be any specific conservation within sub-families. Clearly, the binding site of PHOSPHO1 is more negatively charged than that of PHOSPHO2, and there are subtle changes in the location of potential H-bond donors. In addition, the surface charges of the putative entry sites are also different (figure 4.13): whilst Glu65 in PHOSPHO1 renders the surface rather negative, the respective Lys41 residue in PHOSPHO2 has the opposite effect. Again, these amino acids are fully conserved within their respective sub-families. Changes in surface charges are likely to contribute to the rate of both ligand binding and product release.

These results clearly demonstrate that the two enzymes, PHOSPHO1 and PHOSPHO2, both belong to the HAD superfamily but have different substrate specificities. Asp43 and Asp123 in PHOSPHO1 (and, by inference, presumably also Asp19 and Asp99 in PHOSPHO2) contribute to catalysis but other residues are also involved. The structural models help to identify potential candidates for these residues through the discovery of subtle differences inside the substrate-binding pockets and on the surfaces of the active sites. Given the overall high similarity between PHOSPHO1 and PHOSPHO2, it was important to elucidate whether or not

the enzymes had similar activities. PHOSPHO1 is associated with high levels of expression at mineralising regions of bone and cartilage. The discovery of another phosphatase with comparable PEA and PCho phosphatase activity would have given rise to serious questions regarding a role in mineralisation for PHOSPHO1 as gene expression studies carried out in chicken and EST analysis in mammals have shown that PHOSPHO2 expression is not specific to bone and is indeed expressed in a wide range of soft tissues. In addition, functional redundancy would likely complicate future gene knockout and inhibitory experiments. Furthermore, this is the first investigation of human PHOSPHO2 structure and activity, providing a platform for the further study of this enzyme.

CHAPTER 5

PHOSPHO1 EXPRESSSION AND LOCALISATION

Chapter Contents

5.1 Introduction

As previously revealed by Houston *et al,* (2004) and in section 1.7.1 PHOSPHO1 protein is localised to the mineralising centres of both avian bone and cartilage. This localisation mirrors that of the other major bone phosphatase, TNAP. To allow a link between PHOSPHO1 and bone/cartilage mineralisation in the mammalian system a localisation pattern similar to that found in the chick is required. The process of matrix mineralisation occurs in the extra-cellular matrix which surrounds terminally differentiating chondrocytes, osteoblasts and odontoblasts and is the mechanism by which growth plate cartilage, bone and tooth formation occurs by each of these cell types, respectively. Mineralisation in growth plate cartilage increases as chondrocytes progress through differentiation till they obtain a hypertrophic phenotype resulting in cell death thus leaving a calcified cartilage template for bone growth. The sites of bone mineralisation are characterised by osteoblast activity which is found at various bone forming surfaces such as primary spongiosa, osteons and areas of bone remodelling. Each of these sites are characterised by the presence of TNAP on the surface of mineralising cells as well as among the collagen fibrils within the bone osteoid matrix (Bonucci *et al*, 1994). It is widely regarded that MVs are the initial sites for apatite formation by providing an environment permissive for calcium phosphate precipitation (Ali and Evans, 1973).

The localisation of TNAP to all sites of mineralisation serves to strengthen the potential role it has in this process and it is now thought that this role is to hydrolyse the potent mineralisation inhibitor PPi (Harmey *et al*, 2004). The action of TNAP, however does not seem to be critical for the initial stages of mineralisation as in newborn *Tnap* knockout mice, bone development and mineralisation appear

normal and MVs contain crystals of hydroxyapatite. Skeletal hypomineralisation does subsequently appear in these mice (Narisawa *et al*, 1997; Hessle *et al*, 2002) however this is likely to be due to an increased concentration of PPi at mineralising sites (Meyer 1984). This hypomineralisation can be reversed by NPP1 knockout as this reduces the PPi pool and subsequently allows physiological mineralisation to occur as discussed in 1.6.4.2.

TNAP activity displays a regulatory pattern which is directly related to the stage of cellular differentiation. If differentiation is induced *in vitro* through the addition of AA, chondrocytes display a hypertrophic phenotype which is accompanied by an increased expression of collagen type X and TNAP activity. It has been known for many years that AA is required for the production of a normal extracellular matrix as it is important in stabilising the triple helical structure of collagen (Kivirikko and Myllyla, 1987). It is, however, unclear how exactly AA influences chondrocyte gene expression and the activity of TNAP. It has been hypothesised that it is due to the vitamin inducing an increased matrix production and deposition which subsequently triggers expression of genes required for the development of this matrix (Leboy *et al,* 1989). A similar effect of AA is seen on osteoblast differentiation with an increase in TNAP activity coupled with an increase in collagen expression evident (Sugimoto *et al*, 1986; Franceschi *et al*, 1994). It is unknown whether PHOSPHO1 is regulated in this manner, however if it did show a regulatory pattern similar to TNAP it would further the hypothesis that PHOSPHO1 plays a central role in the formation of a mature cartilage/bone matrix.

5.2 Hypothesis

That PHOSPHO1 is localised in a similar fashion in mammals to that of the already characterised avian model. Also that gene expression mirrors that of the avian model with increased transcript levels observed in mineralising tissues.

5.3 Aims

I. Further analyse the localisation on PHOSPHO1 in the chick model by analysing protein content of MVs.

II. To analyse gene expression quantitatively through the use of real time PCR in a mouse model.

III. To produce a mouse/human specific PHOSPHO1 antibody and use this for immunohistochemical analysis of tissue sections.

IV. To analyse PHOSPHO1s relationship to differentiation factors in both cells and MVs and investigate if PHOSPHO1 is active at these sites.

5.4 Materials and Methods

5.4.1 MV and Chondrocyte Isolation

MVs and chondrocytes were isolated from dissected chick tibial growth plate cartilage as described in section 2.2.7 and shown in figure 5.1. Chondrocytes were cultured as outlined in this section. Briefly the cells were seeded at $1x10^6/cm^2$ in T25 flasks and cultured in DMEM containing 10% FBS and 4units/ml hyaluronidase until confluence had been achieved (day 5). At this point 50 μg/ml ascorbic acid 2-phosphate (AA) was added to the culture medium to induce cellular differentiation. This was classed as day 0. Differentiation was assessed by TNAP histochemistry as outlined in 2.2.9.3. MVs were isolated from the chondrocyte monolayer periodically following this point at 2, 5, 8 and 12 days according to the method outlined in 2.2.7. Protein concentration of the MV preparations were determined as outlined in section 2.5.9.

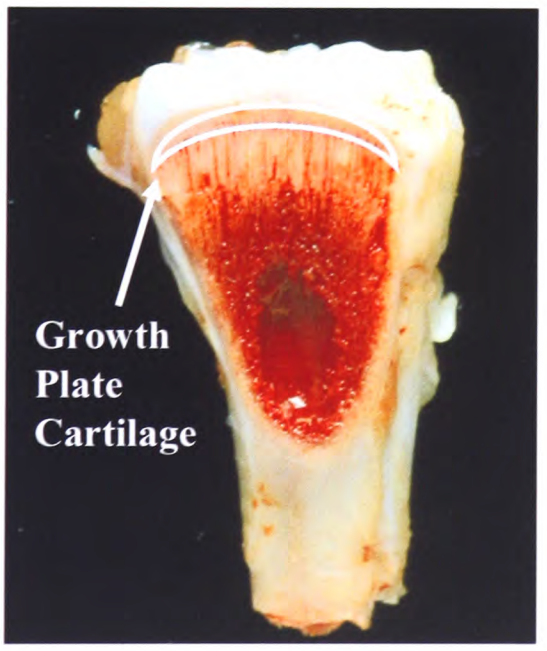

Figure 5.1 Location of the tibial growth plate. The highlighted section represents the growth plate cartilage which was dissected to allow the isolation of chondrocytes and MVs as outline in section 2.2.7.

5.4.2 Purification of anti-PHOSPHO1 Antibodies from Sheep Antisera

Anti chick-PHOSPHO1 antibodies were purified from sheep antisera according to the protocol detailed in 2.5.8. The resultant purified antibody was electrophoresed on a Novex 10% Bis-Tris as outlined in 2.5.1. The antibody protein was either in a reduced or non-reduced state. As IgG is held together by disulphide bonds the reduced antibody should appear on the gel as two bands (heavy and light chains) and the non-reduced should appear as one band (assembled antibody). Following electrophoresis the gel was stained with coomassie blue as outlined in section 2.5.2 and shown in figure 5.2.

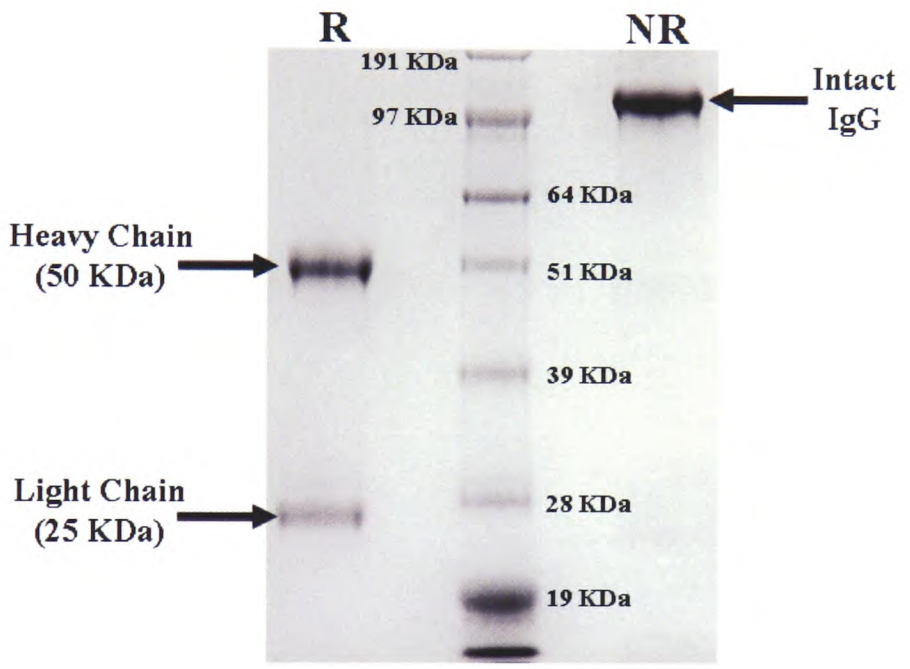

Figure 5.2 Purification of anti-PHOSPHO1 antibodies from sheep sera. Immobilised recombinant PHOSPHO1 used as a matrix to pull specific antibodies from anti-sera. (**R**) Represents antibody reduced with DTT showing bands corresponding to both heavy and light chains (**NR**) corresponds to a non-reduced sample.

5.4.3 Western Blotting

To allow detection of PHOSPHO1 in chick MVs 10μg MV protein was run on a Novex 10% Bis-Tris as outlined in 2.5.1. This was then used for Western

blotting as detailed in 2.5.4. The nitrocellulose was probed with a solution of 2 μg/ml purified antibody in 5% milk protein/TBST solution. The secondary antibody used for this detection was mouse anti sheep IgG-peroxidase (Sigma) diluted 1:2,000. To assess equal loading of the protein lysates an Indian ink stain was carried out on the membrane as outlined in 2.5.4

To test the antisera raised against the recombinant human PHOSPHO1 protein and the synthetic peptide antibody, 50 μg samples of cell line and tissue proteins were subjected to electrophoresis as outlined in 2.5.1. Both antisera were used at a dilution of 1:500 in 5% milk protein/TBST solution to probe Western blots (produced as outlined in 2.5.4). The secondary antibody used for this detection was goat anti rabbit IgG-peroxidase (Dako) diluted 1:2,000.

To detect PHOSPHO1 in differentiating cell lines and murine MVs, 50 μg and 25 μg protein was utilised respectively and run on a Novex 10% Bis-Tris as outlined in 2.5.1. This was then used for Western blotting as detailed in 2.5.4. The nitrocellulose was probed with a 1:750 dilution of anti-mouse PHOSPHO1 antisera in 5% milk protein/TBST solution. The secondary antibody used for this detection was goat anti rabbit IgG-peroxidase (Dako) diluted 1:2,000.

5.4.4 MV TNAP Assay

This was carried out as detailed in section 2.6.3 using approximately 10 μg of MV protein. The final activity was expressed as nmoles pNPP hydrolysed/ min/mg protein (thus normalising the protein content).

5.4.5 Quantitative PCR of Mouse RNA

The quantitative PCR was carried out directly on mouse RNA in a one step reaction using the Brilliant® SYBR® Green QRT-PCR Master Mix Kit (Stratagene), as detailed in section 2.4.5.

5.4.6 Immunohistochemistry

10-day old mice were killed by cervical dislocation and tissues processed as described in section 2.7.1. The protocols for sectioning, wax embedding and probing of these tissues are outlined in section 2.7.

5.4.7 Isolation of MVs from Cultured Osteoblasts

To isolate MVs from cultured osteoblasts a protocol was employed which is similar to that used for chondrocytes, as outlined in section 2.2.8. Firstly the primary murine osteoblasts were cultured for 13 days in alpha MEM (Gibco) containing 10% FBS and 50 μM AA. The cell monolayer was then washed with 50 mM Tris-HCl pH 7.6, 120 mM NaCl and 10 mM KCl, and then incubated with 0.45% collagenase (Worthington, type II) in 50 mM Tris-HCl pH 7.6, 120 mM NaCl and 10 mM KCl at 37°C for 120 minutes at 37°C, with constant agitation. This cell suspension was subjected to differential centrifugation as described in section 2.2.7. Cell phenotype (*Tnap*$^{+/-}$ and wild-type cells) was confirmed using TNAP histochemistry as detailed in 2.2.9.3 and mineralisation capability by von Kossa staining as outlined in 2.2.9.2.

5.4.8 Identification of Active PHOSPHO1 in MVs

The phosphatase assay used for this analysis was identical to that detailed under section 2.6.1 using 12 μg of MV protein in place of recombinant PHOSPHO1. The MV protein was either intact or sonicated thus causing the vesicles to rupture.

5.5 Results

5.5.1 PHOSPHO1 in Isolated MVs

The presence of PHOSPHO1 was examined in MVs isolated from chick growth plate cartilage. Two forms of PHOSPHO1 (30.4 and 28.6 kD) were detected in MVs isolated directly from the tibial growth plates of 3 week-old chicks (figure 5.3A) and from primary cultured chondrocyte cells (figure 5.3B). PHOSPHO1 expression in the MVs isolated from the primary cells was found to increase with time in culture and appeared to be much greater in the presence AA after 12 days in culture. Equal loading of the samples was confirmed by India ink staining of the membrane (figure 5.3C). No overt signs of matrix mineralisation were noted in these cultures. TNAP activity in the presence of AA was found to double after 5 days in culture and was 4-times that of the control after 12 days but was not found to alter with time in the control cultures (figure 5.3D). This was confirmed using TNAP histochemistry where enzyme activity was concentrated in cartilaginous nodules with only low activity present in control cultures (figure 5.4).

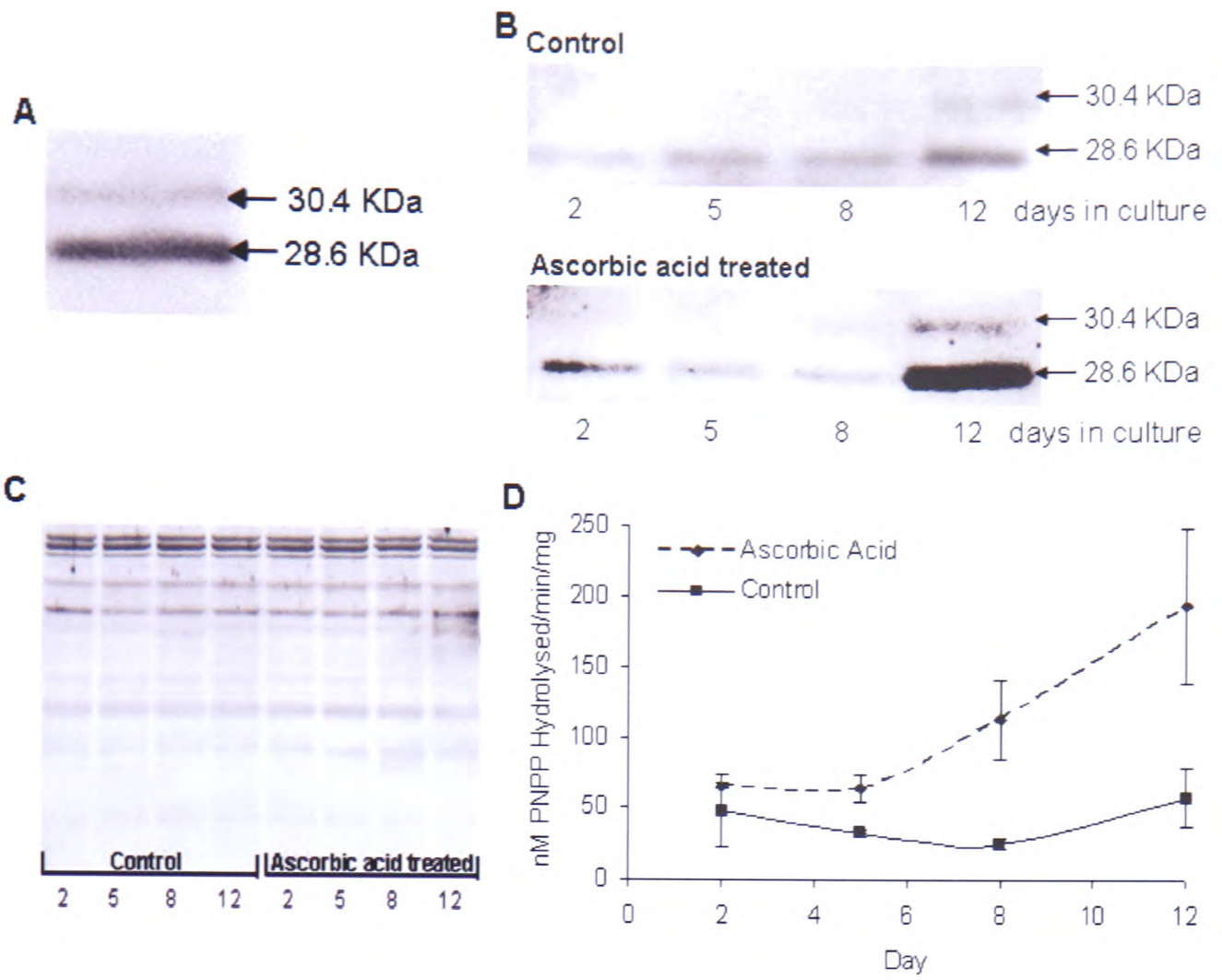

Figure 5.3 Localisation of PHOSPHO1 in chick growth plate MVs (A) Immunoblot showing PHOSPHO1 expression in MVs isolated from the tibial growth plates of 3 week old chicks. **(B)** Immunoblots examining PHOSPHO1 expression in MVs isolated from primary chondrocytes cultured in the presence or absence of 50 μg/ml AA. **(C)** India Ink Staining of MV Immunoblot demonstrating equal loading in each lane. **(D)** TNAP activity of MVs isolated from primary chondrocyte cultures.

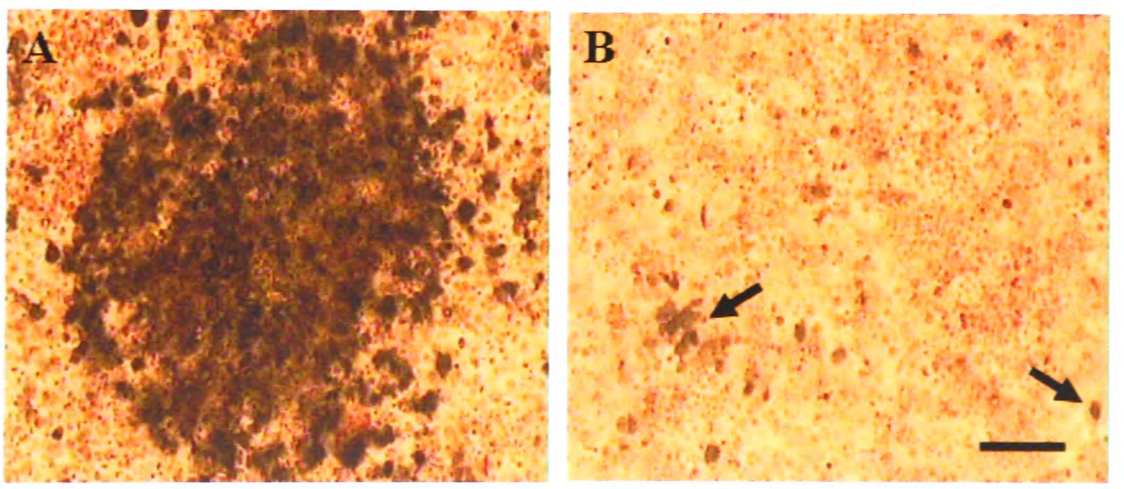

Figure 5.4 TNAP histochemistry on day 12 avian chondrocyte cultures (A) Localisation of TNAP activity to cartilaginous nodules in cells treated with 50 μg/ml AA. **(B)** Localisation of TNAP activity in control cultures, arrows indicate randomly distributed regions. (Scale Bar = 200μm)

5.5.2 Analysis of PHOSPHO1 Expression

To investigate how PHOSPHO1 gene expression varies between mammalian tissues, qPCR was utilised to obtain relative expression values. From this analysis, bone had the highest expression levels with the least amount of PHOSPHO1 transcript found in the liver (figure 5.5). The difference in expression between these two tissue types was 119.4 fold. Low transcript levels were detectable in all tissues examined; heart (5.67), bone marrow (3.57), adipose tissue (3.38), brain (1.96) and gut (1.20) (numbers in brackets represent the fold difference when compared to PHOSPHO1 expression in liver, which was deemed 1).

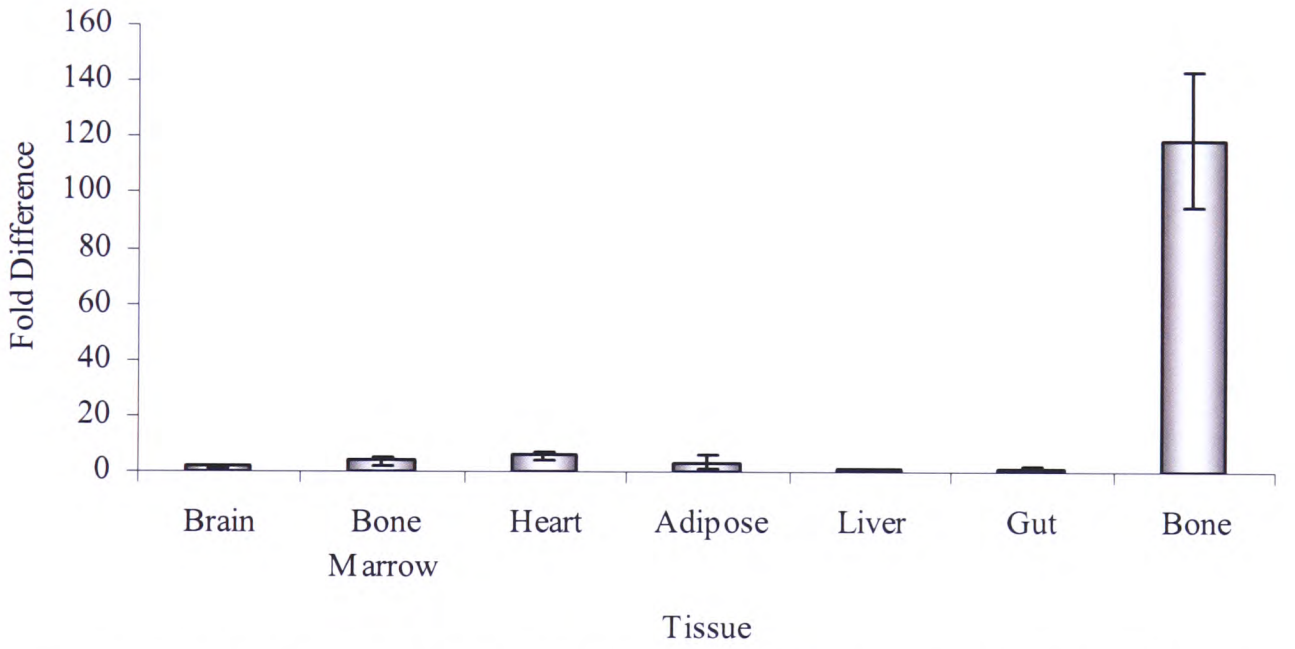

Figure 5.5 Q-PCR of PHOSPHO1 in murine tissues. Data shows relative expression of PHOSPHO1 with liver denoted 1 due to it having the lowest expression profile. RNA was isolated from mouse tissues by phenol chloroform extraction and used directly in a quantitative PCR reaction utilising the DNA intercalating dye, SYBR green. Results are mean ± SD (n = 3).

5.5.3 Antibody Production

Two strategies were utilised to raise an antibody capable of recognising human/mouse PHOSPHO1, firstly immunising rabbits directly with recombinant human PHOSPHO1 protein and secondly producing a synthetic peptide to the c

terminal region of the protein (identical in human and mouse), linking this to KLH (keyhole limpet haemocyanin) and using this as an antigen for immunisation.

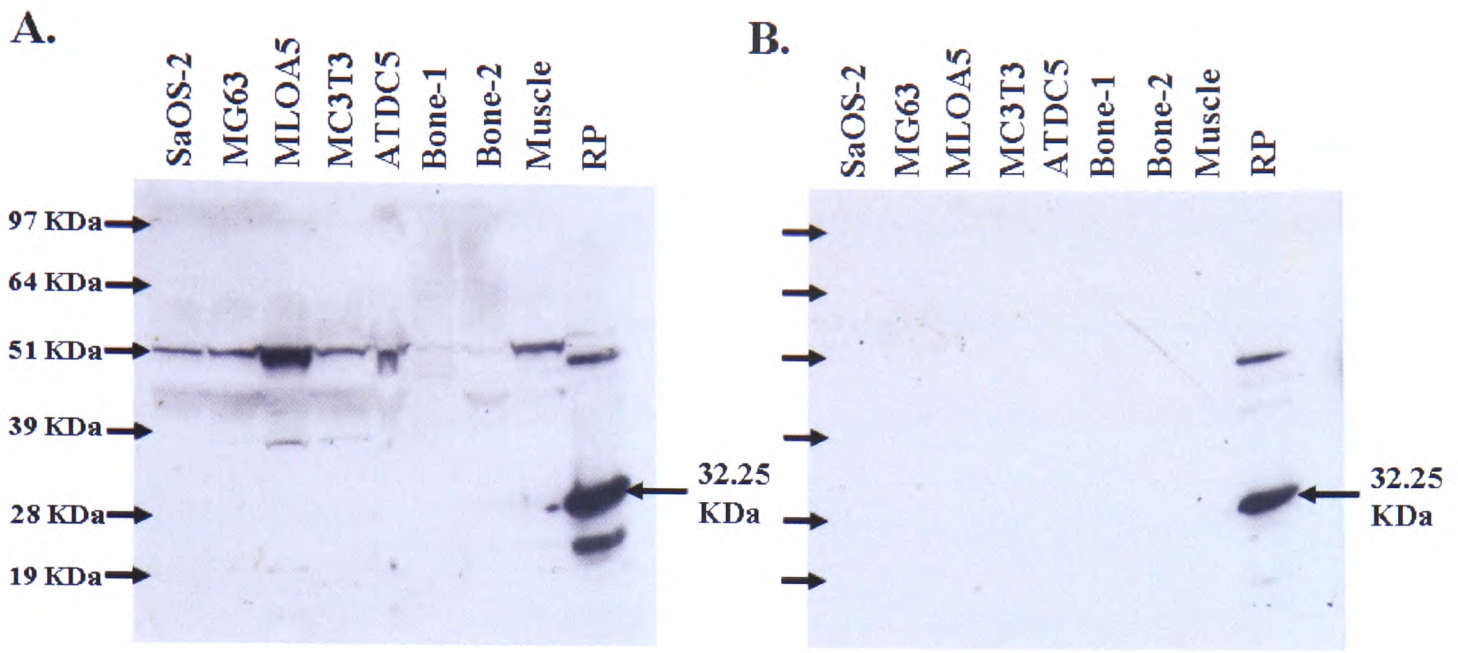

Figure 5.6 Testing antibodies raised against PHOSPHO1 for immunoreactivity towards cell and tissue lysates. (**A**) Immunoblot using an antibody raised against recombinant human PHOSPHO1(**B**) Immunoblot using an antibody raised against the synthetic peptide CGYPMHRLIQEAQKAE. Both of these antibodies were produced in New Zealand white rabbits.

As seen in figure 5.6 both antibodies recognise the recombinant protein, however no bands are present on the western blot at a size corresponding to PHOSPHO1 in either cell line or bone tissue lysates. As discussed in chapter three, the predicted size for the two splice variants are approximately 29 and 32 KDa. These antibodies also failed to stain bone sections positively by immunohistochemistry. Therefore in order to advance my studies a rabbit antiserum to mouse PHOSPHO1 was sourced from Professor Ikramuddin Aukhil, University of Florida, USA. This antiserum was raised against the 32KDa form of mouse recombinant PHOSPHO1.

5.5.4 PHOSPHO1 Protein Levels in Differentiating Cells

To analyse the effect of differentiating factors on the presence of PHOSPHO1 within murine MLOA5 (osteoblast) cells and ATDC5 (chondrocyte), cells were cultured in the presence of 10 mM βGP and 50 μg/ml AA. Two forms of PHOSPHO1 (32 and 29KDa) were detected in each cell type corresponding to two splice variants from the *Phospho1* gene, as seen in figure 5.7. However, PHOSPHO1 appeared to be constitutively expressed and protein levels did not alter during cell differentiation and mineralisation (point where mineralisation is evident depicted by red lettering in figure).

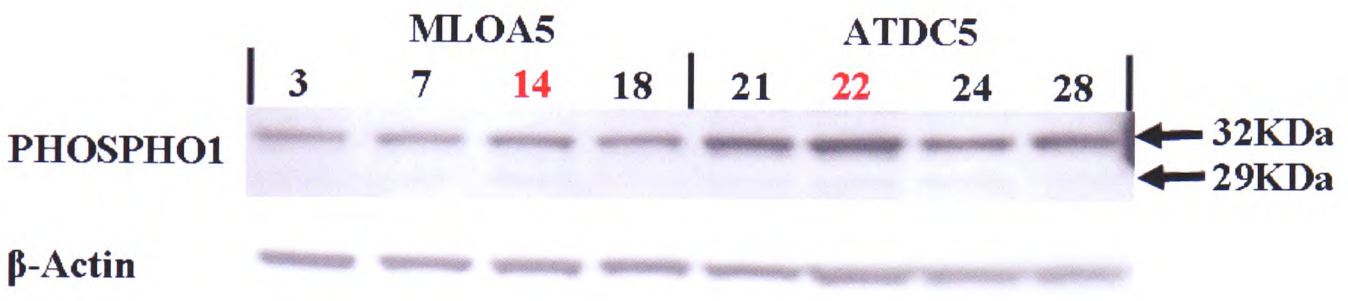

Figure 5.7 Immunoblot showing the effect of mineralising conditions on PHOSPHO1 expression by the murine osteoblast cell line, MLOA5 and the chondrocyte cell line, ATDC5. Each cell line was cultured in the presence of 10 mM βGP and 50 μg/ml AA. The day in red indicates the time point at which mineralisation of the monolayer was evident.

5.5.6 Immunolocalisation of PHOSPHO1 to Skeletal Cells and Identification of PHOSPHO1 in Mouse MVs

Confirmation that, as with the avian model, PHOSPHO1 is present in MVs from a mammalian source was obtained by localisation to MVs isolated from mouse calvarial osteoblasts (figure 5.8). A single band of 29 KDa was detected which agrees with the expe16ted protein size for one of the PHOSPHO1 splice variants.

The high expression levels of PHOSPHO1 in bone noted by qPCR (figure 5.5) was confirmed and extended by the localisation of PHOSPHO1 to primary regions of ossification in growth plate cartilage, trabecular bone and calvarial bone. Positive staining was restricted to the hypertrophic zone of the growth plate with strongest staining observed in the early hypertrophic region, observed both in tibia and fibula (figure 5.9 and 5.10A). No staining was observed in the proliferating chondrocytes and in comparison to the pre-hypertrophic chondrocytes, the terminally differentiated hypertrophic chondrocytes displayed little staining. PHOSPHO1 immunoreactivity was also observed within the chondrocytes of the developing secondary ossification centre of the fibula (figure 5.9).

Positive staining was present on the surface of the trabecular bone of the secondary spongiosa as well as within the osteoblasts lining the bone forming surfaces of the primary osteons within the periosteal area of the cortical bone. Bone forming regions of the calvaria also stained positive for PHOSPHO1 (figure 5.10B).

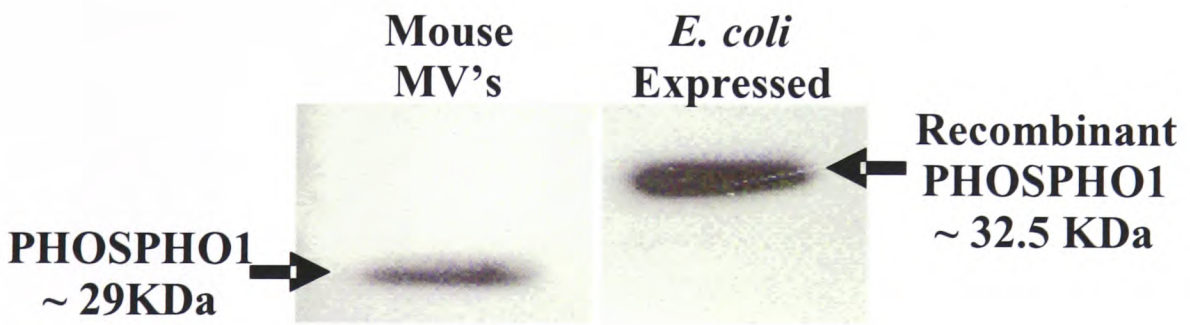

Figure 5.8 Immunoblot showing the localisation of PHOSPHO1 to murine MVs isolated from murine calvarial osteoblasts. MVs were isolated as indicted in 5.4.7 and 20 μg used for western blot analysis, immunoreactivity is compared to that of recombinant PHOSPHO1. The recombinant protein is of greater mass due to the presence of a C-terminal tagged region.

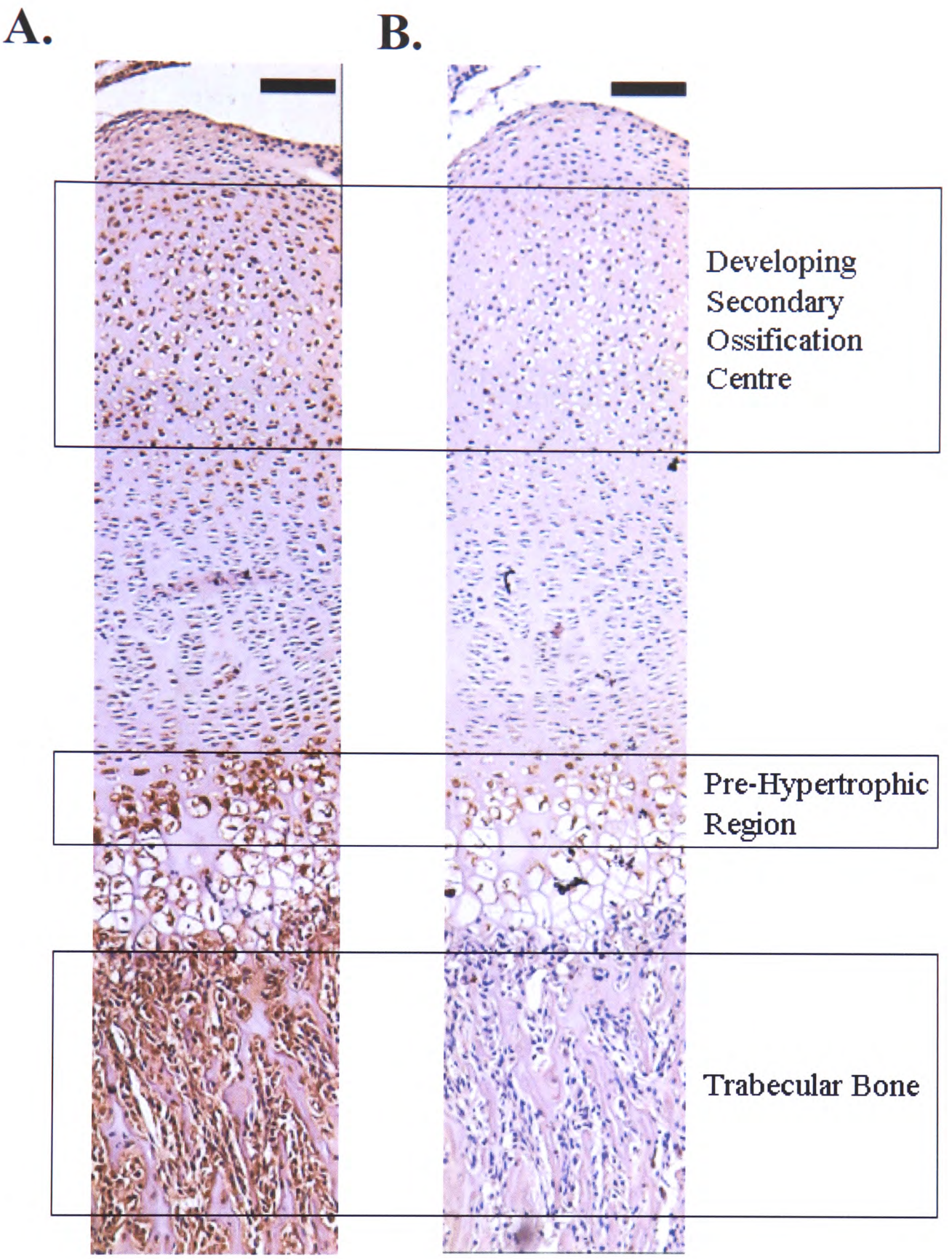

Figure 5.9 Immunohistochemistry showing the localisation of PHOSPHO1 in mouse fibula. (**A**) Section was probed using a PHOSPHO1 specific antisera, localisation was restricted to the mineralising regions of the bone, including (from top to bottom) the developing secondary ossification centre, pre-hypertrophic chondrocytes and trabecular bone (**B**) Control section probed with pre-immune sera. (Scale Bar = 100μm).

A.

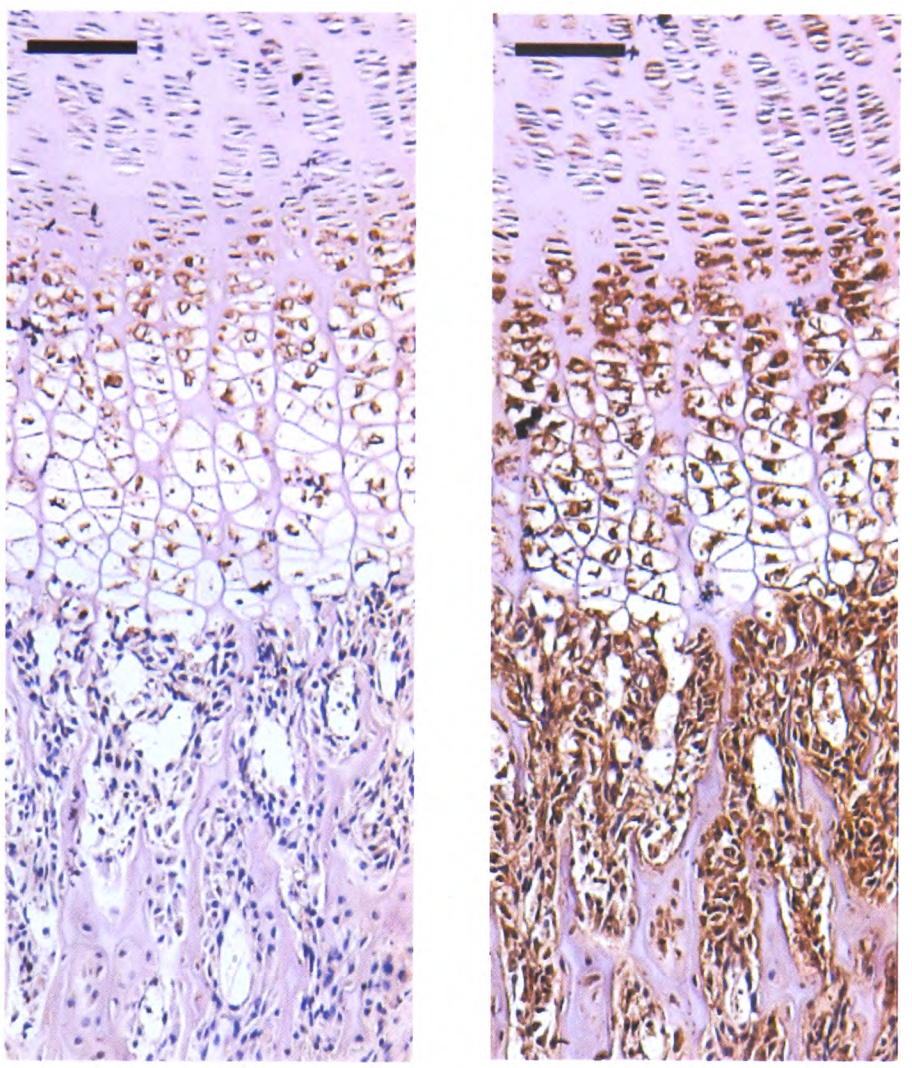

B.

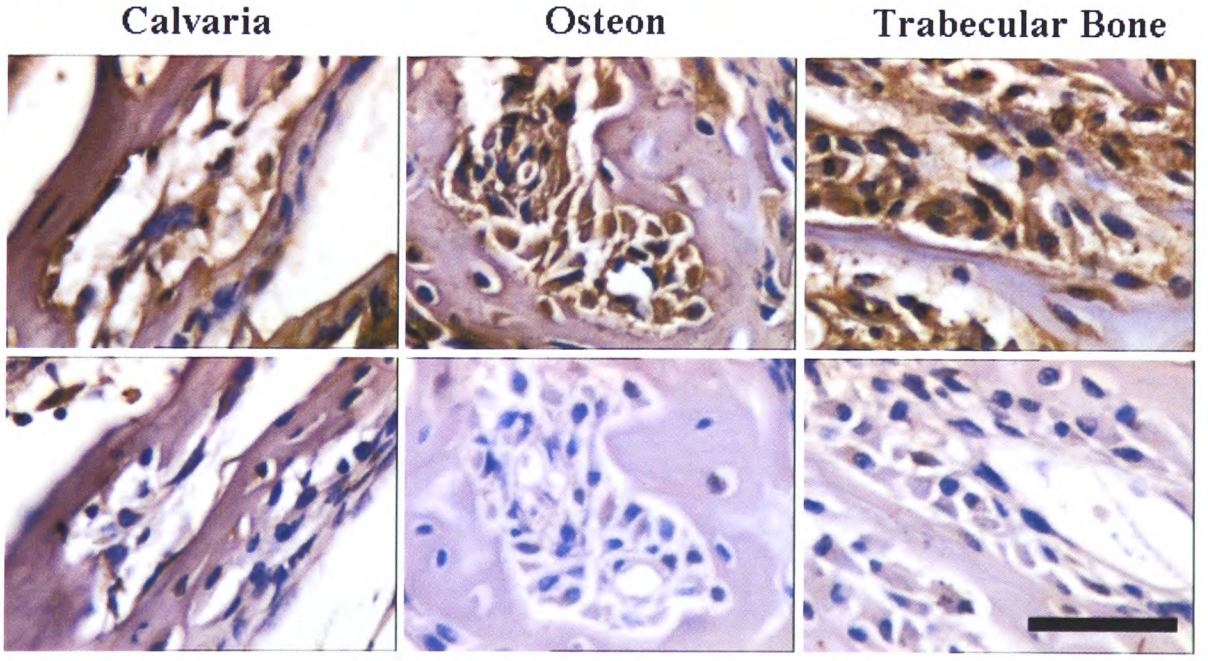

Figure 5.10 Immunohistochemistry showing the localisation of PHOSPHO1 in mouse tibial sections. (**A**) Tibial growth plate probed with PHOSPHO1 specific antisera, Control section to the left (Scale bar = 100μm) (**B**) Higher magnification of mineralising centres including the calvaria, osteon and trabecular bone (control sections displayed in the lower panel). (Scale Bar = 50μm)

5.5.7 Identification of Active PHOSPHO1 in MVs

To determine if the PHOSPHO1 present in murine MVs was active I tested for hydrolase activity within intact and sonicated MVs isolated from cultures of *Tnap*$^{-/-}$, *Tnap* $^{+/-}$ and wild-type osteoblasts. This strategy was adopted to eliminate the possibility that TNAP hydrolysis of PEA may mask PHOSPHO1 activity. Cell phenotype (*Tnap*$^{-/-}$, *Tnap*$^{+/-}$ and wild-type cells) was confirmed using TNAP histochemistry, and mineralisation capability by von Kossa staining (figure 5.11). TNAP activity of MVs purified from these cultures mirrored that of TNAP histochemistry (figure 5.12A). MV preparations were used directly in the standard discontinuous colorimetric assay. It was found that the wild-type and *Tnap*$^{-/-}$ intact MVs had a hydrolase activity of 3.3 $\pm$ 0.4 and 0.07 $\pm$ 0.4 nmol.min^{-1}mg^{-1} MV protein, respectively. *Tnap* heterozygous MVs had an activity of 1.68 $\pm$ 0.5 nmol.min^{-1}mg^{-1} MV protein (figure 5.12B). Sonication of the MV preparation caused an increase of approximately 1 nmol.min^{-1}mg^{-} in all cases ($P<0.05$), suggesting that the enzyme responsible for this increased hydrolysis is cytosolic.

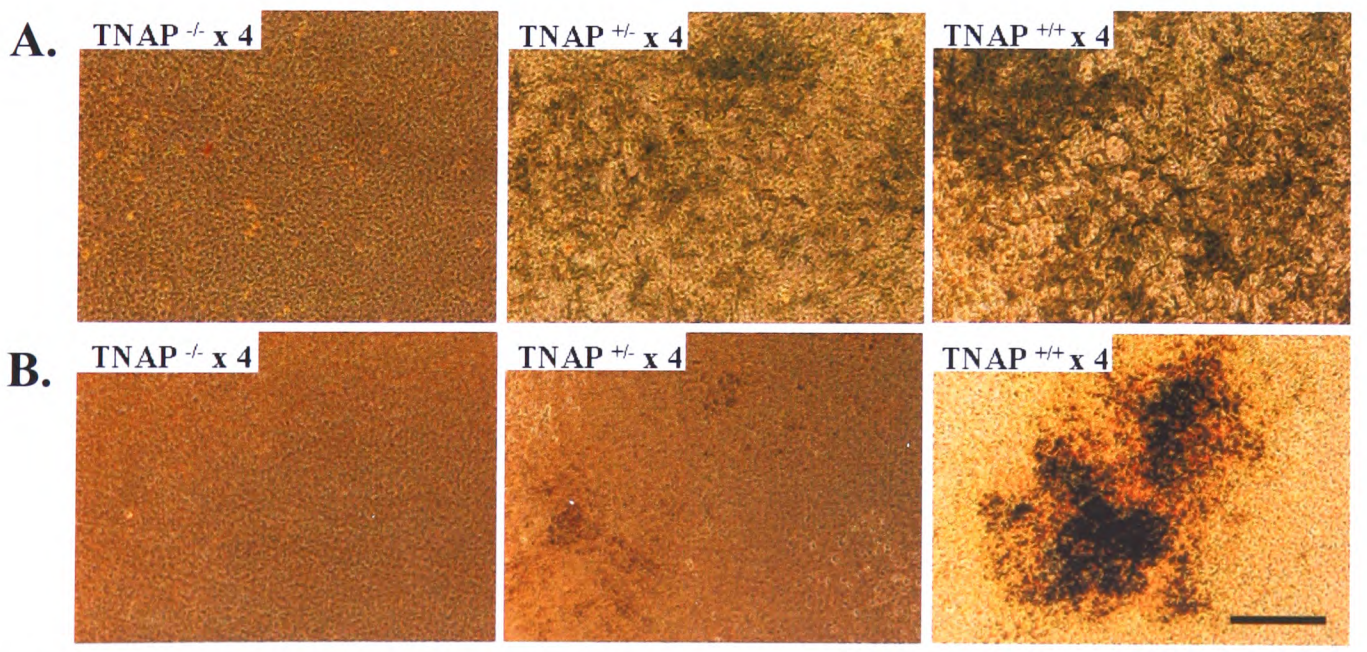

Figure 5.11 Phenotypic confirmation of osteoblasts. (**A**) TNAP histochemistry on osteoblast monolayers (**B**) von Kossa staining of osteoblast monolayers. Both techniques were carried out on day 13 - the same time as MV harvest. (Scale Bar = 500μm)

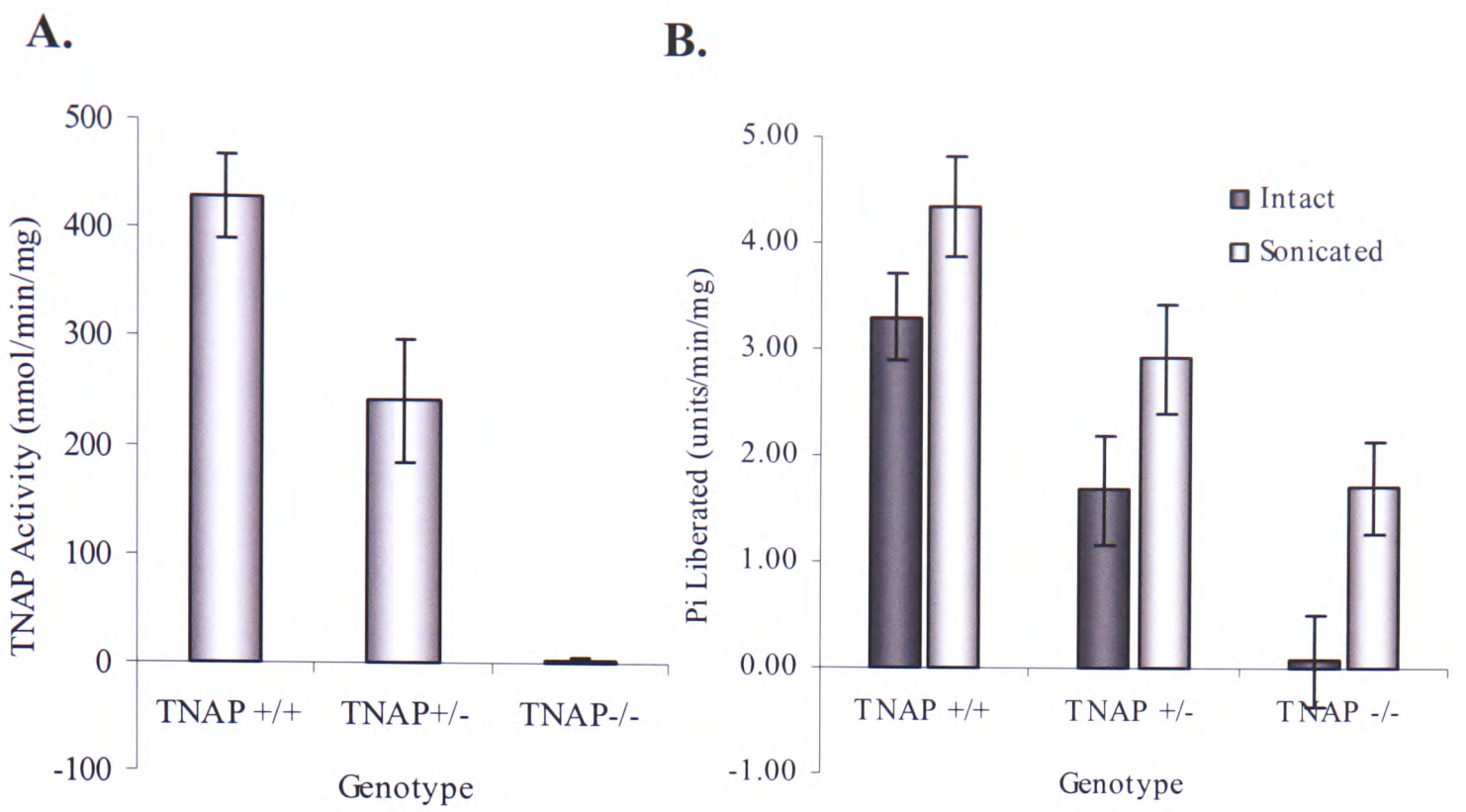

Figure 5.12 Hydrolase activity of MVs from *Tnap*$^{+/+}$, $^{+/-}$, $^{-/-}$ osteoblasts. **(A)** pNPP and **(B)** PEA phosphatase activity of MV preparations. Data is presented as the mean ± SEM of nine replicates from each genotype (units = nmol/min). PEA hydrolase activity was significantly higher ($p<0.05$) in sonicated vs. intact MVs. Two way analysis of variance used for generation of p value.

5.6 Discussion

It has previously been shown that PHOSPHO1 expression is upregulated approximately 100 times in mineralising chondrocytes compared to non skeletal tissues in the avian system (Houston *et al*, 1999). As shown in figure 5.5 PHOSPHO1 expression is approximately 120 times higher in murine bone tissue than in liver, which was deemed the lowest expresser by quantitative PCR. When compared to the chick expression profile the pattern exhibited in the mammalian system would indicate that PHOSPHO1 is involved in a specific pathway that is closely associated with bone development. The data already presented in chapter 3 speculates that due to the high activity PHOSPHO1 exhibits when incubated with PEA this pathway is likely to be that of glycerolipid metabolism, which may be

harnessed during bone mineralisation as a means of generating Pi. Interestingly the expression of PHOSPHO1 in bone is only 20 times higher than that of heart, however under normal development heart muscle should not mineralise as this is associated with pathological disease. Interestingly, PHOSPHO1 has also been shown to be able to cleave PCho, the hydrolysis of which has been studied in hamster heart and has been shown to be catalysed by an unidentified enzyme (Hatch and Choy, 1987). PCho is an important regulatory compound for the metabolism of phosphatidylcholine, the major phospholipid in mammalian tissues (Zelinski and Choy, 1982), thus the action of a phosphocholine phosphatase would provide a means for regulating this system in the heart. It has been documented that the phosphocholine pool in the heart is much lower than that in the liver or HeLa cells (Pelech and Vance, 1984) thus a novel regulatory mechanism may be present in this tissue which is absent in others. This may be controlled by the PCho activity of PHOSPHO1 hence explaining the increased expression in this tissue when compared with others, and implicating PHOSPHO1 in a possible novel pathway which may be mediated by one of the alternate transcript from the PHOSPHO1 gene. The low transcript level in bone marrow (figure 5.5) would indicate that mesenchymal stem cells and osteo-progenitor cells do not express PHOSPHO1 thus indicting that it is perhaps a protein which is found only in mature cells thus implying an involvement in a pathway that is unique to the terminally differentiated cells of the bone.

To allow a link for PHOSPHO1s involvement in tissue mineralisation to be formed, the protein would not only have to be localised to mineralising surfaces of both bone and cartilage, it would also have to be closely associated with MVs, the site of initial crystal formation (Anderson, 1969). Previous studies have shown that

in the avian system PHOSPHO1 protein is localised to the mineralising sites of both bone and cartilage, however no data is present regarding the potential involvement of PHOSPHO1 in MV mediated mineralisation (Houston *et al*, 2004). The immunolocalisation of PHOSPHO1 in the murine system analysed in the present study mirrors that found by Houston and colleagues, namely that PHOSPHO1 is found at every site of mineral production in both bone and cartilage, thus further implicating this protein in matrix mineralisation. As shown in figures 5.9 and 5.10 the PHOSPHO1 protein is localised to mineralising growth plate chondrocytes of the early hypertrophic region and also to bone forming surfaces situated on trabecular, cortical and calvarial bones. This localisation mirrors that of TNAP (Miao and Scutt, 2002), which has been long associated with matrix mineralisation and perhaps indicates synergy between the two enzymes to achieve hydroxyapatite crystal growth through the depletion of the mineralisation inhibitor PPi and the elevation of Pi from PEA hydrolysis. The lower expression of PHOSPHO1 in the terminally differentiated chondrocytes of the mammalian growth plate would indicate that PHOSPHO1 is required for the initial events of mineralisation (Phase 1, as discussed in 1.6.3.1) and not the growth of hydroxyapatite crystal (Phase 2), which is readily seen in this zone. Phase 2 is generally attributed to TNAP action, which is consistent with the localisation of TNAP activity throughout the whole of the hypertrophic zone (Farquharson *et al*, 1999). Interestingly the hypertrophic region of the growth plate is characterised by concentration of MVs in the longitudinal septa (Anderson, 1969), it is within these MVs that hydroxyapatite nucleation occurs hence if PHOSPHO1 is present within these vesicles the distribution would be concordant with a role in the initial events of mineralisation.

It has previously been shown that chick growth plate chondrocytes contain the 30.4 and 28.6 kD forms of PHOSPHO1, corresponding to transcripts derived from alternative start sites in the PHOSPHO1 gene (Houston *et al*, 2004). The amino acid sequences of both putative transcripts contain all three of the catalytic motifs found within the HAD enzyme superfamily (Ridder and Dijkstra, 1999) and so both forms are likely to be catalytically active. It is unknown whether each form has a distinct physiological significance. Both forms of PHOSPHO1 were found to be present in chick MVs providing strong evidence that PHOSPHO1 is involved in the first phase of the mineralisation. Interestingly only the smaller of the two forms was found to be present in MVs from cultured murine calvarial osteoblasts. This may be due to the smaller transcript possessing the higher capacity for Pi generation within MVs. Upon analysis of the immunoblot in figure 5.3A it is evident that the smaller transcript forms higher proportion of PHOSPHO1 content within the chick MV thus also implicating this protein as more important of the two in regard to MV mediated calcification. Primary chick chondrocytes were cultured in the presence and absence of AA. The addition of AA was found to increase both PHOSPHO1 levels and TNAP activity in isolated MVs. AA is a known stimulant for osteogenesis and mineralisation *in vitro* (Peck *et al,* 1967; Spindler *et al*, 1989). This suggests that PHOSPHO1 expression and TNAP activity are both influenced by the state of differentiation and may be controlled by similar mechanisms within growth plate chondrocytes. Interestingly, as seen in figure 5.7, mineralising agents do not increase the cellular content of PHOSPHO1 in either chondrocytes or osteoblasts when cultured over a time period spanning the mineralisation of the cell monolayer. This is in contrast to the protein content observed within MVs and indicates that the protein

is perhaps being targeted to the vesicle in response to mineralising conditions, hence explaining the increase of PHOSPHO1 levels within MVs. When compared with PHOSPHO1, AA does not increase the transcript levels of TNAP found in chondrocytes, but an increased activity is observed and is thought to be due to an interaction of TNAP with collagen during matrix synthesis (Franceschi and Young, 1990; Hitomi *et al*, 1992)

To analyse the ability of MV derived PHOSPHO1 to catalyse the hydrolysis of PEA (the phosphomonoester found to show the most favourable kinetics when incubated with recombinant human PHOSPHO1), MVs were isolated from murine calvarial osteoblasts which had been differentiated with AA, as this has been shown to increase their PHOSPHO1 content in chick matrix vesicles. The cells from which these were isolated were genetically different in relation to the presence of TNAP (*Tnap*$^{-/-}$, *Tnap*$^{+/-}$ and wild-type cells) hence allowing the quantification of PEA hydrolysis with varying degrees of TNAP present. PEA hydrolase activity was observed with wildtype and *Tnap*$^{+/-}$ but not in *Tnap*$^{-/-}$ MVs. However upon sonication of the MV preparations PEA hyrolase activity was observed with all phenotypes. Sonication would cause the MV to rupture thus when these MVs were analysed for PEA hydrolase activity intravesicular proteins would be exposed to the substrate. This would indicate that the enzyme responsible for this degradation is cytosolic and as according the KEGG database only PHOSPHO1 has the ability to cleave PEA at a neutral pH, it is likely that this enzyme is in fact PHOSPHO1, as seen in figure 5.13. It is worth noting that previously documented hydrolysis of PEA by TNAP was under alkaline pH (Muller *et al*, 1989), thus this reaction would not be favourable under assay conditions or in *vivo*. The only other reported mammalian

enzyme capable of hydrolysing PEA is acid phosphatase, however its action against PEA has not been reported in bone (McDonald *et al*, 1980). The rationale behind why hyrolase activity is observed with intact MVs is due to TNAP being anchored to the outer leaflet of the plasma membrane thus TNAP would be exposed to the substrate if the vesicles were intact or ruptured. This is confirmed through the analysis of TNAP activity of intact MVs as this pattern mirrors that of PEA hydrolase activity before sonication.

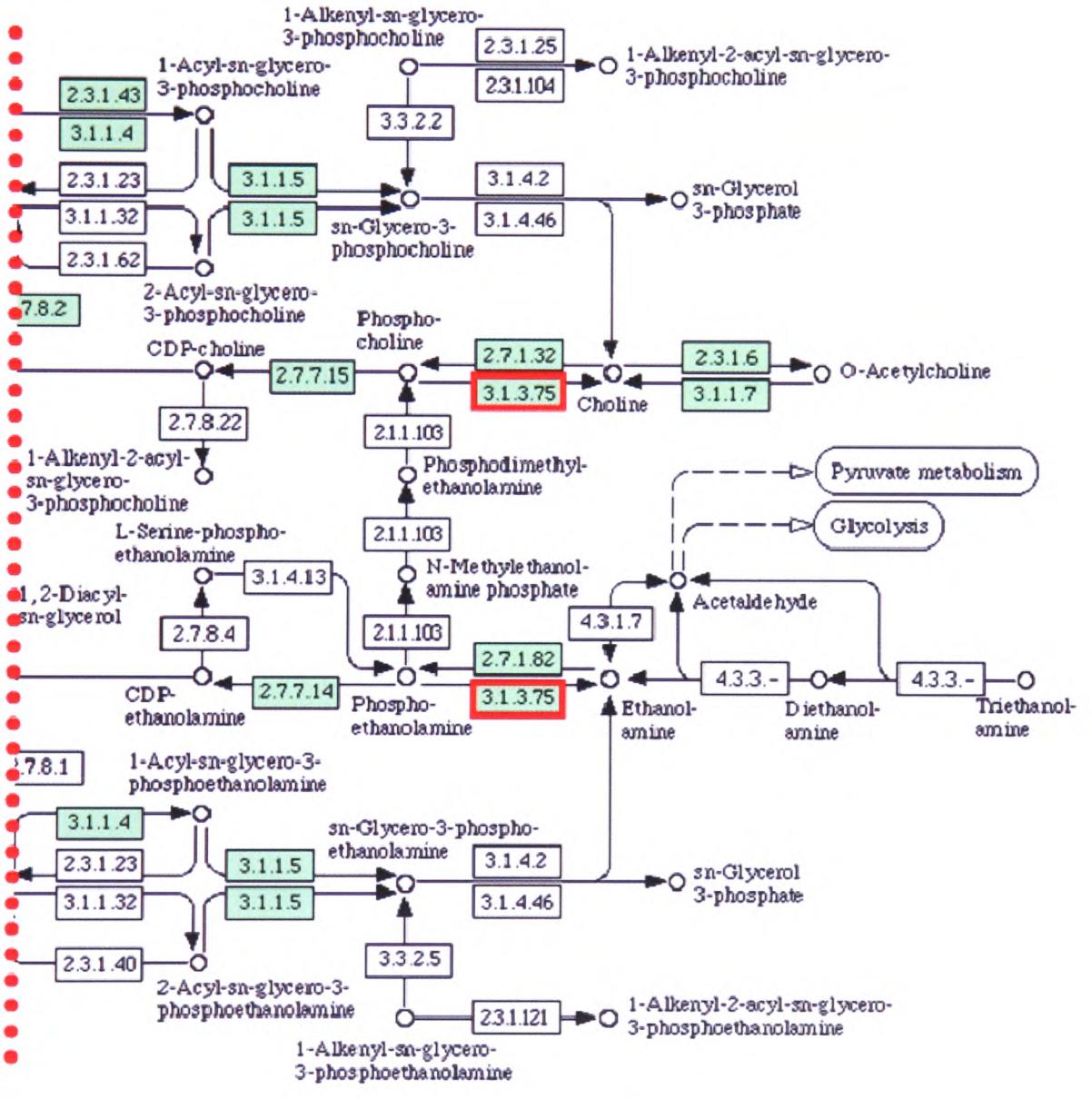

Figure 5.13 Extract of the phosphoglycerolipid metabolism pathway from the KEGG database. This pathway indicates enzymes known to catalyse specific reactions within different metabolic pathways. Note the only enzyme documented to catalyse the hydrolysis of PEA and PCho to ethanolamine and choline respectively is enzyme 3.1.3.75 (PHOSPHO1) as indicated by red boxes.

In conclusion PHOSPHO1 expression is up regulated in bone tissue and protein localisation is restricted to sites of mineralisation in the mammalian model. Further to this, PHOSPHO1 protein is found within chondrocyte and osteoblast derived MVs. This protein is cytosolic and in an active state, retaining the ability to hydrolyse the PEA, as already demonstrated with the recombinant enzyme. In addition to this it is regulated by AA thus exhibiting similar characteristics as TNAP. These data further strengthens the hypothesis that PHOSPHO1 has a role in bone mineralisation, likely to be linked to the glycerolipid metabolism pathways involving the degradation of phosphatidylethanolamine and phosphatidylcholine hence producing Pi for MV mediated mineralisation.

CHAPTER 6

FUNCTIONAL ANALYSIS OF MAMMALIAN PHOSPHO1

Chapter Contents

6.1 Introduction

Although PHOSPHO1 has now been implicated in the glycerolipid metabolism pathway due to its high catalytic activity towards both PCho and PEA its exact function with respect to bone mineralisation is yet to be discovered. The *in vivo* function of PHOSPHO1 appears to be closely associated with the bone mineralisation process due to its location to mineralising sites in both bone and cartilage in both mammals and birds; the identification of PHOSPHO1 in MVs also strengthens the evidence for a role in this process.

To assign function to this protein cells can be modified to have a reduced content of PHOSPHO1 thus creating a line that can be examined for phenotypic alterations and discrepancies in cellular function. The method now commonly used for this type of investigation is short interfering (si) RNAs which function to modulate mRNA levels of the cell. This process known as RNA interference (RNAi) is a natural phenomenon triggered by double stranded RNA, from which a template is formed for the sequence-specific targeting and degradation of endogenous RNAs. This process is observed as a natural anti-viral mechanism in plant immune systems, however pioneering work using C. elegans has further characterised the use of antisense and in particular antisense/sense duplexes for modulation of mRNA (Fire *et al*, 1998; Baulcombe, 2004). Upon detection of dsRNA within a cell the RNA is processed by the dicer enzyme which is a cytoplasmic RNAse like enzyme, to produce siRNAs of approximately 21 nucleotides in length. The siRNAs combine with an RNAi inducing silencing complex (RISC), which triggers the destruction of the complimentary mRNA, upon binding. In addition to this system if the siRNA pairs with the target RNA in the absence of RISC a RNA directed RNA polymerase

can use this as a primer to amplify the mRNA, this can be subsequently cleaved by DICER to produce new siRNAs (Sijen *et al*, 2001). In addition to this, short hairpin (sh)RNAs which can be produced from vector systems are also processed by the DICER thus allowing exploitation of this system for stable transcript knockdown, something that cannot be achieved by conventional 21 nucleotide dsRNA oligonucleotides. This process of stable gene knockdown is desirable when studying proteins thought to be involved in the mineralisation process as matrix mineralisation *in vitro* occurs after 20 days post confluence with the SaOS-2 osteosarcoma cell line (McQuillan *et al*, 1995). The knockdown effect when using synthetic siRNA oligonucleotides is typically around 96 hrs thus to achieve knockdown over a prolonged period multiple transfections would need to be carried out. However cell transfection is only effective pre-confluence (usually 50-70%) thus due to the kinetics of the mineralisation process synthetic dsRNA oligonucleotides are of no value when using these cell lines.

An additional method for attributing functionality to phosphatases is to over express the protein within cells while observing any alterations in phenotype or cell behaviour, this process has successfully aided in attributing function to several phosphatases including the protein phosphatases PTPMEG, PTP-alpha and PTP36 (Gu, *et al*, 1996; Cong *et al*, 1999; Ogata *et al*, 1999). As it has been hypothesised that PHOSPHO1 is involved in the initial stages of the mineralisation process this may be adequate to trigger monolayer calcification. In converse the 'knockdown' of gene transcript may modulate the deposition of hydroxyapatite. If this is the case it would show for the first time that PHOSPHO1 is involved directly in producing Pi, hence aiding calcium phosphate precipitation and matrix mineralisation.

6.2 Hypothesis

That the reduction of PHOSPHO1 within bone cells will reduce their capacity to mineralise and conversely overexpression of PHOSPHO1 within non-skeletal cells will increase their potential to form calcium phosphate.

6.3 Aims

I. To map human PHOSPHO1 RNA to indicate which sites are suitable for siRNA targeting.

II. To produce a construct to stably express shRNA in both osteoblast and chondrocyte cells.

III. To investigate the use of preformed siRNAs with the rapidly mineralising MLO-A5 cells.

IV. To tag the PHOSPHO1 CDS with a Hemagglutinin (HAg) tag and engineer this into a construct suitable for mammalian expression. The tagging of PHOSPHO1 will allow the identification of expressed protein with commercially available antibodies

6.4 Materials and Methods

6.4.1 Secondary Structure Mapping

The secondary structure mapping of PHOSPHO1 mRNA was carried out in conjunction with Expresson Biosystems Ltd. This process utilises a 4069 element degenerate six-base oligonucleotide array, which allows the mapping of *in vitro* transcribed RNA within a 4 hr time frame and at physiological conditions.

To produce gene specific RNA the purified PHOSPHO1 CDS produced in 3.4.2 was cloned into the pGEM-T-Easy vector as described in 2.3.9.2. The ligation reaction was used to transform JM109 competent cells as outlined in 2.3.1. Liquid cultures and plasmid minipreparations of individual clones were subsequently carried out (section 2.3.2 and 2.3.3 respectively). Orientation of the PHOSPHO1 CDS was analysed by digestion with Nco1. A clone in the correct orientation was used for the production of *in vitro* transcribed RNA from the T7 and Sp6 RNA promoters.

The RNA production and array analysis was undertaken at Expression Biosystems Ltd.

6.4.2 Production of a shRNA Expressing Construct

The pSUPER vector (Oligoengine, appendix 1) was supplied linearised with *BglII HindIII* 'sticky' ligation sites. This vector was first described in Science by Brummelkamp *et al* (2002), in a study that detailed stable suppression of p53 in MCF-7 cells. From this study several variants of the original pSuper vector have been developed. The preferred vector for this work would be the pSUPER.gfp/neo, this vector utilises the H1 RNA polymerase III promoter to drive shRNA synthesis, this has many advantages including the ability to function without additional

transcriptional elements unlike other pol III promoters, this promoter also drives endogenous siRNA production. The phosphoglycerate kinase (PGK) promoter drives the production of the gfp/neomycin resistance fusion protein. This is a housekeeping gene promoter thus not tissue specific allowing expression of this protein in all cell types.

The region that was identified in the secondary structure mapping of PHOSPHO1 was designed as a shorthairpin RNA. To produce the shRNA two 60mer complimentary oligonucleotides were synthesised (Sigma-Genosys) containing a 19-mer target region specific to the target region of PHOSPHO1, a loop region and a stem region, as shown in figure 6.1. The oligonucleotides (3 μg of each) were annealed in a 50 μl reaction containing 25 mM Tris-Acetate pH 7.5, 100 mM K-Acetate, 10 mM Mg-Acetate, 1 mM DTT. The reaction was cycled at 90°C for 4 minutes, 70°C for 10 minutes, the reaction was then step cooled to 10°C (2°C /minute). The annealed oligonucleotides were ligated downstream of the H1 promoter via *HindIII/BglII* restriction sites which are engineered to the end regions of the oligonucleotide pair. This was done as outlined in section 2.3.9.1 using a 10:1 ratio. When RNA is transcribed from this region, a gene specific shRNA is produced which is cleaved into a conventional 21mer siRNA by the cells dicer enzyme. The ligated plasmid/oligonucleotide was used to transform SURE-2 cells as described in 2.3.1. Liquid cultures and plasmid minipreparations of individual clones were subsequently carried out (section 2.3.2 and 2.3.3 respectively). Clones containing the oligonucleotide pair were identified by restriction digestion of plasmid minipreparations as described in 2.3.8. Briefly the plasmid DNA was digested with the restriction enzymes EcoR1 and Sal1, a fragment of 302bp would be present if the

oligonucleotides had ligated to the vector successfully. DNA sequencing of plasmids was carried out by the DNA sequencing facility at Dundee University.

Figure 6.1 Design of the oligonucleotides required for shRNA production. Each individual oligonucleotide was synthesised by Sigma-Genosys and annealed to form an insert for the pSUPER vector. When transcribed the two complimentary stem regions come together producing a hairpin like structure.

6.4.3 Transfection of SW1353 and SaOS-2 Cells

These two cell types were transfected with the pSUPER vector, described above, as outlined in 2.2.6. The drug used for selection of stably transfected cells was G418 (neomycin), this was used at concentrations of 700 μg/ml and 500 μg/ml for SW1353 and SaOS-2 cells respectively. These concentrations were deemed the lowest needed for 100% cellular death through kill curve analysis of concentrations between 200 and 800 μg/ml. Selective pressure was kept on until no sign of cellular death was evident and 100% of cells were fluorescing green when viewed over UV light.

6.4.4 Analysis of Transfected Cells

RNA was isolated from cells by Ultraspec extraction, as described in 2.4.1 and reverse transcribed as described in 2.4.3. PHOSPHO1 transcript was amplified as described in 2.4.4 utilising the gene specific primers TACAGGTGGTGCTCACGGTA (forward) and CAAAGGGATGGCTTCGTAGA

(reverse), a 57°C annealing temperature with 200ng cDNA. The PCR products were then electrophoresed on a 2% agarose gel as described in 2.3.5. The band densities were compared using multi-analyst after normalisation to the density of the β-actin band.

The transfected SW1353 cells were cultured, as outlined in section 2.2.3, in DMEM supplemented with 10% FBS and 0.5% genomycin, the cells were initially seeded at a density of $5x10^4$ cells/cm^2 in a 6 well plate (day 0). The cells were either supplemented with 50 μg/ml AA and 10 mM βGP on day 3 or with AA alone. The cells supplemented with AA alone were changed to DMEM containing 5% FBS, 8 amino acids (Ala 7 mM, Asn 0.4 mM, Asp 4 mM, Glu 10 mM, Gly 7 mM, Pro 3 mM, Ser 2 mM, and taurine 2 mM), and insulin (5 μg/ml), transferrin (5 μg/ml), sodium selenite (5 ng/ml), and 1 mM Na_2HPO_4 to bring total inorganic phosphate (Pi) to 1.9 mM and Ca^{2+} to 1.8 mM (DATP5 media) on day 6, along with 50nM retinoic acid. The addition of phosphate to this media means no addition of a phosphoester is required. The cells were cultured to day 12 and then stained with alizarin red as outlined in section 2.2.9.1 and a digital image taken.

6.4.5 Tansfection of MLO-A5 Cells with siRNA

Cells were maintained as outlined in section 2.2, with the following modifications. The cells were cultured in alpha MEM (Gibco) containing 5% FBS, 5% FCS. The cells were seeded into 12 well plates at a density of 10,000 cells/cm^2, and cultured overnight to allow cellular attachment. The transfection protocol was similar to that described in 2.2.6 with the following adjustments. Lipofectamine was utilised as the transfection reagent, 100 pmols of pre-annealed oligonucleotides

(Dharmacon Smart-pool or GFP control) were combined with 250 µl Opti-MEM and the same was carried out for 5 µl Lipofectamine-2000, these were combined after 5 minute incubation at room temperature and incubated for a further 20 minutes. The complexed RNA/Lipofectamine was added to the 1.5ml cell culture media on the cell monolayer and incubated for 6 hrs at 37°C (5% CO_2). The media was then replaced with alpha MEM containing 5% FBS, 5% FCS, 50 µg/ml AA and 10 mM βGP. The cells were culture for 6 days changing the media daily.

6.4.6 Analysis of siRNA Transfected MLO-A5 cells

This analysis was similar to that in 6.4.4 with the following adjustments. The PCR that was carried out utilised the mouse specific PHOSPHO1 primers GACAATGAGCGGGTGTTTTC (forward) GGGGATGGTCTCGTAGACAG (reverse). The external control used for this PCR was 18s RNA in place of β-actin. The cells were cultured to day 6 during differentiation with 50 µg/ml AA and 10 mM βGP, they were then stained with alizarin red and a digital image taken.

6.4.7 Production of a HAg-Tagged PHOSPHO1 Expression Construct

To tag PHOSPHO1 a PCR method was employed. This utilised a protocol as outlined in section 2.4.4, however the reverse primer used was modified to engineer a HAg tag into the amplified product, as shown in figure 4.2. The primer would initially only partly anneal to the template DNA, however subsequent cycles of PCR would ensure all product contained the tagged sequence. The template used for the generation of this tagged PHOSPHO1 was the pBAD-PHOSPHO1 clone detailed in 3.4.2. The reaction conditions were as detailed in section 2.4.4, using 100ng plasmid

DNA and an annealing temperature of 69.2°C. The PCR products were then electrophoresed on a 1.5% agarose gel as described in 2.3.5 and purified using the Qiagen QiaQuick gel extraction kit as outlined in 2.3.6. The PCR products were cloned directly into the pGEM-T-Easy vector (Promega, as shown in appendix 1). The PCR product and plasmid were ligated in a 3:1 ratio using 100ng of PCR product as described in 2.3.9.1. This mixture was used to transform JM109 competent cells as outlined in 2.3.1. Liquid cultures and plasmid minipreparations of individual clones were subsequently carried out (section 2.3.2 and 2.3.3 respectively). DNA sequencing of plasmids was carried out by the DNA sequencing facility at Dundee University.

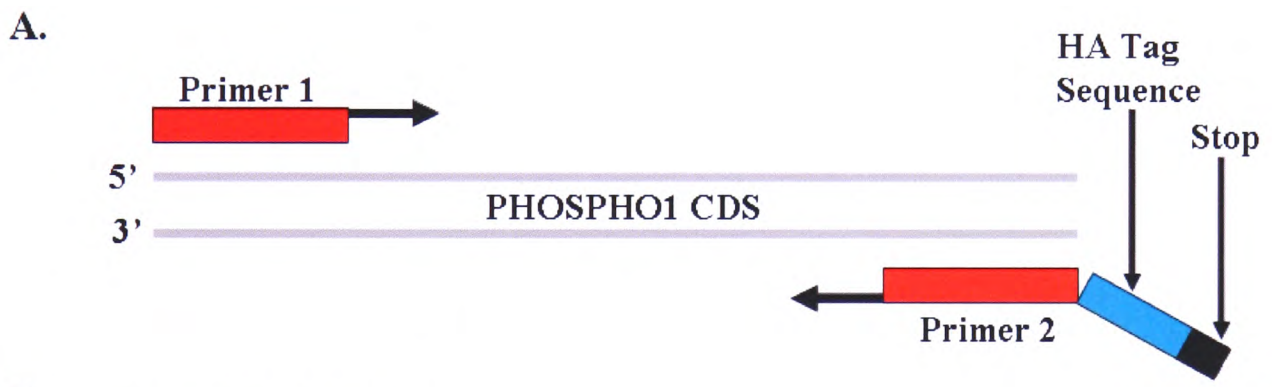

Figure 6.2 Technique used to introduce a C terminal HAg tag to the PHOSPHO1 CDS using PCR. **(A)** The reverse primer contains a non complimentary region coding for the HAg tag which upon PCR would be integrated into the amplified product. **(B)** Primer sequences used for the amplification which allows the introduction of the peptide sequence indicated.

The pWGB10 mammalian expression vector (as shown in appendix 1) was a kind gift from Dr Cui, Roslin Institute. pWGB10 contains a phosphoglycerate kinase (PGK) promoter to drive recombinant protein expression, simian virus 40 (SV40) small t intron/polyA and a SV40/Puromycin to allow cell selection. The plasmid backbone is composed of pBluescript. Both pWGB10 and a pGEM clone containing the correct sequence of tagged PHOSPHO1 were digested with EcoR1 as outlined in 2.3.8. The linerised pWGB10 plasmid was dephosphorylated with shrimp alkaline phosphatase in a reaction containing 100ng vector DNA, 2 units SAP (Roche) and 1x reaction buffer, this was incubated at 37°C for 10 minutes and heat killed at 70°C for 15 minutes, this process stops the re-circularisation of the empty vector. The digested pGEM clone was run on a 1.5% agarose gel as described in 2.3.5 and the PHOSPHO1 fragment purified using the Qiagen QiaQuick gel extraction kit as outlined in 2.3.6. The tagged PHOSPHO1 CDS was ligated to the linerarised pWGB10 vector in a 3:1 ratio as outlined in 2.3.9.1. This ligation reaction was used to transform JM109 competent cells as outlined in 2.3.1. Liquid cultures and plasmid minipreparations of individual clones were subsequently carried out (section 2.3.2 and 2.3.3 respectively). The clones were analysed by multiple restriction digestions with enzymes *Apa1, BamH1, HindIII, Nco1, EcoR1* and *Sma1* to assess insert orientation. A clone containing the insert in the correct orientation with respect to the PGK promoter was used for (Endofree) plasmid production (2.3.4).

6.4.8 Transfection of HeLa Cells

This cell type was transfected with the pWGB10-PHOSPHO1 (HAg) vector (or empty vector as a control) as outlined in 2.2.6. The drug used for the selection of

stably transfected cells was puromycin, this was used at a concentration of 1μg/ml. Selective pressure was kept on until no sign of cellular death was evident.

6.4.9 Analysis of PHOSPHO1 Expressing HeLa Cells

RNA was isolated from the control and overexpressing cells as described in 2.4.1 and reverse transcribed as described in 2.4.3. Transcripts were amplified as described in 2.4.4 utilising gene specific primers for PHOSPHO1 exon3 GACGAAAACAGCGACGATTC (forward) and CGGAGATGAGAATCACCTCG (reverse) (annealing temperature 55.3°C), PHOSPHO1 spanning intron 2 TACAGGTGGTGCTCACGGTA (forward) and CAAAGGGATGGCTTCGTAGA (reverse) (annealing temperature 56.9°C), puromycin resistance gene (puromycin^{r})ATGACCGAGTACAAGCCCAC (forward) and TCAGGCACCGGGCTTGCGGG (reverse) (annealing temperature 60.5°C), 18s primers (ambion) were used as an external control. Each reaction utilised 200ng cDNA, however only the puromycin PCR incorporated 20% betaine (PCR enhancer). The PCR products were then electrophoresed on a 2% agarose gel as described in 2.3.5.

Protein extracts from both cell lines were seperated on a 10% Bis-Tris novex gel as outlined in 2.5.1 and Western blotted (2.5.4). The primary antibodies that were used include and anti mammalian PHOSPHO1 antiserum, an anti HAg antibody (Sigma) an anti β-Actin (Sigma). The anti HAg antibody was also blocked by incubation with 10 μg/ml HAg peptide (Sigma) in blocking buffer for 1Hr and subsequently used to probe the nitrocellulose membrane.

HeLa cells were plated down at 6000/cm^2 and cultured in the presence of 10 mM βGP or PEA and 50 μg/ml AA for 12 days as outlined in 2.2.3. The cell monolayer's were then stained using the von Kossa method as outlined in 2.2.9.2.

6.5 Results

6.5.1 Secondary Structure Mapping of PHOSPHO1

ACCESSarray analysis was used to allow the determination of accessible sites on the human PHOSPHO1 structure. From the mapping of human PHOSPHO1 4 specific regions were identified as potential targets for siRNA, as shown in figure 6.3, between regions 40 – 59, 138-157, 195-214 and 545-564. However the best target from these regions is the one between 138 and 157 due to its increased accessibility compared to the others and also due to its falling 5' to 3' free energy signature, which is a characteristic of effective siRNAs. From this region the siRNA CTCGTTGTAGAAGCCCTCG (and scrambled control, TAGGTACACGCTCTCGCGC) was designed which was further adapted to be produced from a shRNA producing vector by insertion into a 64 mer oligonucleotide consisting of the tail, target and loop regions required for this type of knockdown.

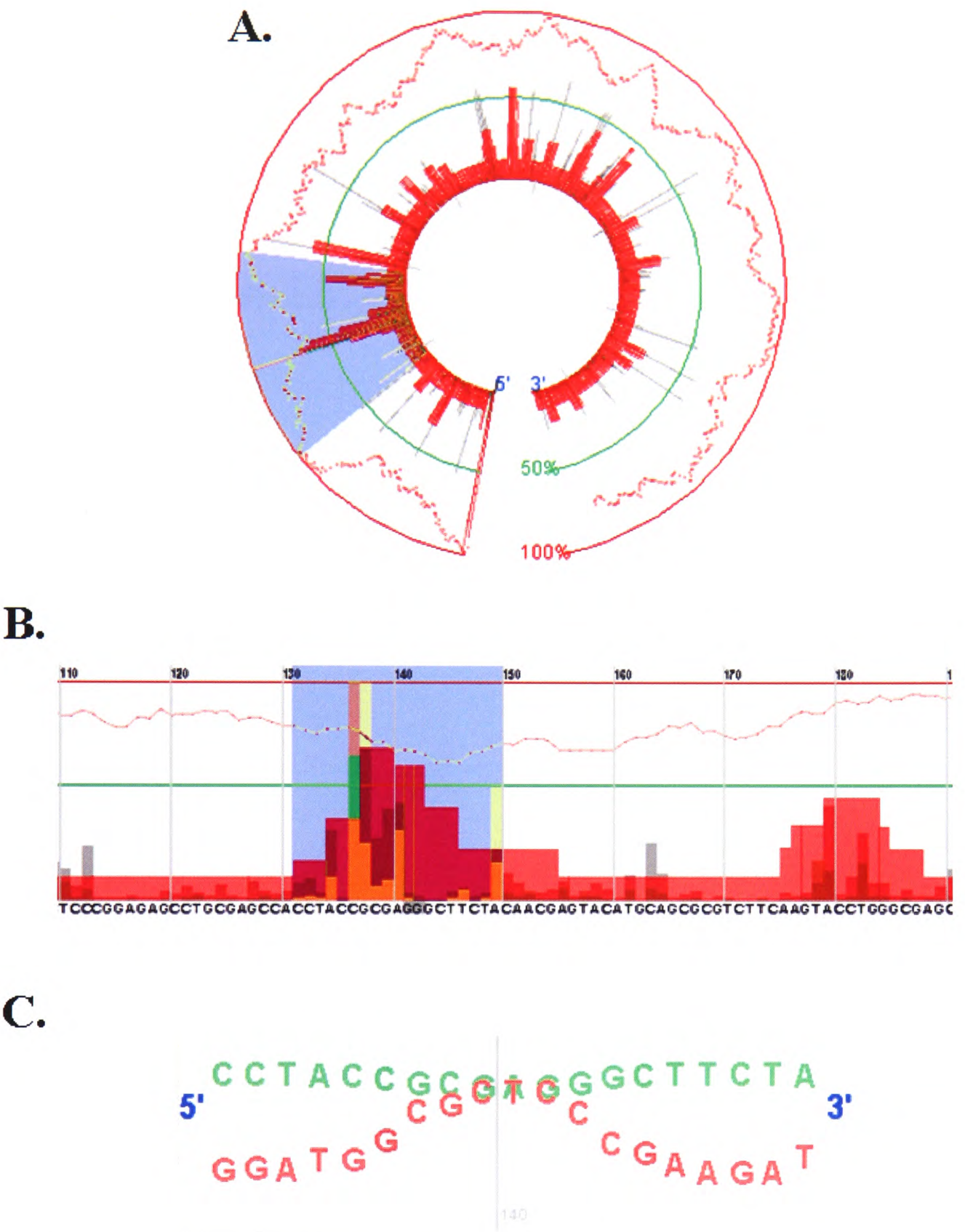

Figure 6.3 Secondary structure mapping of human PHOSPHO1 RNA. (**A**) ACCESSmap of 727 nucleotide region relating to exon 3 of human PHOSPHO1, the horseshoe represents the sequence of RNA from 5' to 3' in a clockwise direction, the red bars indicate accessible regions of the RNA with the red trace indicating the free energy profile. (**B**) Zoomed section of the area indicted by blue shading in (**A**), this area was selected for siRNA design due to its superior properties. (**C**) This sequence is that from the accessible area of the RNA detailed in (**B**) this display details the sequence from 5' to 3'. The green strand (sense) and the red strand (antisense) are shown in their annealed state. This diagram represents how close these stands are thought to be under ideal conditions.

6.5.2 PHOSPHO1 Knockdown in SW1353 and SaOs-2 Cells

To knockdown PHOSPHO1 gene expression in the human chondrocyte (SW1353) and osteoblast (SaOS-2) lines the cells were transfected with the pSUPER shRNA vector, which produces hairpin RNAs which are processed by the cellular machinery to produce an active siRNA. The region targeted was that identified by the secondary structure mapping of PHOSPHO1. A scrambled control was also used which bore no resemblance to any mammalian gene. PHOSPHO1 expression was verified in both cell lines, along with TNAP as a marker of mineralisation capacity. As seen in figure 6.4 both SaOS-2 and SW1353 cells express PHOSPHO1 and TNAP.

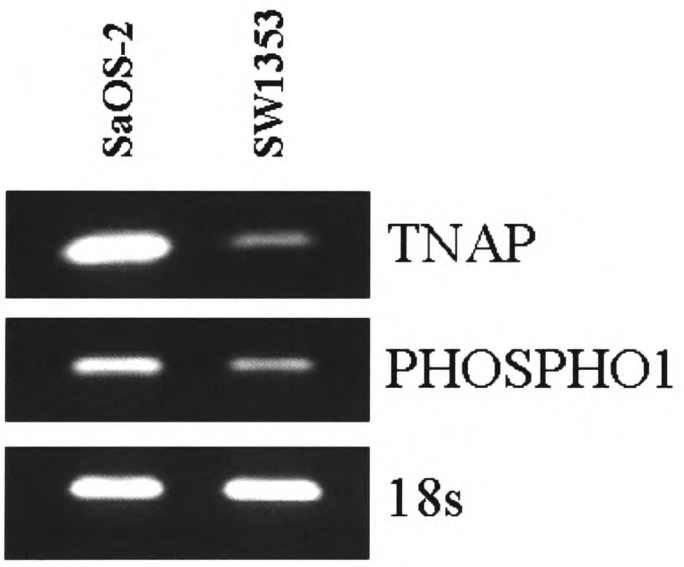

Figure 6.4 Analysis of TNAP and PHOSPHO1 expression in SW1353 and SaOS-2 cells. RNA was extracted from each cell type and reverse transcribed before being amplified by PCR using gene specific primers.

The pSUPER vector contained a GFP marker gene which allowed analysis of tranfection efficiency, this was estimated at 10% for both cell lines. Following 14

days with G418 selective pressure greater than 70% fluorescence was seen for both cell types as shown in figure 6.5. Interestingly the SW1353 cells fluoresced brighter than the SaOS-2 cells, indicated by the obvious fluorescence at 4x magnification to the very low fluorescence at 10x in the SW1353 and SaOS-2 cells respectively. The SaOS-2 cells also contained a greater variation of fluorescent signal with some cells only weakly visible over UV light to the eye.

A.

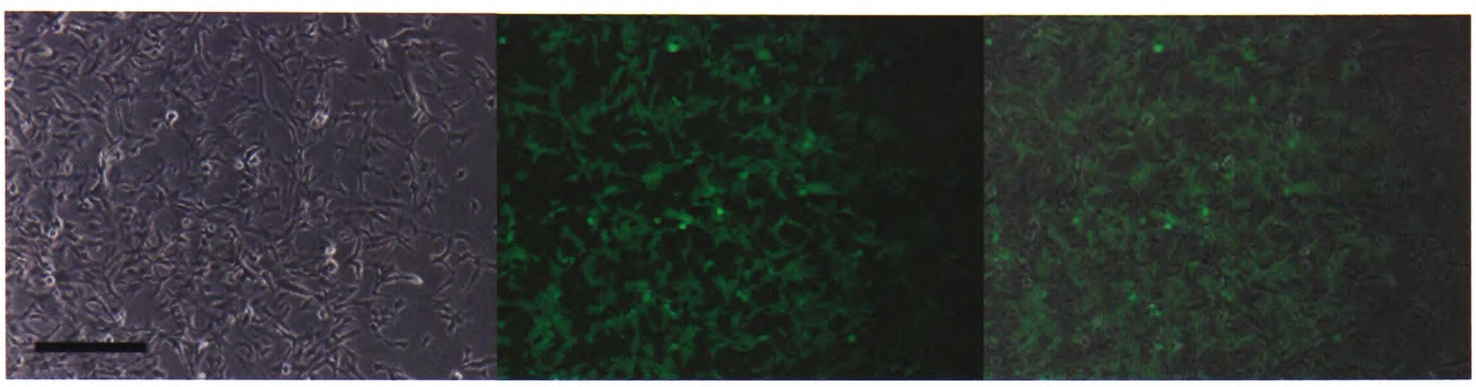

B.

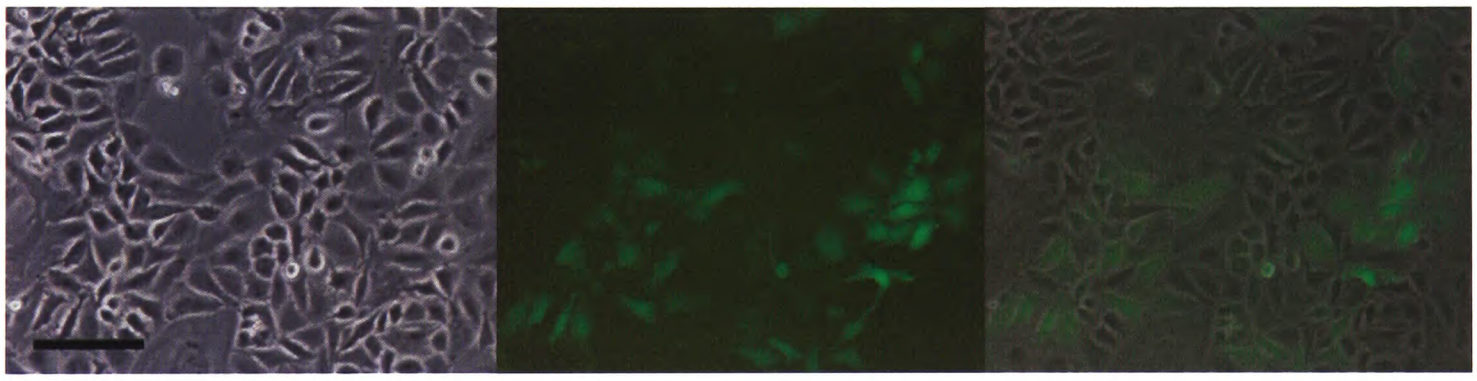

Figure 6.5 Cells stably transfected with the pSUPER shRNA expressing vector construct. **(A)** SW1353 cells viewed on 4x magnification. Left panel represents cells viewed under phase contrast, centre panel represents cells viewed under UV light, right panel represents the two images merged (scale bar = 500μm). **(B)** SaOS-2 cells viewed on 10x magnification. Left panel represents cells viewed under phase contrast, centre panel represents cells viewed under UV light, righ panel represents the two images merged (scale bar = 200μm).

The PHOSPHO1 status of the stably transfected cell lines was analysed by RT-PCR and quantified by band densitometry. No apparent knockdown was seen in

the SaOS-2 cells, however the SW1353 cell line exhibited a knockdown of 59.6 ± 2.92% (SD of 3 replicates), as shown in figure 6.6.

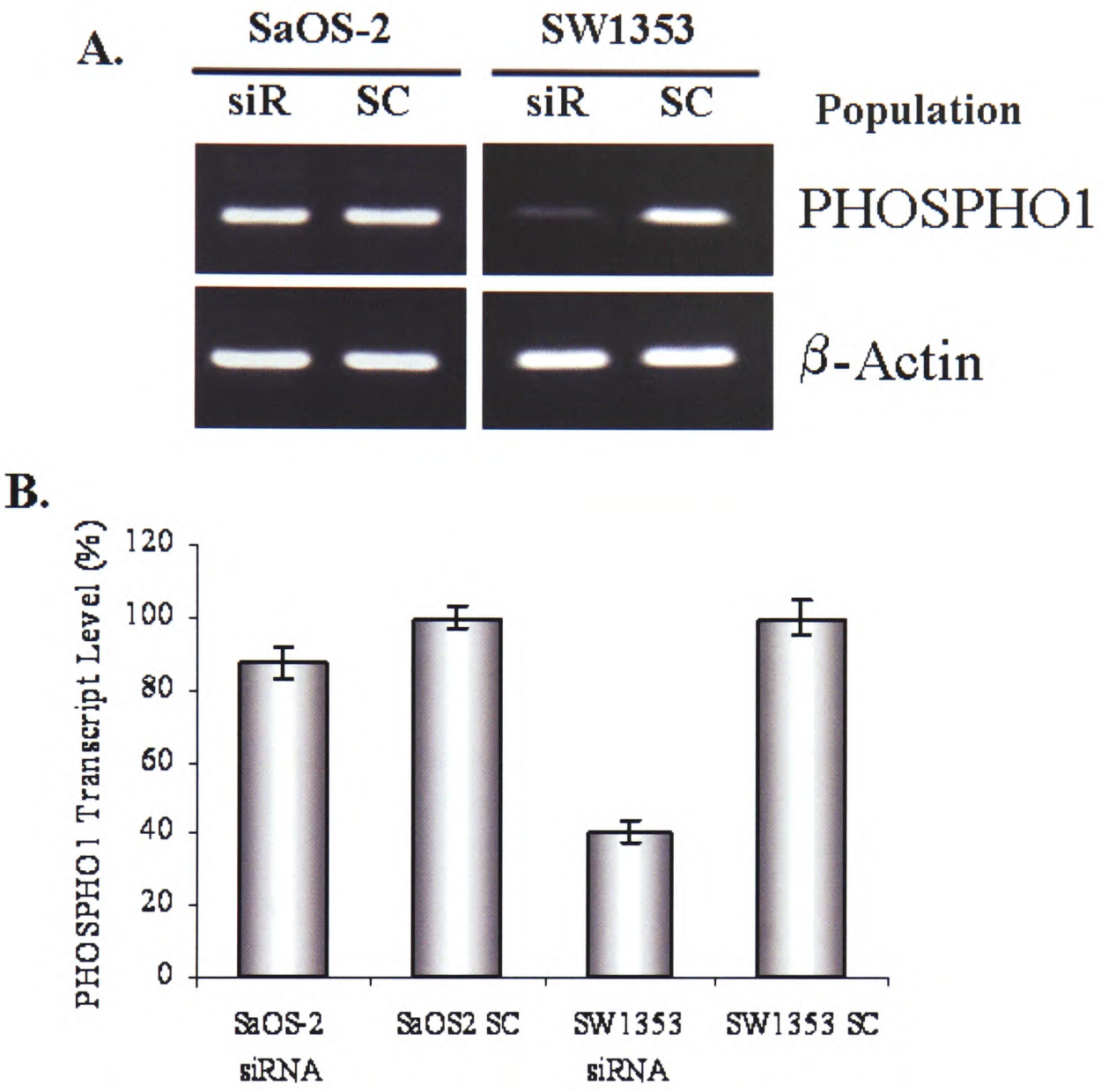

Figure 6.6 Analysis of PHOSPHO1 expression in stably transfected SW1353 and SaOS-2 cells. **(A)** RNA was extracted from each cell type and reverse transcribed before being amplified by PCR using PHOSPHO1 specific primers. The external control β-Actin was used to detect any inconsistencies in initial RNA concentrations. **(B)** Quantification of PHOSPHO1 knockdown by band desitometric analysis. Each band was normalised to the intensity of the β-Actin band. Error bars represent the SD of three replicates.

6.5.3 Mineralisation Potential of the SW1353 Knockdown Cell Line

To analyse the effect of PHOSPHO1 knockdown on chondrocyte mineralisation the SW1353 cells were cultured in two types of mineralisation media previously documented to induce calcification in chondrocyte cells. The well documented method of Tacchetti *et al* (1989) utilising AA and βGP and the method detailed by Ishikawa and Wuthier (1992) which is βGP free and was originally developed for the *in vitro* mineralisation of avian growth plate chondrocytes. After culture for 12 days the cells were stained with alizarin red for detection of calcium phosphate; however no evidence of mineralisation was present in either control or knockdown cells. Upon analysis of cell morphology and monolayer appearance distinct differences were apparent. The knockdown cells produced large lesions in the cell monolayer when differentiation was induced by both culture conditions, which was in contrast to the control cells which had a normal appearance, as seen in figure 6.7.

6.5.4 PHOSPHO1 Knockdown in the Murine MLO-A5 (Osteoblast) Cell Line

The cells were transiently transfected with Dharmacons smart pool of RNA oligonucleotides which contains a pool of four *SMART*selection™ designed siRNA duplexes. Following transfection transcript levels were 62.8 ± 8.8 %, 75.9 ± 5.3% and 96.9 ± 12.9% at 44 hrs 96 hrs and 144 hrs respectively, post transfection when compared to control cells (transfected with a GFP siRNA).

Upon alizarin red staining of the cultures a reduced quantity of mineral was observed in the knockdown cultures when compared to the control cultures. As seen in figure 6.8 the quantity of dye incorporated in the knockdown cells has an OD of

0.029 ± 0.027 which is 3.6 fold less than that observed in the control cells (0.105 ± 0.041).

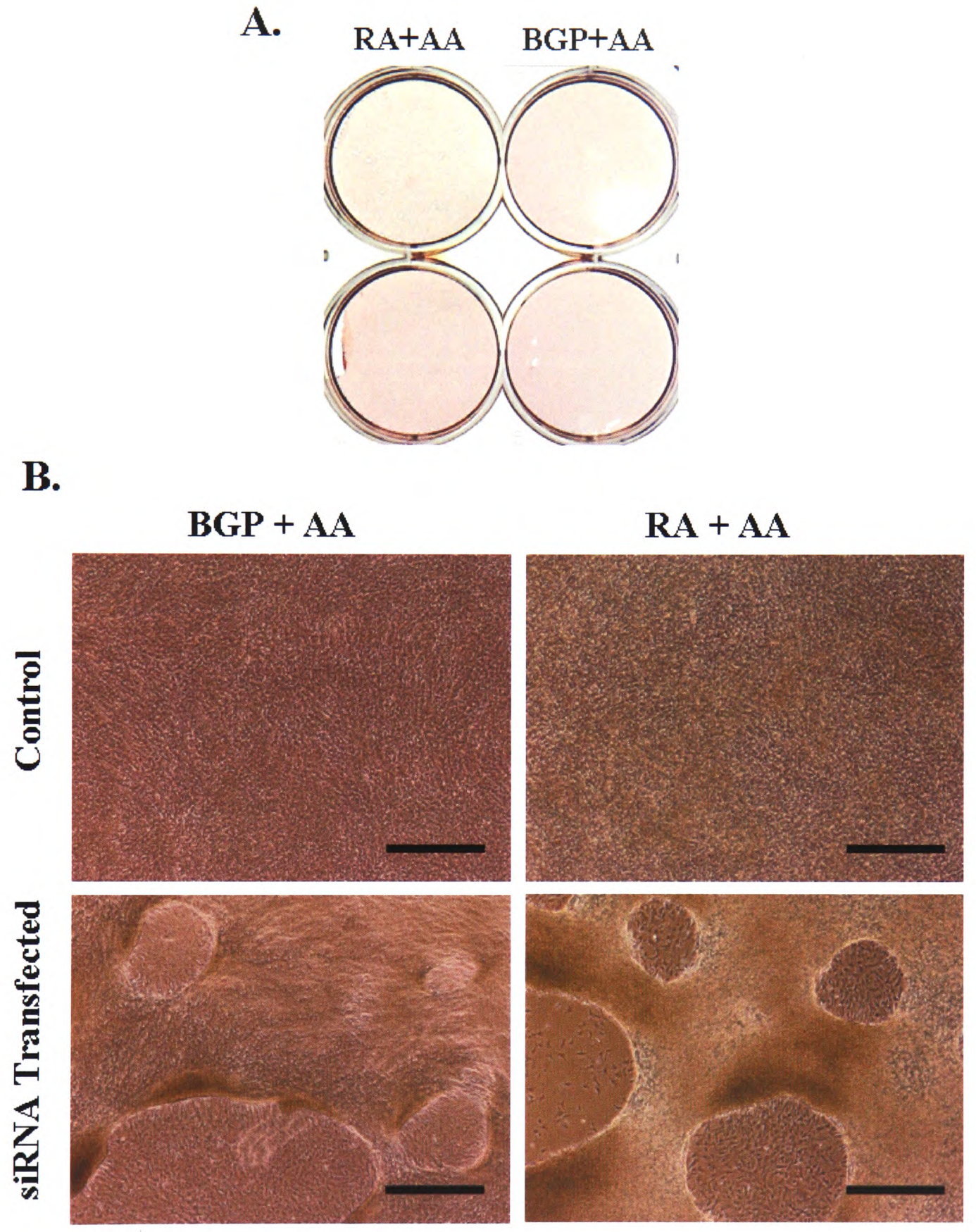

Figure 6.7 Analysis of SW1353 cells which are genetically modified to have a reduced expression of PHOSPHO1 (**A**) Alizarin red staining of knockdown and control cells following 12 days in mineralising media, two protocols were used to induce mineralisation, these utilised either βGP and AA or AA and RA in the culture media (**B**) Analysis of cell morphology, at 4x magnification, following 12 days in mineralising media (scale bar = 500μm).

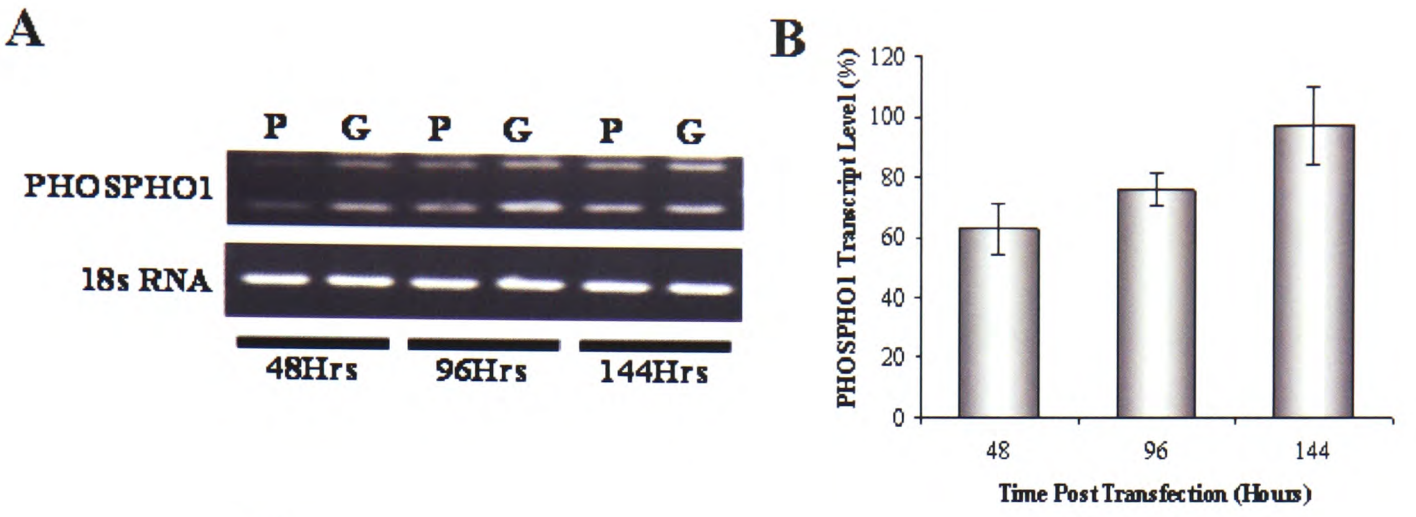

Figure 6.8 Analysis of PHOSPHO1 expression in MLO-A5 cells, transiently transfected with smartpool siRNA mixture. (**A**) RNA was extracted from cells transfected with the PHOSPHO1 siRNAs (P) and a GFP control oligo (G) at three time points. This was reverse transcribed before being amplified by PCR using PHOSPHO1 specific primers. The external control 18s RNA was used to detect any inconsistencies in initial RNA concentrations. (**B**) Quantification of PHOSPHO1 knockdown by band desitometric analysis. Each band was normalised to the intensity of the 18s RNA band and that of the control (G) band. Error bars represent the SD of three replicates. (**C**) Alizarin red staining of cells 144 hrs following transfection, the dye incorporation was quantified; error bars represent the SD of three replicates.

6.5.5 Over-Expression of PHOSPHO1

6.5.5.1 Production of a pWGB10-PHOSPHO1-HAg Clone

A PHOSPHO1 CDS was designed to contain a C-terminal HAg Tag which was subsequently cloned into the pWGB10 mammalian expression vector (appendix 1). pWGB10-PHOSPHO1-HAg clones were analysed for orientation in respect to the mammalian phosphoglycerate kinase promoter. The digested clone shown in figure 6.9 is in the correct orientation as when digested with Apa1 and Nco1, which are both contained within the coding sequence, DNA fragments of 1071 and 1319bp are present, respectively. If this clone was inverted the band sizes when digested with these two enzymes would be 830 and 1560bp respectively.

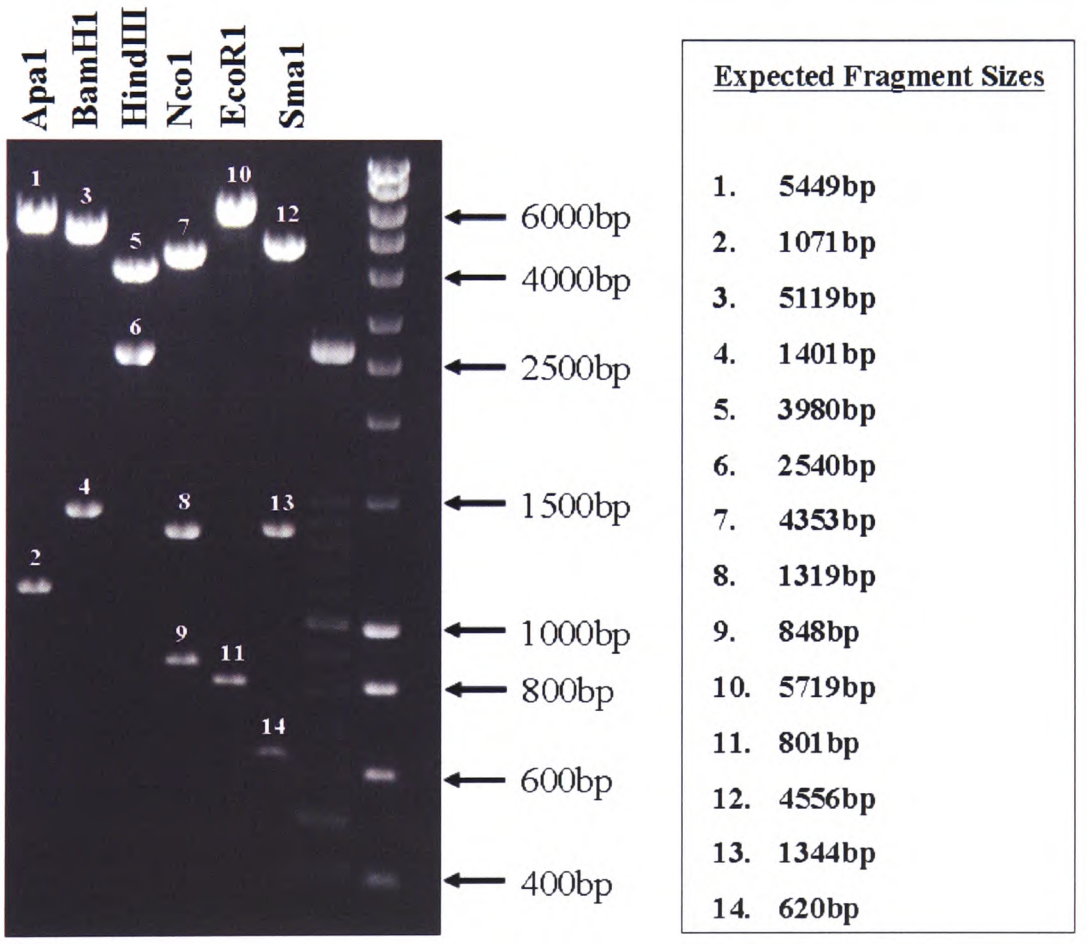

Figure 6.9 Analysis of a pWGB10-PHOSPHO1-HAg clone by restriction digestion with enzymes *Apa1*, *BamH1*, *HindIII*, *Nco1*, *EcoR1* and *Sma1*. Enzymes *Apa1* and *Nco1* both cut the clone within the PHOSPHO1 CDS, close to the 3' region, hence allowing the assessment of orientation. The clone the CDS is aligned in the correct orientation with respect to the PGK promoter, if it was inverted the band sizes of 2 and 8 would be 830 and 1560 respectively. EcoR1 cuts out the CDS which was originally cloned into the vector.

6.5.5.2 Analysis of HeLa cells Expressing PHOSPHO1

To assess if the HeLa cells stably transfected with the PHOSHO1 construct described in 6.5.5.1 were expressing the recombinant protein, extracted RNA and protein was analysed for the presence of transcript and HAg peptide respectively. In addition the protein was also probed with the anti mouse PHOSPHO1 antibody described in chapter 5. As seen in figure 6.10A RNA corresponding to exon 3 of PHOSPHO1 transcript is present within the cells transfected with the over-expression construct, with only a faint band present in the control cells. To assess endogenous expression of PHOSPHO1 in HeLa cells a PCR was carried out to amplify between exon 2 and 3 (spanning intron 2), however no amplification was seen from this PCR indicating no endogenous expression of PHOSPHO1 in HeLa cells. As seen in figure 6.10A both control and over-expression cell lines are also positive for puromycin^r, with an apparent equal expression in both, indicating that the both are stably transfected with the control and over-expression vector.

Upon analysis of the Western blot detailed in 6.10B it can be seen that a band corresponding to the expected size of the recombinant PHOSPHO1 protein (29KDa) is present, in the overexpression cells, when probed with the anti mouse PHOSPHO1 antisera and the anti HAg antibody. This protein is not present in the control cells. In addition the identification of the protein using the anti-HAg antibody can be blocked by incubating the primary antibody with HAg peptide, showing the interaction is specific. The membrane was stripped and probed for β-actin to ensure equal loading.

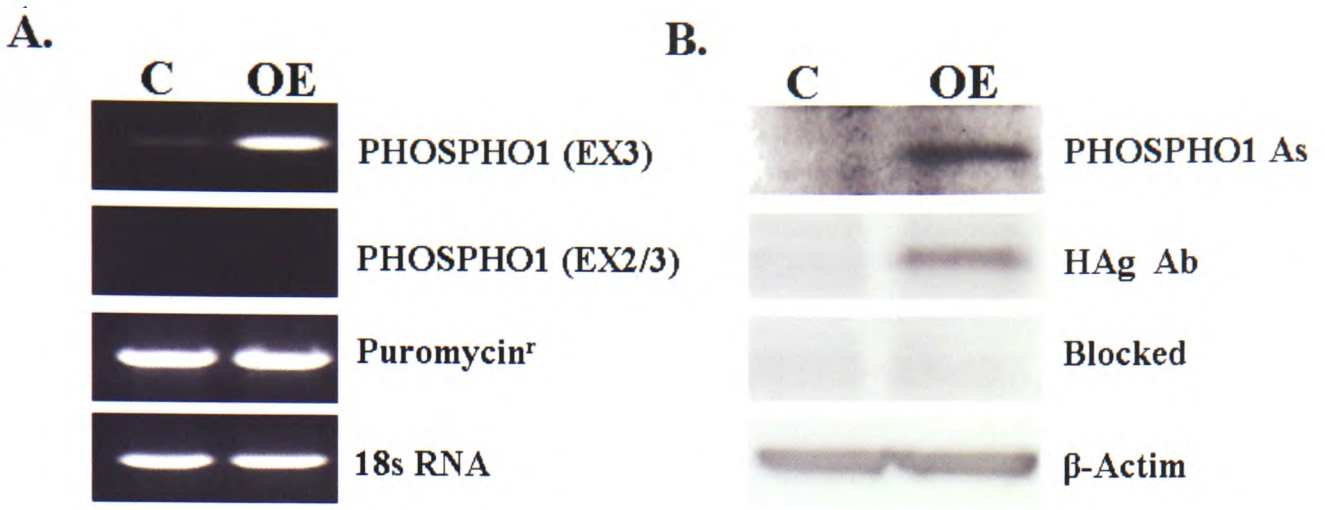

Figure 6.10 Analysis of PHOSPHO1 expression and protein content in stably transfected HeLa cells. (**A**) RT PCR of RNA from HeLa cells modified to express PHOSPHO1. RNA was extracted from both the control and the over-expression cells and reverse transcribed before being amplified by PCR using gene specific primers. The external control 18s RNA was used to detect any inconsistencies in initial RNA concentrations. (**B**) Western blot of proteins from HeLa cells modified to express PHOSPHO1. Antibodies used include and anti mammalian PHOSPHO1 antiserum (top) an anti HAg antibody, as the recombinant protein was designed to contain a C terminal HAg tag, this band can be blocked by the incubation of 10 μg/ml HAg peptide with the primary antibody. The loading control β-Actin was used to detect any inconsistencies in initial protein concentrations.

6.5.5.3 Analysis of Mineralising Potential of PHOSPHO1 Expressing HeLa Cells

To investigate whether HeLa cells expressing the HAg tagged PHOSPHO1 protein had the ability to mineralise they were cultured in the presence of AA and βGP. In a second experiment the cells were cultured in the presence of AA and PEA as from chapter 3 this is now deemed as PHOSPHO1s natural substrate. As seen in figure 6.11 upon von Kossa staining of 12 day old cultures, although sporadic staining of calcium phosphate is present with both treatments, no difference is seen when PHOSPHO1 expressing cultures are compared to control cultures.

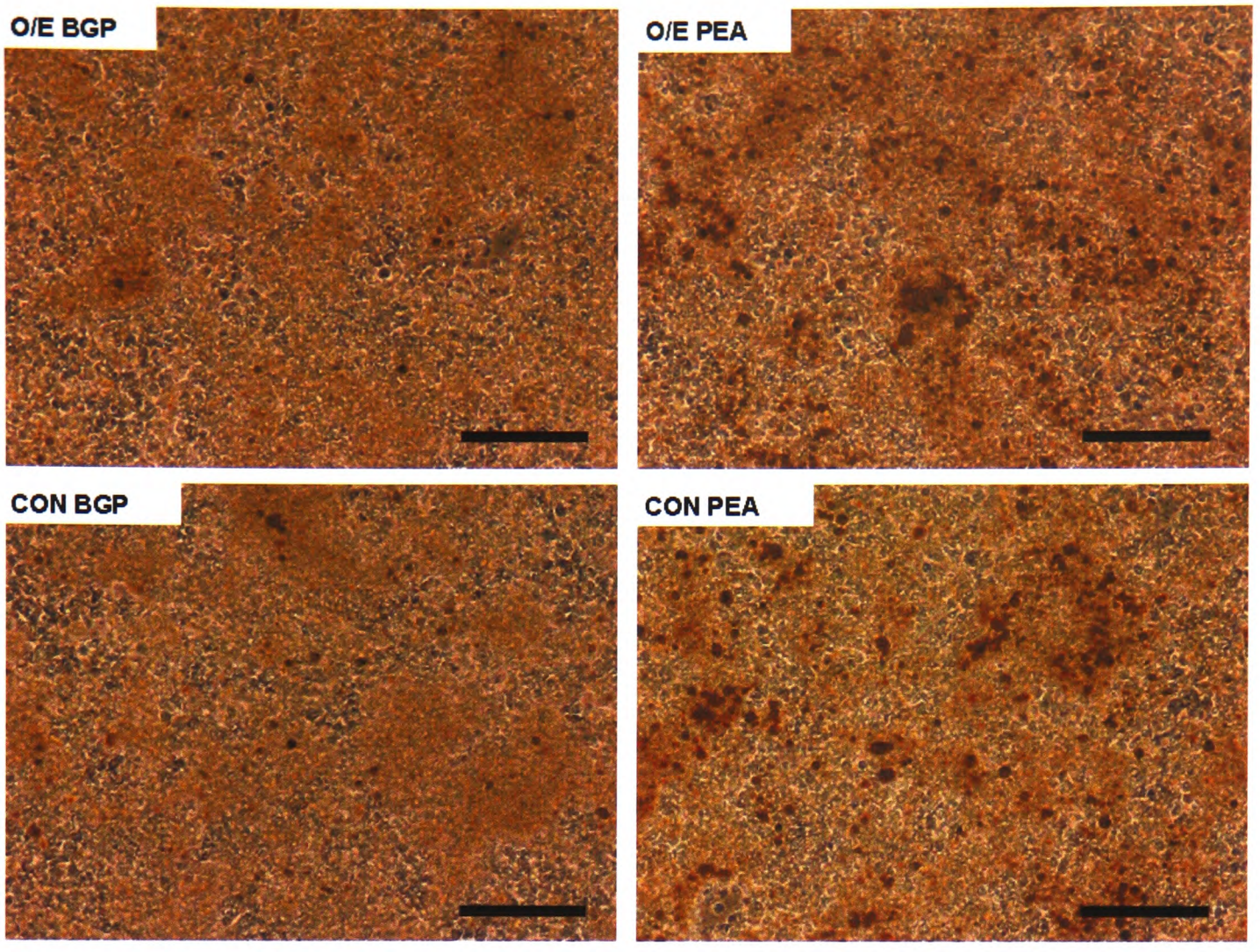

Figure 6.11 Von Kossa staining of HeLa cells which are genetically modified to have an increased expression of PHOSPHO1. Analysis of calcium phosphate staining, at 4x magnification, following 12 days in mineralising conditions. The mineralising media contained either βGP or PEA as a phosphate source for mineral precipitation (scale bar = 500μm).

6.6 Discussion

The analysis of the secondary structure of human PHOSPHO1 allowed the assessment of accessible sites of the mRNA. Target accessibility has been shown to be of the utmost importance for the effective silencing of gene expression as any sites which lie within tightly folded RNA structures may resist RISC mediated targeting (Schubert *et al*, 2005). Identification of effective siRNA targets within mRNA sequences give rise to the potential for a new class of therapeutics. This type

of RNAi therapy is broad spanning and includes any disease which requires a reduction in gene expression. Indeed if PHOSPHO1 is involved in the generation of Pi for mineralisation, diseases characterised by excess mineral production such as osteopetrosis or pathological soft tissue calcification could be combated through novel RNAi therapeutic approaches. Indeed the sequence generated from the accessibility map shown in figure 6.3 allowed the knockdown of PHOSPHO1 in the SW1353 chondrosarcoma cell line of approximately 60%. However no knockdown was observed in the SaOS2 cells, interestingly this was accompanied by a lower degree of fluorescence from the GFP marker. This phenomenon has previously been reported when using retroviral vectors and is thought to be due to DNA methylation (Gram *et al*, 1998). Although this has not been directly reported in non-retroviral vectors it is known that DNA methylation can have a major effect on eukaryotic gene expression. Indeed it has been demonstrate that methylated cytosines present in vector DNA can inhibit a flanking promoter (Curradi *et al*, 2002). It is therefore conceivable that this is occurring in the SaOS2 transfected cells thus causing a decrease in GFP transcription and siRNA transcription. It is however unclear why this does not occur with the SW1353 cells. As these two cell lines were originally isolated from different cancers, and that sarcoma cell lines have been shown to contain differing methylation patterns (Paz *et al*, 2003) and different levels of DNA methyl transferase, the cause of DNA methylation (Vilain *et al*, 1999), this may go some way to explaining why this vector behaves differently in the two lines. Although due to lack of experimental data to reinforce this hypothesis the theory is only speculation.

Upon analysis of the mineralisation capacity of both the control and knockdown SW1353 lines it is evident that this cell type does not have the capacity to mineralise. Interestingly it does express both TNAP and PHOSPHO1 which are a hallmark of SaOS-2 cells, these cells do mineralise and when absent, as with MG63 cells mineralisation cannot be achieved. This obviously raises questions about the potential role of PHOSPHO1 in the mineralisation process, however it cannot be ruled out that the presence of PHOSPHO1 and TNAP transcript is a result of an altered gene expression profile by a transformed line or an *in vitro* artefact. Interestingly the knockdown cells do posses a phenotype that is different to that of the control cells. Upon culture large lesions appear in the cell monolayer resulting in the regression of the cartilaginous matrix. The cells below this appear to be sparse thus perhaps indicating a possible cytotoxic effect of the siRNA, interestingly this has been documented and has been attributed to off-target effects of the siRNA (Fedorov *et al*, 2006). This study (Fedorov *et al*, 2006) revealed that almost 30% of siRNAs in their randomly generated library were able to reduce overall cellular viability. Alternative explanations for this phenotype, in my study, could be that PHOSPHO1 is also involved in matrix maintenance, that gene knockdown causes cellular de differentiation or that this particular phenotype is an *in vitro* artefact. All of these explanations would require extensive experimental evidence to conclude the cause, which is unfortunately out with the scope of this project.

The MLO-A5 pre-osteocyte (post-osteoblast) cell line mineralises in culture in sheets, without nodule formation within 3 days of culture in the presence of βGP and AA (Kato *et al*, 2001). This cell line has previously been shown to express PHOSPHO1 (Stewart *et al*, unpublished data). Thus due to the kinetics of this cell

line it allows the possibility of gene knockdown using 21mer dsRNA oligonucleotides. Upon transfection of the Dharmacon Smartpool (4 gene specific oligonucleotides) transcript levels were calculated at 62.8 ± 8.8 % at 44 hrs rising to 96.9 ± 12.9% after 144 hrs. This strategy gave the potential to monitor mineralisation of this cell line in a PHOSPHO1 reduced environment. As seen in figure 6.8 the incorporated mineral was reduced approximately 3.5 fold when PHOSPHO1 levels were reduced. A greater effect may have been observed if the knockdown had been stable as the transcript, thus protein, content of the cells had returned to normal after a 144 hr period thus allowing a 'normal' environment to be re-established. It would be expected if PHOSPHO1 is critical to the mineralisation process a more severe phenotype would be observed from this knockdown, as seen with *Tnap*$^{-/-}$ osteoblasts where they have a complete inability to form a mineralised matrix (Wennberg *et al*, 2000). However the alternative roles that TNAP exhibits such as depletion of the mineralisation inhibitor PPi and the hydrolysis of the mineralisation promoter βGP to form Pi for HA deposition need to be taken into account. In addition to this as TNAP is still active in the MLO-A5 cells the activity of this enzyme may be partly masking the knockdown of PHOSPHO1. However as a slight reduction in the initial signs of mineralisation were noted this data provides preliminary functional evidence for a role of PHOSPHO1 in the mineralisation process.

To investigate whether PHOSPHO1 was able to initiate deposits of seed crystals, as observed within MVs, the human protein was overexpressed in the HeLa cell line. As seen in figure 6.10 the PHOSPHO1 protein was overexpressed at both the transcript and protein level in cell extracts. This indicates that my overexpression strategy was successful. However upon analysis of cell phenotype and cell

mineralisation capacity no differences were observed between control cells and those overexpressing PHOSPHO1 (figure 6.11). This is most likely due to PHOSPHO1 not having the capacity to induce a mineralised phenotype by itself, rather than an indication that it has no involvement in the mineralisation process. It is known that mineralisation is a multi step, multi component pathway that requires the synchronisation of many factors as previously discussed 1.6.4. As many of these factors will be specific to mineralising skeletal cells and not the fibroblast-like HeLa cells it is likely that such osteoblast/chondrocyte specific genes would need to be expressed along with PHOSPHO1 to induce a mineralised phenotype. However as stated in section 6.1 the function of many phosphatases have been clarified using similar techniques to this, thus the rationale for this investigation is justified.

In conclusion this study demonstrates effective areas of the PHOSPHO1 mRNA which can be targeted for siRNA mediated gene knockdown thus giving rise to potential future study on PHOSPHO1 modulation using siRNA both *in vitro* and *in vivo*. MLO-A5 cells cultured in mineralising conditions, with a reduced cellular content of PHOSPHO1, display a reduction of mineralisation capacity. This data further strengthens the hypothesis that PHOSPHO1 is involved in matrix mineralisation, however further work relating to gene knockdown in primary skeletal cells would need to be undertaken to allow an exact role of PHOSPHO1 in this process to be established.

CHAPTER 7

DISCOVERY AND CHARACTERISATION OF PHOSPHO1 INHIBITORS

Chapter Contents

7.1 Introduction

As outlined in chapter 3 the hydrolysis of PEA by PHOSPHO1 has favourable kinetics thus it is therefore likely that this reaction would occur *in vivo*. This hypothesis is furthered as PEA is one of the most abundant phosphomonoesters in cartilage (Kvam *et al*, 1992), a site that PHOSPHO1 is present at in large quantities. In addition, the proportions of membrane phospholipids containing these groups decrease in MVs during mineralisation, whilst 1,2-diacyl glycerol accumulates, indicative of phospholipase C activity (Wu *et al*, 2002). This gives rise to the possibility of a novel mechanism whereby plasma membrane bound phosphate may be released through the action of PHOSPHO1 and phospholipase C to contribute to the P_i concentration inside the MV.

To further examine this mechanism, the mineralisation potential of cells and cell associated factors such as MVs need to be assessed whilst modulating the activity of PHOSPHO1. The most common way of modulating enzyme activity is to use small molecule inhibitors which can be utilised in biological systems to inhibit the pathway that the enzyme is involved in. However as PHOSPHO1 is a novel enzyme belonging to a specific group of the phosphor-monoesterase section of the HAD superfamily (Tirrell *et al*, 2006), no inhibitors are yet known for this enzyme thus in such circumstances methods such as high throughput screening of chemical libraries are employed in an attempt to find compounds able to modulate enzyme catalysis.

Inhibitors are a powerful tool in both the research and pharmacological industry. Indeed, small molecule inhibitors are used to investigate cellular pathways such as the MEK-ERK signalling pathway (Klein *et al*, 2006) and the AKT pathway

(Yang *et al*, 2004). In addition to this some of the most powerful antiviral agents available at present are enzyme inhibitors. Retroviral protease inhibitors are one of the most successful groups of anti-HIV therapeutics, including drugs such as Ritonavir. This particular drug was launched in 1995 and presented a novel target of interception within this disease (Danner *et al*, 1995). Other powerful pharmaceutical inhibitors include the influenza neuraminidase inhibitor Tamiflu (oseltamivir) which is active against the H5N1 strain of avian influenza (Leneva *et al,* 2000). It will be the main drug of choice in fighting any avian flu epidemic. Discovery of inhibitors to PHOSPHO1 may lead to the generation of reagents that will facilitate future studies aimed at understanding the process of matrix mineralisation and how PHOSPHO1 is involved in this cellular pathway.

It is known that the first step of mineralisation (initiation step) mediates the deposition of seed crystals of HA. It is proposed that this step, which is independent of the function of TNAP, involves the function of PHOSPHO1 in increasing the local concentration of P_i inside the MVs. If correct, it would be envisaged that an inhibition of PHOSPHO1 activity would result in decreased mineralisation within the MV. Therefore, in this study this hypothesis has been tested by affecting the first step of MV-mediated mineralisation and cell mediated matrix mineralisation using a pharmacological approach.

7.2 Hypothesis

That the inhibition of PHOSPHO1 will reduce the concentration of Pi at potential sites of mineralisation thus causing a decrease in HA formation via calcium phosphate precipitation.

7.3 Aims

I. Screen chemical libraries for compounds with an inhibitory potential for recombinant human PHOSPHO1.

II. Characterise these inhibitors through the production of dose response curves and analysis of kinetic values during PHOSPHO1 mediated hydrolysis of PEA in the presence of inhibitor.

III. To study effects of these inhibitors on cell mediated matrix mineralisation.

IV. Assess the ability of these inhibitors to reduce the Pi producing potential and calcification of MVs.

7.4 Materials and Methods

7.4.1 Inhibitor Screening

Recombinant protein produced in the same manner as detailed in section 3.4.2 was utilised in a modified reaction system outlined in section 2.6.5. These reaction conditions used BSA rather than glycerol to stabilise the PHOSPHO1 protein. This was due to the liquid handler not being able to pipette a solution containing glycerol accurately due to liquid retention in the tip. The screening was carried out as outlined in section 2.6.5 in a 96 well plate format. This allowed the screening of 80 compounds per plate, as shown in figure 7.1. These compounds were drawn from the LOPAC^{1280} (Sigma) and Spectrum (Microsource Discovery) libraries. The LOPAC library consists of 1280 pharmacologically active compounds

covering most of the major target classes i.e. G protein coupled receptors and kinases. The spectrum library contains 2000 compounds including known bioactives, natural products and their derivatives. The use of these two libraries allowed the evaluation of hundreds of marketed drugs and biochemical standards. Each compound that exhibited an inhibition of 40% or more using the automated system was reconfirmed manually, in duplicate, to eliminate the possibility of false positives.

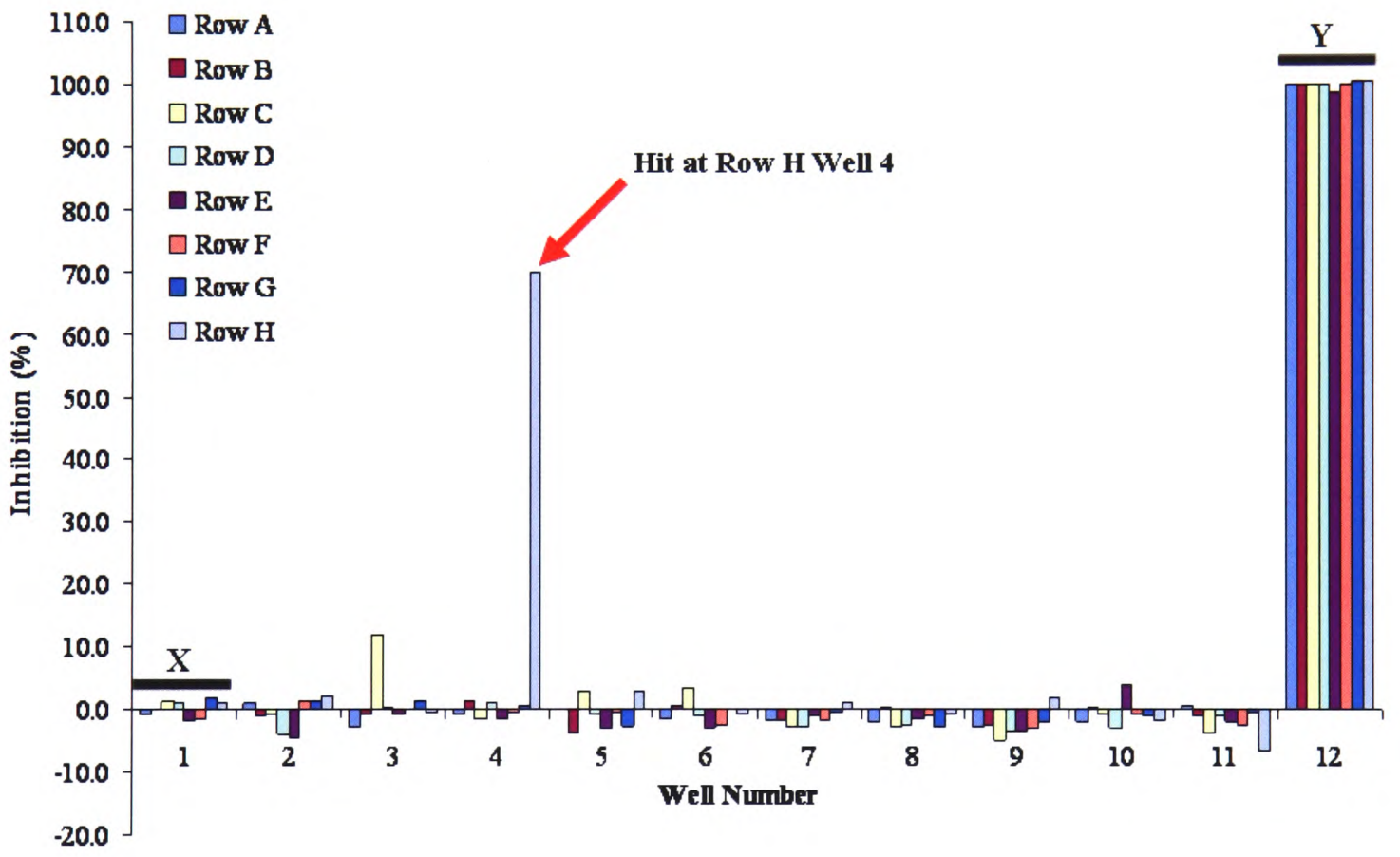

Figure 7.1 Histogram relating to the screen of one plate from the LOPAC Library. This assay was conducted as outlined in section 2.6.5. The section labelled X relates to the negative controls (i.e. no inhibition, contained both enzyme and PEA) and section Y relates to the positive control (i.e. 100% inhibition, contained only PEA)

7.4.2 Characterisation of PHOSPHO1 Inhibitors

The commercially available BIOMOL green assay system (based on the classical malachite green assay detailed by Martin *et al*, (1985)), which measures the amount of Pi in a reaction solution was utilised for the calculation of IC_{50} values. This protocol employs an identical assay to that described in section 2.6.5 for the automated screening, however the reaction was scaled up to 50 µL. Briefly 500ng of purified recombinant PHOSPHO1 protein was incubated with 62.5 µM PEA in the presence of serial dilutions (5:6) of inhibitors from 100 µM to 351 nM in triplicate. The reaction was incubated at room temperature for 60 min. Phosphate released during the reaction was measured by addition of 100 µL BIOMOL Green reagent and absorbance read at 620nm. The data of absorbance vs. inhibitor concentration was plotted using SigmaPlot and four parameter logistic curve fitted. The IC_{50} was calculated using the equation; $y = min + (max\text{-}min/1+ 10^{(logEC50\text{-}x)Hillslope})$.

To analyse kinetic constants for these inhibited reactions a continuous phosphatase assay was employed as described in section 2.6.6. This involved the monitoring of *p*NPP dephosphorylation which causes an absorbance change at 405 nm due to the release of free p-nitrophenol (yellow in colour) and is directly proportional to phosphate bond hydrolysis. Both inhibitor and pNPP concentrations were varied between 0 – 60 µM and 0 – 10 mM respectively and hydrolysis measured in the presence of 1.5 µM recombinant human PHOSPHO1.

7.4.3 Effect of Inhibitors on MLO-A5 Cell Mineralisation

Cells were maintained as outlined in section 2.2, with the following modifications. The cells were cultured in alpha MEM (Gibco) containing 5% FBS,

5% FCS. The cells were seeded into 12 well plates at a density of 40,000 cells/cm^2, and cultured in the presence of 10 mM βGP and 50 μg/ml AA. Inhibitors were supplied at 0, 5, 7.5 and 10 μM in triplicate, the no inhibitor control contained an equal volume of DMSO. The cells were then stained with alizarin red as outlined in section 2.2.9.1.

7.4.4 MV Isolation

MVs were isolated from chick growth plate cartilage as outlined in section 2.2.7 with the following modifications. The diced growth plate cartilage was immersed directly in a solution of 0.45% collagenase (Worthington, type II) in 50 mM Tris-HCl pH 7.6, 120 mM NaCl and 10 mM KCl and incubated at 37 °C for three hrs with constant agitation. The MVs were purified from this suspension by differential ultracentrifugation as outlined in section 2.2.7.

To isolate MVs from cultured osteoblasts a protocol was employed which was similar to that used for chondrocytes, as outlined in section 2.2.8. Firstly the primary murine osteoblasts were cultured for 21 days in alpha MEM (Gibco) containing 10% FBS and 50 μg/ml AA. The cell monolayer was then washed with 50 mM Tris-HCl pH 7.6, 120 mM NaCl and 10 mM KCl, and then incubated with 0.45% collagenase (Worthington, type II) in 50 mM Tris-HCl pH 7.6, 120 mM NaCl and 10 mM KCl at 37°C for 120 minutes at 37°C, with constant agitation. This cell suspension was subjected to differential centrifugation as described in section 2.2.7.

7.4.5 MV Phosphatase Assay

The phosphatase assay used for the analysis of inhibitor effects on Pi production by MVs was identical to that detailed under section 2.6.5 with the following adjustments. The reaction volume was scaled up to 100 µl from 25 µl and 1.2 µg MV protein was used in place of recombinant enzyme. The assay was run in triplicate in the presence of 1 mM PHOSPHO1 inhibitors and 100 µM PEA with a no inhibitor and no substrate control containing equal quantities of DMSO or reaction buffer respectively. The reaction was incubated for 60 minutes at room temperature and stopped by the addition of 100 µl BIOMOL green reagent, the absorbance of each well was measured at 620 nm and converted to standard units (nmol min^{-1} mg^{-1}) by comparison to phosphate standards of known concentration.

7.4.6 MV Calcification Assay

This was carried out according to the procedure detailed in section 2.6.4. This utilised 15 µg samples of chick MVs and 20 µg of TNAP null osteoblast derived MVs. Briefly these were incubated with calcification buffer containing 3 mM PEA or βGP and 1 mM inhibitor in a 200 µl reaction for a period of 6 hrs. The resultant calcium phosphate was harvested, solubilised and calcium content measured as outlined in section 2.6.4.

7.5 Results

7.5.1 Identification and Characterisation of PHOSPHO1 Inhibitors

7.5.1.1 Discovery of PHOSPHO1 Inhibitors

Seventeen compounds in the LOPAC and SPECTRUM chemical libraries were found to inhibit recombinant PHOSPHO1 activity with IC_{50} values of 10 μM or less (structures shown in appendix 7). From these seventeen compounds three were selected based on certain criteria, i.e. having a reconfirmed inhibitory potential of 80% or more and also the absence of any reactive groups such as thiols etc. This led to the identification of SCH 202676, Lansoprazole and Ebseleln as compounds for further investigation (structures shown in figure 7.2).

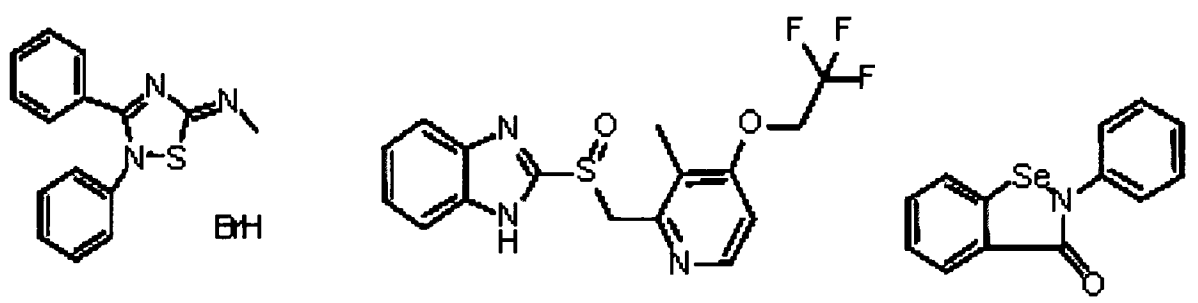

Figure 7.2 Structures of three compounds found to inhibit recombinant PHOSPHO1. The compounds were selected on the basis of their chemical properties i.e. having a reconfirmed inhibitory potential of 80% or more and also the absence of any reactive groups such as thiols etc.

7.5.1.2 Inhibitory Concentration$_{50}$ (IC_{50}) Calculations

The IC_{50} values for each of these compounds were calculated by varying the concentrations of inhibitors, and observing the effect on PHOSPHO1 mediated

hydrolysis of PEA. These values were computed using the; y = min + (max-min/1+ $10^{(logEC50-x)Hillslope}$) and values of 1.97 ± 0.01, 4.71 ± 0.1 and 2.81 ± 0.04 μM were obtained for SCH 202676, Lansoprazole and Ebselen respectively (figure 7.3).

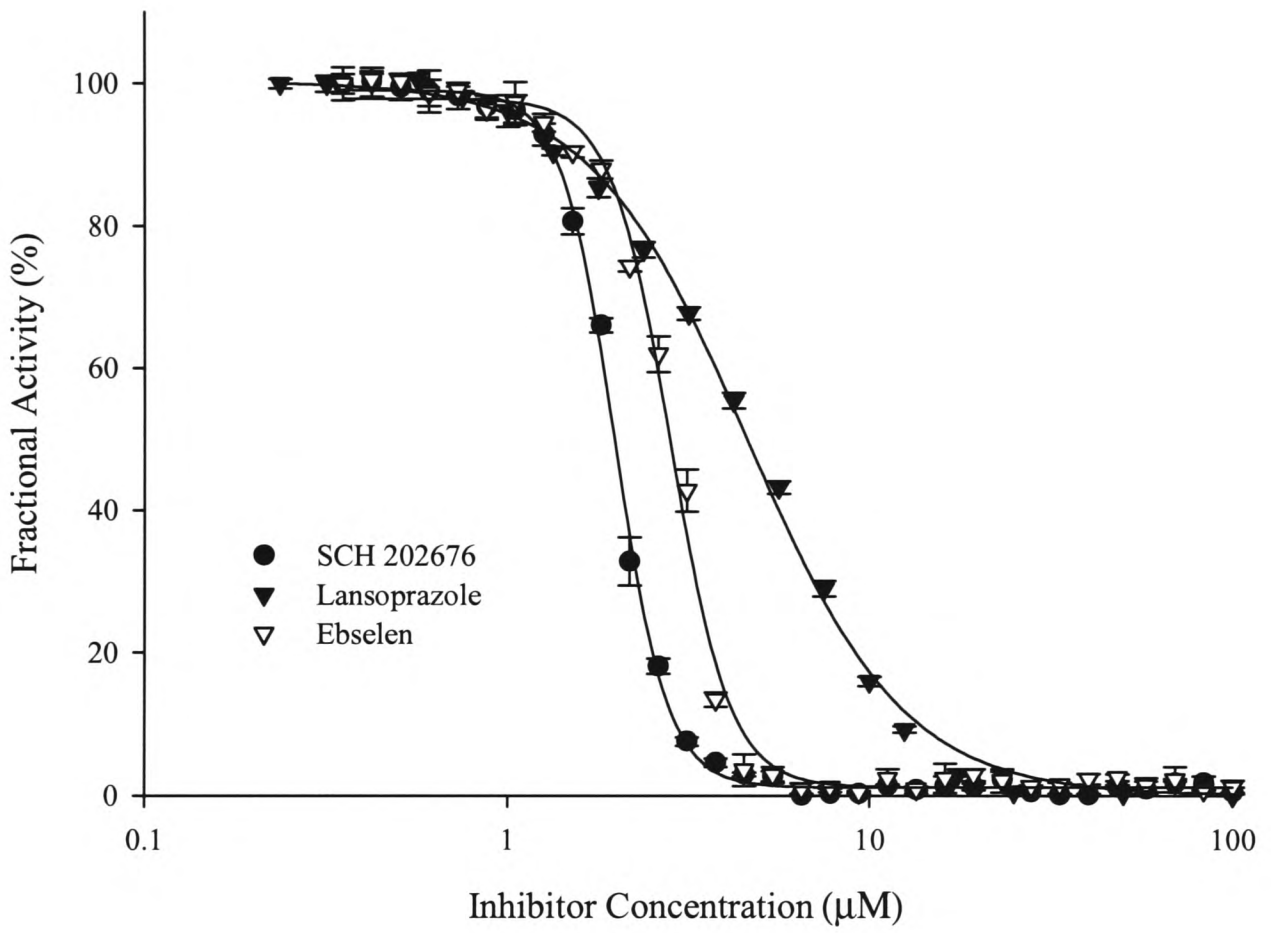

Figure 7.3 IC_{50} determination of each PHOSPHO1 inhibitor. Recombinant human PHOSPHO1 was incubated with various concentrations of SCH 202676, Lansoprazole or Ebseleln at room temperature for 60 min. Phosphate released during the reaction was measured by addition of 100 μL BIOMOL Green reagent and absorbance read at 620nm. Results are mean ± SD (n = 3).

7.5.1.3 Inhibitor Classification

The inhibition type displayed by each of the compounds was investigated by analysis of data relating to the initial velocity of the hydrolysis reaction in the presence of varying concentrations of inhibitor and the colorimetric substrate pNPP. From analysis of the resultant Line-weaver burke plots (figure 7.4) each inhibitor displayed an apparent mixed or non-competitive type inhibitory profile as the lines were not parallel as seen with un-competitive inhibition. All three inhibitors display lines which intercept after the y axis, close to the x axis. A Michaelis Menten curve was constructed under saturating quantities of pNPP as seen in figure 7.5, this also shown the inhibitors are of a non competitive or mixed nature. If these inhibitors were competitive the lines of the inhibited reaction vs. the uninhibited reaction would intercept due to a dilution effect of substrate on inhibitor. Upon analysis of the K_m values for the inhibited reactions displayed in Tables 7.1, 7.2 and 7.3, both SCH 202676 and Lansoprazole display apparent non-competitive characteristics due to the K_m values not altering significantly. However when the data relating to Ebselen is examined it is evident that with increasing concentrations of inhibitor the K_m of the reaction also increases. This is a hallmark of mixed type inhibition. The inhibitor constant K_i, dissociation constant for the inhibitor/enzyme complex, was also calculated for each of these reactions with SCH 202676, Lansoprazole and Ebseleln displaying K_i values of 1.08 ± 0.83 , 71.28 ± 9.21and 31.00 ± 0.74 μM respectively (calculations are shown in tables 7.1 to 7.3).

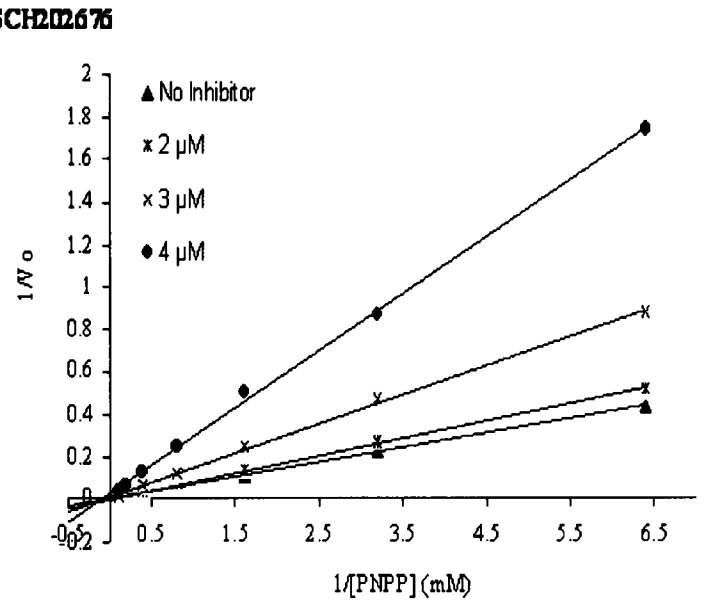

Figure 7.4 Kinetic analysis of PHOSPHO1 mediated hydrolysis of pNPP in the presence of inhibitors. Recombinant human PHOSPHO1 was incubated with various concentrations of SCH 202676, Lansoprazole or Ebselen and various concentrations of pNPP and change in absorbance (405nm) measured over 30 minutes. Initial velocity was calculated from the increment of the graph relating to the start of the reaction. Line weaver burke plots indicate the mode of inhibition is of the non-competitive type due to the lines interception around the x axis.

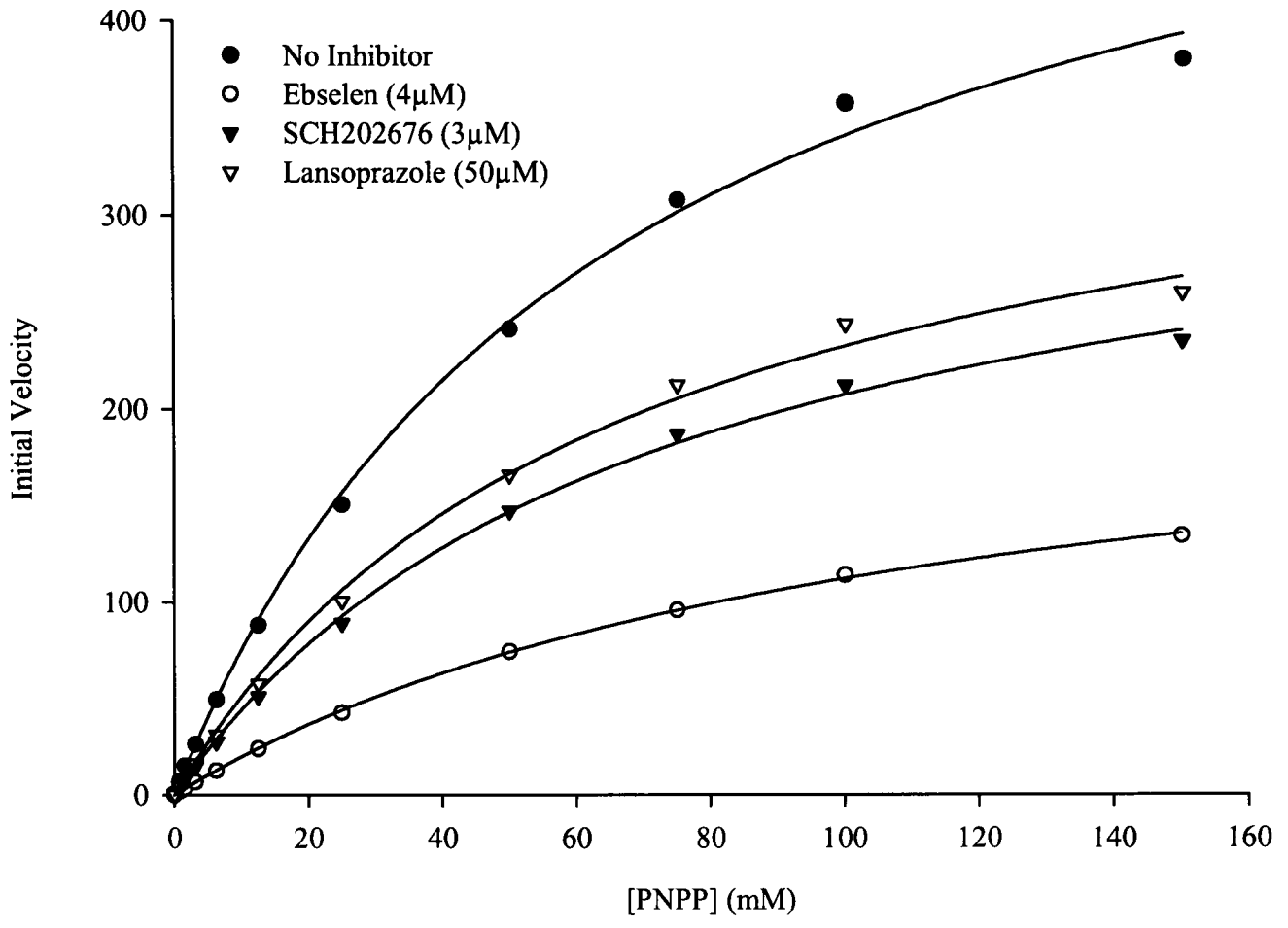

Figure 7.5 Kinetic analysis of PHOSPHO1 mediated hydrolysis of pNPP in the presence of inhibitors. Recombinant human PHOSPHO1 was incubated with various concentrations of SCH 202676, Lansoprazole or Ebseleln and up to saturating concentrations of pNPP. The change in absorbance (405nm) was measured over 30 minutes. Initial velocity was calculated from the increment of the graph relating to the start of the reaction. This plot indicate the mode of inhibition is of the non-competitive type due to the lines not nearing interception with the uninhibited reaction under saturating quantities of substrate. (*units of initial velocity = milliOD/min*).

Inhibitor Concentration (μM)	Equation of Line (y=mx+c)	V_{max} (mOD/min)[a]	K_m (μM)[b]	K_i (μM)[c]
0	y = 0.0734x + 00051	196.10	14.39	**X**
3	y = 0.0858x + 0.0056	178.6	15.32	30.62
6	y = 0.097x + 0.0061	163.9	15.89	30.54
10	y = 0.1261x + 0.0067	149.25	18.82	31.86
		Mean K_i (μM)		31.00 ± 0.74

[a] V_{max} = 1/c, [b] $K_m = V_{max}$ x m, [c] K_i=[I]/((V_{max}/$V_{max'}$)-1)

Table 7.1 Properties of Ebselen on pNPP hydrolysis by PHOSPHO1. Concentrations of Ebselen varied between 0 and 10 μM, constants calculated from equations of Lineweaver-Burke plots

Inhibitor Concentration (μM)	Equation of Line (y=mx+c)	V_{max} (mOD/min)[a]	K_m (μM)[b]	K_i (μM)[c]
0	y = 0.0699x + 0.0057	175.43	12.23	**X**
20	y = 0.0866x + 0.0071	140.84	12.20	81.39
40	y = 0.1191x + 0.009	111.11	13.23	69.11
50	y = 0.1402x + 0.0102	98.03	13.74	63.35
		Mean K_i (μM)		71.28 ± 9.21

[a] V_{max} = 1/c, [b] $K_m = V_{max}$ x m, [c] K_i=[I]/((V_{max}/$V_{max'}$)-1)

Table 7.2 Properties of Lansoprazole on pNPP hydrolysis by PHOSPHO1. Concentrations of Lansoprazole varied between 0 and 50 μM, constants calculated from equations of Lineweaver-Burke plots.

Inhibitor Concentration (μM)	Equation of Line (y=mx+c)	V_{max} (mOD/min)[a]	K_m (μM)[b]	K_i (μM)[c]
0	y = 0.0692x + 0.0052	192.31	13.31	**X**
2	y = 0.0816x + 0.0069	144.93	11.83	1.51
3	y = 0.1384x + 0.0134	74.63	10.33	1.90
4	y = 0.2691x + 0.0277	36.10	9.71	0.92
		Mean K_i (μM)		1.08 ± 0.83

[a] V_{max} = 1/c, [b] K_m = V_{max} x m, [c] K_i=[I]/((V_{max}/$V_{max'}$)-1)

Table 7.3 Properties of SCH 202676 on pNPP hydrolysis by PHOSPHO1. (A) Concentrations of SCH 202676 varied between 0 and 4 μM, constants calculated from equations of Lineweaver-Burke plots

7.5.2 Effect of PHOSPHO1 Inhibitors on Cell Mediated Mineralisation

To analyse whether any of the PHOSPHO1 inhibitors had an effect on matrix mineralisation the rapidly mineralising osteoblast-like cell, MLO-A5 was used. The inhibitors were added directly to the cell suspension on the day of plating and the media/inhibitors changed each day up to day nine. Three twelve well plates were set up for each inhibitor, utilising three wells for each inhibitor concentration (0, 5, 7.5 and 10 μM) and one plate for each time point (4, 7, and 9 days). Mineralisation was observed in all wells on day 4 which increased till day 9. Lansoprazole showed no effect on mineralisation and no apparent cellular toxicity. However SCH 202676 and Ebseleln at all concentrations displayed high levels of cellular toxicity depicted by large unoccupied plaques in the culture well becoming apparent after 4 days in

culture. The remaining cells that did continue to grow in the presence of these inhibitors show no signs of reduced capacity for mineralisation, as shown in figure7.6.

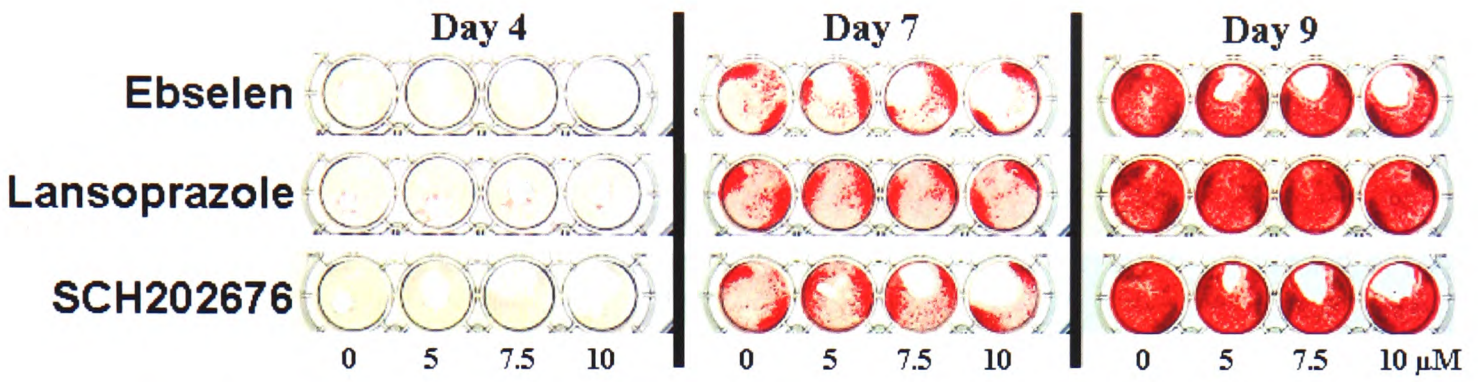

Figure 7.6 Analysis of mineralisation in the presence of PHOSPHO1 inhibitors. Murine MLO-A5 osteoblast like cells were grown in the presence of the mineralisation promoters βGP and AA and incubated with various concentrations of SCH 202676, Lansoprazole or Ebselen. Mineralisation was assessed using the Alizarin red calcium staining technique.

7.5.3 Effect of PHOSPHO1 Inhibitors on MV Phosphatase Activity

MV protein (chick and murine) was used directly as a source of wild type PHOSPHO1 in a malachite green assay to assess Pi generation in the presence of PHOSPHO1 inhibitors. PEA was supplied as PHOSPHO1s preferential substrate and each inhibitor used at a concentration of 1 mM. As seen in figure 7.7 the uninhibited MV protein exhibits a PEA hydrolase activity of 87.1 ± 1.8 nmol min^{-1} mg^{-1} with Lansoprazole and SCH202676 exhibiting the most inhibition of this reaction, 62.9 ± 1.1 nmol min^{-1} mg^{-1} and 73.0 ± 2.7 nmol min^{-1} mg^{-1} respectively. These activities relate to a reduction in activity of approximately 28% for Lansoprazole and 16% for SCH202676.

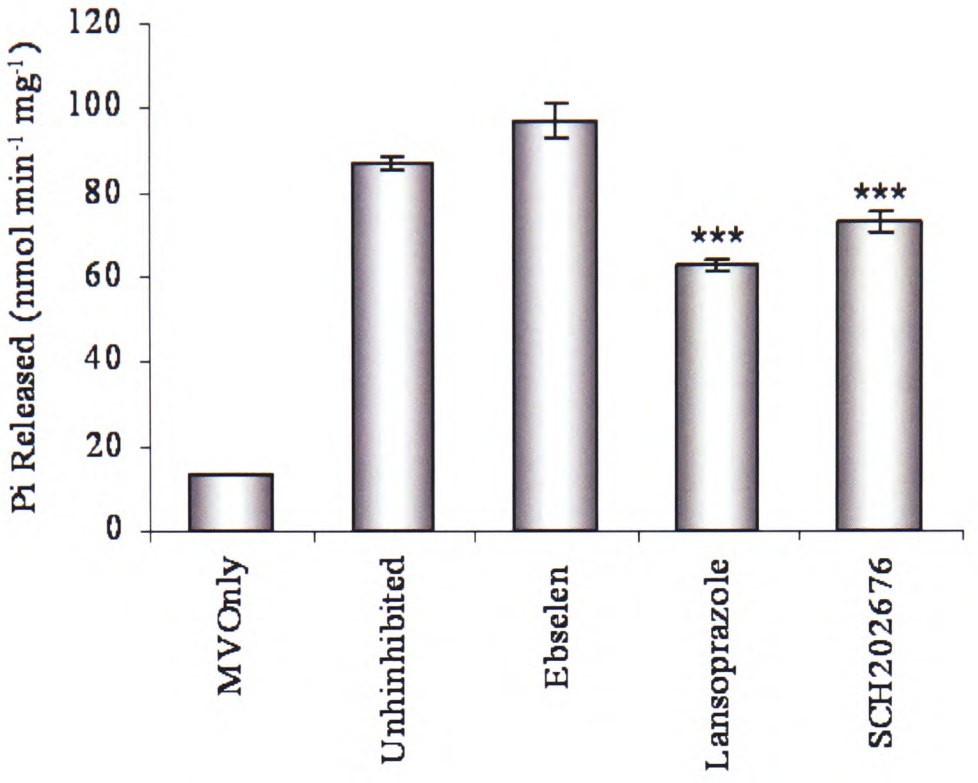

Figure 7.7 Phosphoethanolamine hydrolase potential of chick MVs in the presence of PHOSPHO1 inhibitors. Chick MVs were isolated from tibial growth plate cartilage and used directly to assess PEA hydrolase potential. The reaction was allowed to proceed for 60mins and terminated by the addition of 100 µL BIOMOL Green reagent and absorbance read at 620nm as described under Materials and Methods. Results are mean ± SD (n = 3, *** = $p<0.001$ when inhibited reaction compared to uninhibited).

7.5.4 Effect of PHOSPHO1 Inhibitors on MV Calcification

To investigate the ability of these inhibitors to inhibit the calcification of MV preparations a protocol based on that of Garimella *et al,* (2004) was used. This protocol allows the assessment of the ability of MVs to form calcium phosphate *in vitro*. PEA supports the calcification of chick MVs, purified from growth plate cartilage, comparable to that shown by the phosphoester βGP, 1.0 ± 0.01 and 1.3 ± 0.04 units of calcium precipitated respectively under these assay conditions (figure 7.8a). Chick MV preparations were subsequently incubated with 1 mM of

Lansoprazole or SCH202676 resulting in a slight decrease in calcifying potential in the presence of PEA (approximately 10% with each inhibitor, shown in figure 7.8B).

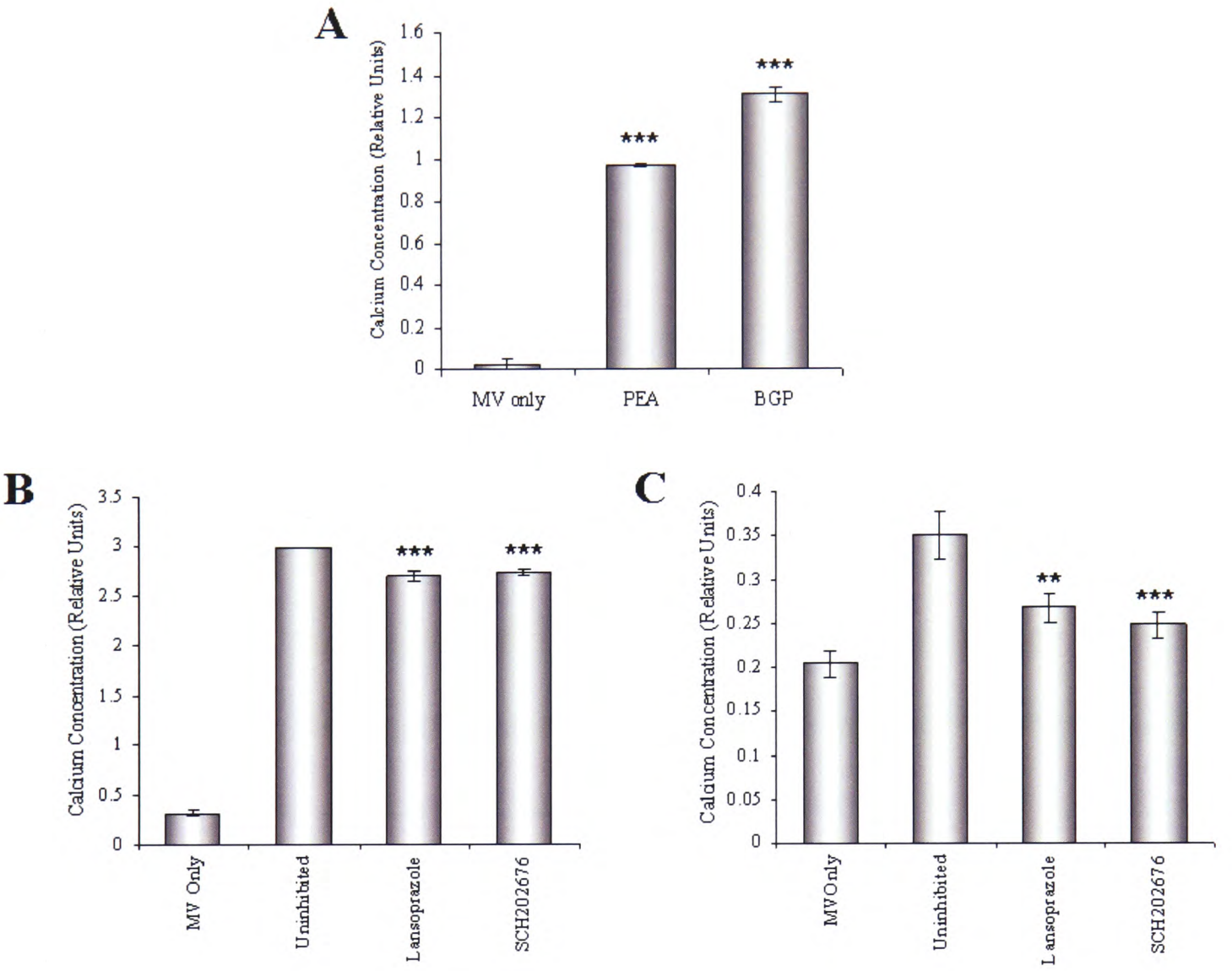

Figure 7.8 Potential for MVs to calcify *in vitro* in the presence of phosphoethanolamine and PHOSPHO1 inhibitors. (**A**) The ability of chick MVs to induce calcification in the presence of PEA and βGP. (**B**) Calcification of chick MVs in the presence of 1 mM Lansoprazole or SCH 202676 (**C**) Calcification of murine TNAP null osteoblast derived MVs in the presence of 1 mM Lansoprazole or SCH 202676. MVs were incubated in calcification buffer with 3 mM phosphoester for 6 hrs, precipitated calcium phosphate was harvested by centrifugation and solubilised for 24Hrs in 0.6N HCl, Calcium concentration was measured by the Calcium-O-cresolpthalein complexone (O-CPC) method as described in section 2.6.4. Results are mean ± SD (n = 3, *** = $p<0.001$, ** = $p<0.01$ when inhibited reaction compared to uninhibited).

To increase the sensitivity of this assay MVs were extracted from cultured $TNAP^{-/-}$ osteoblasts, as these contain no alkaline phosphatase the possibility of this enzyme hydrolysing the phosphoester will be eliminated. When incubated in an identical reaction to that of chick MVs (figures 7.7 -7.8B) a more pronounced inhibitory effect was seen with Lansoprazole and SCH202676. Lansoprazole exhibited a 56.8 % inhibition of calcification by TNAP null MVs whereas SCH202676 inhibited calcification by 70.7%, as detailed in figure 7.8C.

7.6 Discussion

High throughput screening of compounds from the two chemical libraries LOPAC and SPECTRUM revealed 17 inhibitors of PHOSPHO1 mediated hydrolysis of PEA. Many of these inhibitors however had undesirable properties. Compounds such as cisplatinin which could conceivably intercalate between the disulfide bridge in PHOSPHO1. In addition to this, compounds such as the dimeric disulfide containing compound THIRAM would be susceptible to nucleophilic attack and reduction. Other compounds deemed unsuitable include those which posses thiol groups (-SH) due to their propensity to form disulphide bridges with other thiol groups. The functional group of the amino acid cysteine is indeed a thiol thus it is likely that compounds such as mercaptbenzothiazole, which was identified during this screen as a PHOSPHO1 inhibitor, would be causing inhibition through chemical modification of the PHOSPHO1 structure. This compound structure screening led to the identification of three inhibitors for further investigation - SCH 202676, Lansoprazole and Ebselen.

As seen in figure 7.4 and 7.5 all of the inhibitors display characteristics which suggest they do not belong to either the un-competitive or competitive classes i.e. the K_m of the inhibited reaction remains apparently unchanged (due to the interception of the x axis) but there is a reduction in the V_{max}. This is due to the inhibitor binding to a site on the enzyme distinct from the active site causing inactivation of the enzyme molecule. This effectively reduces the total concentration of enzyme available for catalysis. As V_{max} is proportional to enzyme concentration, V_{max} is reduced and as the uninhibited enzyme molecules are unaltered, K_m is unchanged. However upon closer inspection the K_m for Ebselen does seem to rise slightly (table 7.1) with addition of inhibitor thus indicating a mixed inhibition type – characterised by the decrease in V_{max} with a subsequent rise in K_m due to inhibitor binding of both enzyme and enzyme/substrate complex (Stryer, 1995).

The selective inhibition of TNAP within mineralising cultures and tissues has previously been shown to have a negative effect on the mineralisation process. The inhibitory potential of levamisole towards TNAP was first documented in 1973 (Borgers, 1973) and since then has been classified a stereospecific, un-competitive inhibitor of bone alkaline phosphatase (TNAP) (Van Belle, 1976). When levamisole is incubated with cultures of osteoid forming cells, mineralisation is blocked through inhibition of TNAP activity (Tenenbaum, 1987). Although it was originally postulated that the inhibition of TNAP reduced the Pi pool thus decreasing mineralisation it is more likely that the inhibition seen is due to an increase in TNAPs natural substrate and hydroxyapatite inhibitor, PPi (Wang *et al*, 2005). It was investigated, in the present study, whether PHOSPHO1 inhibitors would function in a similar manner to alkaline phosphatase inhibitors when incubated with osteoblast

like cells. The cells of choice were the well characterised MLO-A5 cell type which have the capacity to mineralise their matrix in culture (Kato *et al*, 2001). As seen in figure 7.6 none of the inhibitors had an effect on the mineralisation of cell monolayers by MLO-A5 cells. This may be due to the inaccessibility of the inhibitors to the site where PHOSPHO1 resides, within MVs, however a more likely explanation is that the action of TNAP is masking any effect of the PHOSPHO1 inhibitors. As reported in chapter 3, the mineralisation promoter βGP is a poor substrate for PHOSPHO1, displaying a specific activity of 39.6 ± 6.2 nmol phosphate released/min/mg, over 100x less than that observed with PEA as a substrate. Although it is widely accepted that the main function of TNAP is to hydrolyse the mineralisation inhibitor PPi, a function when studying *in vitro* mineralisation is to cleave βGP thus producing Pi for mineral formation (Chung *et al*, 1992). It has also been shown that βGP increases TNAP transcript levels and hence protein content of cells during the non-mineralisation phase of osteoblast development (Chak *et al*, 1995). Together these data possibly explain why no effect was seen when PHOSPHO1 inhibitors were incubated with osteoblast cultures.

It has been hypothesised that PHOSPHO1 functions at the first step of mineralisation (initiation step), which mediates the deposition of seed crystals of HA within the MV lumen, therefore modulation of PHOSPHO1 activity within these compartments would allow the precise function of this enzyme to be deduced. It has previously been shown that inhibition of TNAP sequestered on the surface of MVs, by levamisole, causes a decrease in both Ca^{2+} and PO_4^{3-} uptake into the vesicle lumen, however apatite growth in this compartment was only weakly affected indicating that TNAP is not directly involved in vesicle mediated calcification

(Register *et al*, 1984). In addition, MVs from TNAP null mice show normal HA formation (Anderson *et al*, 2004). This only strengthens the hypothesis that another enzyme is present at these sites and functions to increase the intravesicular concentrations of Pi to a level which is conducive for calcium phosphate precipitation. To investigate whether PHOSPHO1 could be this enzyme, PEA hydrolase activity was monitored in the presence of PHOSPHO1 inhibitors. As seen in figure 7.7 both Lansoprazole and SCH 202676 decrease the liberated Pi by 28% and 16% respectively. Ebselen had no effect on the PEA hydrolase activity of MVs thus it is likely that it is not effective against wild type enzyme. Also as this is a non-competitive inhibitor it is known that the inhibitor is binding at a site distinct from the active site. As the recombinant protein used for inhibitor screening has a C terminal tagged region, which is not present on the wild type enzyme it is conceivable that Ebselen is binding PHOSPHO1 around this site thus serving to inhibit the recombinant enzyme but not wild type.

SCH 202676 is a thiadiazole compound that acts upon and inhibits signalling through G protein-coupled receptors (Fawzi *et al*, 2001). It is thought that this compound is an allosteric modulator of G protein-coupled receptors and may recognise an intracellular regulatory domain of the protein, however it remains unknown what the exact mode of inhibition is (Lanzafame & Christopoulos, 2004).

Lansoprazole, however, is an extremely well characterised compound. This drug belongs to a class of compounds known as the 2-(2-pyridylmethylsulfinyl)-1*H*-benzimidazoles and is an inhibitor of H+ and K+ (H+/K+)-ATPase of stomach parietal cells. Because this enzyme system is regarded as the acid (proton) pump, Lansoprazole is classified as a gastric acid-pump inhibitor, in that it blocks the final

step of acid production. Interestingly this drug is widely used in the treatment of acid-reflux disorders but no side effects involving bone have been noted, thus the finding that this compound displays PHOSPHO1 inhibition *in vitro* suggests that the drug may be absent at sites of mineralisation or if present, in a altered form. This is consistent with the site of action for this drug – the stomach. Indeed it has been proposed that under acidic conditions, Lansoprazole is converted into an acid activated cationic sulphenamide form (AG2000) which acts as the proton pump inhibitor (Kihira, 1988), this drug is thought to be stomach restricted as the activated sulphenamide form is unable to traverse membranes. At this site it reacts with thiol groups within the catalytic subunit of the H,K-ATPase to form disulfide bonds with cysteine in the α-subunit, as shown in figure 7.9 (Lorentzon *et al*, 1987). It is unlikely that this is the mode of inhibition displayed during Lansoprazole mediated inhibition of PHOSPHO1 as the reaction conditions used during this study are near neutral (pH6.7-7.6) thus the formation of the protonated active form would not be facilitated. In humans this form only occurs when the pH is below 4 (Riel *et al*, 2004) and with the pH of gastric acid being documented as in the 1-2.5 range the conversion of the pro drug to the active form would only be facilitated at acidic sites of the body i.e. the stomach (Evans *et al*, 1988).

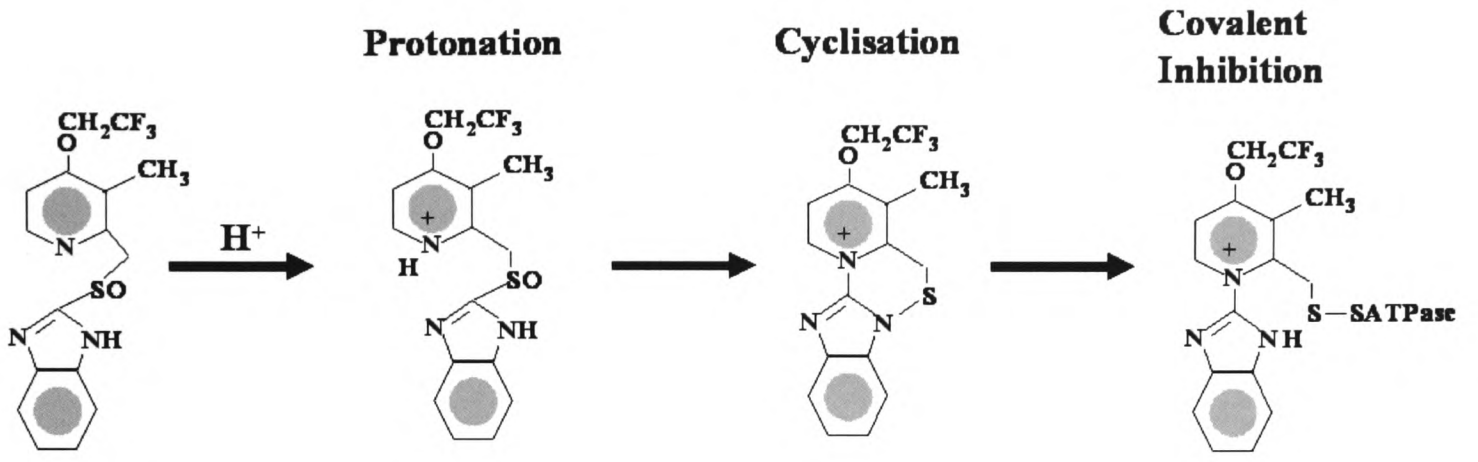

Figure 7.9 Reaction mechanism of Lansoprazole under acidic conditions. The compounds protonate and accumulate in an acid space and undergo an acid-catalysed conversion to a tetracyclic sulfenamide, which then reacts with cysteines in the α subunit of the H,K-ATPase that are accessible from the extracytoplasmic surface (Adapted from Besancon *et al*, 1997)

These two PHOSPHO1 inhibitors were used directly to investigate if they influenced calcification of chick growth plate MVs. As shown in figure 7.8B the effect of these inhibitors was minimal with only around a 10% decrease in calcium detected with each inhibitor. This is not in agreement with the data showing Lansoprazole and SCH 202676 causing a 26% and 16% decrease in Pi release from MV preparations, respectively. It would have been expected that the calcium phosphate deposition from these preparations would also have decreased by a similar ratio. However, as the calcification reaction was done at a higher pH (7.6 compared to 6.7) it is likely that TNAP activity of these MV preps would be higher thus perhaps masking the inhibition of PHOSPHO1 though production of Pi for calcification. In an attempt to overcome this, TNAP null MVs were obtained from osteoblast cultures (isolated from TNAP null calvaria) and used in an identical assay. When the calcification potential of these MV preparations was investigated, and

incubated in the presence of PHOSPHO1 inhibitors, a more profound effect on calcification was observed. Although only a very small quantity of calcium phosphate was produced from these preparations (11.4x less than the equivalent quantity of chick MVs), SCH 202676 caused a 70% decrease in calcification. This would indicate that PHOSPHO1 which is sequestered within the lumen of MVs has the ability to hydrolyse PEA to increase the intravesicular concentrations of Pi and thereby allow mineralisation to occur. This is likely to occur in synergy with phosphate and calcium transporters to facilitate the production of seed crystals for HA deposition, outlined in figure 7.10.

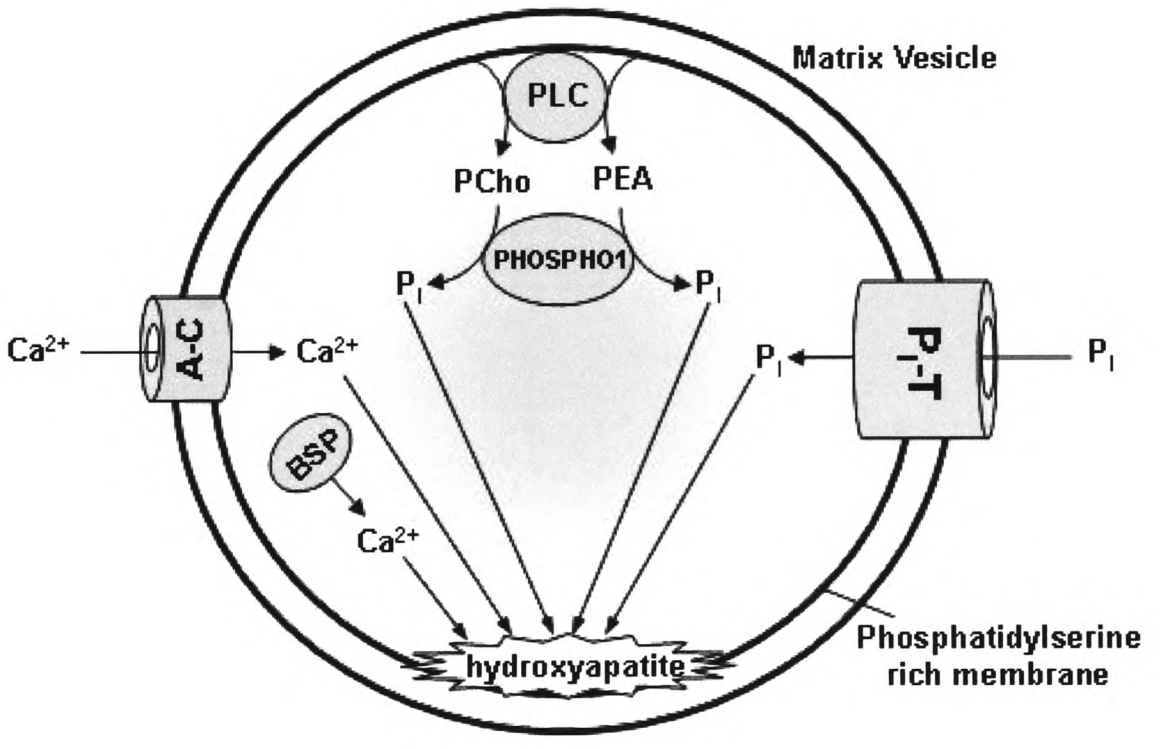

Figure 7.10 Schematic representation of Ca2+ and Pi accumulation in MVs. Inhibition of PHOSPHO1 will decrease the Pi pool within the MV lumen thus causing a decrease in HA production. BSP, bone sialoprotein; PCho, phosphocholine; PEA, phosphoethanolamine; PLC, phospholipase C; A–C, annexin complex; Pi–T, phosphate transporter.

In conclusion the inhibitors, SCH 202676 and Lansoprazole have a certain efficacy in the modulation of *in vitro* mineralisation within MVs. These two compounds, in addition to TNAP inhibitors, may allow further investigation into the initial stages of calcification through the modulation of MV associated phosphatases.

CHAPTER 8

GENERAL DISCUSSION AND FUTURE WORK

8.1 General Discussion

The initiation step of mineralisation is critical for subsequent ordered growth of HA crystals for bone development. Although it is now widely regarded that the production of apatite seed crystals is orchestrated within the confines of the MV, the factors influencing this process are poorly understood. It was originally postulated that TNAP was the catalyst for this process, a master enzyme governing the production of phosphate for calcium phosphate precipitation, however knockout mice lacking functional TNAP displayed mineralised skeletons, and perhaps more critically their MVs contained crystals of hydroxyapatite. This discovery triggered the investigation of other factors which may influence skeletal mineralisation. This work that I present within this thesis concentrated on one protein, PHOSPHO1, which may be involved in this pathway. However before I commence any detailed discussion of the results presented in this thesis I will briefly describe the main findings from this study.

PHOSPHO1 is a phosphatase enzyme which belongs to the HAD superfamily of hydrolases. This enzyme is capable of hydrolysing PEA and PCho, compounds which form the polar head regions of phospholiphid membranes, with high specific activity and favourable kinetics. This would indicate that this reaction is likely to occur *in vivo* and implicates this enzyme in the phosphoglycerolipid metabolism pathway. This enzyme, despite its relatively high sequence identity, displays an entirely different hydrolysis pattern to PHOSPHO2. PHOSPHO2 is expressed within mineralising tissues, as is PHOSPHO1, however out of the tested substrates P5P served as the best ligand for this enzyme. This was somewhat surprising, however upon analysis of molecular models of both PHOSPHO1 and PHOSPHO2 significant

differences were observed between the two structures which may cause the differences in apparent substrate specificity. The active site of PHOSPHO1 was also further characterised with residues previously postulated to be involved in substrate specific interactions mutated to investigate their involvement in PHOSPHO1 mediated catalysis.

Previous to this project, localisation studies had been undertaken using a chick model, the results of which implicated PHOSPHO1 in the mineralisation process due to its localisation to every surface of mineralisation in both bone and cartilage. It was therefore important to replicate this in the mammalian system thus disproving the interpretation that perhaps this protein was merely a caveat of avian bone formation. Indeed mammalian PHOSPHO1 is localised in the mouse model in an identical fashion as previously observed within the chick. Interestingly the protein is also present in MVs of both species, furthering the hypothesis that PHOSPHO1 is involved in the mineralisation process. Further, the mineralisation promoter AA also increases the content of PHOSPHO1 within MVs indicting a similar regulatory pattern to TNAP.

The modulation to PHOSPHO1 has an effect on the mineralisation capacity of both cells and MVs. Reduction of PHOSPHO1 transcript within the MLO-A5 cell line through siRNA mediated knockdown reduces the potential for matrix mineralisation. In addition, reduction of PHOSPHO1 activity through the use of newly discovered small molecule inhibitors causes a decrease in the capacity of MVs to calcify *in vitro*. These data both indicate that PHOSPHO1 has a role in the mineralisation process which is likely to be in the production of Pi for calcium phosphate precipitation.

Collectively these data indicate that PHOSPHO1 is closely associated with the mineralisation process and in particular, due to the results presented in chapter 7, the generation of Pi for hydroxyapatite production. This is an essential phase of mineral formation, not only for the precipitation with calcium but initially to raise the Pi/PPi ratio to a degree that is permissive to mineralisation. This, as discussed previously, is due to PPi acting as a powerful inhibitor of HA formation. The source of substrate for Pi generation by PHOSPHO1 is likely to be that of the MV-membrane which is a reservoir of both phosphatidylethanolamine and phosphatidylcholine. As discussed previously, Wu *et al* (2002) have found that the phosphatidylethanolamine and phosphatidylcholine composition of the MV membrane decreases during mineralisation and that 1,2-diacyl glycerol accumulates in MVs, indicative of phospholipase C activity. In addition to this a recent study has shown that prostaglandin F2α increases PCho production in murine MC3T3-E1 osteoblast-like cells (Sakai *et al*, 2004). The authors suggest that a phospholipase C (PLC) is responsible for this increase in PCho production. This combined with the localisation of PHOSPHO1 in MVs and the differentiation pattern akin to TNAP furthers the initial hypothesis. This would represent a novel means of generating P_i in mineralising cells and offer an explanation as to why HA is observed within the MVs of TNAP null mice. It is apparent though that this is not a form of enzymatic redundancy in the mineralisation process as PHOSPHO1 does not cleave well known TNAP substrates such as PPi and P5P, also TNAP is anchored to the outer leaflet of MVs and mineralising cells whereas PHOSPHO1 appears to be cytosolic. It is more likely that these two enzymes act in a synchronised manner to promote the mineralisation process; TNAP would primarily hydrolyse the mineralisation inhibitor

PPi whereas PHOSPHO1 would produce Pi to facilitate seed crystal deposition. The loss of function of either of these enzymes would only serve to impede skeletal development. It seems however, that neither of these enzymes are powerful enough to cause a complete loss of mineralisation. This is indicated by the data in chapter six referring to the use of siRNA to knockdown PHOSPHO1 transcript and that in chapter seven concerning the inhibition of PHOSPHO1 in TNAP null MVs. Collectively these data strongly suggest that if the function of both enzymes is lost mineralisation would be severely retarded.

If correct this would have implications to the manner in which we treat mineralisation disorders such as osteomalacia and pathological soft-tissue ossification, a process clinically significant in atherosclerosis and heart failure. Intervention of these pathological conditions at a stage prior to mineral growth, at the point of seed crystal initiation may prove to have an efficacy in the treatment of these conditions. Indeed, as it seems from the results presented that bone mineralisation requires both PHOSPHO1 and TNAP, the targeted inhibition of these proteins may be a potential treatment in these disorders. The discovery of novel small molecule inhibitors and the characterisation of the PHOSPHO1 active site may lead to the generation of novel reagents with the ability to modulate PHOSPHO1 activity. In addition since the discovery that siRNAs can be used to selectively knockdown gene expression *in vivo* (Xia *et al*, 2002) a novel therapeutic mechanism could potentially be developed. I have described within this thesis regions of the PHOSPHO1 RNA sequence which can be targeted to ensure knockdown of gene expression, information which would ultimately need to be compiled before the development of a siRNA therapeutic.

In conclusion the data presented within this thesis has linked PHOSPHO1 to a cellular pathway (phosphoglycerolipid metabolism) and to the mineralisation process in the mammalian system. Its elevated expression and localisation in the mouse model only serves to strengthen this hypothesis. Its localisation within MVs also attributes to this conclusion, as these discrete packages are considered the epicentre of mineralisation. A protein that is present within MVs, which is regulated so as content increases in line with cellular differentiation, would presumably be contributing to the processes which are occurring within.

8.2 Future Work

Although the results described within this thesis give an indication that PHOSPHO1 is involved in the bone mineralisation process, to assign true function, a model to study PHOSPHO1 *in vivo* would have to be developed. Knockout technology allows the production of mice lacking functional genes; hence by generating a mouse deficient in PHOSPHO1 it would be possible to assign function through analysis of metabolic abnormalities. This has already been exemplified by the wealth of information gained through the study of the TNAP-deficient mouse model of hypophosphatasia.

As it has been hypothesised that PHOSPHO1 is closely associated with TNAP in the mineralisation process, the PHOSPHO1 null mouse could be compared directly to the TNAP null mouse developed by Dr Millan (Burnham Institute, CA). In addition, inactivation of both the PHOSPHO1 and TNAP genes simultaneously could be investigated by cross breading the two mutants. As it has already been shown that TNAP is involved in the second step (phase 2) of mineralisation and as

PHOSPHO1 has been hypothesised to be involved in the first, initiation step it may be hypothesised that the knockout of both gene products simultaneously could lead to the complete absence of HA crystals. If this were the case, it would clearly implicate the function of PHOSPHO1, and of MV-mediated mineralisation, as a crucial step in skeletal mineralisation. Alternatively, it may be found that the phenotypic changes in the PHOSPHO1/TNAP double mutant mice are not significantly different from the osteomalacia observed in the TNAP null mice. This would imply either that MV-mediated calcification is not dependent on PHOSPHO1 function and/or that other phosphatases or pathways may be operating in addition to, or instead of, PHOSPHO1. Only upon complete characterisation of bone physiology from both the single and double mutant mice could a reasoned evaluation of PHOSPHO1 function be carried out.

Calvarial osteoblasts could also be grown in culture from these mice and used to evaluate phenotypic changes *in vitro*. These cells could be tested directly, utilising mineralisation assays, to investigate differences in their ability to deposit mineral *in vitro* compared to TNAP null cells and also if this ability is restricted further in the PHOSPHO1/TNAP double mutant cells. Using techniques described in this thesis it could also be investigated whether MVs derived from PHOSPHO1 null and TNAP null osteoblasts have an impaired ability to calcify *in vitro* compared with MVs from WT cells and also if calcification is further restricted in MVs derived from PHOSPHO1/TNAP double mutant osteoblasts. This would further give data which could directly be used to assign not only function of PHOSPHO1 but also which stage of the mineralisation process it is involved in.

Finally, as PHOSPHO1 has been implicated in the glycerophospholipid metabolism pathway changes in phospholipid metabolites of MVs from the single and double mutants during calcification could be investigated. As discussed in chapter 3 it has previously been demonstrated by Wu *et al*, 2002 that the phospholipid composition of the MV membrane decreases during mineralisation and that 1,2-diacyl glycerol accumulates in the MV lumen. Although this is directly the result of Phospholipase C activity, the products of the reaction would be PEA and PCho, these could be directly monitored using ^{31}P-nuclear magnetic resonance spectroscopy (NMR) hence indicating PHOSPHO1s involvement in this pathway.

Reference List

Akiyama,H., Chaboissier,M.C., Martin,J.F., Schedl,A., and de Crombrugghe,B. (2002). The transcription factor Sox9 has essential roles in successive steps of the chondrocyte differentiation pathway and is required for expression of Sox5 and Sox6. Genes Dev. *16*, 2813-2828.

Ali,S.Y., Sajdera,S.W., and Anderson,H.C. (1970). Isolation and characterization of calcifying matrix vesicles from epiphyseal cartilage. Proc. Natl. Acad. Sci. U. S. A *67*, 1513-1520.

Ali,S.Y. and Evans,L. (1973). The uptake of [Ca]calcium ions by matrix vesicles isolated from calcifying cartilage (Short Communication). Biochem. J. *134*, 647-650.

Anderson,H.C. (1969). Vesicles Associated with Calcification in Matrix of Epiphyseal Cartilage. Journal of Cell Biology *41*, 59-72.

Anderson,H.C., Matsuzawa,T., Sajdera,S.W., and Ali,S.Y. (1970). Membranous particles in calcifying cartilage matrix. Trans. N. Y. Acad. Sci. *32*, 619-630.

Anderson,H.C. (1992). Conference Introduction and Summary. Bone and Mineral *17,* 107-112.

Anderson,H.C. (1995). Molecular-Biology of Matrix Vesicles. Clinical Orthopaedics and Related Research 266-280.

Anderson,H.C., Hsu,H.H., Morris,D.C., Fedde,K.N., and Whyte,M.P. (1997). Matrix vesicles in osteomalacic hypophosphatasia bone contain apatite-like mineral crystals. Am. J. Pathol. *151*, 1555-1561.

Anderson,H.C. (2003). Matrix vesicles and calcification. Curr. Rheumatol. Rep. *5*, 222-226.

Anderson,H.C., Sipe,J.B., Hessle,L., Dhamyamraju,R., Atti,E., Camacho,N.P., and Millan,J.L. (2004). Impaired calcification around matrix vesicles of growth plate and bone in alkaline phosphatase-deficient mice. American Journal of Pathology *164*, 841-847.

Aravind,L., Galperin,M.Y., and Koonin,E.V. (1998). The catalytic domain of the P-type ATPase has the haloacid dehalogenase fold. Trends Biochem. Sci. *23*, 127-129.

Aubin,J.E. and Triffitt,J.T. (2002), 'Mesenchymal stem cells and osteoblast differentiation', in Bilezikian,J.P., Raisz,L.G. and Rodan,G.A. (eds) *Principles of Bone Biology.* Academic Press, San Diego, 59-81.

Bachner,D., Ahrens,M., Betat,N., Schroder,D., and Gross,G. (1999). Developmental expression analysis of murine autotaxin (ATX). Mech. Dev. *84*, 121-125.

Baldwin,J.C., Karthikeyan,A.S., and Raghothama,K.G. (2001). LEPS2, a phosphorus starvation-induced novel acid phosphatase from tomato. Plant Physiol *125*, 728-737.

Baulcombe,D. (2004). RNA silencing in plants. Nature *431*, 356-363.

Baykov,A.A., Evtushenko,O.A., and Avaeva,S.M. (1988). A malachite green procedure for orthophosphate determination and its use in alkaline phosphatase-based enzyme immunoassay. Anal. Biochem. *171*, 266-270.

Beck,G.R., Jr., Moran,E., and Knecht,N. (2003). Inorganic phosphate regulates multiple genes during osteoblast differentiation, including Nrf2. Exp. Cell Res. *288*, 288-300.

Beier,F., Leask,T.A., Haque,S., Chow,C., Taylor,A.C., Lee,R.J., Pestell,R.G., Ballock,R.T., and LuValle,P. (1999). Cell cycle genes in chondrocyte proliferation and differentiation. Matrix Biology *18*, 109-120.

Belli,S.I., Sali,A., and Goding,J.W. (1994). Divalent cations stabilize the conformation of plasma cell membrane glycoprotein PC-1 (alkaline phosphodiesterase I). Biochem. J. *304 (Pt 1)*, 75-80.

Bendtsen,J.D., Nielsen,H., von Heijne,G., and Brunak,S. (2004). Improved prediction of signal peptides: SignalP 3.0. J. Mol. Biol. *340*, 783-795.

Beninati,S., Senger,D.R., Cordellamiele,E., Mukherjee,A.B., Chackalaparampil,I., Shanmugam,V., Singh,K., and Mukherjee,B.B. (1994). Osteopontin - Its Transglutaminase-Catalyzed Posttranslational Modifications and Cross-Linking to Fibronectin. Journal of Biochemistry *115*, 675-682.

Bertani,G. (2004). Lysogeny at Mid-Twentieth Century: P1, P2, and Other Experimental Systems. J. Bacteriol. *186,* 595-600.

Besancon,M., Simon,A., Sachs,G., and Shin,J.M. (1997). Sites of reaction of the gastric H,K-ATPase with extracytoplasmic thiol reagents. J. Biol. Chem. *272*, 22438-22446.

Bi,W., Deng,J.M., Zhang,Z., Behringer,R.R., and de Crombrugghe,B. (1999). Sox9 is required for cartilage formation. Nat. Genet. *22*, 85-89.

Bohn,W.W., Stein,R.M., Hsu,H.H., Morris,D.C., and Anderson,H.C. (1984). Isolation of a plasma membrane-enriched fraction from collagenase-suspended rachitic rat growth plate chondrocytes. J. Orthop. Res. *1*, 319-324.

Bollen,M., Gijsbers,R., Ceulemans,H., Stalmans,W., and Stefan,C. (2000). Nucleotide pyrophosphatases/phosphodiesterases on the move. Crit Rev. Biochem. Mol. Biol. *35*, 393-432.

Bonucci,E., Silvestrini,G., and Bianco,P. (1992). Extracellular alkaline phosphatase activity in mineralizing matrices of cartilage and bone: ultrastructural localization using a cerium-based method. Histochemistry *97*, 323-327.

Borgers,M. (1973). The cytochemical application of new potent inhibitors of alkaline phosphatases. J. Histochem. Cytochem. *21*, 812-824.

Boskey,A.L., Spevak,L., Paschalis,E., Doty,S.B., and Mckee,M.D. (2002). Osteopontin deficiency increases mineral content and mineral crystallinity in mouse bone. Calcified Tissue International *71*, 145-154.

Bostrom,K. (2001). Insights into the mechanism of vascular calcification. American Journal of Cardiology *88*, 20E-22E.

Bower,M.J., Cohen,F.E., and Dunbrack,R.L., Jr. (1997). Prediction of protein side-chain rotamers from a backbone-dependent rotamer library: a new homology modeling tool. J. Mol. Biol. *267*, 1268-1282.

Bradford,M.M. (1976). A rapid and sensitive method for the quantitation of microgram quantities of protein utilizing the principle of protein-dye binding. Anal. Biochem. *72*, 248-254.

Bradshaw,A.D. and Sage,E.H. (2001). SPARC, a matricellular protein that functions in cellular differentiation and tissue response to injury. Journal of Clinical Investigation *107*, 1049-1054.

Brummelkamp,T.R., Bernards,R., and Agami,R. (2002). A system for stable expression of short interfering RNAs in mammalian cells. Science *296*, 550-553.

Campo,R.D. and Romano,J.E. (1986). Changes in cartilage proteoglycans associated with calcification. Calcif. Tissue Int. *39*, 175-184.

Chak,C.W., Lee,K.M., Leung,K.S., and Fung,K.P. (1995). No change in bone-specific alkaline phosphatase activities in cultured rat osteoblastic cells under L-ascorbate and beta-glycerophosphate-induced mineralization. Cell Biol. Int. *19*, 979-985.

Chen,J.K., Shapiro,H.S., Wrana,J.L., Reimers,S., Heersche,J.N.M., and Sodek,J. (1991). Localization of Bone Sialoprotein (Bsp) Expression to Sites of Mineralized Tissue Formation in Fetal-Rat Tissues by Insitu Hybridization. Matrix *11*, 133-143.

Chenu,C., Colucci,S., Grano,M., Zigrino,P., Barattolo,R., Zambonin,G., Baldini,N., Vergnaud,P., Delmas,P.D., and Zallone,A.Z. (1994). Osteocalcin Induces Chemotaxis, Secretion of Matrix Proteins, and Calcium-Mediated Intracellular Signaling in Human Osteoclast-Like Cells. Journal of Cell Biology *127*, 1149-1158.

Chung,C.H., Golub,E.E., Forbes,E., Tokuoka,T., and Shapiro,I.M. (1992). Mechanism of action of beta-glycerophosphate on bone cell mineralization. Calcif. Tissue Int. *51*, 305-311.

Clarke,D.M., Loo,T.W., and MacLennan,D.H. (1990). Functional consequences of alterations to amino acids located in the nucleotide binding domain of the Ca2(+)-ATPase of sarcoplasmic reticulum. J. Biol. Chem. *265*, 22223-22227.

Collet,J.F., Stroobant,V., Pirard,M., Delpierre,G., and Van Schaftingen,E. (1998). A new class of phosphotransferases phosphorylated on an aspartate residue in an

amino-terminal DXDX(T/V) motif. Journal of Biological Chemistry *273*, 14107-14112.

Collet,J.F., Stroobant,V., and Van Schaftingen,E. (1999). Mechanistic studies of phosphoserine phosphatase, an enzyme related to P-type ATPases. J. Biol. Chem. *274*, 33985-33990.

Colnot,C., Lu,C.Y., Hu,D., and Helms,J.A. (2004). Distinguishing the contributions of the perichondrium, cartilage, and vascular endothelium to skeletal development. Developmental Biology *269*, 55-69.

Cong,L.N., Chen,H., Li,Y., Lin,C.H., Sap,J., and Quon,M.J. (1999). Overexpression of protein tyrosine phosphatase-alpha (PTP-alpha) but not PTP-kappa inhibits translocation of GLUT4 in rat adipose cells. Biochem. Biophys. Res. Commun. *255*, 200-207.

Curradi,M., Izzo,A., Badaracco,G., and Landsberger,N. (2002). Molecular mechanisms of gene silencing mediated by DNA methylation. Mol. Cell Biol. *22*, 3157-3173.

Danner,S.A., Carr,A., Leonard,J.M., Lehman,L.M., Gudiol,F., Gonzales,J., Raventos,A., Rubio,R., Bouza,E., Pintado,V., and . (1995). A short-term study of the safety, pharmacokinetics, and efficacy of ritonavir, an inhibitor of HIV-1 protease. European-Australian Collaborative Ritonavir Study Group. N. Engl. J. Med. *333*, 1528-1533.

DeJong, W.F. (1926). La Substance Minerale Dans Les Os. Journal of the Royal Netherlands Chemical Society *45*, 445- 448.

Delany,A.M., Amling,M., Priemel,M., Howe,C., Baron,R., and Canalis,E. (2000). Osteopenia and decreased bone formation in osteonectin-deficient mice. Journal of Clinical Investigation *105*, 915-923.

Delany,A.M., Kalajzic,I., Bradshaw,A.D., Sage,E.H., and Canalis,E. (2003). Osteonectin-null mutation compromises osteoblast formation, maturation, and survival. Endocrinology *144*, 2588-2596.

Deng,C.X., WynshawBoris,A., Zhou,F., Kuo,A., and Leder,P. (1996). Fibroblast growth factor receptor 3 is a negative regulator of bone growth. Cell *84*, 911-921.

Derfus,B., Steinberg,M., Mandel,N., Buday,M., Daft,L., and Ryan,L. (1995). Characterization of an additional articular cartilage vesicle fraction that generates calcium pyrophosphate dihydrate crystals in vitro. J. Rheumatol. *22*, 1514-1519.

Ducy,P., Desbois,C., Boyce,B., Pinero,G., Story,B., Dunstan,C., Smith,E., Bonadio,J., Goldstein,S., Gundberg,C., Bradley,A., and Karsenty,G. (1996). Increased bone formation in osteocalcin-deficient mice. Nature *382*, 448-452.

Ducy,P., Zhang,R., Geoffroy,V., Ridall,A.L., and Karsenty,G. (1997). Osf2/Cbfa1: A transcriptional activator of osteoblast differentiation. Cell *89*, 747-754.

Ducy,P., Schinke,T., and Karsenty,G. (2000). The osteoblast: A sophisticated fibroblast under central surveillance. Science *289*, 1501-1504.

Durning,W.C. (1958). Submicroscopic structure of frozen-dried epiphyseal plate and adjacent spongiosa of the rat. J. Ultrastruct. Res. *2*, 245-260.

Dziewiatkowski,D.D. and Majznerski,L.L. (1985). Role of Proteoglycans in Endochondral Ossification - Inhibition of Calcification. Calcified Tissue International *37*, 560-564.

Eanes,E.D. and Posner,A.S. (1970), 'Structure and chemistry of bone mineral', in Schraer,H. (ed) *Biological Calcification: Cellular and Molecular Aspects.* Appleton-Century-Crofts, New York, 1-26.

Ellison,D.W., Beal,M.F., and Martin,J.B. (1987). Phosphoethanolamine and ethanolamine are decreased in Alzheimer's disease and Huntington's disease. Brain Res. *417*, 389-392.

Engel,J., Taylor,W., Paulsson,M., Sage,H., and Hogan,B. (1987). Calcium-Binding Domains and Calcium-Induced Conformational Transition of Sparc-Bm-40-Osteonectin, An Extracellular Glycoprotein Expressed in Mineralized and Nonmineralized Tissues. Biochemistry *26*, 6958-6965.

Evans,D.F., Pye,G., Bramley,R., Clark,A.G., Dyson,T.J., and Hardcastle,J.D. (1988). Measurement of gastrointestinal pH profiles in normal ambulant human subjects. Gut *29*, 1035-1041.

Farber,S.A., Slack,B.E., and Blusztajn,J.K. (2000). Acceleration of phosphatidylcholine synthesis and breakdown by inhibitors of mitochondrial function in neuronal cells: a model of the membrane defect of Alzheimer's disease. FASEB J. *14*, 2198-2206.

Farley,J.R., Ivey,J.L., and Baylink,D.J. (1980). Human skeletal alkaline phosphatase. Kinetic studies including pH dependence and inhibition by theophylline. J. Biol. Chem. *255*, 4680-4686.

Farquharson,C., Lester,D., Seawright,E., Jefferies,D., and Houston,B. (1999). Microtubules are potential regulators of growth-plate chondrocyte differentiation and hypertrophy. Bone *25*, 405-412.

Farquharson,C., Seawright,E., and Houston,B. (2002). Specific immunolocalisation of a novel phosphatase to osteoblasts and mineralising growth plate chondrocytes of immature long bones. Journal of Bone and Mineral Research *17*, 1332.

Farquharson,C. (2003), 'Bone Growth', in Scanes,C.G. (ed) *Biology of growth of domestic animals*. Iowa State Press, Iowa, 170-185

Fawzi,A.B., Macdonald,D., Benbow,L.L., Smith-Torhan,A., Zhang,H.T., Weig,B.C., Ho,G., Tulshian,D., Linder,M.E., and Graziano,M.P. (2001). SCH-202676: An allosteric modulator of both agonist and antagonist binding to G protein-coupled receptors. Molecular Pharmacology *59*, 30-37.

Fedde,K.N., Lane,C.C., and Whyte,M.P. (1988). Alkaline phosphatase is an ectoenzyme that acts on micromolar concentrations of natural substrates at physiologic pH in human osteosarcoma (SAOS-2) cells. Arch. Biochem. Biophys. *264*, 400-409.

Fedde,K.N., Blair,L., Silverstein,J., Coburn,S.P., Ryan,L.M., Weinstein,R.S., Waymire,K., Narisawa,S., Millan,J.L., MacGregor,G.R., and Whyte,M.P. (1999). Alkaline phosphatase knock-out mice recapitulate the metabolic and skeletal defects of infantile hypophosphatasia. J. Bone Miner. Res. *14*, 2015-2026.

Fedorov,Y., Anderson,E.M., Birmingham,A., Reynolds,A., Karpilow,J., Robinson,K., Leake,D., Marshall,W.S., and Khvorova,A. (2006). Off-target effects by siRNA can induce toxic phenotype. RNA. *12*, 1188-1196.

Fire,A., Xu,S., Montgomery,M.K., Kostas,S.A., Driver,S.E., and Mello,C.C. (1998). Potent and specific genetic interference by double-stranded RNA in Caenorhabditis elegans. Nature *391*, 806-811.

Fisher,L.W., Whitson,S.W., Avioli,L.V., and Termine,J.D. (1983). Matrix Sialoprotein of Developing Bone. Journal of Biological Chemistry *258*, 2723-2727.

Fisher,L.W., Mcbride,O.W., Termine,J.D., and Young,M.F. (1990). Human-Bone Sialoprotein - Deduced Protein-Sequence and Chromosomal Localization. Journal of Biological Chemistry *265*, 2347-2351.

Franceschi,R.T. and Young,J. (1990). Regulation of alkaline phosphatase by 1,25-dihydroxyvitamin D3 and ascorbic acid in bone-derived cells. J. Bone Miner. Res. *5*, 1157-1167.

Franceschi,R.T., Iyer,B.S., and Cui,Y. (1994). Effects of ascorbic acid on collagen matrix formation and osteoblast differentiation in murine MC3T3-E1 cells. J. Bone Miner. Res. *9*, 843-854.

Franzen,A. and Heinegard,D. (1985). Isolation and characterization of two sialoproteins present only in bone calcified matrix. Biochem. J. *232*, 715-724.

Garimella,R., Sipe,J.B., and Anderson,H.C. (2004). A simple and non-radioactive technique to study the effect of monophosphoesters on matrix vesicle-mediated calcification. Biol. Proced. Online. *6*, 263-267.

Genge,B.R., Sauer,G.R., Wu,L.N., McLean,F.M., and Wuthier,R.E. (1988). Correlation between loss of alkaline phosphatase activity and accumulation of calcium during matrix vesicle-mediated mineralization. J. Biol. Chem. *263*, 18513-18519.

Gergen,J.P. and Wieschaus,E.F. (1985). The Localized Requirements for A Gene Affecting Segmentation in Drosophila - Analysis of Larvae Mosaic for Runt. Developmental Biology *109*, 321-335.

Gram,G.J., Nielsen,S.D., and Hansen,J.E. (1998). Spontaneous silencing of humanized green fluorescent protein (hGFP) gene expression from a retroviral vector by DNA methylation. J. Hematother. *7*, 333-341.

Gregory,C.A., Singh,H., Perry,A.S., and Prockop,D.J. (2003). The Wnt signaling inhibitor dickkopf-1 is required for reentry into the cell cycle of human adult stem cells from bone marrow. J. Biol. Chem. *278*, 28067-28078.

Gu,M., Meng,K., and Majerus,P.W. (1996). The effect of overexpression of the protein tyrosine phosphatase PTPMEG on cell growth and on colony formation in soft agar in COS-7 cells. Proc. Natl. Acad. Sci. U. S. A *93*, 12980-12985.

Hakim,F.T., Cranley,R., Brown,K.S., Eanes,E.D., Harne,L., and Oppenheim,J.J. (1984). Hereditary joint disorder in progressive ankylosis (ank/ank) mice. I. Association of calcium hydroxyapatite deposition with inflammatory arthropathy. Arthritis Rheum. *27*, 1411-1420.

Hale,J.E., Fraser,J.D., and Price,P.A. (1988). The identification of matrix Gla protein in cartilage. J. Biol. Chem. *263*, 5820-5824.

Halleen,J.M. and Ranta,R. (2001). Tartrate-resistant acid phosphatase as a serum marker of bone resorption. Am. Clin. Lab *20* , 29-30.

Hanahan,D. (1983). Studies on Transformation of *Escherichia coli* with Plasmids. J. Mol. Biol. *166,* 557-580.

Harmey,D., Hessle,L., Narisawa,S., Johnson,K.A., Terkeltaub,R., and Millan,J.L. (2004). Concerted regulation of inorganic pyrophosphate and osteopontin by akp2, enpp1, and ank: an integrated model of the pathogenesis of mineralization disorders. Am. J. Pathol. *164*, 1199-1209.

Hashimoto,S., Ochs,R.L., Rosen,F., Quach,J., McCabe,G., Solan,J., Seegmiller,J.E., Terkeltaub,R., and Lotz,M. (1998). Chondrocyte-derived apoptotic bodies and calcification of articular cartilage. Proc. Natl. Acad. Sci. U. S. A *95*, 3094-3099.

Hatch,G.M. and Choy,P.C. (1987). Phosphocholine phosphatase and alkaline phosphatase are different enzymes in hamster heart. Lipids *22*, 672-676.

Havers, C. (1691), 'Osteologia nova, or Some new observations of the bones, and the parts belonging to them, : with the manner of their accretion, and nutrition, communicated to the Royal Society in several discourses. I. Of the membrane, nature, constituent parts, and internal structure of the bones. II. Of accretion, and nutrition, as also of the affections of the bones in the rickets, and of venereal nodes. III. Of the medulla, or marrow. IV. Of the mucilaginous glands, with the etiology or explication of the causes of a rheumatism, and the gout, and the manner how they are

produced. To which is added a fifth discourse of the cartilages.', Printed for Samuel Smith, at the Princes Arms in St. Paul's Church-Yard, London.

Helfrich,M.H., Nesbitt,S.A., Lakkakorpi,P.T., Barnes,M.J., Bodary,S.C., Shankar,G., Mason,W.T., Mendrick,D.L., Vaananen,H.K., and Horton,M.A. (1996). beta(1) Integrins and osteoclast function: Involvement in collagen recognition and bone resorption. Bone *19*, 317-328.

Henthorn,P.S., Raducha,M., Fedde,K.N., Lafferty,M.A., and Whyte,M.P. (1992). Different missense mutations at the tissue-nonspecific alkaline phosphatase gene locus in autosomal recessively inherited forms of mild and severe hypophosphatasia. Proc. Natl. Acad. Sci. U. S. A *89*, 9924-9928.

Hessle,L., Johnson,K.A., Anderson,H.C., Narisawa,S., Sali,A., Goding,J.W., Terkeltaub,R., and Millan,J.L. (2002). Tissue-nonspecific alkaline phosphatase and plasma cell membrane glycoprotein-1 are central antagonistic regulators of bone mineralization. Proceedings of the National Academy of Sciences of the United States of America *99*, 9445-9449.

Hill,T.P., Spater,D., Taketo,M.M., Birchmeier,W., and Hartmann,C. (2005). Canonical Wnt/beta-catenin signaling prevents osteoblasts from differentiating into chondrocytes. Dev. Cell *8*, 727-738.

Hitomi,K., Torii,Y., and Tsukagoshi,N. (1992). Increase in the activity of alkaline phosphatase by L-ascorbic acid 2-phosphate in a human osteoblast cell line, HuO-3N1. J. Nutr. Sci. Vitaminol. (Tokyo) *38* , 535-544.

Ho,A.M., Johnson,M.D., and Kingsley,D.M. (2000). Role of the mouse ank gene in control of tissue calcification and arthritis. Science *289*, 265-270.

Hoang,Q.Q., Sicheri,F., Howard,A.J., and Yang,D.S. (2003). Bone recognition mechanism of porcine osteocalcin from crystal structure. Nature *425*, 977-980.

Horton,M.A., Nesbit,M.A., and Helfrich,M.H. (1995). Interaction of Osteopontin with Osteoclast Integrins. Osteopontin: Role in Cell Signalling and Adhesion *760*, 190-200.

Houston,B. and Peddie,D. (1989). A method for detecting proteins immobilized on nitrocellulose membranes by in situ derivatization with fluorescein isothiocyanate. Anal. Biochem. *177*, 263-267.

Houston,B., Seawright,E., Jefferies,D., Hoogland,E., Lester,D., Whitehead,C., and Farquharson,C. (1999). Identification and cloning of a novel phosphatase expressed at high levels in differentiating growth plate chondrocytes. Biochim. Biophys. Acta *1448*, 500-506.

Houston,B., Paton,I.R., Burt,D.W., and Farquharson,C. (2002). Chromosomal localization of the chicken and mammalian orthologues of the orphan phosphatase PHOSPHO1 gene. Anim Genet. *33*, 451-454.

Houston,B., Stewart,A.J., and Farquharson,C. (2004). PHOSPHO1 - A novel phosphatase specifically expressed at sites of mineralisation in bone and cartilage. Bone *34*, 629-637.

Howell,D.S., Pita,J.C., Marquez,J.F., and Madruga,J.E. (1968). Partition of calcium, phosphate, and protein in the fluid phase aspirated at calcifying sites in epiphyseal cartilage. J. Clin. Invest *47*, 1121-1132.

Hsu,H.H. (1983). Purification and partial characterization of ATP pyrophosphohydrolase from fetal bovine epiphyseal cartilage. J. Biol. Chem. *258*, 3463-3468.

Hsu,H.H. and Anderson,H.C. (1996). Evidence of the presence of a specific ATPase responsible for ATP-initiated calcification by matrix vesicles isolated from cartilage and bone. J. Biol. Chem. *271*, 26383-26388.

Huelsken,J. and Birchmeier,W. (2001). New aspects of Wnt signaling pathways in higher vertebrates. Curr. Opin. Genet. Dev. *11*, 547-553.

Hunter,G.K. and Goldberg,H.A. (1994). Modulation of crystal formation by bone phosphoproteins: role of glutamic acid-rich sequences in the nucleation of hydroxyapatite by bone sialoprotein. Biochemical Journal *302*, 175-179.

Hunter,G.K., Kyle,C.L., and Goldberg,H.A. (1994). Modulation of Crystal-Formation by Bone Phosphoproteins - Structural Specificity of the Osteopontin-Mediated Inhibition of Hydroxyapatite Formation. Biochemical Journal *300*, 723-728.

Hurley,H.M. and Florkiewicz,R.A. (1996), 'Fibroblast growth factor and vascular endothelial cell growth factor families', in Bilezikian,J.P., Raisz,L.G. and Rodan,G.A. (eds) *Principles of Bone Biology.* Academic Press, San Diego, 627–645.

Ihara,H., Denhardt,D.T., Furuya,K., Yamashita,T., Muguruma,Y., Tsuji,K., Hruska,K.A., Higashio,K., Enomoto,S., Nifuji,A., Rittling,S.R., and Noda,M. (2001). Parathyroid hormone-induced bone resorption does not occur in the absence of osteopontin. Journal of Biological Chemistry *276*, 13065-13071.

Inada,M., Yasui,T., Nomura,S., Miyake,S., Deguchi,K., Himeno,M., Sato,M., Yamagiwa,H., Kimura,T., Yasui,N., Ochi,T., Endo,N., Kitamura,Y., Kishimoto,T., and Komori,T. (1999). Maturational disturbance of chondrocytes in Cbfa1-deficient mice. Developmental Dynamics *214*, 279-290.

Irving,J.T. (1963). The sudanophil material at sites of calcification. Arch. Oral Biol. *38*, 735-745.

Ishikawa,Y. and Wuthier,R.E. (1992). Development of an in vitro mineralization model with growth plate chondrocytes that does not require beta-glycerophosphate. Bone Miner. *17*, 152-157.

Johnson,K., Moffa,A., Chen,Y., Pritzker,K., Goding,J., and Terkeltaub,R. (1999). Matrix vesicle plasma cell membrane glycoprotein-1 regulates mineralization by murine osteoblastic MC3T3 cells. J. Bone Miner. Res. *14*, 883-892.

Johnson,K., Hashimoto,S., Lotz,M., Pritzker,K., Goding,J., and Terkeltaub,R. (2001). Up-regulated expression of the phosphodiesterase nucleotide pyrophosphatase family member PC-1 is a marker and pathogenic factor for knee meniscal cartilage matrix calcification. Arthritis Rheum. *44*, 1071-1081.

Johnson,K., Polewski,M., van Etten,D., and Terkeltaub,R. (2005). Chondrogenesis mediated by PPi depletion promotes spontaneous aortic calcification in NPP1-/- mice. Arterioscler. Thromb. Vasc. Biol. *25*, 686-691.

Kagoshima,H., Shigesada,K., Satake,M., Ito,Y., Miyoshi,H., Ohki,M., Pepling,M., and Gergen,P. (1993). The Runt Domain Identifies A New Family of Heteromeric Transcriptional Regulators. Trends in Genetics *9*, 338-341.

Kanehisa,M., Goto,S., Kawashima,S., and Nakaya,A. (2002). The KEGG databases at GenomeNet. Nucleic Acids Research *30*, 42-46.

Kaplan,S.B., Kemp,S.S., and Oh,K.S. (1991). Radiographic manifestations of congenital anomalies of the skull. Radiol. Clin. North Am. *29*, 195-218.

Karsenty,G. (2003). The complexities of skeletal biology. Nature *423*, 316-318.

Kato,Y., Boskey,A., Spevak,L., Dallas,M., Hori,M., and Bonewald,L.F. (2001). Establishment of an osteoid preosteocyte-like cell MLO-A5 that spontaneously mineralizes in culture. J. Bone Miner. Res. *16*, 1622-1633.

Kay,M.I., Young,R.A., and Posner,A.S. (1964). Crystal Structure of Hydroxyapatite. Nature *204*, 1050-1052.

Kelley,L.A., MacCallum,R.M., and Sternberg,M.J. (2000). Enhanced genome annotation using structural profiles in the program 3D-PSSM. J. Mol. Biol. *299*, 499-520.

Kihira,K. (1988). [AG1749: a study of its inhibition of gastric pH after morning or evening dosage]. Nippon Shokakibyo Gakkai Zasshi *85*, 2693.

Kim,H.Y., Heo,Y.S., Kim,J.H., Park,M.H., Moon,J., Kim,E., Kwon,D., Yoon,J., Shin,D., Jeong,E.J., Park,S.Y., Lee,T.G., Jeon,Y.H., Ro,S., Cho,J.M., and Hwang,K.Y. (2002). Molecular basis for the local conformational rearrangement of human phosphoserine phosphatase. J. Biol. Chem. *277*, 46651-46658.

Kingsley,D.M., Bland,A.E., Grubber,J.M., Marker,P.C., Russell,L.B., Copeland,N.G., and Jenkins,N.A. (1992). The mouse short ear skeletal morphogenesis locus is associated with defects in a bone morphogenetic member of the TGF beta superfamily. Cell *71*, 399-410.

Kirsch,T., Ishikawa,Y., Mwale,F., and Wuthier,R.E. (1994). Roles of the nucleational core complex and collagens (types II and X) in calcification of growth plate cartilage matrix vesicles. J. Biol. Chem. *269*, 20103-20109.

Kirsch,T., Wang,W., and Pfander,D. (2003). Functional differences between growth plate apoptotic bodies and matrix vesicles. J. Bone Miner. Res. *18*, 1872-1881.

Kivirikko,K.I. and Myllyla,R. (1987). Recent developments in posttranslational modification: intracellular processing. Methods Enzymol. *144*, 96-114.

Klein,P.J., Schmidt,C.M., Wiesenauer,C.A., Choi,J.N., Gage,E.A., Yip-Schneider,M.T., Wiebke,E.A., Wang,Y., Omer,C., and Sebolt-Leopold,J.S. (2006). The effects of a novel MEK inhibitor PD184161 on MEK-ERK signaling and growth in human liver cancer. Neoplasia. *8*, 1-8.

Klutts,S., Pastuszak,I., Edavana,V.K., Thampi,P., Pan,Y.T., Abraham,E.C., Carroll,J.D., and Elbein,A.D. (2003). Purification, cloning, expression, and properties of mycobacterial trehalose-phosphate phosphatase. Journal of Biological Chemistry *278*, 2093-2100.

Komori,T., Yagi,H., Nomura,S., Yamaguchi,A., Sasaki,K., Deguchi,K., Shimizu,Y., Bronson,R.T., Gao,Y.H., Inada,M., Sato,M., Okamoto,R., Kitamura,Y., Yoshiki,S., and Kishimoto,T. (1997). Targeted disruption of Cbfa1 results in a complete lack of bone formation owing to maturational arrest of osteoblasts. Cell *89*, 755-764.

Komori,T. (2006). Regulation of osteoblast differentiation by transcription factors. J. Cell Biochem.

Kronenberg,H.M. (2003). Developmental regulation of the growth plate. Nature *423*, 332-336.

Kulkarni,N.H., Onyia,J.E., Zeng,Q., Tian,X., Liu,M., Halladay,D.L., Frolik,C.A., Engler,T., Wei,T., Kriauciunas,A., Martin,T.J., Sato,M., Bryant,H.U., and Ma,Y.L. (2006). Orally bioavailable GSK-3alpha/beta dual inhibitor increases markers of cellular differentiation in vitro and bone mass in vivo. J. Bone Miner. Res. *21*, 910-920.

Kvam,B.J., Pollesello,P., Vittur,F., and Paoletti,S. (1992). 31P NMR studies of resting zone cartilage from growth plate. Magn Reson. Med. *25*, 355-361.

Laemmli,U.K. (1970). Cleavage of structural proteins during the assembly of the head of bacteriophage T4. Nature *227*, 680-685.

Lanske,B., Karaplis,A.C., Lee,K., Luz,A., Vortkamp,A., Pirro,A., Karperien,M., Defize,L.H.K., Ho,C., Mulligan,R.C., AbouSamra,A.B., Juppner,H., Segre,G.V., and Kronenberg,H.M. (1996). PTH/PTHrP receptor in early development and Indian hedgehog-regulated bone growth. Science *273*, 663-666.

Lanzafame,A. and Christopoulos,A. (2004). Investigation of the interaction of a putative allosteric modulator, N-(2,3-diphenyl-1,2,4-thiadiazole-5-(2H)-ylidene) methanamine hydrobromide (SCH-202676), with M1 muscarinic acetylcholine receptors. Journal of Pharmacology and Experimental Therapeutics *308*, 830-837.

Laskowski,R.A., Macarthur,M.W., Moss,D.S., and Thornton,J.M. (1993). Procheck - A Program to Check the Stereochemical Quality of Protein Structures. Journal of Applied Crystallography *26*, 283-291.

Leboy,P.S., Vaias,L., Uschmann,B., Golub,E., Adams,S.L., and Pacifici,M. (1989). Ascorbic acid induces alkaline phosphatase, type X collagen, and calcium deposition in cultured chick chondrocytes. J. Biol. Chem. *264*, 17281-17286.

Lefebvre,V., Huang,W.D., Harley,V.R., Goodfellow,P.N., and deCrombrugghe,B. (1997). SOX9 is a potent activator of the chondrocyte-specific enhancer of the pro alpha 1(II) collagen gene. Molecular and Cellular Biology *17*, 2336-2346.

Leneva,I.A., Roberts,N., Govorkova,E.A., Goloubeva,O.G., and Webster,R.G. (2000). The neuraminidase inhibitor GS4104 (oseltamivir phosphate) is efficacious against A/Hong Kong/156/97 (H5N1) and A/Hong Kong/1074/99 (H9N2) influenza viruses. Antiviral Res. *48*, 101-115.

Lindqvist,Y., Branden,C.I., Mathews,F.S., and Lederer,F. (1991). Spinach glycolate oxidase and yeast flavocytochrome b2 are structurally homologous and evolutionarily related enzymes with distinctly different function and flavin mononucleotide binding. J. Biol. Chem. *266*, 3198-3207.

Lorentzon,P., Jackson,R., Wallmark,B., and Sachs,G. (1987). Inhibition of (H+ + K+)-ATPase by omeprazole in isolated gastric vesicles requires proton transport. Biochim. Biophys. Acta *897*, 41-51.

Luo,G., Ducy,P., Mckee,M.D., Pinero,G.J., Loyer,E., Behringer,R.R., and Karsenty,G. (1997). Spontaneous calcification of arteries and cartilage in mice lacking matrix GLA protein. Nature *386*, 78-81.

Majeska,R.J. and Wuthier,R.E. (1975). Studies on matrix vesicles isolated from chick epiphyseal cartilage. Association of pyrophosphatase and ATPase activities with alkaline phosphatase. Biochim. Biophys. Acta *391*, 51-60.

Malone,J.D., Teitelbaum,S.L., Griffin,G.L., Senior,R.M., and Kahn,A.J. (1982). Recruitment of Osteoclast Precursors by Purified Bone-Matrix Constituents. Journal of Cell Biology *92*, 227-230.

Martin,B., Pallen,C.J., Wang,J.H., and Graves,D.J. (1985). Use of fluorinated tyrosine phosphates to probe the substrate specificity of the low molecular weight phosphatase activity of calcineurin. J. Biol. Chem. *260*, 14932-14937.

Maruyama,K., Clarke,D.M., Fujii,J., Inesi,G., Loo,T.W., and MacLennan,D.H. (1989). Functional consequences of alterations to amino acids located in the catalytic

center (isoleucine 348 to threonine 357) and nucleotide-binding domain of the Ca2+-ATPase of sarcoplasmic reticulum. J. Biol. Chem. *264*, 13038-13042.

Masuda,I., Iyama,K.I., Halligan,B.D., Barbieri,J.T., Haas,A.L., McCarty,D.J., and Ryan,L.M. (2001). Variations in site and levels of expression of chondrocyte nucleotide pyrophosphohydrolase with aging. J. Bone Miner. Res. *16*, 868-875.

Matsuzawa,T. and Anderson,H.C. (1971). Phosphatases of epiphyseal cartilage studied by electron microscopic cytochemical methods. J. Histochem. Cytochem. *19*, 801-808.

Mazzali,M., Kipari,T., Ophascharoensuk,V., Wesson,J.A., Johnson,R., and Hughes,J. (2002). Osteopontin--a molecule for all seasons. QJM. *95*, 3-13.

Mccarthy,T.L., Centrella,M., and Canalis,E. (1989). Regulatory Effects of Insulin-Like Growth Factor-I and Factor-Ii on Bone-Collagen Synthesis in Rat Calvarial Cultures. Endocrinology *124*, 301-309.

McDonald,D.F., Schofield,B.H., Geffert,M.A., and Coleman,R.A. (1980). A comparative study of new substrates for the histochemical demonstration of acid phosphomonoesterase activity in tissues which secrete acid phosphatase. J. Histochem. Cytochem. *28*, 316-322.

McLean,F.M., Keller,P.J., Genge,B.R., Walters,S.A., and Wuthier,R.E. (1987). Disposition of preformed mineral in matrix vesicles. Internal localization and association with alkaline phosphatase. J. Biol. Chem. *262*, 10481-10488.

McQuillan,D.J., Richardson,M.D., and Bateman,J.F. (1995). Matrix deposition by a calcifying human osteogenic sarcoma cell line (SAOS-2). Bone *16*, 415-426.

Meyer,J.L. (1984). Can biological calcification occur in the presence of pyrophosphate? Arch. Biochem. Biophys. *231*, 1-8.

Miao,D. and Scutt,A. (2002). Histochemical localization of alkaline phosphatase activity in decalcified bone and cartilage. J. Histochem. Cytochem. *50*, 333-340.

Miyazono,K., Kusanagi,K., and Inoue,H. (2001). Divergence and convergence of TGF-beta/BMP signaling. Journal of Cellular Physiology *187*, 265-276.

Montessuit,C., Caverzasio,J., and Bonjour,J.P. (1991). Characterization of a Pi transport system in cartilage matrix vesicles. Potential role in the calcification process. J. Biol. Chem. *266*, 17791-17797.

Morais,M.C., Zhang,W., Baker,A.S., Zhang,G., Dunaway-Mariano,D., and Allen,K.N. (2000). The crystal structure of bacillus cereus phosphonoacetaldehyde hydrolase: insight into catalysis of phosphorus bond cleavage and catalytic diversification within the HAD enzyme superfamily. Biochemistry *39*, 10385-10396.

Mornet,E., Stura,E., Lia-Baldini,A.S., Stigbrand,T., Menez,A., and Le Du,M.H. (2001) Structural evidence for a functional role of human tissue nonspecific alkaline phosphatase in bone mineralization. J Biol Chem. *276*, 31171-31178.

Morris,D.C., Masuhara,K., Takaoka,K., Ono,K., and Anderson,H.C. (1992). Immunolocalization of alkaline phosphatase in osteoblasts and matrix vesicles of human fetal bone. Bone Miner. *19*, 287-298.

Moss,D.W., Eaton,R.H., Smith,J.K., and Whitby,L.G. (1967). Association of inorganic-pyrophosphatase activity with human alkaline-phosphatase preparations. Biochem. J. *102*, 53-57.

Mostov,K. and Werb,Z. (1997). Cell biology - Journey across the osteoclast. Science *276*, 219-220.

Mulari,M.T.K., Zhao,H., Lakkakorpi,P.T., and Vaananen,H.K. (2003). Osteoclast ruffled border has distinct subdomains for secretion and degraded matrix uptake. Traffic *4*, 113-125.

Muller,K., Schulz,J., and Oemus,R. (1989). [Phosphoethanolamine--a substrate of alkaline phosphatase isolated from rat calvaria.]. Biomed. Biochim. Acta *48*, 495-504.

Munroe,P.B., Olgunturk,R.O., Fryns,J.P., Van Maldergem,L., Ziereisen,F., Yuksel,B., Gardiner,R.M., and Chung,E. (1999). Mutations in the gene encoding the human matrix Gla protein cause Keutel syndrome. Nat. Genet. *21*, 142-144.

Nakano,Y., Kawamoto,T., Oda,K., and Takano,Y. (2003). Alkaline and acid phosphatases in bone cells serve as phosphohydrolases at physiological pH in vivo: a histochemical implication. Connect. Tissue Res. *44 Suppl 1*, 219-222.

Nakashima,K., Zhou,X., Kunkel,G., Zhang,Z., Deng,J.M., Behringer,R.R., and de Crombrugghe,B. (2002). The novel zinc finger-containing transcription factor osterix is required for osteoblast differentiation and bone formation. Cell *108*, 17-29.

Narasaraju,T.S.B. (1972). Preparation and Some Physicochemical Aspects of Solid-Solutions of Hydroxylapatite and Fluorapatite. Indian Journal of Chemistry *10*, 309.

Narasaraju,T.S.B. and Phebe,D.E. (1996). Some physico-chemical aspects of hydroxylapatite. Journal of Materials Science *31*, 1-21.

Narisawa,S., Frohlander,N., and Millan,J.L. (1997). Inactivation of two mouse alkaline phosphatase genes and establishment of a model of infantile hypophosphatasia. Developmental Dynamics *208*, 432-446.

Narita,M., Goji,J., Nakamura,H., and Sano,K. (1994). Molecular cloning, expression, and localization of a brain-specific phosphodiesterase I/nucleotide pyrophosphatase (PD-I alpha) from rat brain. J. Biol. Chem. *269*, 28235-28242.

Nesbitt,S., Nesbit,A., Helfrich,M., and Horton,M. (1993). Biochemical-Characterization of Human Osteoclast Integrins - Osteoclasts Express Alpha-V-Beta-3, Alpha-2-Beta-1, and Alpha-V-Beta-1 Integrins. Journal of Biological Chemistry *268*, 16737-16745.

Newman,B., Gigout,L.I., Sudre,L., Grant,M.E., and Wallis,G.A. (2001). Coordinated expression of matrix Gla protein is required during endochondral ossification for chondrocyte survival. J. Cell Biol. *154*, 659-666.

Niida,S., Kaku,M., Amano,H., Yoshida,H., Kataoka,H., Nishikawa,S., Tanne,K., Maeda,N., Nishikawa,S.I., and Kodama,H. (1999). Vascular endothelial growth factor can substitute for macrophage colony-stimulating factor in the support of osteoclastic bone resorption. Journal of Experimental Medicine *190*, 293-298.

Noti,J.D. (2000). Adherence to osteopontin via alphavbeta3 suppresses phorbol ester-mediated apoptosis in MCF-7 breast cancer cells that overexpress protein kinase C-alpha. Int. J. Oncol. *17*, 1237-1243.

Nurnberg,P., Thiele,H., Chandler,D., Hohne,W., Cunningham,M.L., Ritter,H., Leschik,G., Uhlmann,K., Mischung,C., Harrop,K., Goldblatt,J., Borochowitz,Z.U., Kotzot,D., Westermann,F., Mundlos,S., Braun,H.S., Laing,N., and Tinschert,S. (2001). Heterozygous mutations in ANKH, the human ortholog of the mouse progressive ankylosis gene, result in craniometaphyseal dysplasia. Nat. Genet. *28*, 37-41.

Oda,Y., Kuo,M.D., Huang,S.S., and Huang,J.S. (1991). The plasma cell membrane glycoprotein, PC-1, is a threonine-specific protein kinase stimulated by acidic fibroblast growth factor. J. Biol. Chem. *266*, 16791-16795.

Ogata,M., Takada,T., Mori,Y., Oh-hora,M., Uchida,Y., Kosugi,A., Miyake,K., and Hamaoka,T. (1999). Effects of overexpression of PTP36, a putative protein tyrosine phosphatase, on cell adhesion, cell growth, and cytoskeletons in HeLa cells. J. Biol. Chem. *274*, 12905-12909.

Okawa,A., Nakamura,I., Goto,S., Moriya,H., Nakamura,Y., and Ikegawa,S. (1998). Mutation in Npps in a mouse model of ossification of the posterior longitudinal ligament of the spine. Nat. Genet. *19*, 271-273.

Orengo,C.A., Flores,T.P., Jones,D.T., Taylor,W.R., and Thornton,J.M. (1993). Recurring structural motifs in proteins with different functions. Curr. Biol. *3*, 131-139.

Palmer,G., Bonjour,J.P., and Caverzasio,J. (1997). Expression of a newly identified phosphate transporter/retrovirus receptor in human SaOS-2 osteoblast-like cells and its regulation by insulin-like growth factor I. Endocrinology *138*, 5202-5209.

Paz,M.F., Fraga,M.F., Avila,S., Guo,M., Pollan,M., Herman,J.G., and Esteller,M. (2003). A systematic profile of DNA methylation in human cancer cell lines. Cancer Res. *63*, 1114-1121.

Peck,W.A., Birge,S.J., Jr., and Brandt,J. (1967). Collagen synthesis by isolated bone cells: stimulation by ascorbic acid in vitro. Biochim. Biophys. Acta *142*, 512-525.

Pelech,S.L. and Vance,D.E. (1984). Trifluoperazine and chlorpromazine inhibit phosphatidylcholine biosynthesis and CTP:phosphocholine cytidylyltransferase in HeLa cells. Biochim. Biophys. Acta *795*, 441-446.

Pizette,S. and Niswander,L. (2000). BMPs are required at two steps of limb chondrogenesis: formation of prechondrogenic condensations and their differentiation into chondrocytes. Dev. Biol. *219*, 237-249.

Posner,A.S., Perloff,A., and Diorio,A.F. (1958). Refinement of the Hydroxyapatite Structure. Acta Crystallographica *11*, 308-309.

Price,P.A., Urist,M.R., and Otawara,Y. (1983). Matrix Gla protein, a new gamma-carboxyglutamic acid-containing protein which is associated with the organic matrix of bone. Biochem. Biophys. Res. Commun. *117*, 765-771.

Price,P.A. and Williamson,M.K. (1985). Primary structure of bovine matrix Gla protein, a new vitamin K-dependent bone protein. J. Biol. Chem. *260*, 14971-14975.

Prince,C.W. (1989). Secondary Structure Predictions for Rat Osteopontin. Connective Tissue Research *21*, 345-350.

Proudfoot,D., Skepper,J.N., Hegyi,L., Bennett,M.R., Shanahan,C.M., and Weissberg,P.L. (2000). Apoptosis regulates human vascular calcification in vitro: evidence for initiation of vascular calcification by apoptotic bodies. Circ. Res. *87*, 1055-1062.

Rarey,M., Kramer,B., Lengauer,T., and Klebe,G. (1996). A fast flexible docking method using an incremental construction algorithm. J. Mol. Biol. *261*, 470-489.

Rasmussen,K. (1968). Phosphorylethanolamine and hypophosphatasia. Dan. Med. Bull. *15*, Suppl-112.

Register,T.C., Warner,G.P., and Wuthier,R.E. (1984). Effect of L- and D-tetramisole on 32Pi and 45Ca uptake and mineralization by matrix vesicle-enriched fractions from chicken epiphyseal cartilage. J. Biol. Chem. *259*, 922-928.

Register,T.C., McLean,F.M., Low,M.G., and Wuthier,R.E. (1986). Roles of alkaline phosphatase and labile internal mineral in matrix vesicle-mediated calcification. Effect of selective release of membrane-bound alkaline phosphatase and treatment with isosmotic pH 6 buffer. J. Biol. Chem. *261*, 9354-9360.

Ridder,I.S. and Dijkstra,B.W. (1999). Identification of the Mg2+-binding site in the P-type ATPase and phosphatase members of the HAD (haloacid dehalogenase) superfamily by structural similarity to the response regulator protein CheY. Biochemical Journal *339*, 223-226.

Riel,M.A., Kyle,D.E., Bhattacharjee,A.K., and Milhous,W.K. (2002). Efficacy of proton pump inhibitor drugs against Plasmodium falciparum in vitro and their probable pharmacophores. Antimicrob. Agents Chemother. *46*, 2627-2632.

Roach,H.I. (1999). Association of matrix acid and alkaline phosphatases with mineralization of cartilage and endochondral bone. Histochem. J. *31*, 53-61.

Robison,R. (1923). The Possible Significance of Hexosephosphoric Esters in Ossification. Biochem. J. *17*, 286-293.

Rollo,E.E. and Denhardt,D.T. (1996). Differential effects of osteopontin on the cytotoxic activity of macrophages from young and old mice. Immunology *88*, 642-647.

Romberg,R.W., Werness,P.G., Riggs,B.L., and Mann,K.G. (1986). Inhibition of Hydroxyapatite Crystal-Growth by Bone-Specific and Other Calcium-Binding Proteins. Biochemistry *25*, 1176-1180.

Sakai,T., Sugiyama,T., Banno,Y., Kato,Y., and Nozawa,Y. (2004). Involvement of phosphatidylcholine hydrolysis by phospholipase C in prostaglandin F2alpha-induced 1,2-diacylglycerol formation in osteoblast-like MC3T3-E1 cells. J. Bone Miner. Metab *22*, 198-206.

Sali,A. and Blundell,T.L. (1993). Comparative protein modelling by satisfaction of spatial restraints. J. Mol. Biol. *234*, 779-815.

Sali,A., Favaloro,J.M.,Terkeltaub, R. and Goding,J.W. (2000), 'Germline deletion of the nucleoside triphosphate pyrophosphohydrolase (NTPPPH) plasma cell membrane glycoprotein (PC-1) produces abnormal calcification of periarticular tissues', in Vanduffel,L. and Lemmens,R. (eds.) *Ecto-ATPases and Related Ectonucleotidases.*, Shaker Publishing B.V., Maastricht, 267–280.

Sambrook,P., Kelly,P., and Eisman,J. (1993). Bone mass and ageing. Baillieres Clin. Rheumatol. *7*, 445-457.

Sampson,H.W. (1988). Spondyloarthropathy in Progressive Ankylosis (Ank Ank) Mice - Morphological Features. Spine *13*, 645-649.

Sauer,G.R. and Wuthier,R.E. (1988). Fourier transform infrared characterization of mineral phases formed during induction of mineralization by collagenase-released matrix vesicles in vitro. J. Biol. Chem. *263*, 13718-13724.

Schubert,S., Grunweller,A., Erdmann,V.A., and Kurreck,J. (2005). Local RNA target structure influences siRNA efficacy: systematic analysis of intentionally designed binding regions. J. Mol. Biol. *348*, 883-893.

Selengut,J.D. (2001). MDP-1 is a new and distinct member of the haloacid dehalogenase family of aspartate-dependent phosphohydrolases. Biochemistry *40*, 12704-12711.

Serra,R., Johnson,M., Filvaroff,E.H., LaBorde,J., Sheehan,D.M., Derynck,R., and Moses,H.L. (1997). Expression of a truncated, kinase-defective TGF-beta type II receptor in mouse skeletal tissue promotes terminal chondrocyte differentiation and osteoarthritis. Journal of Cell Biology *139*, 541-552.

Shibata,H., Fukushi,M., Igarashi,A., Misumi,Y., Ikehara,Y., Ohashi,Y., and Oda,K. (1998). Defective intracellular transport of tissue-nonspecific alkaline phosphatase with an Ala162-->Thr mutation associated with lethal hypophosphatasia. J. Biochem. (Tokyo) *123*, 968-977.

Shipley,P.G., Kramer,B., and Howland,J. (1926). Studies upon Calcification in vitro. Biochem. J. *20*, 379-387.

Shum,L. and Nuckolls,G. (2002). The life cycle of chondrocytes in the developing skeleton. Arthritis Res. *4*, 94-106.

Sijen,T., Fleenor,J., Simmer,F., Thijssen,K.L., Parrish,S., Timmons,L., Plasterk,R.H., and Fire,A. (2001). On the role of RNA amplification in dsRNA-triggered gene silencing. Cell *107*, 465-476.

Skedros,J.G., Mason,M.W., Nelson,M.C., and Bloebaum,R.D. (1996). Evidence of structural and material adaptation to specific strain features in cortical bone. Anat. Rec. *246*, 47-63.

Sohn,P., Crowley,M., Slattery,E., and Serra,R. (2002). Developmental and TGF-beta-mediated regulation of Ank mRNA expression in cartilage and bone. Osteoarthritis. Cartilage. *10*, 482-490.

Sok,D.E. (1999). Oxidative inactivation of brain alkaline phosphatase responsible for hydrolysis of phosphocholine. J. Neurochem. *72*, 355-362.

Sommerfeldt,D.W. and Rubin,C.T. (2001). Biology of bone and how it orchestrates the form and function of the skeleton. Eur. Spine J. *10 Suppl 2*, S86-S95.

Spindler,K.P., Shapiro,D.B., Gross,S.B., Brighton,C.T., and Clark,C.C. (1989). The effect of ascorbic acid on the metabolism of rat calvarial bone cells in vitro. J. Orthop. Res. *7*, 696-701.

Stenzel,I., Ziethe,K., Schurath,J., Hertel,S.C., Bosse,D., and Kock,M. (2003). Differential expression of the LePS2 phosphatase gene family in response to phosphate availability, pathogen infection and during development. Physiol Plant *118*, 138-146.

Stern,P.H. and Vance,D.E. (1987). Phosphatidylcholine metabolism in neonatal mouse calvaria. Biochem. J. *244*, 409-415.

Stewart,A.J., Schmid,R., Blindauer,C.A., Paisey,S.J., and Farquharson,C. (2003). Comparative modelling of human PHOSPHO1 reveals a new group of phosphatases within the haloacid dehalogenase superfamily. Protein Engineering *16*, 889-895.

Stewart,A.J., Roberts,S.J., Seawright,E., Davey,M.G., Fleming,R.H., and Farquharson,C. (2006). The presence of PHOSPHO1 in matrix vesicles and its developmental expression prior to skeletal mineralization. Bone. *39,* 1000-1007.

Stryer,L. (1995), 'Enzymes: basic concepts and kinetics', in Stryer, L. (ed) *Biochemistry*. W.H. Freeman and Company, New York, 181-207.

Sugimoto,T., Nakada,M., Fukase,M., Imai,Y., Kinoshita,Y., and Fujita,T. (1986). Effects of ascorbic acid on alkaline phosphatase activity and hormone responsiveness in the osteoblastic osteosarcoma cell line UMR-106. Calcif. Tissue Int. *39*, 171-174.

Sutherland,M.W. and Skerritt,J.H. (1986). Alkali Enhancement of Protein Staining on Nitrocellulose. Electrophoresis *7*, 401-406.

Tacchetti,C., Quarto,R., Campanile,G., and Cancedda,R. (1989). Calcification of in vitro developed hypertrophic cartilage. Dev. Biol. *132*, 442-447.

Tenenbaum,H.C. and Palangio,K. (1987). Phosphoethanolamine- and fructose 1,6-diphosphate-induced calcium uptake in bone formed in vitro. Bone Miner. *2*, 201-210.

Tenenbaum,H.C. (1987). Levamisole and Inorganic Pyrophosphate Inhibit Beta-Glycerophosphate Induced Mineralization of Bone Formed Invitro. Bone and Mineral *3*, 13-26.

Termine,J.D., Kleinman,H.K., Whitson,S.W., Conn,K.M., Mcgarvey,M.L., and Martin,G.R. (1981). Osteonectin, A Bone-Specific Protein Linking Mineral to Collagen. Cell *26*, 99-105.

Thirunavukkarasu,K., Mahajan,M., McLarren,K.W., Stifani,S., and Karsenty,G. (1998). Two domains unique to osteoblast-specific transcription factor Osf2/Cbfa1 contribute to its transactivation function and its inability to heterodimerize with Cbfbeta. Mol. Cell Biol. *18*, 4197-4208.

Tirrell,I.M., Wall,J.L., Daley,C.J., Denial,S.J., Tennis,F.G., Galens,K.G., and O'Handley,S.F. (2006). YZGD from Paenibacillus thiaminolyticus, a pyridoxal phosphatase of the HAD (haloacid dehalogenase) superfamily and a versatile member of the Nudix (nucleoside diphosphate x) hydrolase superfamily. Biochemical Journal *394*, 665-674.

Tootle,T.L., Silver,S.J., Davies,E.L., Newman,V., Latek,R.R., Mills,I.A., Selengut,J.D., Parlikar,B.E., and Rebay,I. (2003). The transcription factor Eyes absent is a protein tyrosine phosphatase. Nature *426*, 299-302.

Tsuji,M., Funahashi,S., Takigawa,M., Seiki,M., Fujii,K., and Yoshida,T. (1996). Expression of c-fos gene inhibits proteoglycan synthesis in transfected chondrocyte. FEBS Lett. *381*, 222-226.

Tu,Q., Valverde,P., and Chen,J. (2006). Osterix enhances proliferation and osteogenic potential of bone marrow stromal cells. Biochem. Biophys. Res. Commun. *341*, 1257-1265.

Urist,M.R. (1965). Bone: formation by autoinduction. Science *150*, 893-899.

Vaananen,H.K., Zhao,H., Mulari,M., and Halleen,J.M. (2000). The cell biology of osteoclast function. J. Cell Sci. *113 (Pt 3)*, 377-381.

Van Belle,H. (1976). Alkaline phosphatase. I. Kinetics and inhibition by levamisole of purified isoenzymes from humans. Clin. Chem. *22*, 972-976.

van Dijk,M.C., Muriana,F.J., de Widt,J., Hilkmann,H., and van Blitterswijk,W.J. (1997). Involvement of phosphatidylcholine-specific phospholipase C in platelet-derived growth factor-induced activation of the mitogen-activated protein kinase pathway in Rat-1 fibroblasts. J. Biol. Chem. *272*, 11011-11016.

Vilain,A., Vogt,N., Dutrillaux,B., and Malfoy,B. (1999). DNA methylation and chromosome instability in breast cancer cell lines. FEBS Lett. *460*, 231-234.

Vriend,G. (1990). WHAT IF: a molecular modeling and drug design program. J. Mol. Graph. *8*, 52-6, 29.

Walkey,C.J., Donohue,L.R., Bronson,R., Agellon,L.B., and Vance,D.E. (1997). Disruption of the murine gene encoding phosphatidylethanolamine N-methyltransferase. Proc. Natl. Acad. Sci. U. S. A *94*, 12880-12885.

Wang,W., Kim,R., Jancarik,J., Yokota,H., and Kim,S.H. (2001). Crystal structure of phosphoserine phosphatase from Methanococcus jannaschii, a hyperthermophile, at 1.8 A resolution. Structure. *9*, 65-71.

Wang,W., Xu,J.P., Du,B., and Kirsch,T. (2005). Role of the progressive ankylosis gene (ank) in cartilage mineralization. Molecular and Cellular Biology *25*, 312-323.

Wang,W.R., Cho,H.S., Kim,R., Jancarik,J., Yokota,H., Nguyen,H.H., Grigoriev,I.V., Wemmer,D.E., and Kim,S.H. (2002). Structural characterization of the reaction pathway in phosphoserine phosphatase: Crystallographic "snapshots" of intermediate states. Journal of Molecular Biology *319*, 421-431.

Waymire,K.G., Mahuren,J.D., Jaje,J.M., Guilarte,T.R., Coburn,S.P., and MacGregor,G.R. (1995). Mice lacking tissue non-specific alkaline phosphatase die from seizures due to defective metabolism of vitamin B-6. Nat. Genet. *11*, 45-51.

Webb,M.R. (1992). A continuous spectrophotometric assay for inorganic phosphate and for measuring phosphate release kinetics in biological systems. Proc. Natl. Acad. Sci. U. S. A *89*, 4884-4887.

Weiner,S., Traub,W., and Wagner,H.D. (1999). Lamellar bone: structure-function relations. J. Struct. Biol. *126*, 241-255.

Wennberg,C., Hessle,L., Lundberg,P., Mauro,S., Narisawa,S., Lerner,U.H., and Millan,J.L. (2000). Functional characterization of osteoblasts and osteoclasts from alkaline phosphatase knockout mice. J. Bone Miner. Res. *15*, 1879-1888.

Whyte,M.P. (1994). Hypophosphatasia and the role of alkaline phosphatase in skeletal mineralization. Endocr. Rev. *15*, 439-461.

Whyte,M.P. (1995), 'Hypophosphatasia', In Scriver,C.R., Beaudet,A.L., Sly,W.S., and Valle,D. (eds) *The metabolic and molecular bases of inherited disease, 7th ed.* McGraw-Hill, New York, 4095-4112.

Whyte,M.P., Landt,M., Ryan,L.M., Mulivor,R.A., Henthorn,P.S., Fedde,K.N., Mahuren,J.D., and Coburn,S.P. (1995). Alkaline phosphatase: placental and tissue-nonspecific isoenzymes hydrolyze phosphoethanolamine, inorganic pyrophosphate, and pyridoxal 5'-phosphate. Substrate accumulation in carriers of hypophosphatasia corrects during pregnancy. J. Clin. Invest *95*, 1440-1445.

Wolf,G. (1996). Function of the bone protein osteocalcin: definitive evidence. Nutr. Rev. *54*, 332-333.

Wu,J. and Woodard,R.W. (2003). Escherichia coli YrbI is 3-deoxy-D-manno-octulosonate 8-phosphate phosphatase. J. Biol. Chem. *278*, 18117-18123.

Wu,L.N.Y., Ishikawa,Y., Sauer,G.R., Genge,B.R., Mwale,F., Mishima,H., and Wuthier,R.E. (1995). Morphological and Biochemical-Characterization of Mineralizing Primary Cultures of Avian Growth-Plate Chondrocytes - Evidence for Cellular Processing of Ca2+ and Pi Prior to Matrix Mineralization. Journal of Cellular Biochemistry *57*, 218-237.

Wu,L.N.Y., Wuthier,M.G., Genge,B.R., and Wuthier,R.E. (1997). In situ levels of intracellular Ca2+ and pH in avian growth plate cartilage. Clinical Orthopaedics and Related Research 310-324.

Wu,L.N.Y., Genge,B.R., Kang,M.W., Arsenault,A.L., and Wuthier,R.E. (2002). Changes in phospholipid extractability and composition accompany mineralization of chicken growth plate cartilage matrix vesicles. Journal of Biological Chemistry *277*, 5126-5133.

Wuthier,R.E. (1968). Lipids of mineralizing epiphyseal tissues in the bovine fetus. J. Lipid Res. *9*, 68-78.

Wuthier,R.E. (1977). Electrolytes of Isolated Epiphyseal Chondrocytes, Matrix Vesicles, and Extracellular Fluid. Calcified Tissue Research *23*, 125-133.

Xia,H., Mao,Q., Paulson,H.L., and Davidson,B.L. (2002). siRNA-mediated gene silencing in vitro and in vivo. Nat. Biotechnol. *20,* 1006-1010.

Xuan,J.W., Hota,C., Shigeyama,Y., D'Errico,J.A., Somerman,M.J., and Chambers,A.F. (1995). Site-directed mutagenesis of the arginine-glycine-aspartic

acid sequence in osteopontin destroys cell adhesion and migration functions. J. Cell Biochem. *57*, 680-690.

Yang,L., Dan,H.C., Sun,M., Liu,Q., Sun,X.M., Feldman,R.I., Hamilton,A.D., Polokoff,M., Nicosia,S.V., Herlyn,M., Sebti,S.M., and Cheng,J.Q. (2004). Akt/protein kinase B signaling inhibitor-2, a selective small molecule inhibitor of Akt signaling with antitumor activity in cancer cells overexpressing Akt. Cancer Res. *64*, 4394-4399.

Yoshida,C.A., Yamamoto,H., Fujita,T., Furuichi,T., Ito,K., Inoue,K., Yamana,K., Zanma,A., Takada,K., Ito,Y., and Komori,T. (2004). Runx2 and Runx3 are essential for chondrocyte maturation, and Runx2 regulates limb growth through induction of Indian hedgehog. Genes Dev. *18*, 952-963.

Young,M.F., Kerr,J.M., Termine,J.D., Wewer,U.M., Wang,M.G., Mcbride,O.W., and Fisher,L.W. (1990). cDNA Cloning, Messenger-Rna Distribution and Heterogeneity, Chromosomal Location, and Rflp Analysis of Human Osteopontin (Opn). Genomics *7*, 491-502.

Zelinski,T.A. and Choy,P.C. (1982). Choline regulates phosphatidylethanolamine biosynthesis in isolated hamster heart. J. Biol. Chem. *257*, 13201-13204.

Zhang,J., Driscoll,T.A., Hannun,Y.A., and Obeid,L.M. (1998). Regulation of membrane release in apoptosis. Biochem. J. *334 (Pt 2)*, 479-485.

Zurutuza,L., Muller,F., Gibrat,J.F., Taillandier,A., Simon-Bouy,B., Serre,J.L., and Mornet,E. (1999). Correlations of genotype and phenotype in hypophosphatasia. Hum. Mol. Genet. *8*, 1039-1046.

Appendix 1: Vector Maps

pBAD-TOPO (Invitrogen) as used in chapters 3 and 4 for PHOSPHO1 and PHOSPHO2 expression

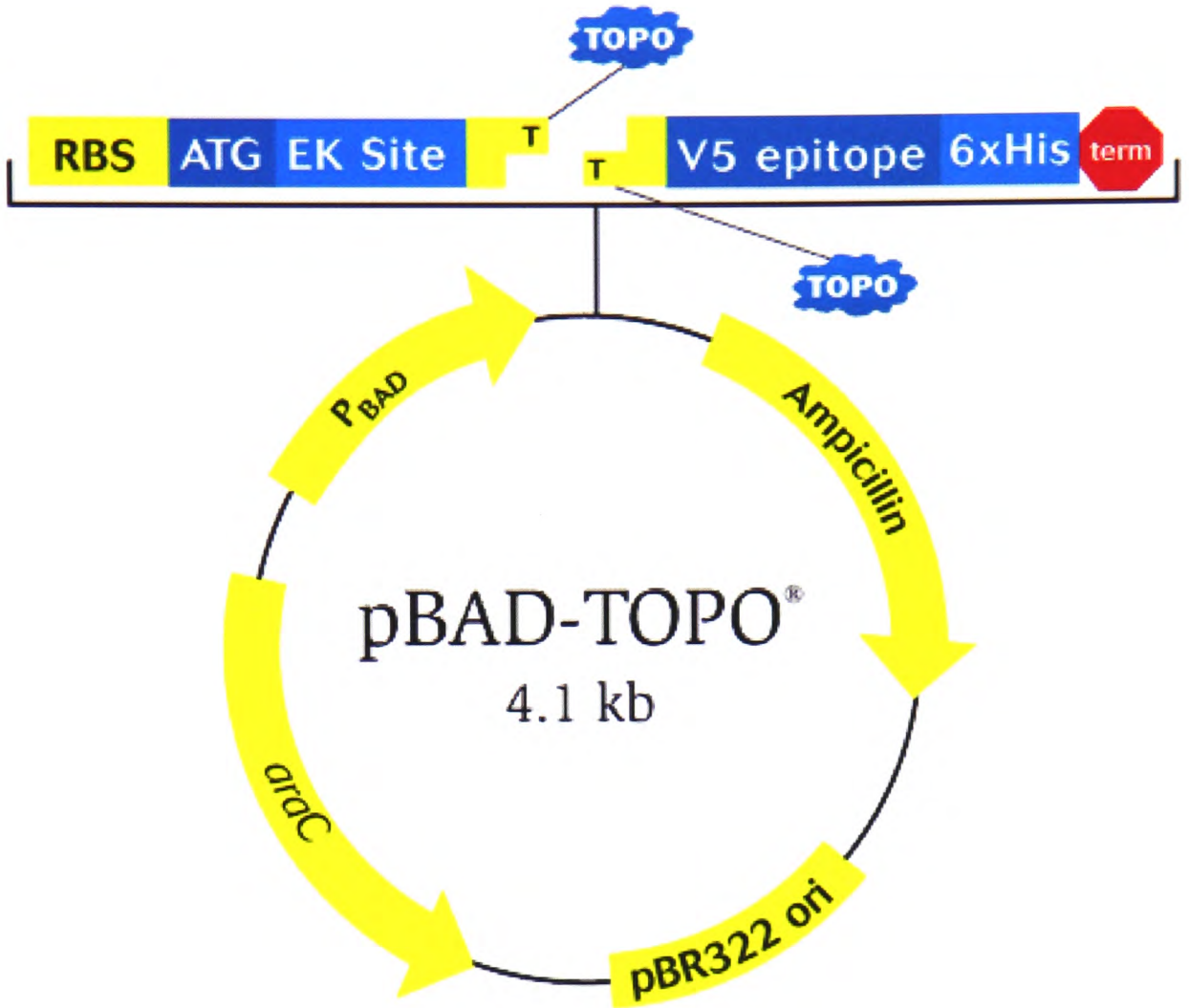

TOPO Represents covalently bound topoisomerase I

Vector Features
Arabinose promoter and regulatory elements: 4-276
pBAD Forward priming site: 208-227
Ribosome binding site: 328-331
Initiation ATG codon: 345-347
Enterokinase recognition site: 363-377
TOPO Cloning site: 387-388
V5 epitope: 402-443
Polyhistidine region: 453-470
pBAD Reverse priming site: 526-543
rrnB T1 and T2 transcription terminators: 576-733
Ampicillin resistance gene: 1013-1873
pBR322 origin: 2018-2691
AraC ORF: 4100-3222 (ORF on the opposite strand)

pGEM-T-Easy (Promega) as used in chapter 5 for cloning of PHOSPHO1 CDS

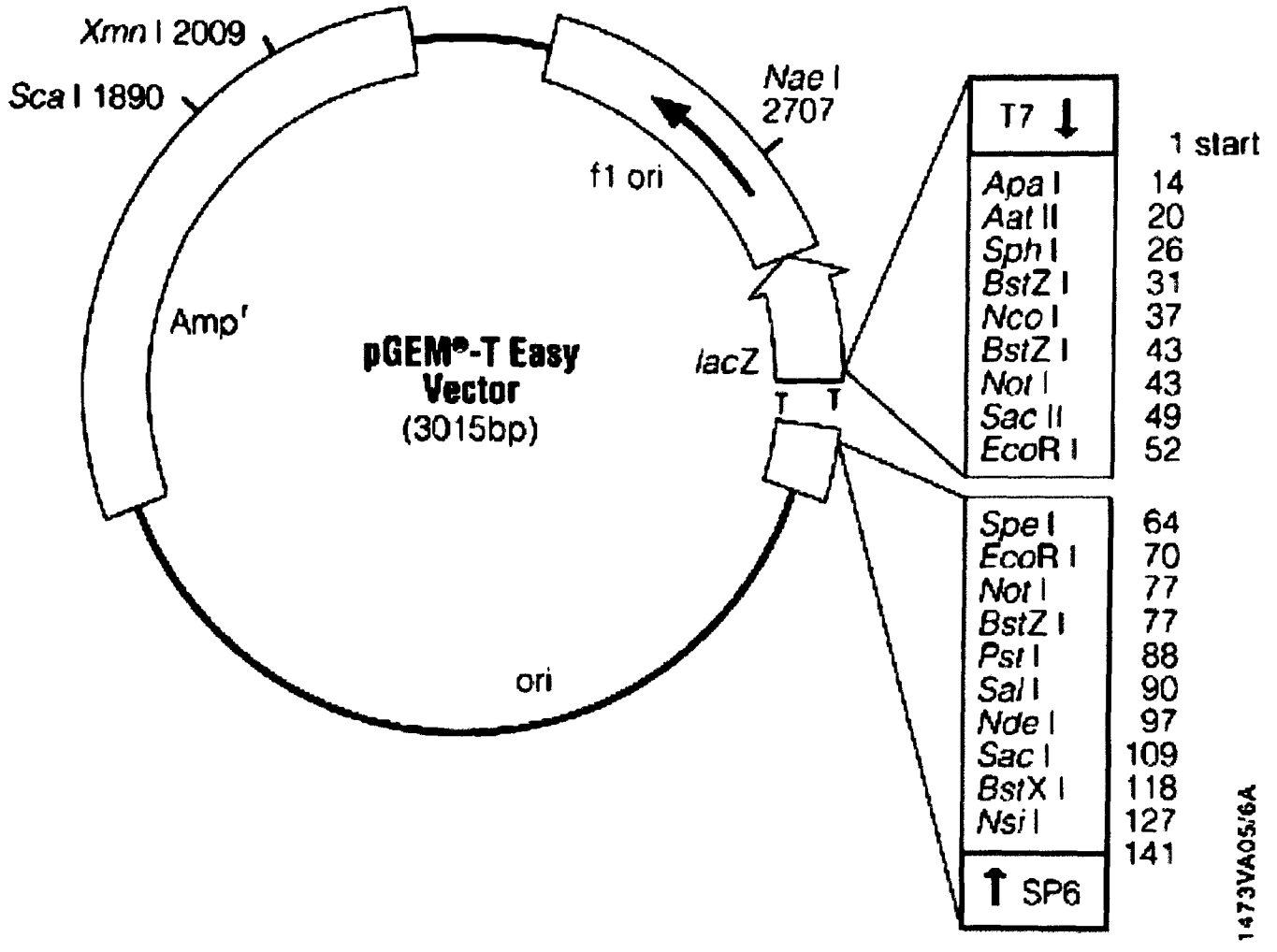

Vector Features

T7 RNA Polymerase transcription initiation site: 1
SP6 RNA Polymerase transcription initiation site: 141
T7 RNA Polymerase promoter (-17 to +3): 2999-3
SP6 RNA Polymerase promoter (-17 to +3): 139-158
Multiple cloning region: 10-128
LacZ start codon: 180
Lac operon sequences: 2996, 166-395
Lac operator: 200-216
Beta-lactamase coding region: 1337-2197
Phage f1 region: 2380-2835
Binding site of pUC/M13 Forward Sequencing Primer: 2956-2972
Binding site of pUC/M13 Reverse Sequencing Primer: 176-192

pSUPER-Neo-GFP (Oligoengine) as used in chapter 5 for shRNA mediated knockdown of gene expression

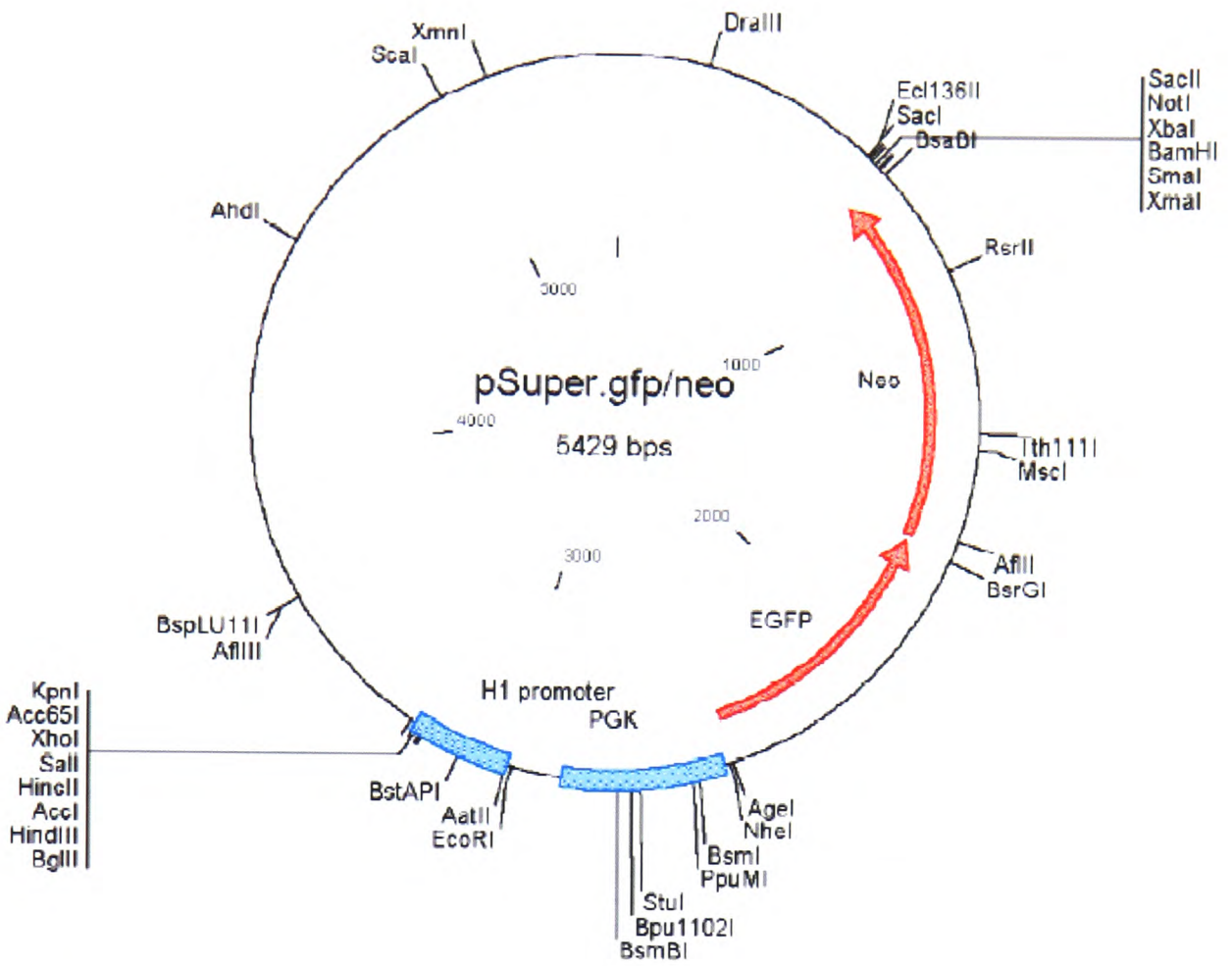

Key Sites

BglII: 3181
HindIII: 3187
EcoRI: 2960
SalI: 3202
XhoI: 3208

Vector Features

f1(+) origin: 135-441
PGK promoter: 2840-2442
Neo ORF: 1684-715
EGFP ORF: 2424-1691
H1 promoter: 2965-3213
Ampicillin resistance ORF: 5301-4444

T7 primer binding site (AATACGACTCACTATAG): 627-643
T3 primer binding site (CTTTAGTGAGGGTTAAT): 3242-3258
M13(-20) primer binding site (GTAAAACGACGGCCAGT): 600-616
M13 reverse primer binding site (CATGGTCATAGCTGTT): 3276-3291

pWGB10 as used in chapter 5 for Mammalian PHOSPHO1 expression

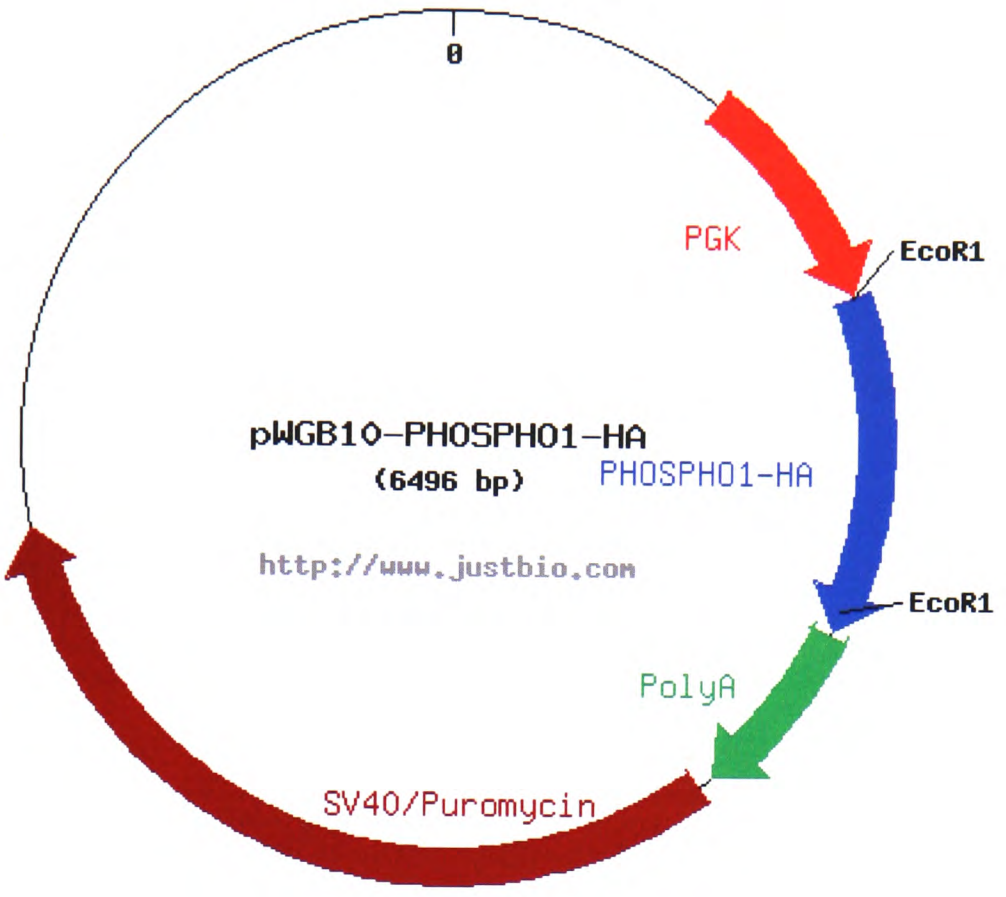

Vector Features

pWGB10 contains a phosphoglycerate kinase (PGK) promoter to drive PHOSPHO1 expression, simian virus 40 (SV40) small t intron/polyA and SV40/Puromycin to allow cell selection. The plasmid Backbone is composed of pBluescript.

Primer Pair	Primer Name	Primer Sequence	Target Exon	Splice Varient	Amplicon Size (bp)	Expressed
1	Exon1F3	CCCCCTTCCCCACTTCTTAC	1b	1	353	No
	Exon1-2-3aR3	CCGGGAGAGGCTGGTTAG	3a	2	120	Yes
2	Exon1F	TACCTCAGCTAGCCCCCTTC	1b	1	761	No
	Exon1-2-3bR	CGGAGATGAGAATCACCTCG	3b	2	638	Yes
				3	511	Yes
3	Exon1-2F	GGCTCAGACGCACATCATC	1a	1,2,3	361	Yes
	Exon1-2R	GGAGGCCAGAAACTGGAAA	2	4	202	Yes

Primer used for analysis of splice variants of PHOSPHO1. The amplicon size relates directly to the band sizes observed in figure 3.5.

Appendix 3: Nucleotide and Protein Sequences

Nucleotide Sequences

>Human PHOSPHO1 CDS

ATGGCCGCGCAGGGCGCGCCGCGCTTCCTCCTGACCTTCGACTTCGACGAGACTATCGTGGACGAAAA
CAGCGACGATTCGATCGTGCGCGCCGCGCCGGGCCAGCGGCTCCCGGAGAGCCTGCGAGCCACCTACC
GCGAGGGCTTCTACAACGAGTACATGCAGCGCGTCTTCAAGTACCTGGGCGAGCAGGGCGTGCGGCCG
CGGGACCTGAGCGCCATCTACGAAGCCATCCCTTTGTCGCCAGGCATGAGCGACCTGCTGCAGTTTGT
GGCAAAACAGGGCGCCTGCTTCGAGGTGATTCTCATCTCCGATGCCAACACCTTTGGCGTGGAGAGCT
CGCTGCGCGCCGCCGGCCACCACAGCCTGTTCCGCCGCATCCTCAGCAACCCGTCGGGGCCGGATGCG
CGGGGACTGCTGGCTCTGCGGCCGTTCCACACACACAGCTGCGCGCGCTGCCCCGCCAACATGTGCAA
GCACAAGGTGCTCAGCGACTACCTGCGCGAGCGGGCCCACGACGGCGTGCACTTCGAGCGCCTCTTCT
ACGTGGGCGACGGCGCCAACGACTTCTGCCCCATGGGGCTGCTGGCGGGCGGCGACGTGGCCTTCCCG
CGCCGCGGCTACCCCATGCACCGCCTCATTCAGGAGGCCCAGAAGGCCGAGCCCAGCTCGTTCCGCGC
CAGCGTGGTGCCCTGGGAAACGGCTGCAGATGTGCGCCTCCACCTGCAACAGGTGCTGAAGTCGTGCT
GA

>Human PHOSPHO2 CDS

ATGAAAATTTTGCTAGTTTTTGACTTTGACAATACAATCATAGATGACAATAGTGACACTTGGATTGT
ACAATGTGCTCCCAACAAAAAGCTTCCTATTGAACTACGTGATTCTTATCGAAAAGGATTTTGGACAG
AATTTATGGGCAGAGTCTTTAAGTATTTGGGAGATAAGGGTGTAAGAGAACATGAAATGAAAAGAGCA
GTGACATCATTGCCTTTCACTCCAGGGATGGTGGAACTCTTCAACTTTATAAGAAAGAATAAGGATAA
ATTTGACTGCATTATTATTTCAGATTCAAATTCGGTCTTCATAGATTGGGTTTTAGAAGCTGCCAGTT
TTCATGACATATTTGATAAAGTGTTTACAAATCCAGCAGCTTTTAATAGCAATGGTCATCTCACTGTT
GAAAATTATCATACTCATTCTTGCAATAGATGCCCAAAGAATCTTTGCAAAAAGGTAGTTTTGATAGA
ATTTGTAGATAAACAGTTACAACAGGGAGTGAATTATACACAAATTGTTTATATTGGTGATGGTGGAA
ATGATGTCTGTCCAGTCACCTTTTTTAAAGAATGATGATGTTGCCATGCCACGGAAAGGATATACCTTA
CAGAAAACTCTTTCCAGAATGTCTCAAAATCTTGAGCCTATGGAATATTCTGTTGTAGTTTGGTCCTC
AGGTGTTGATATAATTTCTCATTTACAATTTCTAATAAAGGATTAA

Nucleotide Sequences of PHOSPHO1 and PHOSPHO2. This CDS was used for recombinant protein production, producing prteins with the sequence defined on the next page

Protein Sequences

>Recombinant PHOSPHO1 sequence

MGSGSGDDDDKLALMAAQGAPRFLLTFDFDETIVDENSDDSIVRAAPGQRLPESLRATYREGFYNEYM
QRVFKYLGEQGVRPRDLSAIYEAIPLSPGMSDLLQFVAKQGACFEVILISDANTFGVESSLRAAGHHS
LFRRILSNPSGPDARGLLALRPFHTHSCARCPANMCKHKVLSDYLRERAHDGVHFERLFYVGDGANDF
CPMGLLAGGDVAFPRRGYPMHRLIQEAQKAEPSSFRASVVPWETAADVRLHLQQVLKSCKGELEGKPI
PNPLLGLDSTRTGHHHHHH

>Recombinant PHOSPHO2 sequence

MGSGSGDDDDKLALMKILLVFDFDNTIIDDNSDTWIVQCAPNKKLPIELRDSYRKGFWTEFMGRVFKY
LGDKGVREHEMKRAVTSLPFTPGMVELFNFIRKNKDKFDCIIISDSNSVFIDWVLEAASFHDIFDKVF
TNPAAFNSNGHLTVENYHTHSCNRCPKNLCKKVVLIEFVDKQLQQGVNYTQIVYIGDGGNDVCPVTFL
KNDDVAMPRKGYTLQKTLSRMSQNLEPMEYSVVVWSSGVDIISHLQFLIKDKGELEGKPIPNPLLGLD
STRTGHHHHHH

Amino acid sequence of recombinant PHOSPHO1 and PHOSPHO2. Red regions indicate vector associated amino acids, Blue region the V5 epitope and green region the six His tag.

Antibody	Supplier	Antigen	Specificity	Raised In	Application	Dillution
Anti-chick PHOSPHO1 (Purified)	Roslin	Reombinant chick PHOSPHO1 (E. coli)	Chick	Sheep	Western Blotting	2μg/ml
Anti-human PHOSPHO1 (Sera)	Roslin	Reombinant human PHOSPHO1 (E. coli)	Human	Rabbit	Western Blotting	1:500
Anti-human/mouse PHOSPHO1 (Sera)	Roslin	Synthetic peptide C-G-Y-P-M-H-R-L-I-Q-E-A-Q-K-A-E, conjugated to KLH.	Human/Mouse	Rabbit	Western Blotting	1:500
Anti-mouse PHOSPHO1 (Sera)	Professor Ikramuddin Aukhil, Florida	Recombinant mouse PHOSPHO1 (mammalian)	Human/Mouse	Rabbit	Western Blotting IHC	1:750 1:300
Anti B-Actin	Sigma	Synthetic peptide D-D-D-I-A-A-L-V-I-D-N-G-S-G-L, conjugated to KLH.	Wide range	Mouse	Western Blotting	1:2000
Anti-sheep IgG (HRP conjugate)	Sigma	Heavy Chain IgG1 and IgG2	Bovine/Goat/Sheep	Mouse	Western Blotting	1:2000
Anti-rabbit IgG (HRP conjugate)	DAKO	Rabbit IgG	Rabbit	Goat	IHC	1:100
Anti-mouse IgG (HRP conjugate)	Sigma	IgG Fab	Mouse	Goat	Western Blotting	1:2000

Properties of all antibodies used during this study. Roslin supplied antibodies have been produced as part of this project with the exception of the chick antibody which was produced by Dr. B Houston. Immunohistochemistry (IHC) carried out as outlined in section 2.7 and Western blotting as in 2.5.4

Appendix 5: Predicted Masses of Tryptic Fragments from Recombinant Human PHOSPHO1

Mass	Position	Peptide Sequence
2702.2741	194-219	LFYVGDGANDFCPMGLLAGG DVAFPR
2590.2195	23-44	FLLTFDFDETIVDENSDDSI VR
2578.3472	84-107	DLSAIYEAIPLSPGMSDLLQ FVAK
2456.2125	108-130	QGACFEVILISDANTFGVES SLR
2006.0916	265-283	GELEGKPIPNPLLGLDSTR
1678.8958	152-166	GLLALRPFHTHSCAR
1400.7168	241-253	ASVVPWETAADVR
1336.5626	61-70	EGFYNEYMQR
1174.6327	74-83	YLGEQGVRPR
1126.5851	141-151	ILSNPSGPDAR
1098.6088	44896	LALMAAQGAPR
1083.3895	39022	MGSGSGDDDDK
1067.5017	185-193	AHDGVHFER
999.4404	284-291	TGHHHHHH
995.5169	131-139	AAGHHSLFR
978.6094	254-261	LHLQQVLK
865.4778	176-182	VLSDYLR
829.4778	227-233	LIQEAQK
793.3839	234-240	AEPSSFR
766.3045	167-173	CPANMCK
760.3559	221-226	GYPMHR
714.4144	51-56	LPESLR

Appendix 6: Sequence of Mutagenesis Primers

Oligonucleotide Name	Sequence
PH1mut(D32N)F	GCTTCCTCCTGACCTTCAACTTCGACGAGACTATCG
PH1mut(D32N)R	CGATAGTCTCGTCGAAGTTGAAGGTCAGGAGGAAGC
PH1mut(D203S)F	CCTCTTCTACGTGGGCAGCGGCGCCAACGACTTCTGC
PH1mut(D203S)R	GCAGAAGTCGTTGGCGCCGCTGCCCACGTAGAAGAGG
PH1mut(D43N)F	CGTGGACGAAAACAGCAACGATTCGATCGTGCG
PH1mut(D43N)R	CGCACGATCGAATCGTTGCTGTTTTCGTCCACG
PH1mut(D123N)F	GGTGATTCTCATCTCCAATGCCAACACCTTTGGCG
PH1mut(D123N)R	CGCCAAAGGTGTTGGCATTGGAGATGAGAATCACC

The sequence of the reverse and forward primers used in the mutagenesis reactions to generate the 5 mutant proteins, D32N, D43N, D123N, D123N/D3N and D203N.

Appendix 7: Hits from Chemical Screen for PHOSPHO1 Inhibitors

LOPAC Library

Structure	Initial Inhibition	Reconfirmed Inhibition	Compound Name
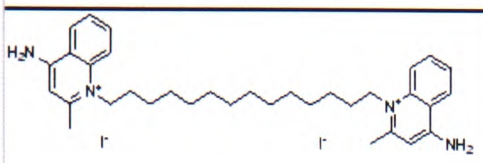	44	42	Dequalinium analog, C-14 linker
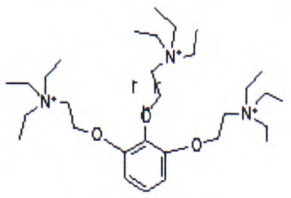	38	27	Gallamine triethiodide
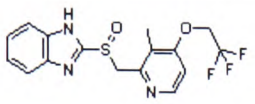	100	85	Lansoprazole
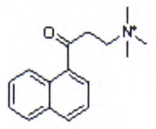	80	28	2-(alpha-Naphthoyl) ethyltrimethylammonium iodide
	98	97	Cisplatin
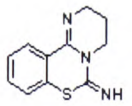	76	94	PD 404,182
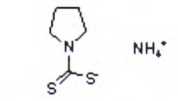	69	100	Ammonium pyrrolidinedithiocarbamate
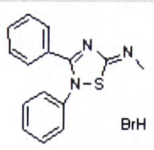	100	98	SCH-202676 hydrobromide
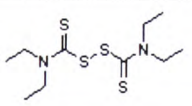	100	98	Tetraethylthiuram disulfide

Each hit was reconfirmed manually, (Green = Inhibition > 40%, Blue = Inhibition > 60%, Red = Inhibition > 80%)

Spectrum Library

Structure	Initial Inhibition	Reconfirmed Inhibition	Compound Name
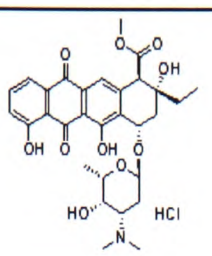	45	35	AKLAVINE HYDROCHLORIDE
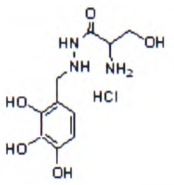	49	26	BENSERAZIDE HYDROCHLORIDE
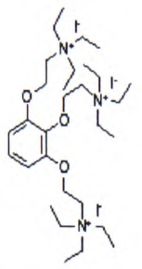	58	49	GALLAMINE
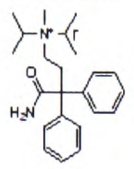	38	38	ISOPROPAMIDE IODIDE
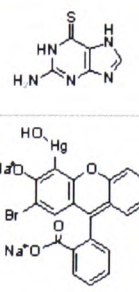	68	99	THIOGUANINE
	98	99	MERBROMIN
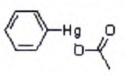	89	84	PHENYLMERCURIC ACETATE
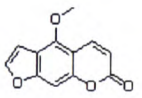	91	86	BERGAPTENE
	99	100	CISPLATIN
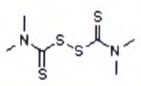	99	101	THIRAM
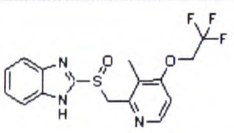	95	89	LANSOPRAZOLE

Each hit was reconfirmed manually, (Green = Inhibition > 40%, Blue = Inhibition > 60%, Red = Inhibition > 80%)

Spectrum Library (Continued)

Structure	Initial Inhibition	Reconfirmed Inhibition	Compound Name
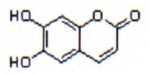	50	26	ESCULETIN
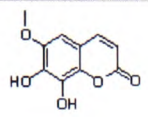	45	31	FRAXETIN
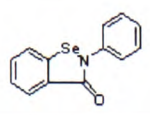	100	96	EBSELEN
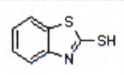	98	82	2-MERCAPTOBENZOTHIAZOLE
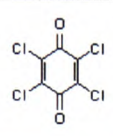	100	100	CHLORANIL

Each hit was reconfirmed manually, (Green = Inhibition > 40%, Blue = Inhibition > 60%, Red = Inhibition > 80%)

Human PHOSPHO1 exhibits high specific phosphoethanolamine and phosphocholine phosphatase activities

Scott J. ROBERTS*, Alan J. STEWART*[1], Peter J. SADLER† and Colin FARQUHARSON*

*Roslin Institute, Roslin, Midlothian EH25 9PS, U.K. and †School of Chemistry, The University of Edinburgh, Edinburgh EH9 3JJ, U.K.

Human PHOSPHO1 is a phosphatase enzyme for which expression is upregulated in mineralizing cells. This enzyme has been implicated in the generation of P_i for matrix mineralization, a process central to skeletal development. PHOSPHO1 is a member of the haloacid dehalogenase (HAD) superfamily of Mg^{2+}-dependent hydrolases. However, substrates for PHOSPHO1 are, as yet, unidentified and little is known about its activity. We show here that PHOSPHO1 exhibits high specific activities toward phosphoethanolamine (PEA) and phosphocholine (PCho). Optimal enzymic activity was observed at approx. pH 6.7. The enzyme shows a high specific Mg^{2+}-dependence, with apparent K_m values of 3.0 μM for PEA and 11.4 μM for PCho. These results provide a novel mechanism for the generation of P_i in mineralizing cells from PEA and PCho.

Key words: bone, haloacid dehalogenase (HAD) superfamily, mineralization, PHOSPHO1, phosphocholine (PCho), phosphoethanolamine (PEA).

INTRODUCTION

Matrix vesicle (MV)-mediated mineralization is a process central to the formation of bone, cartilage and teeth. Inside the MV, calcium phosphate accumulates until sufficient amounts are present for precipitation to occur. This is then converted to an intermediate, octa-calcium phosphate, crystals of which are transformed into the less soluble hydroxyapatite [1]. The MV membranes then breakdown and release preformed hydroxyapatite into the extracellular fluid. Calcium accumulation is controlled by Ca^{2+}-binding molecules, such as annexin I and phosphatidylserine [2,3]. P_i accumulation is associated with the action of alkaline and acid phosphatases [4,5]. The most abundant of these being tissue non-specific alkaline phosphatase (TNAP), an isoenzyme of alkaline phosphatase expressed in bone, liver and kidney [6]. In addition to its structural role, P_i has also been shown to regulate multiple genes during osteoblast differentiation, including the immediate response gene, *Nrf2* [7].

Deficiency of P_i in skeletal tissue (termed hypophosphatasia) is highly variable in its clinical expression, ranging from death *in utero* with an unmineralized skeleton to premature loss of teeth [8]. Hypophosphatasia is usually attributed to a reduction in TNAP activity. In newborn TNAP knockout mice, bone development and mineralization appear to be normal, although hypomineralization and other abnormalities of the skeleton and dentition have subsequently been observed [9–11]; failure occurs in the propagation of the mineral from the MV to the surrounding extracellular matrix [12,13]. Support for this concept comes from earlier work [14], which shows that the catalytic activity of TNAP decreases in direct proportion to the extent that MVs induce mineral formation. TNAP is known to hydrolyse inorganic PP_i [15], which is a potent inhibitor of hydroxyapatite crystal formation [16]. Abnormalities found in TNAP knockout mice are, however, not present in TNAP/PC-1 double-knockout mice [9]. PC-1 (now known as NPP1) encodes the enzyme, phosphodiesterase I in mineralizing cells and generates PP_i from nucleotide triphosphates [17]. Studies have also shown that TNAP can be removed from some preparations of MVs without reducing their potential to mineralize [18], whilst specific inhibitory studies on TNAP provide additional evidence that other phosphatases are present within mineralizing chondrocytes [19]. These observations suggest that the primary role of TNAP in skeletal development is to hydrolyse PP_i, preventing its inhibition of mineral crystal growth. It therefore appears that TNAP is not essential, at least for the initial events leading to MV-induced mineralization and implies that other phosphatases are involved.

Recently a novel phosphatase, PHOSPHO1, was identified which is expressed at levels approximately 100-fold higher in mineralizing chondrocytes than in non-skeletal tissues [20]. Immunolocalization studies have since shown that PHOSPHO1 is specifically localized to mineralizing regions of skeletal tissue [21]. The amino acid sequence of PHOSPHO1 contains three peptide motifs that are conserved within the haloacid dehalogenase (HAD) superfamily of Mg^{2+}-dependent hydrolases. Human PHOSPHO1 shares approximately 30 % homology at the amino acid level with the LePS2 family of phosphatases [22,23]. Molecular modelling of human PHOSPHO1, based upon the crystal structure of phosphoserine phosphatase from *Methanococcus jannaschii*, shows that all the characteristic features of the catalytic site, with regard to the HAD superfamily, are preserved [24]. Despite these structural data, little is known about the phosphatase activity of PHOSPHO1. We report here a biochemical characterization of the enzyme and establish its substrate specificity and conditions for optimal activity. The data allow us to propose a new pathway for the generation of P_i in mineralizing cells that is coupled to the degradation of phospholipids.

EXPERIMENTAL

Materials

SaOS-2 osteosarcoma cells were purchased from the European Collection of Cell Cultures (ECACC; CAMR Centre for Applied Microbiology & Research, Porton Down, Salisbury, Wilts, U.K.).

Abbreviations used: BAP, brain alkaline phosphatase; CDP-Cho, cytidine 5′-diphosphocholine; CDP-EA, cytidine 5′-diphosphoethanolamine; HAD, haloacid dehalogenase; MALDI–TOF-MS, matrix-assisted laser-desorption ionization–time-of-flight mass spectrometry; MESG, 2-amino-6-mercapto-7-methylpurine ribonucleoside; MV, matrix vesicle; Ni-NTA, nickel-nitrilotriacetate; PEA, phosphoethanolamine; PCho, phosphocholine; PNPase, purine nucleoside phosphorylase; TBS, Tris-buffered saline; TNAP, tissue non-specific alkaline phosphatase.

[1] To whom correspondence should be addressed (email alan.stewart@bbsrc.ac.uk).

© 2004 Biochemical Society

Reverse transcriptions were carried out using the Gibco Super-Script™ First-Strand Synthesis System for RT-PCR. Custom DNA oligonucleotides were purchased from MWG-Biotech UK Ltd. (Milton Keynes, U.K.). Plasmid isolation and purification was carried out using the Promega Wizard DNA purification kit. The chemically competent *Escherichia coli* TOP10 cells, the pBAD TOPO TA expression kit and the V5 antibody were purchased from Invitrogen (Paisley, U.K.). Restriction enzymes were purchased from New England BioLabs (Hitchin, Herts., U.K.). Thermal cycling was performed using a Hybaid PCR Express Thermal Cycler. Nickel-nitrilotriacetate (Ni-NTA)-agarose was purchased from Qiagen (Crawley, West Sussex, U.K.). Complete® protease inhibitor cocktail was purchased from Roche. SDS/PAGE was performed on precast 10 % acrylamide mini-gels using a Bis-Tris buffered system (NuPAGE, Invitrogen). Gels were stained directly for protein using Coomassie Brilliant Blue R (Sigma). Tryptic digests and matrix-assisted laser-desorption ionization–time-of-flight mass spectrometry (MALDI–TOF-MS) were carried out by the Functional Genomics Unit at the Moredun Research Institute. BioDesign dialysis tubing (8,000 Molecular mass cut-off) was purchased from VWR International. Human PHOSPHO1 concentrations were determined in 96-well plates using the Bio-Rad protein assay kit with gammaglobulin as standard. Optical spectroscopy of 96-well plates was performed using a Dynatech MR7000 plate-reader unless otherwise stated. Ammonium molybdate, L-arabinose, ATP, β-glycerol phosphate, fructose 6-phosphate, glycone phosphate, Hepes, imidazole, $MgCl_2$ (99 % pure), Malachite Green, NaCl, *p*-nitrophenylphosphate, PCho (phosphocholine), PEA (phosphoethanolamine), phospho-L-serine, phospho-L-tyrosine, pyridoxal-5-phosphate, pyrophosphate sodium salt, ribose-5-phosphate and Trizma base were purchased from Sigma Chemical Co. $CaCl_2$, $CoCl_2$, $NiCl_2$ and $MnCl_2$ (all AnalaR grade) were purchased from BDH–Merck Ltd. (Lutterworth, Leics., U.K.). $ZnCl_2$ (99.99 % pure) was purchased from Acros Organics (Den Bosch, The Netherlands).

Production of recombinant human PHOSPHO1

RNA was isolated from SaOS-2 osteoblast-like cells by phenol/chloroform extraction and reverse transcribed. cDNA corresponding to Met^{19}–Cys^{267} of human PHOSPHO1 was amplified with the specific primers, hs_phos1-f1 primer (5′-ATGGCCG-CGCAGGGC-3′) and hs_phos1-r1 primer (5′-GCACGACTTC-AGCACCTGTTGC-3′). This strategy was adopted in view of the ambiguity concerning the initiation codon of PHOSPHO1 and, therefore, we expressed a protein containing only the region that would be common to all predicted forms. The cDNA fragment was subcloned into the pBAD TOPO TA vector. The construct was designed to express PHOSPHO1 fused to a V5 epitope and 6 His-tag at the C-terminus. A clone (pBAD-PHOSPHO1) containing the PHOSPHO1 fragment in the correct orientation was identified by restriction digestion of plasmid minipreps. The *E. coli* cells were grown in Luria–Bertani broth (10 litres, 37 °C) and recombinant protein expression was induced by treatment with 0.1 % (w/v) L-arabinose for 4 h. Bacteria were harvested by centrifugation and were resuspended in a lysis buffer containing 50 mM potassium phosphate pH 8.0, 300 mM NaCl, 10 mM imidazole and 1.6 mg/ml of Complete® protease inhibitor cocktail. Cells were lysed using a French press (16 000 p.s.i., 16 °C). A clarified lysate was prepared by centrifugation at 20 000 ***g*** for 1 h. A 5 ml Ni-NTA–agarose column was equilibrated with 50 ml of lysis buffer. Following equilibration, a 20 ml aliquot of the clarified lysate was applied to the column. The column was then washed with 50 ml of Tris-buffered saline (TBS) pH 8.0 containing 20 mM imidazole, and eluted in 5 ml fractions each by addition of a single column volume of TBS, pH 8.0, containing 250 mM imidazole. The fraction containing the pure recombinant protein was then dialysed three times in TBS, pH 7.2 (5 l, 4 °C, 24 h) and stored at 4 °C prior to use.

Western blotting

Following dialysis, 1 μg of purified protein was subjected to SDS/PAGE as described above and transferred to nitrocellulose filters using the transfer buffer supplied by the manufacturer. After transfer, filters were blocked for 1 h in PBS containing 4 % dried milk powder and 20 % horse serum. The filters were then incubated in blocking solution containing 1:3000 dilution of mouse monoclonal horseradish peroxidase-labelled anti-V5 antibody and washed three times in PBS. They were then developed by incubation in a solution containing 25 mM Tris/HCl, pH 7.2, 75 mM NaCl, 0.25 mg/ml diaminobenzidine, 0.1 mg/ml $CoCl_2$, 0.15 mg/ml urea hydrogen peroxide.

Phosphatase assays

The standard discontinuous colorimetric assay used was based on that of Baykov et al. [25]. The reactions were measured in 96-well plates containing 200 μl of 25 % (w/v) glycerol, 20 mM TBS, pH 7.2, 25 μg/ml BSA, 2.5 mM substrate, 2 mM of the corresponding divalent metal chloride salt and 600 ng of purified recombinant PHOSPHO1. For investigation of the effect of pH on PHOSPHO1 activity, 20 mM Mes was used to obtain pH values between 5.0 and 6.7, and 20 mM 3-(cyclohexylamino)propane-1-sulphonic acid (Caps) for pH 9.0, in place of TBS. The ionic strength of each buffer was adjusted to that of 20 mM TBS by addition of NaCl. Standard solutions containing known concentrations of KH_2PO_4 were included in each plate. Reactions were allowed to proceed for 15 min at 37 °C then stopped by the addition of 50 μl of 3.75 M sulphuric acid containing 3 % ammonium molybdate, 0.2 % Tween 20 and 0.12 % Malachite Green. The absorbance of each well at 630 nm was measured and the specific activity was calculated in units of activity per mg of enzyme, where 1 unit of activity represents the hydrolysis of 1 nmol of phosphate per min.

The continuous spectrophotometric assay was performed using the EnzChek® Phosphatase Assay Kit (Molecular Probes, Eugene, OR, U.S.A.), which is based upon the purine nucleoside phosphorylase (PNPase)-coupled assay reported by Webb [26]. The reactions were measured in 96-well plates containing 25 % (w/v) glycerol, 20 mM Mes, pH 6.7, 500 mM NaCl, 2 mM $MgCl_2$, 0.2 unit PNPase, 200 μM MESG (2-amino-6-mercapto-7-methylpurine ribonucleoside) and 144 ng of purified recombinant PHOSPHO1 at 37 °C. PNPase and MESG concentrations were optimized to ensure that the phosphatase activity was rate-limiting. PHOSPHO1 substrate concentrations were varied accordingly. Absorbances were measured continuously at 355 nm using a VICTOR HTS plate-reader.

RESULTS

Purification of recombinant human PHOSPHO1

Recombinant His-tagged PHOSPHO1 protein in fractions eluted from a Ni-NTA–agarose column was assayed by SDS/PAGE. Typically, fraction 2 yielded a single band of the expected mass (32 kDa) consistent with > 99 % purity (Figure 1A). The final yield of protein was approx. 35 mg per 10 litres of culture. Western blotting of the purified protein yielded a band of expected

© 2004 Biochemical Society

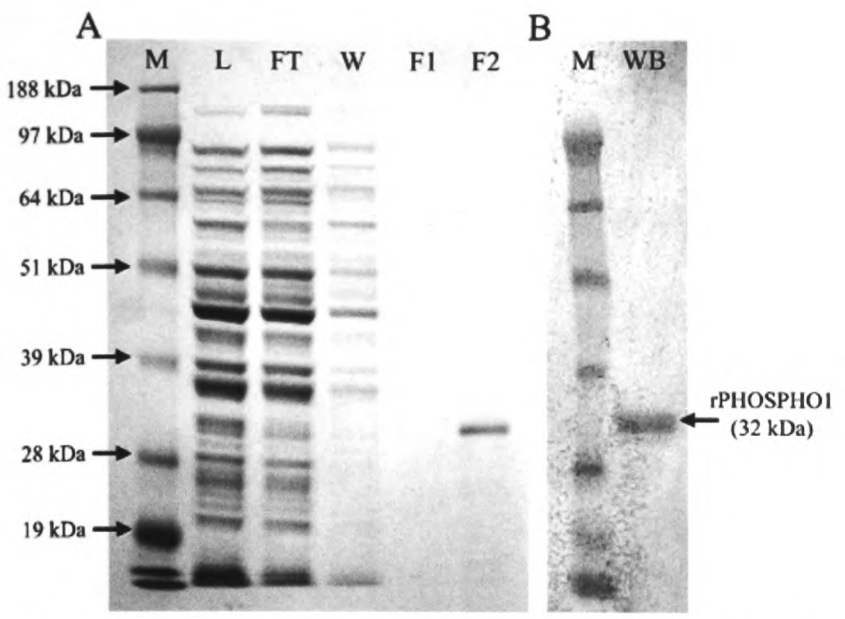

Figure 1 SDS/PAGE and Western analysis of purified recombinant human PHOSPHO1

(**A**) The cell lysate (L) and the flow-through (FT), wash (W) and eluted fractions 1 and 2 (F1 and F2) from each stage of Ni-NTA purification were subjected to SDS/PAGE under reducing conditions and visualized by Coomassie Blue staining. Molecular mass standards are also shown (M). (**B**) Western blot (WB) of the purified protein (1.2 μg) with anti-V5 antibody, which recognizes the V5 epitope tag fused to the recombinant protein near its C-terminus.

Table 1 Substrate specificity of recombinant human PHOSPHO1

Recombinant human PHOSPHO1 (3 μg/ml) was incubated with each substrate and assayed for phosphatase activity by the discontinuous assay at 37 °C. The 200 μl reaction mixture contained 25% (w/v) glycerol, 20 mM TBS, pH 7.2, 25 μg/ml BSA, 2.5 mM substrate and 2 mM $MgCl_2$. The results are the means ± S.E.M. of triplicate assays.

Compound	Specific activity (units/mg)
Phosphoethanolamine	4600 ± 582
Phosphocholine	2980 ± 335
Ribose 5-phosphate	74.8 ± 6.2
p-Nitrophenyl phosphate	64.5 ± 36.6
β-Glycerol phosphate	39.6 ± 6.2
Pyridoxal-5-phosphate	17.6 ± 12.4
Pyrophosphate	< 0.1
Phospho-L-serine	< 0.1
Glycone phosphate	< 0.1
Fructose 6-phosphate	< 0.1
Phospho-L-tyrosine	< 0.1
ATP	< 0.1

size and showed the presence of the V5-epitope tag (Figure 1B). The purified protein was also confirmed as recombinant PHOSPHO1 by MALDI–TOF MS of tryptic fragments (results not shown).

Catalytic properties of recombinant human PHOSPHO1

Twelve phosphate compounds were investigated as potential substrates for human PHOSPHO1. The resultant specific activities are shown in Table 1. PHOSPHO1 was found to have the highest specific activities toward PEA and PCho, with PEA being hydrolysed approx. 1.5 times faster than PCho. Six of the potential substrates tested (PP_i, phospho-L-serine, glycone phosphate, fructose 6-phosphate, phospho-L-tyrosine and ATP) yielded no detectable phosphatase activity.

The concentration of $MgCl_2$ was varied between 2 μM and 200 mM and activity was found to be maximum at 2 mM $MgCl_2$.

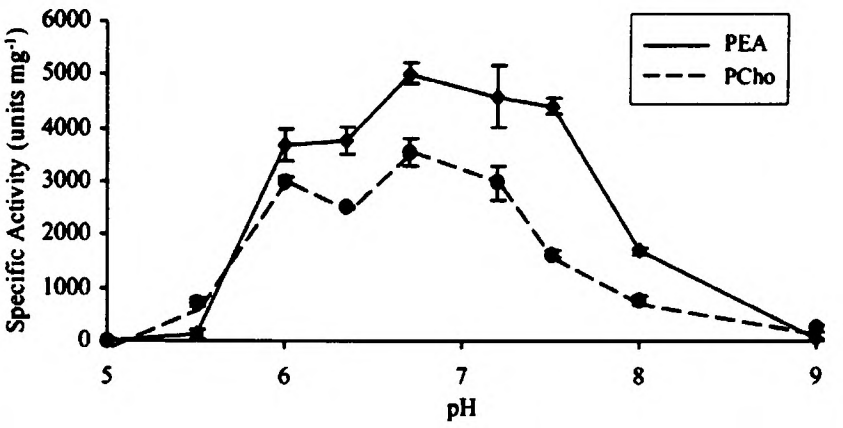

Figure 2 The pH optimum for activity of recombinant PHOSPHO1

Enzymic activity was measured in the presence of 3 μg/ml enzyme and 2 mM Mg^{2+} by the discontinuous assay (as described in the Experimental procedures) for phosphoethanolamine (solid line) and phosphocholine (broken line).

In the presence of 2 mM Mg^{2+} at 37 °C, the recombinant enzyme exhibited a pH optimum around 6.7 for both PEA and PCho (Figure 2). High catalytic activity (> 70% of maximum) was observed between pH 6.0 and 7.2. This high level of activity extends up to at least pH 7.5 for PEA but begins to decline significantly for PCho at pH values higher than pH 7.2. The kinetic constants of recombinant PHOSPHO1 were determined for PEA and PCho using the continuous coupled assay in the presence of 2 mM Mg^{2+} at 37 °C. The enzyme exhibited Michaelis–Menten kinetics for both substrates (Hill coefficients = 1.00). A plot of reaction rate versus substrate concentration for PEA and PCho and also Lineweaver–Burke plots, allowing the calculation of K_m and V_{max} values, are shown in Figure 3. PHOSPHO1 displayed an apparent K_m of 3.0 μM and a k_{cat} of 2.27 s^{-1} for PEA, and a K_m of 11.4 μM and a k_{cat} of 1.98 s^{-1} for PCho.

Requirement for metals

To investigate the requirement of metal ions for the recombinant enzyme, the purified enzyme solution was extensively dialysed against metal-free buffer to remove any weakly bound metal ions. The effect of different metal ions on the hydrolysis of PEA and PCho was assessed by addition of 2 mM concentrations of various metal salts. As controls, reactions were also carried out in buffers without added metal ions. The results are shown in Figure 4. The phosphatase activity was approximately 80-fold higher for both substrates in the presence of Mg^{2+} compared with the metal-free control. Co^{2+}, Mn^{2+} and Ni^{2+} also stimulated activity but to a lesser extent than Mg^{2+}, whereas the presence of Ca^{2+} and Zn^{2+} had no significant effect on activity compared with the control ($Mg^{2+} > Co^{2+} > Mn^{2+} > Ni^{2+} > Ca^{2+} = Zn^{2+}$ = no metal). Interestingly, PHOSPHO1 has a higher activity toward PCho than to PEA in the presence of Co^{2+} and Mn^{2+}. This is most probably due to an allosteric effect caused by a difference in the metal-binding properties of each enzyme–substrate complex.

DISCUSSION

The results presented here show that PHOSPHO1 has activity which is typical of most enzymes within the HAD superfamily, with a strong Mg^{2+}-dependence and a pH optimum within the acid-to-neutral pH range [27–29]. A high level of activity extends to pH values at least as high as pH 7.5 for PEA but begins to decline significantly for PCho at pH values higher than pH 7.2. The pH of the extracellular fluid of growth plate cartilage is close to pH 7.6 [30] and so the activity of PHOSPHO1 may be restricted

© 2004 Biochemical Society

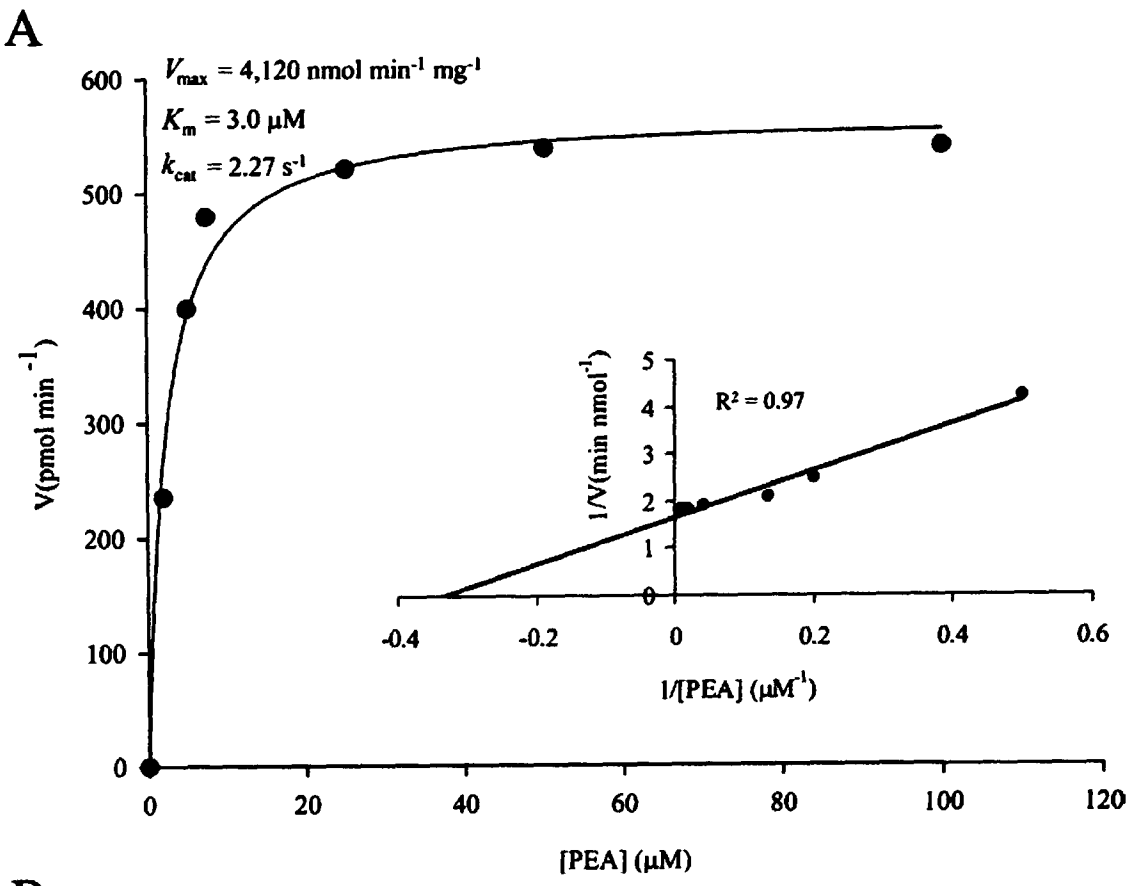

Figure 3 Kinetic analysis of the hydrolysis reactions catalysed by recombinant PHOSPHO1

Kinetic activity toward (**A**) PEA and (**B**) PCho, measured using a method based upon the purine nucleoside phosphorylase-coupled assay [26] as described in the Experimental procedures. Shown are the reaction velocities (V) as a function of substrate concentration. *Insets*, Lineweaver–Burke plots from which K_m and V_{max} values were calculated.

mainly to PEA at this region. Overall, PHOSPHO1 has a high specific activity toward PEA and PCho compared with the other phosphomonoesters investigated. The results are highly significant for the mineralization process in cells. Both PCho and PEA are present in mineralizing cells and are the two most abundant phosphomonoesters in cartilage [31]. The very low K_m values for both PEA and PCho (μM range) suggest that they would be half-saturated at levels of 3 and 11.4 μM, respectively. This indicates that under the reported conditions both substrates would be rapidly hydrolysed. These compounds are therefore likely to be natural substrates of PHOSPHO1.

The hydrolysis of PEA and PCho is known to occur *in vivo*, although the enzyme responsible has not been identified previously. It has been hypothesized that PEA is a natural substrate for TNAP [8,32] due to an increase in its urinary excretion in patients diagnosed with hypophosphatasia [33]. However, this appears unlikely following examination of kinetic data for the TNAP-catalysed hydrolysis reaction at physiological pH, with

© 2004 Biochemical Society

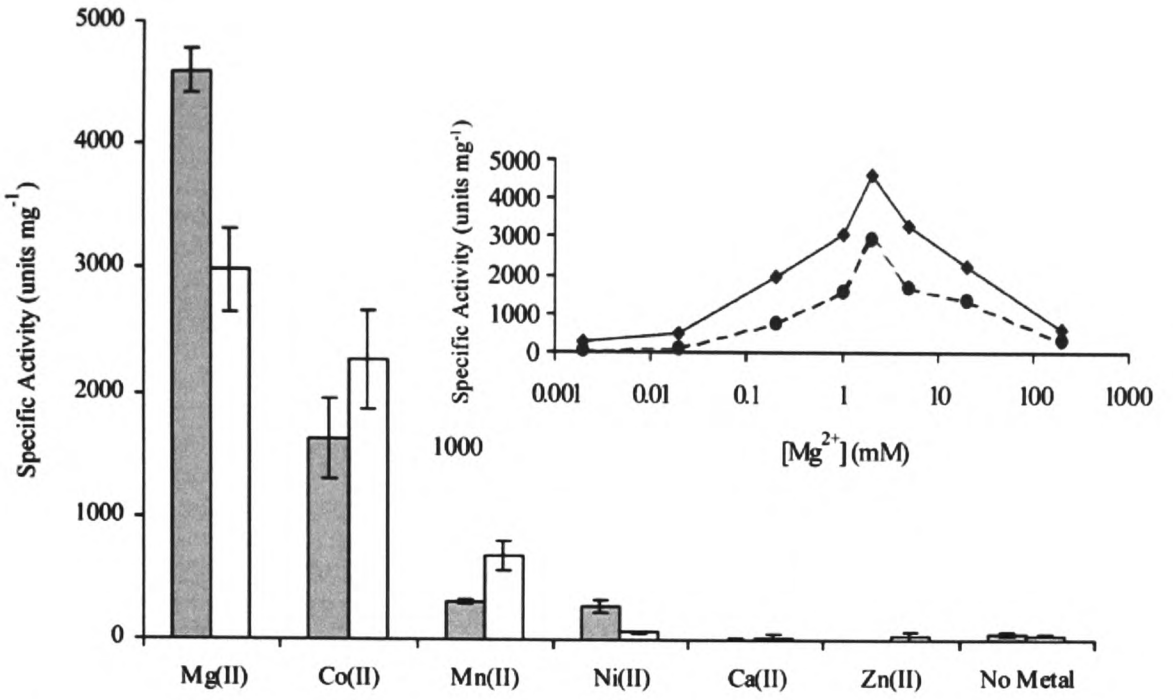

Figure 4 Metal requirement for activity of recombinant PHOSPHO1

Enzyme activity toward phosphoethanolamine (filled bars) and phosphocholine (open bars) was measured in the presence of the indicated metal ions (final concentration 2 mM). The activity of the apoenzyme was measured in the absence of added metals (No Metal). Inset, concentration dependence of apoenzyme activation by Mg^{2+} for PEA (solid line) and PCho (broken line); enzyme activity was measured by the discontinuous assay.

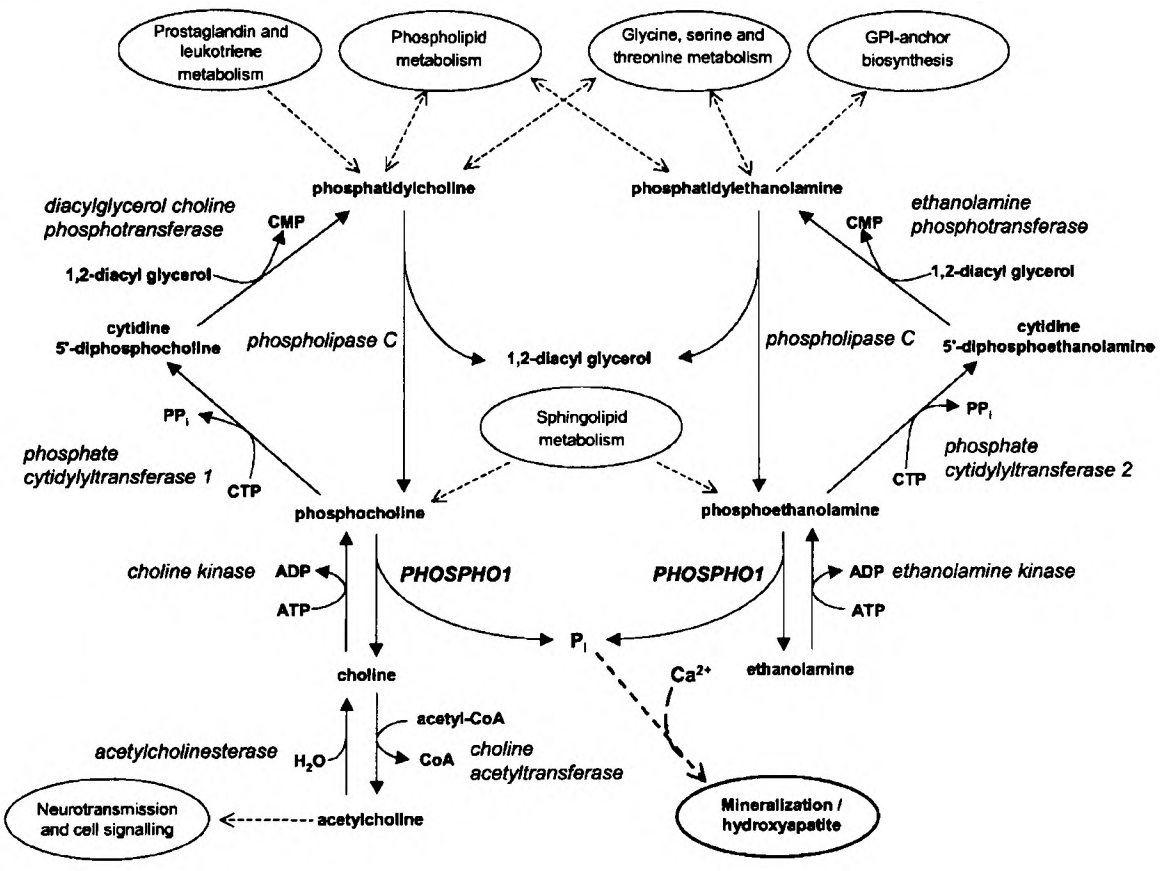

Scheme 1 Human PEA and PCho metabolism

Proposed metabolic pathways for the generation of PEA and PCho. The basis of the diagram is information from the Kyoto Encyclopedia of Genes and Genomes (KEGG) [41].

reported high K_m values at millimolar concentrations [34–36]. It is therefore possible that the genetic defect assumed to be caused by a loss of TNAP in hypophosphatasia is actually due to a loss or defect of PHOSPHO1. Brain alkaline phosphatase (BAP), an isoenzyme of TNAP, is reported to have PCho phosphatase activity [37]. However, the specific activity of BAP toward PCho in the reported study was measured under alkaline conditions (pH 8.5) and is likely to be much lower at physiological pH. PCho hydrolysis has been studied in hamster heart and is not catalysed by alkaline phosphatase, but by a separate unidentified enzyme [38]. It has also been shown that the hydrolysis of PEA and PCho is due to the action of an acid phosphatase in a variety of tissues, including bone and teeth [39], a study which agrees well with our present finding that PHOSPHO1 displays high activity toward both substrates between pH 6.0 and 7.2.

PEA and PCho are metabolites in the cytidine 5′-diphosphoethanolamine (CDP-EA) and cytidine 5′-diphosphocholine (CDP-Cho) pathways respectively (Scheme 1). These are the main

© 2004 Biochemical Society

pathways involved in the formation of phosphatidylcholine and phosphatidylethanolamine [40], which are involved in the metabolism of complex glycerolipids, glycosylphosphatidylinositol-anchors, prostaglandins, leukotrienes and the amino acids glycine, serine and threonine [41]. These pathways are also implicated in the pathogenesis of Alzheimer's and Huntington's disease [42,43]. Therefore the identification of a phosphatase with specificity toward PEA and PCho is highly significant. Conversely, phosphatidylethanolamine and phosphatidylcholine may be hydrolysed by phospholipase C to form PEA and PCho respectively [44]. The synthesis of phosphatidylcholine from choline by the CDP-Cho pathway in mineralizing cells has previously been investigated. PCho accumulation is much decreased in neo-natal rat calvaria compared with the liver of the same animal [45]. PCho concentration is usually determined by the relatively higher activity of choline kinase compared with that of phosphate cytidylyltransferase 1. However, the low PCho accumulation in mineralizing compared with non-mineralizing cells may be due to the upregulation of PHOSPHO1. PHOSPHO1 is highly expressed at sites of mineralization [21], and as a consequence will reduce the levels of PCho and PEA in chondrocytes and osteoblasts. P_i may be scavenged from PEA and PCho during the mineralization process in order to generate the concentration required for hydroxyapatite crystal formation.

The MV-membrane is a rich source of both phosphatidylethanolamine and phosphatidylcholine and may act as a pool for PEA and PCho in MVs. Wuthier et al. have found that the phosphatidylethanolamine and phosphatidylcholine composition of the MV membrane decreases during mineralization and that 1,2-diacyl glycerol accumulates in MVs, indicative of phospholipase C activity [46]. However, in the absence of any kinetic data relating to phosphatidylethanolamine or phosphatidylcholine degradation in MVs it is impossible to say at this time whether such a mechanism exists as a viable means of generating PEA or PCho. Ca^{2+} and P_i are present at high levels in MVs even before induction of mineral formation, and are derived from cellular activity prior to MV formation [47]. Since the ambient concentration of P_i in the extracellular fluid is close to 2 mM [48], it is doubtful that the amount of P_i released from MV lipids would be sufficient to increase the overall level of extracellular P_i. However, the local effect of this limited release may be sufficient to facilitate mineral formation.

In conclusion, these results show for the first time that human PHOSPHO1 is a phosphoethanolamine and phosphocholine phosphatase. PHOSPHO1 is known to be upregulated in mineralizing cells, these findings therefore provide a novel means of generating P_i in mineralizing cells and may have implications for the diagnosis of hypophosphatasia and treatment of bone mineralization abnormalities such as osteomalacia and pathological soft-tissue ossification, a process clinically significant in atherosclerosis and heart failure.

We thank the Wellcome Trust for support for the Edinburgh Protein Interaction Centre and Dr John White for his assistance with the expression of the recombinant protein. We also thank BBSRC for funding and Immunodiagnostic Systems Ltd, Boldon, U.K. for a Council for Advancement and Support of Education (CASE) award (to S. J. R.).

REFERENCES

1 Sauer, G. R. and Wuthier, R. E. (1988) Fourier transform infrared characterization of mineral phases formed during induction of mineralization by collagenase-released matrix vesicles *in vitro*. J. Biol. Chem. **263**, 13718–13724
2 Wu, L. N. Y., Ishikawa, Y., Sauer, G. R., Genge, B. R., Mwale, F., Mishima, H. and Wuthier, R. E. (1995) Morphological and biochemical characterization of mineralizing primary cultures of avian growth plate chondrocytes: evidence for cellular processing of Ca^{2+} and P_i prior to matrix mineralization. J. Cell. Biochem. **57**, 218–237
3 Anderson, H. C. (2003) Matrix vesicles and calcification. Curr. Rheumatol. Rep. **5**, 222–226
4 Roach, H. I. (1999) Association of matrix acid and alkaline phosphatases with mineralization of cartilage and endochondral bone. Histochem. J. **31**, 53–61
5 Nakano, Y., Kawamoto, T., Oda, K. and Takano, Y. (2003) Alkaline and acid phosphatases in bone cells serve as phosphohydrolases at physiological pH *in vivo*: a histochemical implication. Connect. Tissue Res. **44**, 219–222
6 Anderson, H. C. (1995) Molecular biology of matrix vesicles. Clin. Orthopaed. **314**, 266–280
7 Beck, Jr, G. R., Moran, E. and Knecht, N. (2003) Inorganic phosphate regulates multiple genes during osteoblast differentiation, including *Nrf2*. Exp. Cell Res. **288**, 288–300
8 Whyte, M. P. (1994) Hypophosphatasia and the role of alkaline phosphatase in skeletal mineralization. Endocr. Rev. **15**, 439–461
9 Hessle, L., Johnson, K. A., Anderson, H. C., Narisawa, S., Sali, A., Goding, J. W., Terkeltaub, R. and Millán, J. L. (2002) Tissue-nonspecific alkaline phosphatase and plasma cell membrane glycoprotein-1 are central antagonistic regulators of bone mineralization. Proc. Natl. Acad. Sci. U.S.A. **99**, 9445–9449
10 Narisawa, S., Frohlander, N. and Millán, J. L. (1997) Inactivation of two mouse alkaline phosphatase genes and establishment of a model of infantile hypophosphatasia. Dev. Dyn. **208**, 432–446
11 Waymire, K. G., Mahuren, J. D., Jaje, J. M., Guilarte, T. R., Coburn, S. P. and MacGregor, G. R. (1995) Mice lacking tissue non-specific alkaline phosphatase die from seizures due to defective metabolism of vitamin B-6. Nat. Genet. **11**, 45–51
12 Anderson, H. C., Hsu, H. H., Morris, D. C., Fedde, K. N. and Whyte, M. P. (1997) Matrix vesicles in osteomalacic hypophosphatasia bone containing apatite-like mineral crystals. Am. J. Pathol. **151**, 1555–1561
13 Anderson, H. C., Sipe, J. B., Hessle, L., Dhamyamraju, R., Atti, E., Camacho, N. P. and Millán, J. L. (2004) Impaired calcification around matrix vesicles of growth plate and bone in alkaline phosphatase-deficient mice. Am. J. Pathol. **164**, 841–847
14 Genge, B. R., Sauer, G. R., Wu, L. N., McLean, F. M. and Wuthier, R. E. (1988) Correlation between loss of alkaline phosphatase activity and accumulation of calcium during matrix vesicle-mediated mineralization. J. Biol. Chem. **263**, 18513–18519
15 Moss, D. W., Eaton, R. H., Smith, J. K. and Whitby, L. G. (1967) Association of PPi activity with human alkaline-phosphatase preparations. Biochem J. **102**, 53–57
16 Meyer, J. L. (1984) Can biological calcification occur in the presence of pyrophosphate? Arch. Biochem. Biophys. **231**, 1–8
17 Narita, M., Goji, J., Nakamura, H. and Sano, K. (1994) Molecular cloning, expression, and localization of a brain-specific phosphodiesterase I/nucleotide pyrophosphatase (PD-Iα) from rat brain. J. Biol. Chem. **269**, 28235–28242
18 Register, T. C., McLean, F. M., Low, M. G. and Wuthier, R. E. (1986) Roles of alkaline phosphatase and labile internal mineral in matrix vesicle-mediated calcification. Effect of selective release of membrane-bound alkaline phosphatase and treatment with isosmotic pH 6 buffer. J. Biol. Chem. **261**, 9354–9360
19 Hsu, H. H. T. and Anderson, H. C. (1996) Evidence of the presence of a specific ATPase responsible for ATP-initiated calcification by matrix vesicles isolated from cartilage and bone. J. Biol. Chem. **271**, 26383–26388
20 Houston, B., Seawright, E., Jefferies, D., Hoogland, E., Lester, D., Whitehead, C. and Farquharson, C. (1999) Identification and cloning of a novel phosphatase expressed at high levels in differentiating growth plate chondrocytes. Biochim. Biophys. Acta **1448**, 500–506
21 Houston, B., Stewart, A. J. and Farquharson, C. (2004) PHOSPHO1 – a novel phosphatase specifically expressed at sites of mineralization in bone and cartilage. Bone **34**, 629–637
22 Baldwin, J. C., Karthikeyan, A. S. and Raghothama, K. G. (2001) LEPS2, a phosphorus starvation-induced novel acid phosphatase from tomato. Plant Physiol. **125**, 728–737
23 Stenzel, I., Ziethe, K., Schurath, J., Hertel, S. C., Bosse, D. and Kock, M. (2003) Differential expression of the LePS2 phosphatase gene family in response to phosphate availability, pathogen infection and during development. Physiol. Plant. **118**, 138–146
24 Stewart, A. J., Schmid, R., Blindauer, C. A., Paisey, S. J. and Farquharson, C. (2003) Comparative modelling of human PHOSPHO1 reveals a new group of phosphatases within the haloacid dehalogenase superfamily. Protein Eng. **16**, 889–895
25 Baykov, A. A., Evtushenko, O. A. and Avaeva, S. M. (1988) A malachite green procedure for orthophosphate determination and its use in alkaline phosphatase-based enzyme immunoassay. Anal. Biochem. **171**, 266–270
26 Webb, M. R. (1992) A continuous spectrophotometric assay for inorganic phosphate and for measuring phosphate release kinetics in biological systems. Proc. Natl. Acad. Sci. U.S.A. **89**, 4884–4887
27 Morais, M. C., Zhang, W., Baker, A. S., Zhang, G., Dunaway-Mariano, D. and Allen, K. N. (2000) The crystal structure of *Bacillus cereus* phosphonoacetaldehyde hydrolase: insight into catalysis of phosphorus bond cleavage and catalytic diversification within the HAD enzyme superfamily. Biochemistry **39**, 10385–10396

© 2004 Biochemical Society

28 Wu, J. and Woodard, R. W. (2003) *Escherichia coli* YrbI is 3-deoxy-D-manno-octulosonate 8-phosphate phosphatase. J. Biol. Chem. **278**, 18117–18123
29 Klutts, S., Pastuszak, I., Edavana, V. K., Thampi, P., Pan, Y.-T., Abraham, E. C., Carroll, J. D. and Elbein, A. D. (2003) Purification, cloning, expression, and properties of mycobacterial trehalose-phosphate phosphatase. J. Biol. Chem. **278**, 2093–2100
30 Howell, D. S., Pita, J. C., Marquez, J. F. and Madruga, J. E. (1968) Partition of calcium, phosphate and protein in the fluid phase aspirated at calcifying sites in epiphyseal cartilage. J. Clin. Invest. **47**, 1121–1132
31 Kvam, B. J., Pollesello, P., Vittur, F. and Paoletti, S. (1992) ^{31}P NMR studies of resting zone cartilage from growth plate. Magn. Reson. Med. **25**, 355–361
32 Whyte, M. P., Landt, M., Ryan, L. M., Mulivor, R. A., Henthorn, P. S., Fedde, K. N., Mahuren, J. D. and Coburn, S. P. (1995) Alkaline phosphatase: placental and tissue-nonspecific isoenzymes hydrolyse phosphoethanolamine, inorganic pyrophosphate, and pyridoxal 5′-phosphate. Substrate accumulation in carriers of hypophosphatasia corrects during pregnancy. J. Clin. Invest. **95**, 1440–1445
33 Rasmussen, K. (1968) Phosphorylethanolamine and hypophosphatasia. Dan. Med. Bull. **15**, Suppl. 2, 1–112
34 Fedde, K. N., Lane, C. C. and Whyte, M. P. (1988) Alkaline phosphatase is an ectoenzyme that acts on micromolar concentrations of natural substrates at physiologic pH in human osteosarcoma (SAOS-2) cells. Arch. Biochem. Biophys. **264**, 400–409
35 Muller, K., Schulz, J. and Oemus, R. (1989) Phosphoäthanolamin – ein substrat der alkalischen phosphatase aus ratten-calvaria. Biomed. Biochim. Acta **48**, 495–504
36 Tenenbaum, H. C. and Palangio, K. (1987) Phosphoethanolamine- and fructose 1,6-diphosphate-induced calcium uptake in bone formed *in vitro*. Bone Miner. **2**, 201–210
37 Sok, D.-E. (1999) Oxidative inactivation of brain alkaline phosphatase responsible for hydrolysis of phosphocholine. J. Neurochem. **72**, 355–362
38 Hatch, G. M. and Choy, P. C. (1987) Phosphocholine phosphatase and alkaline phosphatase are different enzymes in hamster heart. Lipids **22**, 672–676
39 McDonald, D. F., Schofield, B. H., Geffert, M. A. and Coleman, R. A. (1980) A comparative study of new substrates for the histochemical demonstration of acid phosphomonoesterase activity in tissues which secrete acid phosphatase. J. Histochem. Cytochem. **28**, 316–322
40 Walkey, C. J., Donohue, L. R., Bronson, R, Agellon, L. B. and Vance, D. E. (1997) Disruption of the murine gene encoding phosphatidylethanolamine N-methyltransferase. Proc. Natl. Acad. Sci. U.S.A. **94**, 12880–12885
41 Kanehisa, M., Goto, S., Kawashima, S. and Nakaya, A. (2002) The KEGG databases at GenomeNet. Nucleic Acids Res. **30**, 42–46
42 Ellison, D. W., Beal, M. F. and Martin, J. B. (1987) Phosphoethanolamine and ethanolamine are decreased in Alzheimer's disease and Huntington's disease. Brain Res. **417**, 389–392
43 Farber, S. A., Slack, B. E. and Blusztajn, J. K. (2000) Acceleration of phosphatidylcholine synthesis and breakdown by inhibitors of mitochondrial function in neuronal cells: a model of the membrane defect of Alzheimer's disease. FASEB J. **14**, 2198–2206
44 van Dijk, M. C., Muriana, F. J., de Widt, J., Hilkmann, H. and van Blitterswijk, W. J. (1997) Involvement of phosphatidylcholine-specific phospholipase C in platelet-derived growth factor-induced activation of the mitogen-activated protein kinase pathway in Rat-1 fibroblasts. J. Biol. Chem. **272**, 11011–11016
45 Stern, P. H. and Vance, D. E. (1987) Phosphatidylcholine metabolism in neonatal mouse calvaria. Biochem. J. **244**, 409–415
46 Wu, L. N. Y., Genge, B. R., Kang, M. W., Arsenault, A. L. and Wuthier, R. E. (2002) Changes in phospholipid extractability and composition accompany mineralization of chicken growth plate cartilage matrix vesicles. J. Biol. Chem. **277**, 5126–5133
47 Wu, L. N., Wuthier, M. G., Genge, B. R. and Wuthier, R. E. (1997) *In situ* levels of intracellular Ca^{2+} and pH in avian growth plate cartilage. Clin. Orthop. **335**, 310–314
48 Wuthier, R. E. (1977) Electrolytes of isolated epiphyseal chondrocytes, matrix vesicles, and extracellular fluid. Calcif. Tissue Res. **23**, 125–133

Received 29 March 2004/6 May 2004; accepted 3 June 2004
Published as BJ Immediate Publication 3 June 2004, DOI 10.1042/BJ20040511

© 2004 Biochemical Society

Available online at www.sciencedirect.com
SCIENCE DIRECT
Biochimica et Biophysica Acta 1752 (2005) 73 – 82
BIOCHIMICA ET BIOPHYSICA ACTA
BBA
http://www.elsevier.com/locate/bba

Probing the substrate specificities of human PHOSPHO1 and PHOSPHO2

Scott J. Roberts[a,*,1], Alan J. Stewart[a,1], Ralf Schmid[b], Claudia A. Blindauer[c,d], Stephanie R. Bond[a], Peter J. Sadler[c], Colin Farquharson[a]

[a]*Division of Gene Function and Development, Roslin Institute, Roslin, Midlothian EH25 9PS, UK*
[b]*Institute of Evolutionary Biology, Ashworth Laboratories, The University of Edinburgh, Edinburgh EH9 3JT, UK*
[c]*School of Chemistry, University of Edinburgh, West Mains Road, Edinburgh EH9 3JJ, UK*
[d]*Department of Chemistry, University of Warwick, Coventry CV4 7AL, UK*

Received 16 May 2005; received in revised form 16 June 2005; accepted 16 June 2005
Available online 13 July 2005

Abstract

PHOSPHO1, a phosphoethanolamine/phosphocholine phosphatase, is upregulated in mineralising cells and is thought to be involved in the generation of inorganic phosphate for bone mineralisation. PHOSPHO2 is a putative phosphatase sharing 42% sequence identity with PHOSPHO1. Both proteins contain three catalytic motifs, conserved within the haloacid dehalogenase superfamily. Mutation of Asp32 and Asp203, key residues within two motifs, abolish PHOSPHO1 activity and confirm it as a member of this superfamily. We also show that Asp43 and Asp123, residues that line the substrate-binding site in our PHOSPHO1 model, are important for substrate hydrolysis. Further comparative modelling reveals that the active sites of PHOSPHO1 and PHOSPHO2 are very similar, but surprisingly, recombinant PHOSPHO2 hydrolyses phosphoethanolamine and phosphocholine relatively poorly. Instead, PHOSPHO2 shows high specific activity toward pyridoxal-5-phosphate (V_{max} of 633 nmol min^{-1} mg^{-1} and K_m of 45.5 μM). Models of PHOSPHO2 and PHOSPHO1 suggest subtle differences in the charge distributions around the putative substrate entry site and in the location of potential H-bond donors.
© 2005 Elsevier B.V. All rights reserved.

Keywords: Bone mineralisation; Haloacid dehalogenase superfamily; Molecular modelling; Phosphatase; Site-directed mutagenesis

1. Introduction

Human PHOSPHO1, a phosphatase with upregulated expression in mineralising tissue [1], is localised to the mineralising regions of bone [2] and has been implicated in the generation of inorganic phosphate for matrix mineralisation. PHOSPHO1 has been identified in a number of vertebrates including humans, mice, chickens, zebrafish and puffer fish [3,4] and has recently been shown to exhibit high specific phosphohydrolase activity toward phosphoethanolamine (PEA) and phosphocholine (PCho) substrates [5]. PEA and PCho are involved in the biosynthesis of phosphatidylethanolamine and phosphatidylcholine, respectively, and form the polar headgroups of phospholipids in biological membranes. Both PEA and PCho levels are controlled in vivo by the expression of CTP-dependent cytidyltransferases, which catalyse the formation of CDP-ethanolamine and CDP-choline, respectively [6,7]. Both PEA and PCho are known to accumulate in mineralising cells. Indeed these compounds have been shown to be the two most abundant phosphomonoesters in cartilage [8]. The discovery of PHOSPHO1 provides a close link between PEA and PCho accumulation and the generation of inorganic phosphate in mineralising cells. PHOSPHO1 is therefore a potential target in the design of new therapeutics toward diseases such as osteopetrosis and craniosynostosis,

Abbreviations: CD, circular dichroism; HAD, haloacid dehalogenase; MESG, 2-amino-6-mercapto-7-methylpurine ribonucleoside; *Mj*PSP, phosphoserine phosphatase from *Methanococcus jannaschii*; Ni-NTA, nickel-nitrilotriacetate; P5P, pyridoxal-5-phosphate; PCho, phosphocholine; PEA, phosphoethanolamine; PNPase, purine nucleoside phophorylase; TBS, Tris-buffered saline

* Corresponding author. Tel.: +44 131 527 4221; fax: +44 131 440 0434.
E-mail address: scott.roberts@bbsrc.ac.uk (S.J. Roberts).
[1] Both authors contributed equally to this work.

1570-9639/$ - see front matter © 2005 Elsevier B.V. All rights reserved.
doi:10.1016/j.bbapap.2005.06.009

which lead to skeletal abnormalities characterised by excess or premature mineral formation [9]. Inhibition of PHOSPHO1 may also be of benefit in the treatment of vascular calcification, a process that shares many similarities with the mineralisation of bone and is clinically significant in atherosclerosis and heart failure [10].

Enzymes of the haloacid dehalogenase (HAD) superfamily catalyse the hydrolysis of C-Cl, C-OP and C-P bonds from a wide range of substrates and demonstrate great functional diversity from a single protein fold. The amino acid sequence of PHOSPHO1 contains three motifs that are conserved within the HAD superfamily. These motifs form the active site of this group of enzymes, which includes a variety of magnesium-dependent phosphatases [11]. In motif 1, DXDX(T/V), both Asp residues coordinate to the catalytic Mg^{2+} ion, and the first Asp also forms a phosphoprotein intermediate during hydrolysis [12]. In motif 2, (S/T), the conserved serine or threonine is involved in hydrogen bonding to a phosphoryl oxygen. Motif 3, $K(X)_{18-30}(G/S)(D/S)XXX(D/N)$, is also involved in phosphoryl oxygen hydrogen bonding and coordination to the Mg^{2+} ion [12,13].

A search for homologous proteins to PHOSPHO1 revealed the sequence of PHOSPHO2, a putative human phosphatase that shares 42% sequence identity with human PHOSPHO1. Analysis of expressed sequence tags (ESTs) in dbEST indicates that PHOSPHO2 is expressed in a wide range of tissues. Orthologous proteins to PHOSPHO2 were also found. Fig. 1 shows a sequence alignment of PHOSPHO1 and PHOSPHO2 proteins from a number of species. Analysis of sequences with the program SignalP v3.0 [14] suggests the absence of any signal sequences in

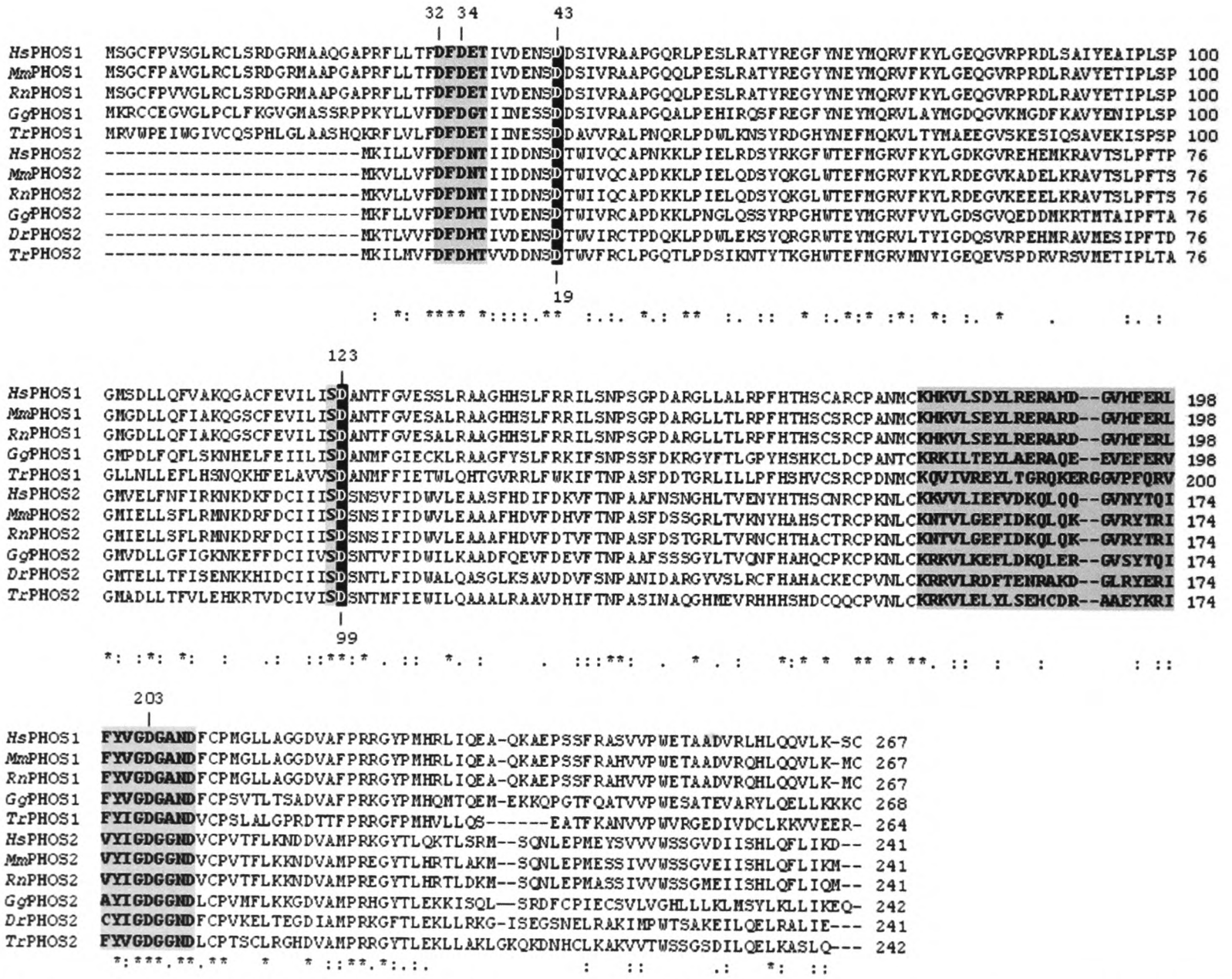

Fig. 1. Alignment of the amino acid sequences of PHOSPHO1 proteins with PHOSPHO2 and its homologues. The three catalytic motifs are highlighted in grey. The white on black letters denotes residues which are proposed to be involved in substrate specific interactions. The following sequences are used (accession numbers are shown in parentheses): *Hs*PHOS1, human PHOSPHO1 (Q8TCT1); *Mm*PHOS1, mouse PHOSPHO1 (Q8R2H9); *Rn*PHOS1, rat PHOSPHO1; *Gg*PHOS1, chicken PHOSPHO1 (O73884); *Tr*PHOS1, puffer fish PHOSPHO1; *Hs*PHOS2, human PHOSPHO2 (Q8TCD6); *Mm*PHOS2, mouse PHOSPHO2 (Q9D9M5); *Rn*PHOS2, rat PHOSPHO2 (XP_230005); *Gg*PHOS2, chicken PHOSPHO2 (XP_422006); *Dr*PHOS2, zebrafish PHOSPHO2 (ENSDARP00000004689); *Tr*PHOS2, puffer fish PHOSPHO2 (SINFRUP00000138420). "*"=identical or conserved residues in all sequences in the alignment, ":"=indicates conserved substitutions and "."=indicates semi-conserved substitutions.

the PHOSPHO1 or PHOSPHO2 proteins suggesting both enzymes are cytosolic. Closer inspection of the amino acid sequence of PHOSPHO2 protein revealed that all three catalytic motifs are conserved. Also conserved are Asp19 and Asp99, which correspond to two residues (Asp43 and Asp123) previously postulated to be involved in substrate-specific interactions in PHOSPHO1 [4]. These two residues were found to line the substrate-binding pocket in a structural model of PHOSPHO1, and are the only residues in this region that are conserved between orthologous proteins from other species, but not in phosphoserine phosphatases (PSPs), which are a closely related group of enzymes within the HAD superfamily. In contrast, in PSP with bound substrate (PDB: 1L7P; Asp11Asn mutant), Glu20, Met43, Phe49 and Arg56 have been shown to be involved in phospho-L-serine binding, and these residues are fully conserved in PSPs, but not present in PHOSPHO1 or PHOSPHO2 [12]. These observations have led to the suggestion that PHOSPHO1 and PHOSPHO2 might utilise the same, or highly similar substrate. If true, this would intimate functional redundancy between PHOSPHO1 and PHOSPHO2 in vivo.

In this study, we have used site directed mutagenesis to confirm PHOSPHO1 as a member of the HAD superfamily and also to ascertain the importance of Asp43 and Asp123 residues for the catalysed hydrolysis of PEA and PCho. The activity of PHOSPHO2 protein toward PEA and PCho as well as a range of other potential substrates is investigated. In addition, we present structural models of PHOSPHO1 and PHOSPHO2 based upon the X-ray crystal structure of phosphoserine phosphatase from *Methanococcus jannaschii* and examine potential enzyme-substrate interactions using in silico ligand docking experiments.

2. Materials and methods

2.1. Site-directed mutagenesis of human PHOSPHO1

DNA corresponding to Met19-Cys267 of human PHOSPHO1 was amplified and cloned into the pBAD TOPO TA vector (Invitrogen) as described [5]. Oligonucleotide-directed mutagenesis was used to prepare cDNAs encoding the PHOSPHO1 mutants. Mutagenesis was performed using the QuikChange Site-Directed Mutagenesis kit (Stratagene). Five mutants were prepared (D32N, D43N, D123N, D203S and a double mutant D43N/D123N). Clones containing the desired mutation(s) were identified commercially (The UK Centre for Functional Genomics in Farm Animals (ARK-Genomics), Roslin, UK) by nucleotide sequence analysis across the mutation site. The *Escherichia coli* cells with transformed mutated plasmids were grown in Luria–Bertani broth containing 100 μg/ml ampicillin (1 l, 37 °C) and recombinant protein expression was induced by treatment with 0.1% (w/v) L-arabinose for 4 h. Bacteria were harvested by centrifugation and were lysed in CellLytic™ B-II lysis reagent (Sigma) containing 1.6 mg/ml of Complete® protease inhibitor cocktail (Roche), 50 mg/ml lysozyme (Sigma), 5 μg/ml DNase I (Sigma), 500 mM NaCl and 10 mM imidazole. Clarified lysates were prepared by centrifugation at 20,000×*g* for 1 h. A 5 ml Ni-NTA-agarose column was equilibrated with 50 ml of lysis buffer (Tris-buffered saline (TBS; 20 mM Tris–HCl, 500 mM NaCl, pH 8.0) containing 10 mM imidazole. Following equilibration, a 20 ml aliquot of each clarified lysate was applied to each column. The columns were washed with 50 ml of TBS, pH 8.0 containing 20 mM imidazole and eluted in 5 ml fractions each by addition of a single column volume of TBS, pH 8.0 containing 250 mM imidazole. The secondary structures of the mutants were compared to that of wild type recombinant PHOSPHO1 using circular dichroism (CD) to confirm that in each case, the mutation(s) had not affected the overall fold of the enzyme. CD spectra were recorded on a JASCO J-600 spectropolarimeter by using 0.5 mg/ml solutions of the recombinant PHOSPHO1 proteins in 20 mM potassium phosphate, pH 7.2, 130 mM sodium sulfate. The SELCON procedure [15] was used for secondary structure analysis. The CD spectra of the mutants were similar to the native protein (data not shown) showing that the mutations did not cause any significant changes in secondary structure.

2.2. Production of recombinant PHOSPHO2 protein

DNA corresponding to PHOSPHO2 was amplified from human genomic DNA as the whole coding sequence was found to be on the same exon. The DNA fragment was subcloned into the pBAD TOPO TA vector. The construct was designed to express PHOSPHO2 fused to a 6-His tag at the C-terminus. A clone (pBAD-PHOSPHO2) containing the PHOSPHO2 fragment in the correct orientation was identified by restriction digestion of plasmid minipreps. The *E. coli* cells were grown in Luria–Bertani broth (10 l, 37 °C) and recombinant protein expression was induced by treatment with 0.1% (w/v) L-arabinose for 4 h. Bacteria were harvested by centrifugation and were resuspended in a lysis buffer containing 20 mM Tris–HCl, pH 8.0, 500 mM NaCl, 10 mM imidazole and 1.6 mg/ml of Complete® protease inhibitor cocktail (Roche). Cells were lysed using a French press (16,000 psi, 16 °C). A clarified lysate was prepared by centrifugation at 20,000×*g* for 1 h. Purification of the PHOSPHO2 enzyme was carried using the same method as that described for the recombinant PHOSPHO1 mutant protein. The fraction containing the pure recombinant protein was then dialysed three times in TBS, pH 7.2 (5 l, 4 °C, 24 h) and stored at 4 °C prior to use.

2.3. Phosphatase assays

Phosphatase assays were carried out as described previously [5] in order to provide a direct comparison with human PHOSPHO1. The standard discontinuous colorimetric assay is based on that of Baykov et al. [16]. The

reactions were measured in 96-well plates containing 200 μl of 25% (w/v) glycerol, 20 mM respective buffer, 25 μg/ml bovine serum albumin, 2.5 mM substrate, 2 mM $MgCl_2$ and 600 ng of purified recombinant enzyme. Buffers used were 20 mM MES, pH 6.7 for the PHOSPHO1 and mutants assays and 20 mM Tris–HCl for the PHOSPHO2 experiments to allow the direct comparison with previous results. Standard solutions containing known concentrations of KH_2PO_4 were included in each plate. Reactions were allowed to proceed for 15 min at 37 °C then stopped by the addition of 50 μl of 3.75 M sulphuric acid containing 3% ammonium molybdate, 0.2% Tween 20 and 0.12% malachite green. The absorbance of each well at 630 nm was measured and the specific activity was calculated in units of activity per mg of enzyme, where 1 unit of activity represents the hydrolysis of 1 nmol of phosphate per min.

The continuous spectrophotometric assay was performed using the EnzChek® Phosphatase Assay Kit (Molecular Probes). The reactions were measured in 96-well plates containing 25% (w/v) glycerol, 20 mM MES, pH 6.7 (20 mM Tris, pH 7.2 for PHOSPHO2), 500 mM NaCl, 2 mM $MgCl_2$, 0.2 units purine nucleoside phosphorylase (PNPase), 200 μM 2-amino-6-mercapto-7-methylpurine ribonucleoside (MESG) and 650 ng of PHOSPHO1 or 10 μg PHOSPHO2 at 37 °C. The concentration of PEA was varied from 2 μM to 100 μM for PHOSPHO1 and from 2 μM to 150 μM for PHOSPHO2. PNPase and MESG concentrations were optimised to ensure that the phosphatase activity was rate-limiting. PHOSPHO1 substrate concentrations were varied accordingly. Absorbances were measured continuously at 355 nm using a VICTOR HTS plate-reader.

2.4. Structural modelling and ligand docking

The protein sequence of PHOSPHO2 was subjected to homology modelling as described previously for PHOSPHO1 [4]. Submitting the protein sequence of human PHOSPHO2 to the 3D-PSSM fold recognition server [17] revealed the high resolution (1.8 Å) X-ray structure of phosphoserine phosphatase (*Mj*PSP) from *Methanococcus jannaschii* (PDB code: 1F5S) [18] as the most suitable template for homology modelling. A pairwise alignment between the target and template sequence was manually adjusted, taking into consideration multiple sequence alignments, structural alignments and the continuity of secondary structure elements (Fig. 2). Twenty models were built using MODELLER v6.2 [19], keeping the active site Mg^{2+} and its bound phosphate and water molecules in the positions found in the template. A disulfide bridge was introduced between Cys152 and Cys185, both of which are conserved within the PHOSPHO1/PHOSPHO2 multiple sequence alignment (Fig. 1), since these residues were found in close proximity to each other in the structural model. Non-identical side-chains between template and target were optimised using SCWRL [20].

Hydrogen atoms and bonds between Mg^{2+} and its coordinating amino acids were introduced in SYBYL v.6.9 (Tripos Associates, St. Louis). The resulting pdb files were used as input files for FlexX [21]. Based on our

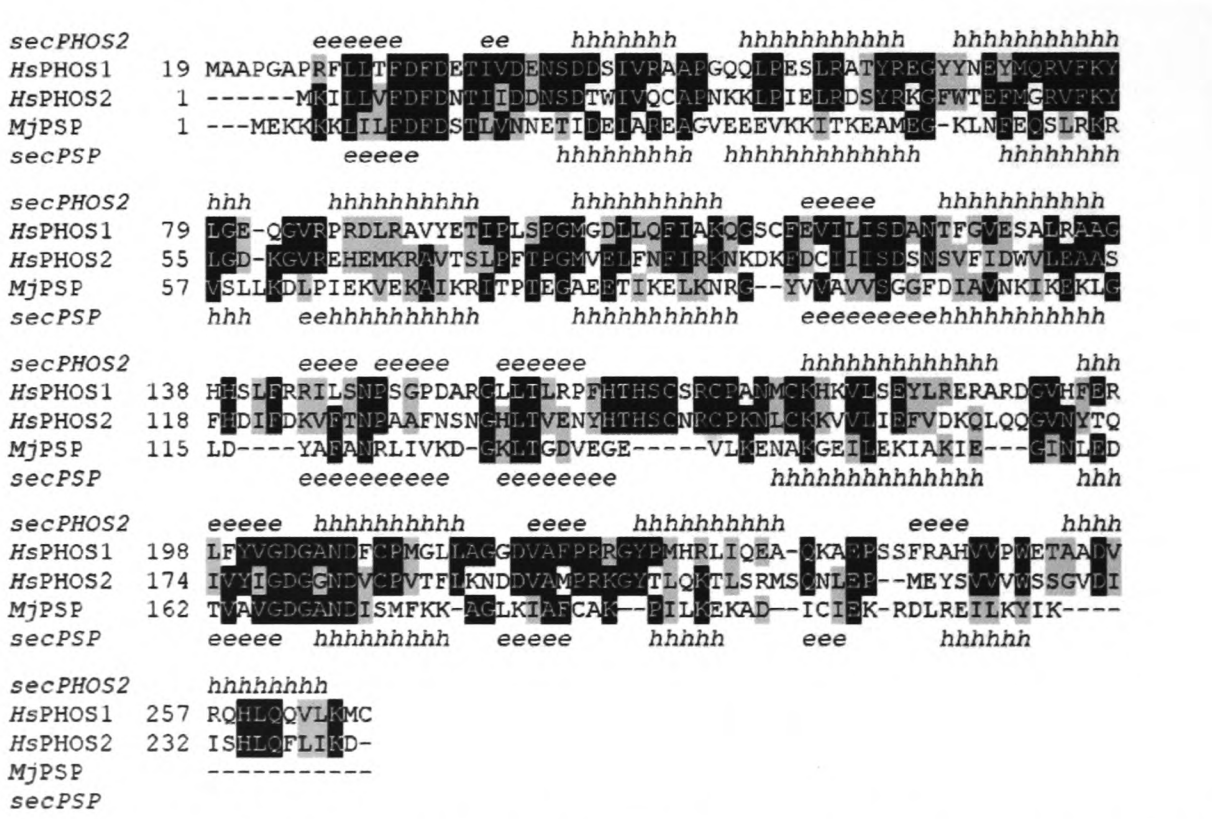

Fig. 2. Alignment of *Hs*PHOSPHO1, *Hs*PHOSPHO2 and the scaffold protein *Mj*PSP, showing the secondary structure for PSP and secondary structure prediction for PHOSPHO2. The following sequences are used (accession numbers are shown in parentheses): *Hs*PHOS1, human PHOSPHO1 (Q8TCT1); *Hs*PHOS2, human PHOSPHO2 (Q8TCD6); *Mj*PSP, phosphoserine phosphatase from *Methanococcus jannaschii* (Q58989). Secondary structure elements for PHOSPHO2 (secPHOS2) and MjPSP (secPSP) are denoted as h=α-helix, e=β-strand. Black shading indicates identical, and grey shading highly similar amino acid residues.

Table 1
Specific activities of recombinant human PHOSPHO1 mutants

Protein	Specific activity (units/mg) PEA	PCho
Wild-type	4959±327	2203±147
D32N	<0.1	<0.1
D203S	<0.1	<0.1
D43N	92±42	<0.1
D123N	277±12	40±18
D43N/D123N	<0.1	<0.1

Wild-type recombinant human PHOSPHO1 and the five mutants (3 μg/ml) were incubated with 2.5 mM PEA or PCho and assayed for phosphatase activity by the discontinuous assay at 37 °C. The 200-μl reaction mixture contained 25% (w/v) glycerol, 20 mM TBS, pH 7.2, 25 μg/ml BSA, 2.5 mM substrate and 2 mM $MgCl_2$. The results are the averages of triplicate assays.

previous findings [4], the active sites were defined manually, and included the Mg^{2+} ion, the two water molecules, the residues 32, 34, 43, 60, 64, 71 and 123 for PHOSPHO1, or 8, 10, 19, 36, 40, 47 and 99 for PHOSPHO2, plus a 2.9-Å margin around these residues. Substrate starting structures (PEA, PCho, and pyridoxal-5-phosphate) were built and energy-minimised in SYBYL v6.9. As our initial homology models were necessarily generated without a substrate in the active site, it appears as if the sidechain of Arg60 (or Arg36) is trying to fill the "empty space" of the active site. Therefore, for subsequent FlexX runs, the side-chain of this residue was manually adjusted. Thirty docked structures were generated for each protein, and the best was selected based on the overall FlexX score. The resulting protein–substrate complexes were energy-minimised in SYBYL v6.9 applying 50 steps of minimisation, restricted to the substrate, the Mg^{2+} ion, and Arg60 for PHOSPHO1 or Arg36 for PHOSPHO2 and their immediate surroundings, followed by 100 steps of energy minimisation applied to the entire protein. The minimisation protocol used the Powell algorithm and an improved version of the Tripos force-field. The validity of the resulting model was assessed using PROCHECK v3.5 [22] and WHAT IF v4.99 [23], which are available on-line at the "Biotech validation suite" at http://biotech.embl-ebi.ac.uk. The validity of this approach was tested by docking phospho-L-serine into *Mj*PSP (PDB code: 1F5S). The resulting docked model corresponded well with the structure of the D11N mutant of *Mj*PSP with bound substrate (PDB code: 1L7P).

3. Results

3.1. PEA and PCho phosphatase activity in PHOSPHO1 mutants

Phosphatase activities toward PEA and PCho were assayed using the standard discontinuous assay for the five PHOSPHO1 mutants. The resultant specific activities are shown in Table 1. No detectable phosphatase activity was observed with either of the two active site mutations (D32N and D203S). Mutations of Asp43 (D43N) and Asp123 (D123N) dramatically decreased the reactivity toward both substrates when compared with the wild-type enzyme, the D123N mutation reduced activity ~20-fold for PEA and ~60-fold for PCho. The D43N mutation reduced activity ~60-fold for PEA, whilst no activity was observed with PCho. No activity was detected with the double mutant, D43N/D123N-PHOSPHO1, with either substrate.

The reaction with PEA catalysed by the D43N mutant was too slow to allow accurate determination of the kinetic

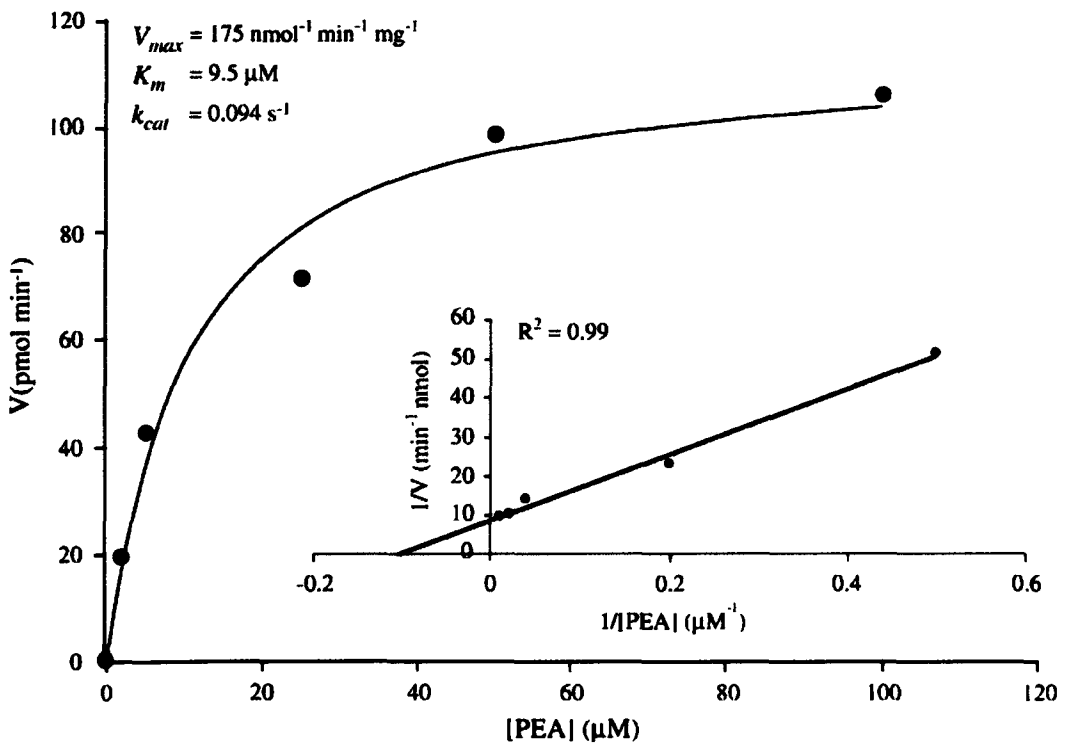

Fig. 3. Kinetic analysis of the hydrolysis reactions catalysed by recombinant PHOSPHO1 D123N mutant. Plot of the reaction velocity (V) as a function of substrate concentration. *Inset*, Lineweaver–Burke plot from which K_m and V_{max} values were calculated. Kinetic activity toward phosphoethanolamine was measured using a method based upon the PNPase-coupled assay [5] as described under Materials and methods.

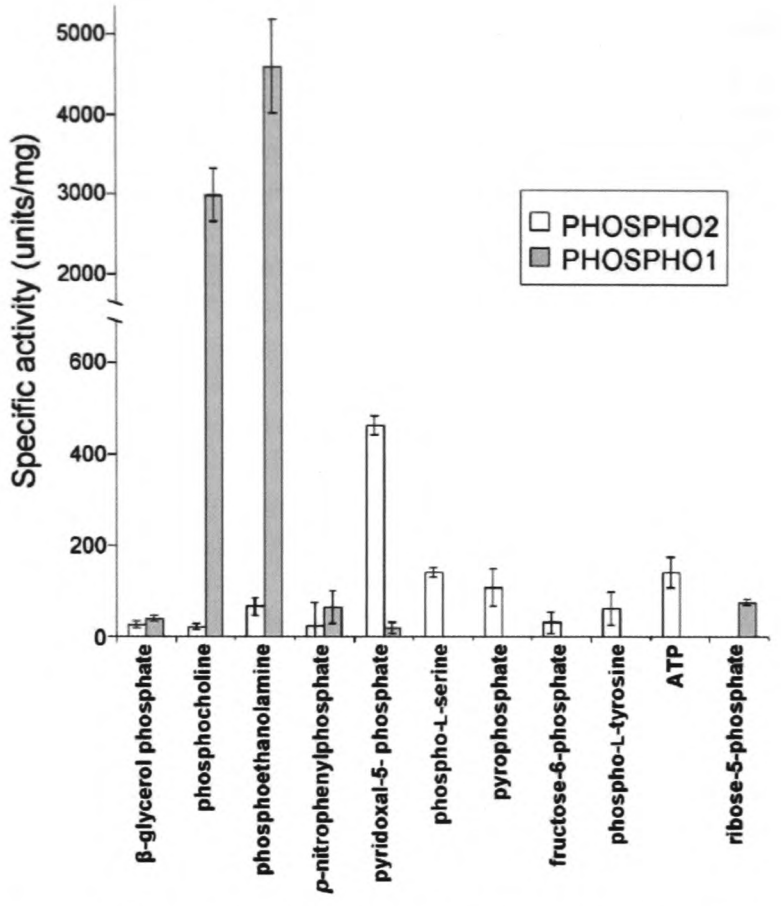

Fig. 4. Specific activities of PHOSPHO2 and PHOSPHO1 in the presence of a range of substrates. PHOSPHO1 data were taken from ref [5]. Activities for PHOSPHO2 were determined using the same method and under the same conditions as described previously to allow a direct comparison with the previously published results for PHOSPHO1.

parameters. However, the kinetic constants were determined for recombinant D123N-PHOSPHO1-catalysed hydrolysis of PEA in the presence of 2 mM Mg^{2+} at 37 °C. The reaction exhibited Michaelis–Menten kinetics. A plot of reaction rate versus PEA concentration and also a Lineweaver–Burke plot for the D123N-PHOSPHO1-catalysed reaction are shown in Fig. 3. The enzyme displayed apparent K_m, V_{max} and k_{cat} values of 9.5 μM, 175 nmol min^{-1} mg^{-1} and 0.094 s^{-1}, respectively.

3.2. Substrate specificity of recombinant PHOSPHO2 protein

Eleven phosphate compounds were investigated as potential substrates for human PHOSPHO2. A comparison of the resultant specific activities with those previously reported for human PHOSPHO1 [5] is shown in Fig. 4. Of the phosphate compounds tested, pyridoxal-5-phosphate (P5P) was hydrolysed by PHOSPHO2 with the highest specific activity (464.1±19.5 units/mg), which was approximately 3 times higher than that towards ATP and phospho-L-serine. PHOSPHO2 also hydrolysed pyrophosphate, PEA, phospho-L-tyrosine, fructose-6-phosphate, *p*-nitrophenyl phosphate, β-glycerophosphate and PCho. No hydrolysis of ribose-5-phosphate was observed in the presence of PHOSPHO2. PHOSPHO1 has previously been shown to have high specific activities toward PEA and PCho (4600±582 and 2980±335 units/mg, respectively). Five of the potential substrates that previously yielded no detectable phosphatase activity with PHOSPHO1 showed activity with PHOSPHO2 (pyrophosphate, phospho-L-serine, fructose-6-phosphate, phospho-L-tyrosine and ATP).

Kinetic constants were determined for recombinant PHOSPHO2-catalysed hydrolysis of P5P in the presence of 2 mM Mg^{2+} at 37 °C. The reaction exhibited Michaelis–Menten kinetics. A plot of reaction rate versus PEA

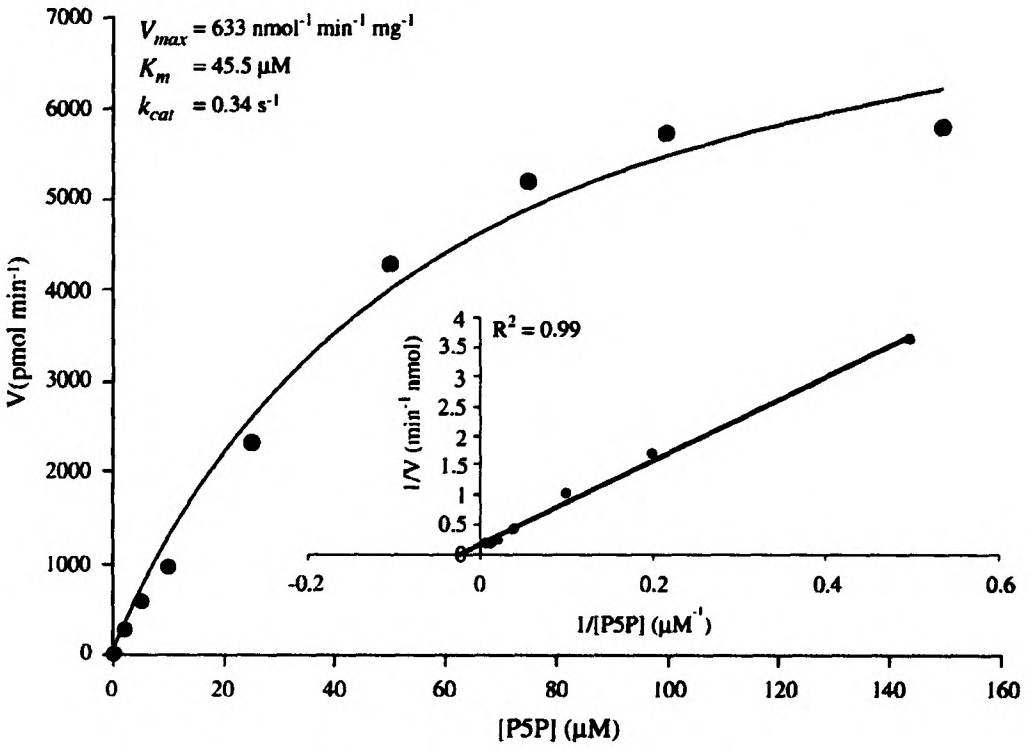

Fig. 5. Kinetic analysis of the hydrolysis reactions catalysed by recombinant PHOSPHO2. Plot of the reaction velocity (V) as a function of substrate concentration. Inset, Lineweaver–Burke plot from which K_m and V_{max} values were calculated. Kinetic activity toward pyridoxal-5-phosphate was measured using a method based upon the PNPase-coupled assay [5] as described under Materials and methods.

concentration and also a Lineweaver–Burke plot for the PHOSPHO2-catalysed reaction are shown in Fig. 5. The enzyme displayed apparent K_m, V_{max} and k_{cat} values of 45.5 μM, 633.3 nmol min^{-1} mg^{-1} and 0.34 s^{-1}, respectively.

3.3. Homology model of PHOSPHO2

In the absence of structural data for PHOSPHO2, a three-dimensional model was built based on the X-ray crystal structure coordinates of *Mj*PSP (PDB: 1F5S). Sequence identity between *Mj*PSP and PHOSPHO1 is 19.4% whilst identity between *Mj*PSP and PHOSPHO2 is 18.0%. Despite the low sequence identity, fold recognition strongly suggests that PHOSPHO2 (and PHOSPHO1) and PSPs belong to the same fold (alignment shown in Fig. 2), therefore allowing us to build a meaningful structural model (Fig. 6). The protein model consists of two domains: the catalytic α/β domain and a four-helix-bundle. The α/β domain forms a Rossman fold structure consisting of a six-stranded parallel β-sheet, surrounded by six α-helices.

3.4. Ligand docking

The homology models of PHOSPHO2 and PHOSPHO1 were subjected to in silico docking calculations, a model of PHOSPHO2 incorporating P5P as substrate is presented in Fig. 6, compared to the structure of the D11N mutant of *Mj*PSP (PDB:1L7P). In this model, a hexadentate Mg^{2+} ion is bound in an octahedral geometry via three Asp residues (Asp8, Asp10 (backbone oxygen) and Asp179), O-ligands are also provided by the phosphate group of P5P and two water molecules.

Previous modelling studies of PHOSPHO1 suggested that as well as Asp43 and Asp123, two additional residues, Arg60 and Tyr71, also line the substrate-binding pocket [4]. A comparison of this region in both the PHOSPHO1 and PHOSPHO2 models is shown in Fig. 7. The active sites of PHOSPHO1 and PHOSPHO2 in our models are very similar. Apart from the conserved Mg^{2+}-binding site (side-chains of Asp8 and Asp179, backbone-CO of Asp10 in PHOSPHO2), and phosphate-binding site (backbone-NH of Phe9, side-chains of Ser98, Lys153 and Asn182; PHOSPHO2), residues in or close to the predicted substrate pocket are: Asn11, Asn17, Asp19, Thr20, Arg36, Tyr39, Arg40, Phe47, Tyr54, Asp99, and Ser100 in PHOSPHO2 (corresponding to Glu35, Asn41, Asp43, Asp44, Arg60, Tyr63, Arg64, Tyr71, Tyr78, Asp123 and Ala124 in PHOSPHO1 respectively).

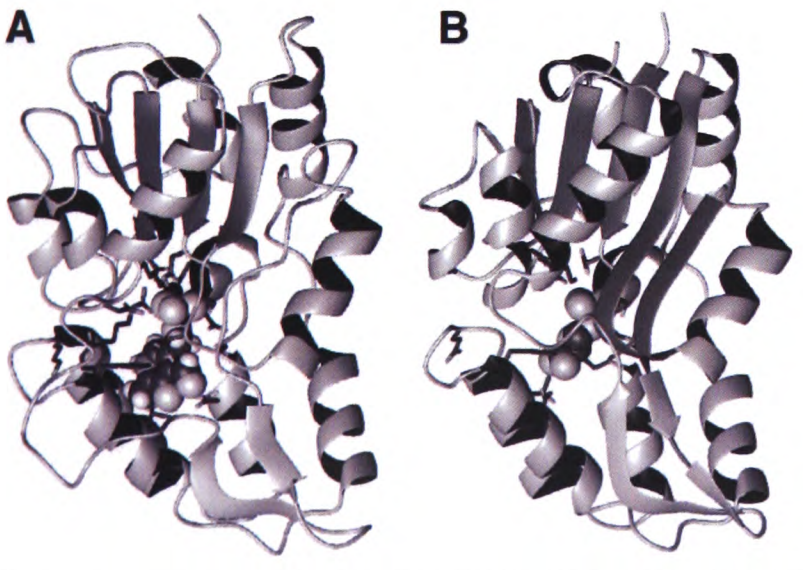

Fig. 6. Comparison of the PHOSPHO2 model structure (A) with the crystal structure of phosphoserine phosphatase from *Methanococcus jannaschii* with bound phospho-L-serine (B; *Mj*PSP; PDB code: 1L7P). Pyridoxal-5-phosphate was modelled into the catalytic site of PHOSPHO2 as this was found to be the best substrate for PHOSPHO2 of those tested.

4. Discussion

Mutation of active-site residues Asp32 (D32N) and Asp203 (D203S) of PHOSPHO1 resulted in a complete loss of activity toward PEA and PCho. This observation is a hallmark for HAD superfamily proteins [24–28], and confirms PHOSPHO1 as a member of this family. PHOSPHO1-induced hydrolysis of PEA and PCho is therefore likely to be catalysed by the same Mg^{2+}-dependent mechanism as other HAD-like phosphatases. The substitutions D32N and D203S are likely to have dramatically reduced the affinity of Mg^{2+} towards the site, whilst the D32N mutation would also prevent the formation of a phospho-protein intermediate during the reaction.

The mutations D43N and D123N also greatly affected PHOSPHO1 activity towards PEA and PCho. Both mutations reduced the specific activity, by varied degrees toward PEA and PCho, with D43N having the more pronounced effect. The double mutant, D43N/D123N, exhibited no activity toward either PEA or PCho. Kinetic analysis revealed that PEA hydrolysis by the D123N mutant is reduced by a factor of 24 compared to wild type PHOSPHO1 under the same conditions [5]. This suggests that Asp123 is important for hydrolysis of PEA. The mutation of Asp123 has only a moderate effect on substrate binding (reduction of K_m by a factor of ca. 3). The K_m value is, under true Michaelis–Menten conditions, an estimate for the dissociation constant of enzyme and substrate. A probable explanation for these kinetic data is that Asp123 of PHOSPHO1 does not interact directly with the substrate but plays a similar role to that of Glu20 in *Mj*PSP, which stabilises an attacking nucleophilic water molecule during phosphoserine hydrolysis and is conserved in all known PSPs [12]. Such a role for Asp123 during the reaction would account for the relatively larger difference in V_{max} and k_{cat} values and small difference in K_m value observed between the D123N mutant and wild type enzyme. The D43N mutation has a much more dramatic effect than D123N. No activity toward PCho was observed with the D43N mutant and activity toward PEA was reduced ~60-fold compared to wild type. This suggests that Asp43 is a more likely candidate than Asp123 to directly interact with the substrate.

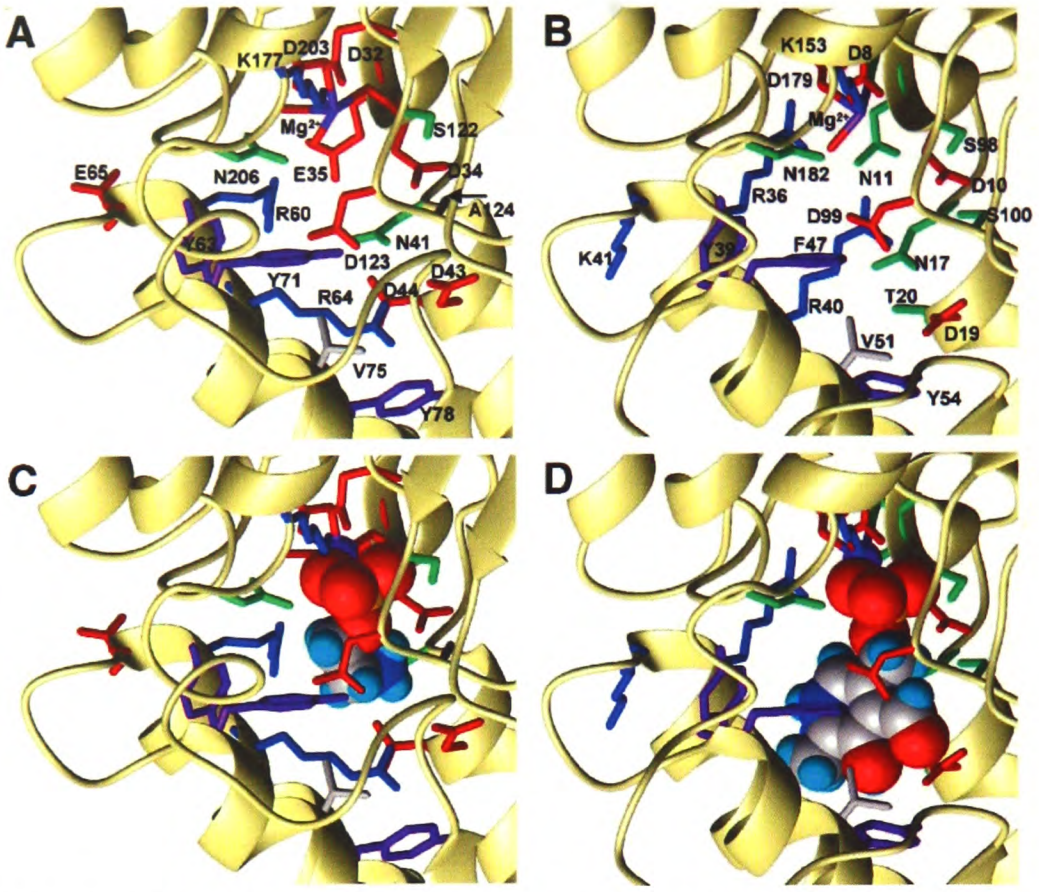

Fig. 7. Models of the active sites of PHOSPHO1 without and with phosphoethanolamine (A and C) and PHOSPHO2 with pyridoxal-5-phosphate (B and D), respectively. Key residues around the sites likely to be involved in substrate binding and catalysis are shown. Amino acid residues are coloured according to type: negatively charged (red), positively charged (blue), hydrophilic uncharged (green), aromatic (violet) and hydrophobic (grey). Atoms of the ligands are coloured as follows: hydrogen (cyan), carbon (grey), nitrogen (blue), oxygen (red), phosphorus (orange); the magnesium ion is shown in purple.

Such an interaction would presumably be more important for the binding of the bulkier choline moiety of PCho than the smaller ethanolamine moiety of PEA as our results suggest.

Recombinant PHOSPHO2 protein was assayed for phosphatase activity in the presence of a number of phosphomonoesters. Surprisingly, activities toward PEA and PCho were ~100 times lower for PHOSPHO2 compared to PHOSPHO1 under the same conditions [5]. The highest activity corresponded to the hydrolysis of P5P (ca. 464.1±19.5 nmol min^{-1} mg^{-1}). This activity is ~10-fold less than that measured for PHOSPHO1 catalysed hydrolysis of PEA under the same conditions. The relatively low K_m (ca. 45.5 μM) suggests that this molecule may be hydrolysed by PHOSPHO2 in vivo, however the existence of a more specific ligand is conceivable.

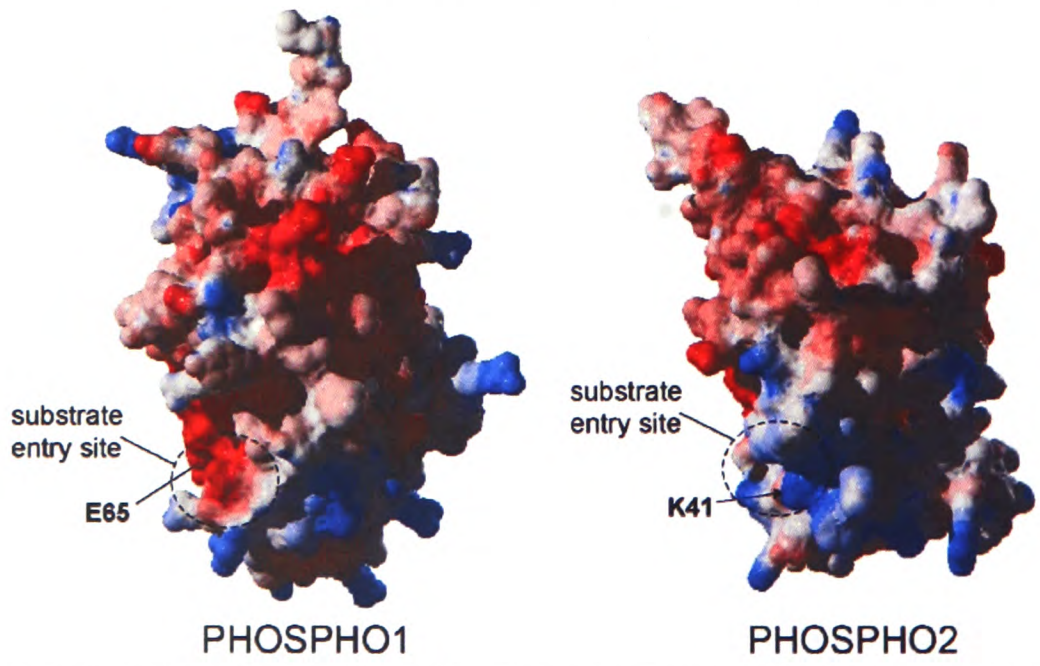

Fig. 8. Electrostatic potential surfaces for PHOSPHO1 (left) and PHOSPHO2 (right). Negative and positive potentials on the surface of each protein are shown in red and blue, respectively. The models suggest that a large difference in potential exists between the two proteins around the entrance to their catalytic sites. The large negative charge at this region of PHOSPHO1 is partly due to Glu65, which corresponds to a positively charged Lys41 in PHOSPHO2.

These results show that despite the overall high level of identity (ca. 42%), PHOSPHO1 and PHOSPHO2 are distinct enzymes with different substrate specificities. Even though high sequence similarity in proteins with distinct functions is well documented [29], it is surprising that two related enzymes that share such close similarity outwith the catalytic motifs have such different specificities.

We have modelled the human PHOSPHO2 protein based on the crystal structure of *Mj*PSP to better understand why these two proteins are functionally distinct. The model shows that the characteristic features of the catalytic site found in the HAD superfamily are all preserved. This includes all residues involved in the recognition of the phosphate group in *Mj*PSP, with the exception of Gly100 (in PSP), which is replaced by Asp99 (in PHOSPHO2). Considering that only the backbone oxygen of this residue is involved in substrate binding in PSP, the modelled catalytic site in PHOSPHO2 closely resembles the catalytic site in *Mj*PSP [18]. The models including bound substrate molecules have been generated by in silico docking. The conformation shown for each substrate is just one of many possible, but is probably a reasonable representation of the general orientations of the molecules. Although no restraints were used during the docking procedure, the interactions between the phosphate group and the amino acid side-chains (Ser122, Lys177, Asn206 for PHOSPHO1 or Ser98, Lys153 and Asn182 for PHOSPHO2) agree very well with those observed in the X-ray structures of related phosphatases [12,18,30]. The situation is slightly more complicated for the remainder of the binding pocket, as the residues defining the "non-phosphate" moiety of the substrate-binding site are not conserved between our template and the two target proteins. Although it is therefore not possible to predict reliably the orientation of the side-chains of these residues, the models allow us to define the residues lining the binding pocket and to predict some of the interactions likely to define substrate specificities. In the theoretical PHOSPHO1/PEA model, the negatively charged side-chains of Asp34, Asp43, and Asp123 are all in the vicinity of the positively charged ammonium group of PEA, potentially providing both a highly negatively charged pocket as well as H-bond acceptor atoms. These interactions are consistent with the decrease in activity for the D43N, the D123N, and the D43N/D123N mutants. Residues in or near the substrate pocket that are not highly conserved between PHOSPHO2 and PHOSPHO1 are Asn11/Glu35, Thr20/Asp44, Ser100/Ala124 and Phe47/Tyr71. Of these, only Thr20/Asp44 and Ser100/Ala124 are fully conserved within the two subfamilies. With the exception of chicken PHOSPHO1, Glu35 is also conserved within the PHOSPHO1 subfamily; PHOSPHO2 proteins carry either an Asn or a His residue at this position. In the case of Tyr71, there does not appear to be any specific conservation within sub-families. Clearly, the binding site of PHOSPHO1 is more negatively charged than that of PHOSPHO2, and there are subtle changes in the location of potential H-bond donors. In addition, the surface charges of the putative entry sites are also different (Fig. 8): whilst Glu65 in PHOSPHO1 renders the surface rather negative, the respective Lys41 residue in PHOSPHO2 has the opposite effect. Again, these amino acids are fully conserved within their respective sub-families. Changes in surface charges are likely to contribute to the rate of both ligand binding and product release.

Our experimental findings clearly demonstrate that the two enzymes, PHOSPHO1 and PHOSPHO2, have different substrate specificities. Structural modelling has helped to identify subtle differences inside the substrate-binding pockets and on the surfaces of the active sites. Given the overall high similarity between PHOSPHO1 and PHOSPHO2, it was important to elucidate whether or not the enzymes had similar activities. PHOSPHO1 is associated with high levels of expression at mineralising regions of bone and cartilage. The discovery of another phosphatase with comparable PEA and PCho phosphatase activity would have given rise to serious questions regarding a role in mineralisation for PHOSPHO1 as gene expression studies carried out in chicken and EST analysis in mammals have shown that PHOSPHO2 expression is not specific to bone (data not shown) and is indeed expressed in a wide range of soft tissues. In addition, functional redundancy would likely complicate future gene knockout and inhibitory experiments. Furthermore, this is the first investigation of human PHOSPHO2 structure and activity, providing a platform for the further study of this enzyme.

Acknowledgements

We thank the Wellcome Trust for support for the Edinburgh Protein Interaction Centre, Dr. John White for his assistance with the expression of recombinant protein, Dr. Sharon Kelly from the Scottish Circular Dichroism Facility, University of Glasgow, for secondary structure analysis of the recombinant proteins using CD. We also thank BBSRC for funding and Immunodiagnostic Systems Ltd., Boldon, UK for a Cooperative Awards in Science and Engineering (CASE) award (to S.J.R.).

References

[1] B. Houston, E. Seawright, D. Jefferies, E. Hoogland, D. Lester, C. Whitehead, C. Farquharson, Identification and cloning of a novel phosphatase expressed at high levels in differentiating growth plate chondrocytes, Biochim. Biophys. Acta 1448 (1999) 500–506.

[2] B. Houston, A.J. Stewart, C. Farquharson, PHOSPHO1-A novel phosphatase specifically expressed at sites of mineralisation in bone and cartilage, Bone 34 (2004) 629–637.

[3] B. Houston, I.R. Paton, D.W. Burt, C. Farquharson, Chromosomal localisation of the chicken and mammalian orthologues of the orphan phosphatase PHOSPHO1 gene, Anim. Genet. 33 (2002) 451–454.

[4] A.J. Stewart, R. Schmid, C.A. Blindauer, S.J. Paisey, C. Farquharson, Comparative modelling of human PHOSPHO1 reveals a new group of phosphatases within the haloacid dehalogenase superfamily, Protein Eng. 16 (2003) 889–895.

[5] S.J Roberts, A.J. Stewart, P.J. Sadler, C. Farquharson, Human PHOSPHO1 exhibits high specific phosphoethanolamine and phosphocholine phosphatase activities, Biochem. J. 382 (2004) 59–65.
[6] O.B. Bleijerveld, W. Klein, A.B. Vaandrager, J.B. Helms, M. Houweling, Control of the CDPethanolamine pathway in mammalian cells: effect of CTP: phosphoethanolamine cytidylyltransferase overexpression and the amount of intracellular diacylglycerol, Biochem. J. 379 (2004) 711–719.
[7] C. Kent, CTP: phosphocholine cytidylyltransferase, Biochim. Biophys. Acta 1348 (1997) 79–90.
[8] B.J. Kvam, P. Pollesello, F. Vittur, S. Paoletti, ^{31}P NMR studies of resting zone cartilage from growth plate, Magn. Reson. Med. 25 (1992) 355–361.
[9] S.B. Kaplan, S.S. Kemp, K.S. Oh, Radiographic manifestations of congenital anomalies of the skull, Radiol. Clin. North Am. 29 (1991) 195–218.
[10] K. Boström, Insights into the mechanism of vascular calcification, Am. J. Cardiol. 88 (Suppl. 1) (2001) 20E–22E.
[11] I.S. Ridder, B.W. Dijkstra, Identification of the Mg^{2+}-binding site in the P-type ATPase and phosphatase members of the HAD (haloacid dehalogenase) superfamily by structural similarity to the response regulator protein CheY, Biochem. J. 339 (1999) 223–226.
[12] W. Wang, H.S. Cho, R. Kim, J. Jancarik, H. Yokota, H.H Nguyen, I. Grigoriev, D.E. Wemmer, S.-H. Kim, Structural characterization of the reaction pathway in phosphoserine phosphatase: crystallographic "snapshots" of intermediate states, J. Mol. Biol. 319 (2002) 421–431.
[13] J.-F. Collet, V. Stroobant, E. van Schaftingen, Mechanistic studies of phosphoserine phosphatase, an enzyme related to P-type ATPases, J. Biol. Chem. 274 (1999) 33985–33990.
[14] J.D. Bendtsen, H. Nielsen, G. von Heijne, S. Brunak, Improved prediction of signal peptides: SignalP 3.0, J. Mol. Biol. 340 (2004) 783–795.
[15] N. Sreerama, R.W. Woody, Poly(pro)II helices in globular proteins: identification and circular dichroic analysis, Biochemistry 33 (1994) 10022–10025.
[16] A.A. Baykov, O.A. Evtushenko, S.M. Avaeva, A malachite green procedure for orthophosphate determination and its use in alkaline phosphatase-based enzyme immunoassay, Anal. Biochem. 171 (1988) 266–270.
[17] L.A. Kelley, R.M. MacCallum, M.J. Sternberg, Enhanced genome annotation using structural profiles in the program 3D-PSSM, Mol. Biol. 299 (2000) 499–520.
[18] W. Wang, R. Kim, J. Jancarik, H. Yokota, S.-H. Kim, Crystal structure of phosphoserine phosphatase from *Methanococcus jannaschii*, a hyperthermophile, at 1.8 Å resolution, Structure 10 (2001) 65–71.
[19] A. Sali, T.L. Blundell, Comparative protein modelling by satisfaction of spatial restraints, J. Mol. Biol. 234 (1993) 779–815.
[20] M.J. Bower, F.E. Cohen, R.L. Dunbrack, Prediction of protein side-chain rotamers from a backbone-dependent rotamer library: a new homology modeling tool, J. Mol. Biol. 267 (1997) 1268–1282.
[21] M. Rarey, B. Kramer, T. Lengauer, G. Klebe, A fast flexible docking method using an incremental construction algorithm, J. Mol. Biol. 261 (1996) 470–489.
[22] R.A. Laskowsky, M.W. McArthur, D.S. Moss, J.M. Thornton, PROCHECK: a program to check the stereochemical quality of protein structures, J. Appl. Crystallogr. 26 (1993) 283–291.
[23] G. Vriend, WHAT IF: a molecular modeling and drug design program, J. Mol. Graph. 8 (1990) 52–55.
[24] J.D. Selengut, MDP-1 is a new and distinct member of the haloacid dehalogenase family of aspartate-dependent phosphohydrolases, Biochemistry 40 (2001) 12704–12711.
[25] L. Aravind, M.Y. Galperin, E.V. Koonin, The catalytic domain of the P-type ATPase has the haloacid dehalogenase fold, Trends Biochem. Sci. 23 (1998) 127–129.
[26] T.L. Tootle, S.J. Silver, E.L. Davies, V. Newman, R.R. Latek, I.A. Mills, J.D. Selengut, B.E. Parlikar, I. Rebay, The transcription factor Eyes absent is a protein tyrosine phosphatase, Nature 426 (2003) 299–302.
[27] D.M. Clarke, T.W. Loo, D.H. MacLennan, Functional consequences of alterations to amino acids located in the nucleotide binding domain of the Ca2(+)-ATPase of sarcoplasmic reticulum, J. Biol. Chem. 265 (1990) 22223–22227.
[28] K. Maruyama, D.M. Clarke, J. Fujii, G. Inesi, T.W. Loo, D.H. MacLennan, Functional consequences of alterations to amino acids located in the catalytic center (isoleucine 348 to threonine 357) and nucleotide-binding domain of the Ca^{2+}-ATPase of sarcoplasmic reticulum, J. Biol. Chem. 264 (1989) 13038–13042.
[29] C.A. Orengo, T.P. Flores, D.T. Jones, W.R. Taylor, J.M. Thornton, Recurring structural motifs in proteins with different functions, Curr. Biol. 3 (1993) 131–139.
[30] H.Y. Kim, Y.S. Heo, J.H. Kim, M.H. Park, J. Moon, E. Kim, D. Kwon, J. Yoon, D. Shin, E.J. Jeong, et al., Molecular basis for the local conformational rearrangement of human phosphoserine phosphatase, J. Biol. Chem. 277 (2002) 46651–46658.

ELSEVIER

Bone 39 (2006) 1000–1007

BONE

www.elsevier.com/locate/bone

The presence of PHOSPHO1 in matrix vesicles and its developmental expression prior to skeletal mineralization

Alan J. Stewart [1], Scott J. Roberts [1], Elaine Seawright, Megan G. Davey, Robert H. Fleming, Colin Farquharson *

Roslin Institute, Roslin, Midlothian, EH25 9PS, United Kingdom

Received 2 February 2006; revised 12 April 2006; accepted 15 May 2006
Available online 11 July 2006

Abstract

PHOSPHO1 is a phosphoethanolamine/phosphocholine phosphatase that has previously been implicated in generating inorganic phosphate (P_i) for matrix mineralization. In this study, we have investigated PHOSPHO1 mRNA expression during embryonic development in the chick. Whole-mount in situ hybridization indicated that PHOSPHO1 expression occurred prior to E6.5 and was initially restricted to the bone collar within the mid-shaft of the diaphysis of long bones but by E11.5 expression was observed over the entire length of the diaphysis. Alcian blue/alizarin red staining revealed that PHOSPHO1 expression seen in the primary regions of ossification preceded the deposition of mineral, suggesting that it is involved in the initial events of mineral formation. We isolated MVs from growth plate chondrocytes and confirmed the presence of high levels of PHOSPHO1 by immunoblotting. Expression of PHOSPHO1, like TNAP activity, was found to be up-regulated in MVs isolated from chondrocytes induced to differentiate by the addition of ascorbic acid. This suggests that both enzymes may be regulated by similar mechanisms. These studies provide for the first time direct evidence that PHOSPHO1 is present in MVs, and its developmental expression pattern is consistent with a role in the early stages of matrix mineralization.
© 2006 Elsevier Inc. All rights reserved.

Keywords: Bone; Gene expression; Matrix mineralization; PHOSPHO1; Skeletal development

Introduction

Matrix mineralization is a biphasic process that occurs in the matrix surrounding terminally differentiating chondrocytes, osteoblasts and ondontoblasts and is the mechanism by which growth plate cartilage, bone and tooth formation occurs by each of these cell types, respectively [1,2]. The initial phase concerns the formation of Ca^{2+} ions and inorganic phosphate (P_i) within matrix vesicles (MVs) [3,4]. The accumulation of Ca^{2+} is controlled by calcium binding molecules such annexins, phosphatidylserine and bone sialoprotein [5–7], however, the source of P_i is less clear. It has long been speculated that the generation of P_i results from the action of phosphatases, the most abundant being tissue non-specific alkaline phosphatase (TNAP), an isozyme of alkaline phosphatase expressed in bone, liver and kidney [4]. Once sufficient, levels of Ca^{2+} and P_i have accumulated within the MVs, calcium phosphate precipitates, before the formation of insoluble hydroxyapatite [8]. The second phase involves the breakdown of the MV membranes, which expose the preformed hydroxyapatite to the extracellular fluid.

Generation of P_i for mineralization does not appear to be entirely due to the activity of TNAP as, in newborn TNAP knockout mice, bone development and mineralization appear normal. Hypomineralization and other abnormalities do subsequently appear [9–11] but have been shown primarily to be due to a build up of inorganic pyrophosphate (PP_i), a known substrate of TNAP [12] and a potent inhibitor of hydroxyapatite crystal formation [13]. However, hypomineralization is greatly reduced in TNAP/PC-1 double-knockout mice and only observed in the long bones and not the vertebrae or cranium [11,14]. PC-1 encodes the enzyme, phosphodiesterase I, which generates PP_i from nucleotide triphosphates [15]. Additional studies have shown that TNAP can be removed from MVs without reducing their potential to mineralize

* Corresponding author. Fax: +44 131 440 0434.
E-mail address: colin.farquharson@bbsrc.ac.uk (C. Farquharson).
[1] Both authors contributed equally to this work.

8756-3282/$ - see front matter © 2006 Elsevier Inc. All rights reserved.
doi:10.1016/j.bone.2006.05.014

[16], while specific inhibitory studies on TNAP provide further evidence that other phosphatases are required for P_i generation [17].

PHOSPHO1 is a phosphatase with up-regulated expression in avian growth plate chondrocytes [18] and is localized to mineralizing regions of chick bone [19]. Since its identification in the chicken, PHOSPHO1 orthologues have also been identified in a number of other species including, humans, mice and zebrafish [20,21]. Analysis of PHOSPHO1 sequences using the web-based program SignalP v1.1 [22] predicts the absence of a signal peptide. This suggests PHOSPHO1 to be a soluble cytoplasmic phosphatase. We have recently shown that human PHOSPHO1 exhibits high specific activity toward the phospholipid metabolites, phosphoethanolamine and phosphocholine [23]. It has been demonstrated that phosphoethanolamine and phosphocholine are the two most abundant phosphomonoesters in cartilage [24]. In addition, the proportions of membrane phospholipids containing these groups decrease in MVs during mineralization, while 1,2-diacyl glycerol has been shown to accumulate, indicative of phospholipase C activity [25]. This gives rise to the possibility of a novel mechanism whereby phosphate locked within the plasma membrane may be unleashed through the action of PHOSPHO1

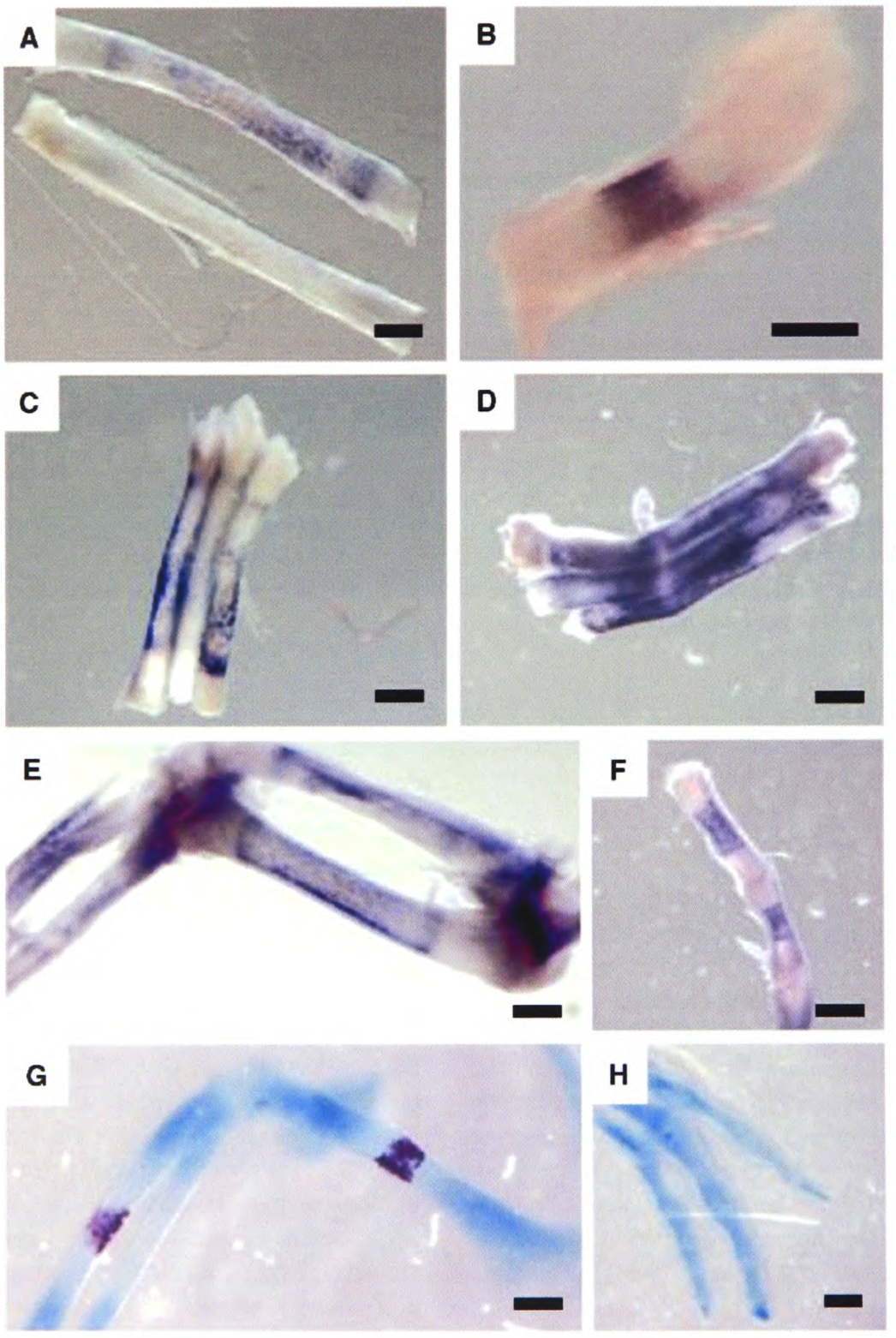

Fig. 1. Whole-mount in situ hybridization showing PHOSPHO1 mRNA expression in the long bones. (A) Metatarsi from chicken embryos (E9.5) incubated with antisense (above) and sense (below) PHOSPHO1 oligonucleotides. The staining can be seen only around the ossification center (or bone collar) of the bone from the embryo incubated with the antisense probe. (B–D) PHOSPHO1 expression in metatarsi from embryos (E6.5, E9.5 and E11.5, respectively). The region of PHOSPHO1 expression extends from the mid-shaft region to the tips between these stages. (E and F) PHOSPHO1 expression pattern in front limb (E9.5) and hind limb phalange (11.5), respectively. (G and H) Alcian blue/alizarin red staining showing the presence of cartilaginous matrix/mineral in front limb (E9.5) and hind limb phalange (11.5), respectively. Magnification bars represent 1 mm.

and phospholipase C to contribute to the P_i concentration inside the MV.

Despite the localization of PHOSPHO1 to mineralizing regions of bone in chicks, little is known about its expression in relation to the onset of mineralization during embryonic development or in adult bone. More importantly, it has also yet to be demonstrated whether PHOSPHO1 is present within MVs. In the present work, we investigate PHOSPHO1 expression from the initial stages of skeletal formation in chick embryos to adult and assay for the presence of PHOSPHO1 in

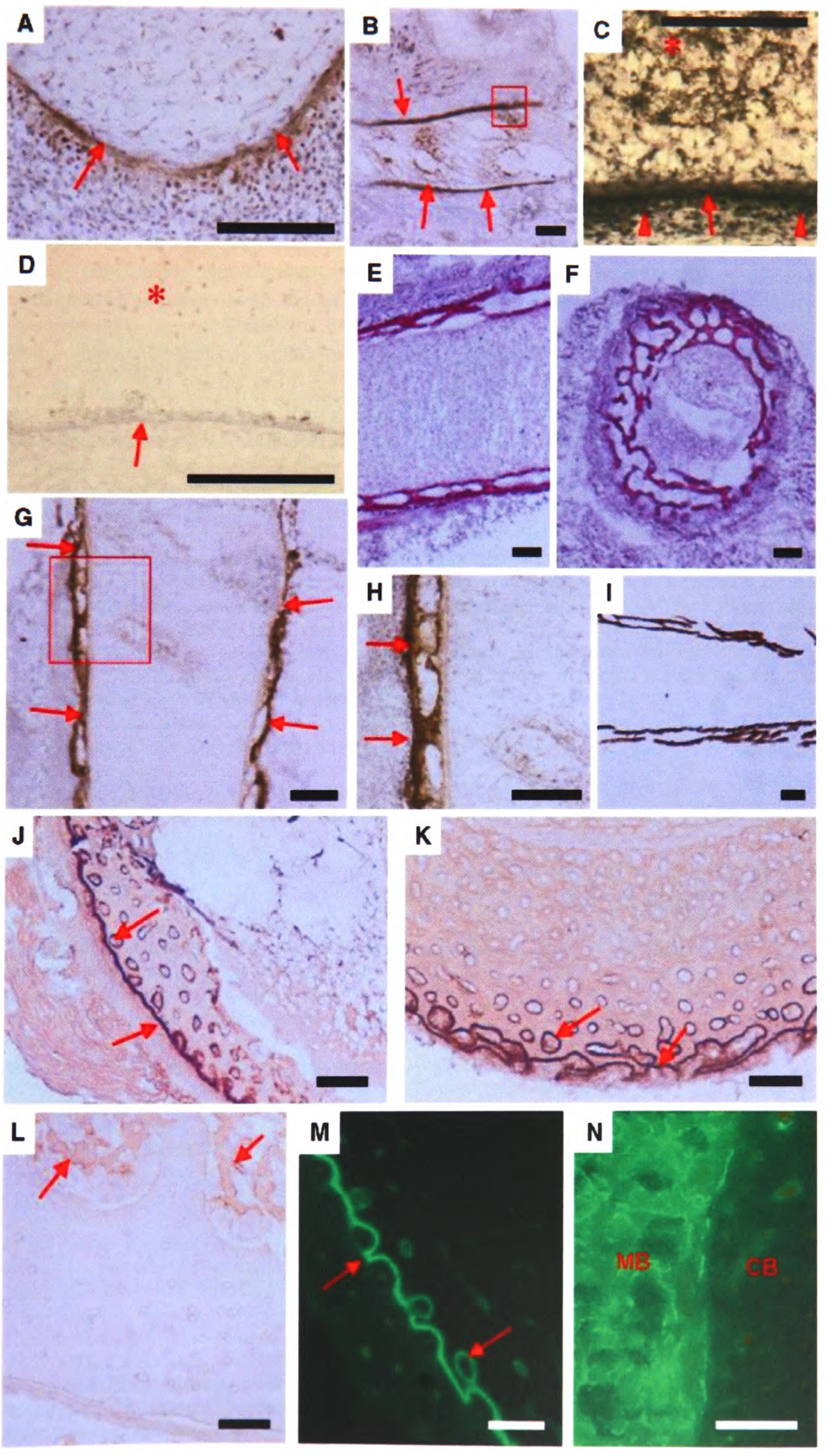

MVs isolated from the growth plate and primary chondrocyte cultures.

Materials and methods

Whole-mount in situ hybridization

A 750 bp DNA fragment corresponding to the third exon of the chicken PHOSPHO1 gene was obtained via PCR amplification of cDNA derived from RNA isolated from chick growth plate chondrocytes using primers F; ATGGCAGCTCCCGGC and R; GCAGTTCTTGAGGAGCTCCG and cloned into a pGEM-T Easy vector (Promega, Southampton, UK). Digoxigenin (DIG)-labeled sense and anti-sense RNA probes were synthesized by in vitro transcription of the DNA template in the presence of ribonucleotides using the DIG-labeling mix (Roche, Lewes, UK) with SP6 and T7 RNA polymerases (both from Roche), respectively. Embryos (E6.5, E9.5 and E11.5) were fixed in 4% paraformaldehyde/phosphate-buffered saline (PBS) overnight and dehydrated in methanol. One milliliter of 50% methanol/50% DMSO was added on ice, then 0.25 ml of 10% Triton X-100 was added and incubated at room temperature for 30 min. Embryos were then washed three times in PBT (PBS plus 0.1% Tween 20), pre-hybridized for 1 h (67°C) then hybridized at 67°C for 4 days with 5.0 μg/ml of each respective probe. Following hybridization, the embryos were washed twice in 2× SSC (300 mM NaCl, 30 mM sodium citrate, pH 7.0) at 70°C, three times in 2× SSC/0.1% CHAPS (3-[3-cholamidopropyl)dimethylammonio]-1-propanesulfonate) at 70°C, three times in 0.2 × SSC/0.1% CHAPS at 70°C and twice with KTBT (50 mM Tris–HCl, pH 7.5, 150 mM NaCl, 10 mM KCl, 1% Triton X-100) at room temperature. Embryos were blocked in 20% heat-inactivated fetal calf serum/KTBT for 3 h. Alkaline-phosphatase-conjugated mouse anti-DIG antibody (Roche) was added (1:1000 dilution) and allowed to react overnight at 4°C. The next day, the embryos were washed five times with KTBT and incubated overnight at 4°C. The embryos were washed twice in NTMT (100 mM NaCl, 100 mM Tris–HCl, pH 9.5, 50 mM MgCl, 0.1% Triton X-100) then a solution containing 3.5 μl/ml *p*-nitrotetrazolium blue, 3.5 μl/ml 5-bromo-4-chloro-3-indoyl-phosphate in NTMT was added for color detection. This reaction was carried out in the dark and was stopped by addition of 4% formal saline.

Alcian blue/alizarin red staining

The embryos (E9.5 and E11.5) were fixed in 90% ethanol, and prior to staining, skin and viscera were removed. Alcian blue solution (0.01% alcian blue, 3% acetic acid) was added to the embryos and left for 3 days. The embryos were rehydrated in increasing dilutions of ethanol. Embryos were then placed in 1% KOH for 2 days to clear and then in alizarin red solution (0.001% alizarin red, 1% KOH) for 3 days. Embryos were washed with 1% KOH and stored in 100% glycerol.

Immunohistochemistry and calcein labeling

Tibiae were removed from female chickens aged 1 day, 3 weeks and 2 years and E6.5 and E.9.5 embryonic chickens. The mineralized tissue was briefly immersed in 5% polyvinyl alcohol (Sigma, Poole, UK) and chilled in an *n*-hexane freezing bath at −70°C [26]. In some cases, the tibiae were decalcified in 10% EDTA at 4°C for up to 14 days before. Sections were cut (10 μm thickness), fixed in ice-cold acetone and stored at −80°C until required. Immunolocalization of PHOSPHO1 was performed using a standard immunoperoxidase procedure which included an overnight incubation at 4°C with affinity purified antiserum diluted to 4 μg/ml of IgG in PBS containing 5% fetal bovine serum (FBS) or 4 μg/ml of normal sheep IgG as control (Sigma). In some cases, DAB peroxidase substrate tablets containing cobalt chloride (Sigma) were used. All sections were mounted without counterstaining. The antiserum to PHOSPHO1 was raised in sheep against recombinant chicken PHOSPHO1 as previously described and shows specificity with avian tissues only [19]. For calcein labeling, 3- and 24-week-old female chickens were injected with 10 mg/kg calcein and culled by cervical dislocation 3 days after injection. The presence of calcein stain in sections of tibiae was visualized by fluorescence microscopy. Some sections were stained with hematoxylin and eosin or von Kossa using standard protocols to identify mineralizing regions.

Matrix vesicle isolation

Three-week-old chickens were culled by cervical dislocation and the tibias removed. The growth plate was dissected from the overlying and underlying tissue and diced into small pieces (1 mm^3). Cartilage pieces were incubated at 37°C in the presence of 0.1% trypsin type II (Sigma) in HBSS (Hank's buffered salt solution) for 30 min. The tissue was washed in HBSS and incubated in 0.07% collagenase at 37°C for 3 h. The cell suspension was passed through a sieve (45 μm) to remove remaining tissue fragments and spun (1000×*g* for 5 min) to pellet the cells. Supernatants were subjected to differential centrifugation. Briefly, the supernatant from the chondrocytes was spun at 30,000×*g* for 20 min to remove sub-cellular debris and finally at 100,000 × *g* for 1 h to pellet MVs. To obtain primary chondrocyte cultures, cartilage pieces were digested by collagenase and hyluronidase as previously described [27]. Chondrocytes were seeded in T25 culture flasks at a density of 1 × 10^6 cells/cm^2 in Dulbecco's modified eagles medium containing 10% FBS, 2 mM L-Glutamine. Following cellular attachment, the cells were treated with or without ascorbic acid (100 μg/ml) and cultured for up to 12 days (37°C, 5% CO_2). When harvesting the cells, the monolayer was washed with HBSS and incubated in 0.07% collagenase type II solution at 37°C for 90 min. The mixture was then subjected to differential centrifugation as described above.

TNAP activity was assayed using the ALP bio-assay kit (Thermo Electron, Melbourne, Australia). MVs activity was determined by measuring the cleavage of *p*-nitrophenyl phosphate (pNPP) at 405 nm, pH 10.7. Total TNAP activity was expressed as nmol pNPP hydrolyzed/min/mg of total protein.

Immunoblotting

The resultant MVs were analyzed for the presence of PHOSPHO1 by immunoblotting. LDS sample buffer was added to the MV lysate extracted from the primary chondrocyte culture, while MVs extracted directly from chick cartilage were lysed in lithium dodecyl sulfate (LDS) sample buffer prior to electrophoresis. Samples corresponding to 10 μg total protein were incubated at 70°C for 10 min before loading. Samples were run on a 10% Bis–Tris NuPAGE gel and electroblotted to nitrocellulose, which were then blocked in 5% non-fat milk in Tris-buffered saline with 0.1% Tween 20 (TBST). The membranes were then

Fig. 2. (A) Immunohistochemical staining of the bone collar (arrows) and chondrocytes with affinity purified antibodies to PHOSPHO1 in a cross-section of a tibia from E6.5 chick embryo. (B) Immunohistochemical staining of longitudinal tibial section from E6.5 embryo showing positive staining is present in the bone collar of the mid-section of the diaphysis (arrows). The area delineated by the box is shown at higher magnification in (C) where the staining is present in the bone collar (arrows), periosteal osteoblasts (arrow heads) and chondrocytes (*). (D) Control longitudinal section of E6.5 chick incubated with normal sheep IgG. The bone collar (arrows) and chondrocytes (*) are unstained. (E and F) Hematoxylin and eosin-stained sections showing trabecularized morphology of the developing cortical bone in longitudinal (E) and cross-section (F) of E9.5 chick tibia. (G and H) Immunohistochemical staining of longitudinal tibial section from E9.5 embryo. Panel (H) shows the box in panel (G) at higher magnification. Staining is limited to the bone forming surfaces (arrows) and is not present on all mineralized bone surfaces. (I) von Kossa staining of mineral in longitudinal section of E9.5 chick tibia. Immunohistochemical staining of PHOSPHO1 in sections of tibia from (J) 1-day-old, (K) 3-week-old and (L) 2-year-old chickens and calcein fluorescence showing (M) mineralization within the periosteum and primary osteons of cortical bone in 3-week-old chick and (N) mineralizing surface of medullary bone in 24-week-old chickens. MB, medullary bone; CB, cortical bone. Staining within the cortical bone (J and K) was limited to the osteoid layer of the periosteum and the bone forming surfaces of the primary osteons (arrows) and mirrored that of the calcein fluorescence (M), with no staining present in the fibroblastic or osteogenic layers. No immunostaining was observed within the cortical bone of the adult (L). DAB peroxidase substrate tablets containing cobalt chloride giving a gray/black end product were used in B, C, G and H. Magnification bars represent 0.1 mm in A–I and 0.2 mm in J–N.

probed with 2 μg/ml sheep–anti-PHOSPHO1 antibody in blocking solution [19] and washed three times with TBST. Blots were then incubated with mouse anti-sheep/goat IgG-peroxidase (DAKO, Cambridgeshire, UK) diluted 1:2000 in blocking solution followed by three washes in TBST. The immune complexes were then visualized by enhanced chemiluminescence. Finally, the proteins on the blot were stained with India ink after alkali pre-treatment, as described by Sutherland and Skerrit [28]. Briefly, the membranes were washed in TBST before incubation with 0.2 M NaOH for 5 min. The membrane was then submerged in 10% India ink solution for 120 min and finally washed repeatedly in TBST until only the protein bands were visible.

Results

Embryonic localization of PHOSPHO1

PHOSPHO1 mRNA expression during embryonic development was investigated in the chick using whole-mount in situ hybridization, staining was seen in embryos incubated with the antisense oligonucleotides corresponding to PHOSPHO1 gene expression at the ossification centers of the long bones. No hybridization was observed in any other tissues or in embryos incubated with the sense oligonucleotides (Fig. 1A). PHOSPHO1 expression began prior to E6.5 around the mid-shaft of metatarsi and by E11.5 had spread to the ends of the diaphysis (Figs. 1B–D). The unmineralized cartilaginous ends of the bones remain unstained.

The temporal expression of PHOSPHO1 in relation to deposition of mineral was also investigated in the chick embryos. Figs. 1E and F show PHOSPHO1 staining of the front limb bones (E9.5) and hind phalange (E11.5), respectively. The entire diaphysis of the front limb bones appeared to be stained, whereas staining had a more restricted location within the diaphysis of the hind phalanges of the older mice. This developmental feature was confirmed by alcian blue and alizarin red staining. Between E9.5 and E11.5, these bones consisted primarily of a cartilaginous matrix with alizarin red staining of mineral restricted only to a small region around the center of the bones in the front limb by E9.5 (Fig. 1G) whereas the phalanges at E11.5 show a complete lack of mineralization (Fig. 1H). Immunohistochemical staining of frozen sections of tibia from embryonic chicks (E6.5 and E9.5) mirrored that of the in situ hybridization and revealed that the PHOSPHO1 staining was localized to the osteoid (bone collar) and associated periosteal osteoblasts within the mid-diaphyseal region (Figs. 2A–C). There were also indications that some chondrocytes within the rudiment also stained positively (Fig. 2C). At this developmental stage, the PHOSPHO1 stained osteoid and the matrix of the differentiating chondrocytes were not mineralized as assessed by von Kossa staining (data not shown). Control sections in which the primary antibody was substituted with normal sheep IgG showed no positive staining (Fig. 2D). By developmental stage E9.5, cortical bone formation had began and had a trabecularized appearance (Figs. 2E and F), which was distinct from osteonal bone present in post-hatch birds (Figs. 2J–L). PHOSPHO1 staining was limited to the bone forming surfaces within cortical bone (Figs. 2G and H) and not on pre-existing mineralized surfaces as visualized by von Kossa staining (Fig. 2I).

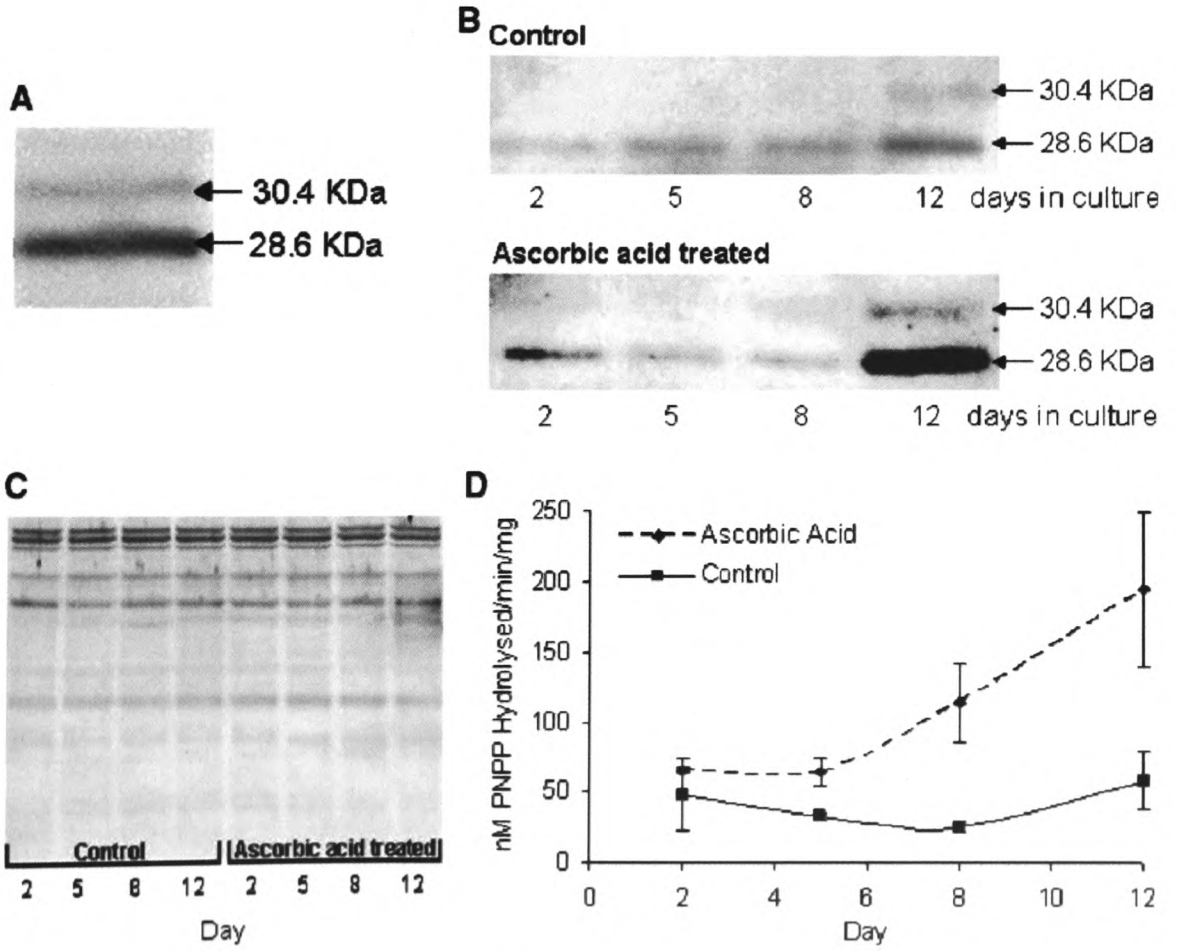

Fig. 3. (A) Immunoblot showing PHOSPHO1 expression in MVs isolated from the tibial growth plates of 3-week-old chicks. (B) Immunoblots examining PHOSPHO1 expression in MVs isolated from primary chondrocytes cultured in the presence or absence of 100 μg/ml ascorbic acid. (C) India ink staining of MV immunoblot demonstrating equal loading in each lane. (D) TNAP activity of MVs isolated from primary chondrocyte cultures.

PHOSPHO1 in growing and adult bone

Strong immunoreactivity was observed at the periosteum and also the bone forming surfaces of the primary osteons situated within the cortical bone (Figs. 2J and K) of the 1-day-old and 3-week-old chicks. All osteons within the cortical bone of the 1-day-old chick were immunoreactive, whereas only those within the periosteal area of the 3-week-old bone were positive. Staining within the periosteum of the 1-day-old and 3-week-old chicks was limited to the osteoid layer and mirrored that of the calcein fluorescence (Fig. 2M), with no staining present in the fibroblastic or osteogenic layers. In the 3-week-old chicks, closed osteons were negative and staining was also absent from the endosteal surface and the cells within the marrow cavity. PHOSPHO1 immunostaining was also present on medullary bone surfaces (Fig. 2L) but not within the periosteum or osteons of a 2-year-old adult chicken. At this age, bone apposition has ceased and no mineralization within osteons or at the periosteal surface takes place. Mineralization in medullary bone of adult female birds was observed by calcein fluorescence (Fig. 2N).

PHOSPHO1 in isolated matrix vesicles

The presence of PHOSPHO1 was examined in MVs isolated from chick growth plate cartilage. Two forms of PHOSPHO1 (30.4 and 28.6 kDa) were detected in MVs isolated directly from the tibial growth plates of 3-week-old chicks (Fig. 3A) and from primary cultured chondrocyte cells (Fig. 3B). PHOSPHO1 expression in the MVs isolated from the primary cells was found to increase with time in culture and appeared to be much greater in the presence of ascorbic acid after 12 days in culture. Equal loading of the samples was confirmed by India ink staining of the membrane (Fig. 3C). No overt signs of matrix mineralization were noted in these cultures. TNAP activity in the presence of ascorbic acid was found to double after 5 days in culture and was 4 times that of the control after 12 days but was not found to alter significantly with time in the control cultures (Fig. 3D).

Discussion

In the embryo, bones begin as condensations of mesenchymal cells that act as models (anlages) for further development. In the developing long bone, capillary invasion of the perichondrium coincides with a switch in perichondrial cell differentiation to the osteoblast lineage. These cells secrete a primary bone collar, which is a thin layer of mineralized bone, lying around the outside of the mid-section of the bone. The bone collar maintains the structural integrity of the bone that is weakened by osteoblasts eroding the internal calcified cartilage scaffold. The ossification process begins at the mid-diaphyseal region and progresses towards the bone extremities [29,30].

PHOSPHO1 has previously been shown to be localized to mineralizing regions of chick bone [19] and has therefore been implicated in the generation of P_i for mineralization. If this hypothesis is true, then developmental expression of PHOSPHO1 should precede the deposition of mineral and follow the same pattern. Whole-mount in situ hybridization indicated that PHOS PHO1 expression occurred prior to E6.5 and was present within the bone collar within the mid-shaft of the diaphysis of the long bones. This was confirmed by immunohistochemistry where both the non-mineralized bone collar and associated periosteal osteoblasts, which first appear at E6.5–7 [31], stained strongly. The matrix staining of PHOSPHO1 on bone forming surfaces may reflect the presence of the enzyme in osteoblast derived MVs, which are deposited within newly formed osteoid [32]. The expression of PHOSPHO1 preceded the mineralization of the osteoid which is known not to occur until E7.5 in the chick [29]. Furthermore, the appearance of PHOSPHO1 in the cartilage rudiment at E6.5 is coincident with chondrocyte hypertrophy in the mid-diaphysis [33] and agrees with our previous observations that PHOSPHO1 is

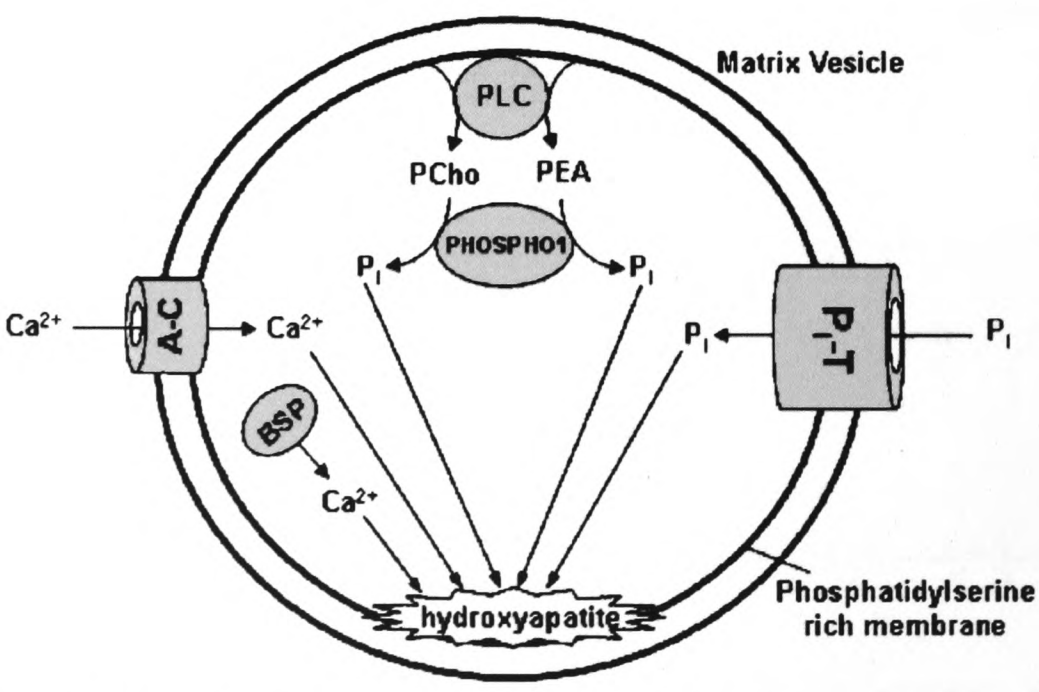

Fig. 4. Schematic representation of Ca^{2+} and Pi accumulation in MVs. BSP, bone sialoprotein; PCho, phosphocholine; PEA, phosphoethanolamine; PLC, phospholipases C; A–C, annexin complex; P_i–T, phosphate transporter.

expressed by hypertrophic chondrocytes prior to them mineralizing their extracellular matrix [19].

By E11.5, expression was observed over the entire length of the diaphysis. In addition, mRNA expression preceded the deposition of mineral as revealed by alcian blue/alizarin red staining. The absence of PHOSPHO1 immunoreactivity on the surface of existing mineralized cortical bone is in accord with previous observations by us where PHOSPHO1 immunoreactivity was absent from terminally differentiated chondrocytes situated deep in the mineralized zone [19]. This suggests that PHOSPHO1 is required for the *de novo* formation of the inorganic phase but not for the continued crystal growth of hydroxyapatite. It is therefore likely that PHOSPHO1 has a pivotal role in first phase of the mineralization process during embryonic development.

By the time of hatching, the chick skeleton is essentially mineralized but continues to grow by periosteal apposition until adulthood. Expression of PHOSPHO1 was observed in all osteons within the cortical bone of the 1-day-old chick but only those situated in the periosteal region of the 3-week-old chick. This difference in PHOSPHO1 distribution reflects the vastly different bone apposition rates between the two ages of birds and is similar to TNAP protein localization, which has previously been shown to be present at the surface of growing osteons but absent in closed osteons where mineralization is complete [34]. Further compelling evidence that PHOSPHO1 plays a role in mineralization comes from the observation that it is present in medullary bone but not cortical bone of adult chicks. In adults, bone apposition has ceased and no mineralization at the periosteum takes place. However, medullary bone in adult female birds constantly undergoes remodeling [35] as illustrated by calcein fluorescence.

Previous studies by us have shown that 30.4 and 28.6 kDa forms of PHOSPHO1 exist in growth plate chondrocytes, corresponding to transcripts derived from alternative start sites in the PHOSPHO1 gene [19]. The amino acid sequences of both putative transcripts contain all three of the catalytic motifs found within the HAD enzyme superfamily [36], and so both forms are likely to be catalytically active. It is unknown whether each form has a distinct physiological significance. Both forms of PHOSPHO1 were found to be present in MVs providing strong evidence that PHOSPHO1 is involved in the first phase of the mineralization. Primary chondrocytes were cultured in the presence and absence of ascorbic acid. The addition of ascorbic acid was found to increase both PHOSPHO1 levels and TNAP activity in isolated MVs. Ascorbic acid is a known stimulant for osteogenesis and mineralization in vitro [37,38]. This suggests that PHOSPHO1 expression and TNAP activity are both influenced by the state of differentiation and may be controlled by similar mechanisms within growth plate chondrocytes.

Ca^{2+} and P_i are known to be present at high levels in MVs even before induction of mineral formation [39]. The action of PHOSPHO1 in MVs will contribute to the P_i generated, although the extent of this contribution is unknown. As well as its generation inside MVs, it is also clear that some P_i is imported from the extracellular matrix with at least two types of P_i transporter known to be present in growth plate chondrocytes [40–43]. The ambient concentration of P_i in the extracellular fluid is close to 2 mM [44]. This may be due to TNAP, which is GPI-anchored to the outer MV membrane [45], as its proposed role in the bone matrix is to generate the P_i needed for hydroxyapatite crystallization [46–48]. However, TNAP has also been hypothesized to hydrolyze the mineralization inhibitor PP_i [13] to facilitate mineral precipitation and growth [12,49,50]. It is therefore doubtful that the amount of P_i released from MV lipids would be sufficient to increase the overall level of extracellular P_i. However, the local effect of PHOSPHO1 within MVs may be sufficient to facilitate mineral formation. A schematic representation of this process is shown in Fig. 4.

In conclusion, PHOSPHO1 is expressed at the primary regions of ossification in developing embryonic bone prior to deposition of mineral and is thus likely to play a role in the initial events leading up to mineralization. We also show for the first time that PHOSPHO1 is enriched in MVs. This study provides further evidence that PHOSPHO1 expression is associated with skeletal mineralization and indirectly supports our hypothesis that PHOS PHO1 is involved in generating P_i within MVs for mineralization.

Acknowledgments

Supported by the Biotechnology and Biological Sciences Research Council and a CASE award to SJR.

References

[1] Cecil RNA, Anderson HC. Freeze-fracture studies of matrix vesicle calcification in epiphyseal growth plate. Metab Bone Dis 1978;1:89–97.
[2] Anderson HC, Stechschulte Jr DJ, Collins DE, Jacobs DH, Morris DC, Hsu HHT, et al. Matrix vesicle biogenesis in vitro by rachitic and normal rat chondrocytes. Am J Pathol 1990;136:391–7.
[3] Wu LNY, Sauer GR, Genge BR, Wuthier RE. Induction of mineral deposition by primary cultures of chicken growth plate chondrocytes in ascorbate-containing media. Evidence of an association between matrix vesicles and collagen. J Biol Chem 1989;264:21346–55.
[4] Anderson HC. Molecular biology of matrix vesicles. Clin Orthop Relat Res 1995;314:266–80.
[5] Wu LNY, Ishikawa Y, Sauer GR, Genge BR, Mwale F, Mishima H, et al. Morphological and biochemical characterization of mineralizing primary cultures of avian growth plate chondrocytes: evidence for cellular processing of Ca^{2+} and Pi prior to matrix mineralization. J Cell Biochem 1995;57:218–37.
[6] Anderson HC. Matrix vesicles and calcification. Curr Rheumatol Rep 2003;5:222–6.
[7] Hunter GK, Goldberg HA. Nucleation of hydroxyapatite by bone sialoprotein. Proc Natl Acad Sci U S A 1993;90:8562–5.
[8] Sauer GR, Wuthier RE. Fourier transform infrared characterization of mineral phases formed during induction of mineralization by collagenase-released matrix vesicles in vitro. J Biol Chem 1988;263:13718–24.
[9] Waymire KG, Mahuren JD, Jaje JM, Guilarte TR, Coburn SP, MacGregor GR. Mice lacking tissue non-specific alkaline phosphatase die from seizures due to defective metabolism of vitamin B-6. Nat Genet 1995;11:45–51.
[10] Narisawa S, Frohlander N, Millán JL. Inactivation of two mouse alkaline phosphatase genes and establishment of a model of infantile hypophosphatasia. Dev Dyn 1997;208:432–46.
[11] Hessle L, Johnson KA, Anderson HC, Narisawa S, Sali A, Goding JW, et al. Tissue-nonspecific alkaline phosphatase and plasma cell membrane glycoprotein-1 are central antagonistic regulators of bone mineralization. Proc Natl Acad Sci U S A 2002;99:9445–9.
[12] Moss DW, Eaton RH, Smith JK, Whitby LG. Association of inorganic-pyrophosphatase activity with human alkaline-phosphatase preparations. Biochem J 1967;102:53–7.

[13] Meyer JL. Can biological calcification occur in the presence of pyrophosphate? Arch Biochem Biophys 1984;231:1–8.
[14] Anderson HC, Harmey D, Camacho NP, Garimella R, Sipe JB, Tague S, et al. Sustained osteomalacia of long bones despite major improvement in other hypophosphatasia-related mineral deficits in tissue nonspecific alkaline phosphatase/nucleotide pyrophosphatase phosphodiesterase 1 double-deficient mice. Am J Pathol 2005;166:1711–20.
[15] Narita M, Goji J, Nakamura H, Sano K. Molecular cloning, expression, and localization of a brain-specific phosphodiesterase I/nucleotide pyrophosphatase (PD-I alpha) from rat brain. J Biol Chem 1994;269:28235–42.
[16] Register TC, McLean FM, Low MG, Wuthier RE. Roles of alkaline phosphatase and labile internal mineral in matrix vesicle-mediated calcification. Effect of selective release of membrane-bound alkaline phosphatase and treatment with isosmotic pH 6 buffer. J Biol Chem 1986;261:9354–60.
[17] Hsu HHT, Anderson HC. Evidence of the presence of a specific ATPase responsible for ATP-initiated calcification by matrix vesicles isolated from cartilage and bone. J Biol Chem 1996;271:26383–8.
[18] Houston B, Seawright E, Jefferies D, Hoogland E, Lester D, Whitehead C, et al. Identification and cloning of a novel phosphatase expressed at high levels in differentiating growth plate chondrocytes. Biochim Biophys Acta 1999;1448:500–6.
[19] Houston B, Stewart AJ, Farquharson C. PHOSPHO1—a novel phosphatase specifically expressed at sites of mineralization in bone and cartilage. Bone 2004;34:629–37.
[20] Houston B, Paton IR, Burt DW, Farquharson C. Chromosomal localization of the chicken and mammalian orthologues of the orphan phosphatase PHOSPHO1 gene. Anim Genet 2002;33:451–4.
[21] Stewart AJ, Schmid R, Blindauer CA, Paisey SJ, Farquharson C. Comparative modelling of human PHOSPHO1 reveals a new group of phosphatases within the haloacid dehalogenase superfamily. Protein Eng 2003;16:889–95.
[22] Nielsen H, Engelbrecht J, Brunak S, von Heijne G. Identification of prokaryotic and eukaryotic signal peptides and prediction of their cleavage sites. Protein Eng 1997;10:1–6.
[23] Roberts SJ, Stewart AJ, Sadler PJ, Farquharson C. Human PHOSPHO1 exhibits high specific phosphoethanolamine and phosphocholine phosphatase activities. Biochem J 2004;382:59–65.
[24] Kvam BJ, Pollesello P, Vittur F, Paoletti S. ^{31}P NMR studies of resting zone cartilage from growth plate. Magn Reson Med 1992;25:355–61.
[25] Wu LNY, Genge BR, Kang MW, Arsenault AL, Wuthier RE. Changes in phospholipid extractability and composition accompany mineralization of chicken growth plate cartilage matrix vesicles. J Biol Chem 2002;277:5126–33.
[26] Farquharson C, Lester D, Seawright E, Jefferies D, Houston B. Cell proliferation and enzyme activities associated with the development of avian tibial dyschondroplasia—an in situ biochemical study. Bone 1992;13:59–67.
[27] Farquharson C, Lester D, Seawright E, Jefferies D, Houston B. Microtubules are potential regulators of growth-plate chondrocyte differentiation and hypertrophy. Bone 1999;25:405–12.
[28] Sutherland MW, Skerrit JH. Alkali enhancement of protein staining on nitrocellulose. Electrophoresis 1986;7:401–6.
[29] Hall BK. Earliest evidence of cartilage and bone development in embryonic life. Clin Orthop Relat Res 1987;225:255–72.
[30] Eyre-Brook AL. The periosteum: its function reassessed. Clin Orthop Relat Res 1984;189:300–7.
[31] Scott-Savage P, Hall BK. The timing of the onset of osteogenesis in the tibia of the embryonic chick. J Morphol 1979;162:453–63.
[32] Morris DC, Masuhara K, Takaoka K, Ono K, Anderson HC. Immunolocalization of alkaline phosphatase in osteoblasts and matrix vesicles of human fetal bone. Bone Miner 1992;19:287–98.
[33] Schmid TM, Linsenmayer TF. Developmental acquisition of type X collagen in the embryonic chick tibiotarsi. Dev Biol 1985;107:373–81.
[34] Gomez S, Rizzo R, Pozzi-Mucelli M, Bonucci E, Vittur F. Zinc mapping in bone tissues by histochemistry and synchrotron radiation-induced X-ray emission: correlation with the distribution of alkaline phosphatase. Bone 1999;25:33–8.
[35] Wilson S, Duff SR. Morphology of medullary bone during the egg formation cycle. Res Vet Sci 1990;48:216–20.
[36] Ridder IS, Dijkstra BW. Identification of the Mg^{2+}-binding site in the P-type ATPase and phosphatase members of the HAD (haloacid dehalogenase) superfamily by structural similarity to the response regulator protein CheY. Biochem J 1999;339:223–6.
[37] Peck WA, Birge Jr SJ, Brandt J. Collagen synthesis by isolated bone cells: stimulation by ascorbic acid in vitro. Biochim Biophys Acta 1967;142:512–25.
[38] Spindler KP, Shapiro DB, Gross SB, Brighton CT, Clark CC. The effect of ascorbic acid on the metabolism of rat calvarial bone cells in vitro. J Orthop Res 1989;7:696–701.
[39] Wu LNY, Wuthier MG, Genge BR, Wuthier RE. In situ levels of intracellular Ca^{2+} and pH in avian growth plate cartilage. Clin Orthop Relat Res 1997;35:310–4.
[40] Montessuit C, Caverzasio J, Bonjour JP. Characterization of a Pi transport system in cartilage matrix vesicles. Potential role in the calcification process. J Biol Chem 1991;266:17791–7.
[41] Montessuit C, Bonjour JP, Caverzasio J. Expression and regulation of Na-dependent Pi transport in matrix vesicles produced by osteoblast-like cells. J Bone Miner Res 1995;10:625–31.
[42] Mansfield K, Teixeira CC, Adams CS, Shapiro IM. Phosphate ions mediate chondrocyte apoptosis through a plasma membrane transporter mechanism. Bone 2001;28:1–8.
[43] Wu LNY, Guo Y, Genge BR, Ishikawa Y, Wuthier RE. Transport of inorganic phosphate in primary cultures of chondrocytes isolated from the tibial growth plate of normal adolescent chickens. J Cell Biochem 2002;86:475–89.
[44] Wuthier RE. Electrolytes of isolated epiphyseal chondrocytes, matrix vesicles, and extracellular fluid. Calcif Tissue Res 1977;23:125–33.
[45] Ierardi DF, Pizauro JM, Ciancaglini P. Erythrocyte ghost cell-alkaline phosphatase: construction and characterization of a vesicular system for use in biomineralization studies. Biochim Biophys Acta 2002;1967:183–92.
[46] Robison R. The possible significance of hexosephosphoric esters in ossification. Biochem J 1923;17:286–93.
[47] Majeska RJ, Wuthier RE. Studies on matrix vesicles isolated from chick epiphyseal cartilage. Association of pyrophosphatase and ATPase activities with alkaline phosphatase. Biochim Biophys Acta 1975;391:51–60.
[48] Fallon MD, Whyte MP, Teitelbaum SL. Stereospecific inhibition of alkaline phosphatase by L-tetramisole prevents in vitro cartilage calcification. Lab Invest 1980;43:489–94.
[49] Rezende A, Pizauro J, Ciancaglini P, Leone F. Phosphodiesterase activity is a novel property of alkaline phosphatase from osseous plate. Biochem J 1994;301:517–22.
[50] Anderson HC, Garimella R, Tague SE. The role of matrix vesicles in growth plate development and biomineralization. Front Biosci 2005;10:822–37.